Oral bioavailability studies of S-nitrosoglutathione using intestinal barrier models by liquid chromatography coupled with mass spectrometry after labeling with the nitrogen isotope 15

Haiyan Yu

Ecole Doctorale BioSE (Biologie-Santé-Environnement)

Thèse

Présentée et soutenue publiquement pour l'obtention du titre de

DOCTEUR DE l'UNIVERSITE DE LORRAINE

Mention : « Sciences de la Vie et de la Santé » par

Haiyan YU

Etude de la biodisponibilité orale du *S*-nitrosoglutathion au moyen de modèles de la barrière intestinale par chromatographie en phase liquide couplée à la spectrométrie de masse après marquage par l'isotope 15 de l'azote

Le 29 août 2018

Membres du jury:

Rapporteurs:	**Emilie DESTANDAU**	**Dr HDR, UMR 7311, Institut de Chimie Organique et Analytique, Université d'Orléans, Orléans, France**
	Elke RICHLING	**Pr, Department of Food Chemistry and Toxicity, University of Kaiserslautern, Kaiserslautern, Germany**
Examinateurs:	**Pierre LEROY**	**Pr, EA 3452, Université de Lorraine, Nancy, France (directeur de thèse)**
	Patrick CHAIMBAULT	**Pr, EA 4632, Université de Lorraine, Metz, France (co-directeur de thèse)**
Membres invités:	**Igor CLAROT**	**Pr, EA 3452, Université de Lorraine, Nancy, France**
	Thierry OSTER	**Pr, UR AFPA USC INRA 340, Biochimie et Biologie Moléculaire, Université de Lorraine, Nancy, France**

EA 3452 CITHEFOR "Cibles thérapeutiques, formulation et expertise préclinique du médicament", 5, rue Albert Lebrun, BP 80403, 54001 NANCY Cedex, France

Acknowledgements

When I start to write acknowledgements, I feel a little sad, because the day to say good-bye is coming. The past three years is a gift to me, I like Nancy, I like the sweet dessert coupled with bitter coffee, I like being with you.

Dear Dr. Emilie Destandau (Université d'Orléans - Pôle de chimie) and Pr. Elke Richling (University of Kaiserslautern), thank you very much for agreeing to be “Rapporteurs” of my PhD thesis. Dear Pr. Igor Clarot (Université de Lorraine) and dear Pr. Thierry Oster (Université de Lorraine), thank you so much for accepting as the jury member of my work. Hope you will enjoy the day.

Dear Pr. Pierre Leroy, thank you for giving me the chance to be your student, it is an honor. Many students are jealous of me, because I have you as my supervisor. Thank you for your serious working attitude and strong exutive ability. You always tell me not to depend on you too much, it is not easy because you are too reliable. Thank you for training me, inspiring me, caring me. Thank you for allowing me to act like a child and always forgiving me, I really enjoy the time with you. You are a responsible teacher, a truly friend, an interesting person.

Dear Pr. Patrick Chaimbault, thank you for being my co-supervisor, the work in Metz is like a vocation, it makes me very relaxed. Thank you for trusting me, explaining and teaching me how to use LC coupled with mass spectrometry. Thank you for showing me how to balance family and work, you are a great father and patient teacher. Thank you for giving me such happy periods.

Dear Pr. Philippe Maincent, thank you for creating the collaboration between falcuty of pharmacy in Wuhan University and university of Lorraine. It contributes to both science and friendship development. Thank you for inviting Chinese students to your home, you make us feel welcomed.

Dear Dr. Anne Sapin, you are always so gentle, so kind, thank you for giving me advices about my mork. You make me realize that eventhough every person in the lab has her/his individual work, but we are family. Thank you for caring about my personal life.

Dear Dr. Ariane Boudier, thank you for showing your principles. I remember the moment that you tell us to wear glasses when carrying out the experiments. This is for our safety. Our lab needs you. Thank you for giving us Chinese money.

Dear Dr. Caroline Gaucher, thank you for your caring about me, you come to the lab on weekends to support my work relating to cells. I know you have done more but without saying anything. Thank you very much for being so nice to me.

Dear Marianne Parent, thank you for staying in our lab, I like you. You work efficiently, you are easygoing, and you have inspired me that I have the potential to be a talent person in the future if I have good plans and work hard.

Dear Pr. Alain Le Faou, Pr. Isabelle Lartaud, thank you for your help and suggestions in my work.

Dear friends, Marie-Lynda Bouressam, Justine Bonetti, Romain Schmitt, Yi Zhou, Hui Ming, Arnaud Pallotta, Eugenia Belcastro…, thank you for accompanying me, working with me. You are my sisters and brothers in France. I miss the time we drink, eat, and chat together.

Dear Isabelle Fries, Philippe Giummelly, Nathalie Degousee, Pascale Carnet, and other colleagues in EA 3452 CITHEFOR, thank you for your help in my work and my personal life.

I will never forget my families in China, especially dear Zhang Liao, without your selfless love, it will be difficult for me to live abroad. I will keep on loving you for the rest of my life.

It is my luck to meet you guys. I am a little shy to tell you how wonderful you are in my eyes, but I am really grateful to meet you, know you and have feelings for you. I hope you will travel in China some day in the future, and I will be exicited to be your tourist guide. I wish all of you are healthy, strong, joyfull and live happily forever.

Table of contents

Scientific works

Publications

(1) Yu Haiyan, Chaimbault Patrick, Clarot Igor, Chen Zilin, Leroy Pierre. Labeling nitrogen species with the stable isotope ^{15}N for their measurement by separative methods coupled with mass spectrometry: a review *(Talanta, 191 (2018) 491–503).*

(2) Yu Haiyan, Schmitt Romain, Sapin Anne, Chaimbault Patrick, Leroy Pierre. Comparison between two derivatization methods of nitrite ion labeled with ^{15}N applied to liquid chromatography-tandem mass spectrometry *(Analytical Methods, 10 (2018) 3830–3836)*

(3) Yu Haiyan, Bonetti Justine, Gaucher Caroline, Fries-Raeth Isabelle, Vernex-Loset Lionel, Leroy Pierre, Chaimbault Patrick. Higher-energy Collision Dissociation for the quantification by liquid chromatography/tandem ion trap mass spectrometry of nitric oxide metabolites coming from S-nitrosoglutathione in an in vitro model of intestinal barrier (*Rapid Communications in Mass Spectrometry, under minor revision)*

(4) Bonetti Justine, Zhou Yi, Parent Marianne, Clarot Igor, Yu Haiyan, Fries-Raeth Isabelle, Leroy Pierre, Lartaud Isabelle, Gaucher Caroline. Intestinal absorption of *S*-nitrosothiols: permeability and transport mechanisms (*Biochemical Pharmacology, 155 (2018) 21–31).*

(5) Yu Haiyan, Schmitt Romain, Sapin Anne, Gaucher Caroline, Fries Isabelle, Leroy Pierre. Degradation of *S*-nitrosoglutathione in rat intestine: roles of denitrosating enzymatic and chemical factors on absorption and permeation (to be submitted to *Drug Metabolism and Disposition).*

Oral presentations

(1) NutriOx (Luxembourg, November 19-20, 2015): Development of a liquid chromatography-mass spectrometry method for the biodistribution studies of nitric oxide species following administration of nitric oxide donors labeled with ^{15}N isotope.

(2) Journée de Rentrée de l'école doctorale BioSE (Nancy, November 23, 2016): Development of a liquid chromatography-mass spectrometry method for studying the intestine permeability of *S*-nitrosothiols labeled with ^{15}N isotope.

(3) Journée scientifique de l'école doctorale BioSE (Nancy, March 28, 2018): Derivatization methods with liquid chromatography- mass spectrometry for the measurement of nitric oxide species originated from *S*-nitrosoglutathione.

Poster communications

(1) Agnieszka Łyczykowska, Haiyan Yu, Igor Clarot, Stéphane Gibaud, Janina Lulek, Patrick Chaimbault, Pierre Leroy. Development of a liquid chromatography-mass spectrometry method for the biodistribution studies of nitric oxide species following administration of nitric oxide donors labeled with ^{15}N isotope (*HTC-14, Ghent, Belgium - January 27-29, 2016*)

(2) Yu Haiyan, Chaimbault Patrick, Leroy Pierre. Development of a liquid chromatography-mass spectrometry method for studying the intestine permeability of *S*-nitrosothiols labeled with ^{15}N isotope (*Journée de Rentrée de l'école doctorale BioSE, Nancy, Novembre 23, 2016*)

(3) Bonetti Justine, Yu Haiyan, Ming Hui, Sapin-Minet Anne, Fries-Raeth Isabelle, Clarot Igor, Chaimbault Patrick, Leroy Pierre, Gaucher Caroline. Intestine permeability of *S*-nitrosoglutathione as a potential nitric oxide donor *via* oral administration (*Oxygen Club of California World Congress 2017 and Annual Society for Free Radical Research-E Conference, Berlin, Germany, June 21-23, 2017*)

(4) Yu Haiyan, Vernex-Loset Lionel, Leroy Pierre, Chaimbault Patrick. Development of a liquid chromatography- HCD tandem mass spectrometry method for the measurement of nitric oxide species coming from *S*-nitrosoglutathione in an *in vitro* model of intestinal (*European Mass Spectrometry Conference (EMSC), Saarbrücken, Germany, March 11-15, 2018*)

List of tables, figures and abbreviations

Tables

Introduction

Review in *Talanta (191 (2018) 491–503)*:

1st Chapter

1. Experimental paper in *Analytical Methods (10 (2018) 3830–3836):*

2. Experimental paper in *Rapid Communications in Mass Spectrometry (under minor revision)*:

Figures

Introduction

Review in *Talanta (191 (2018) 491–503)*:

1st Chapter

^{15}N-nitrites ① after incubation is directly obtained after DAN derivatization followed by LC-ITMS/MS. Free ^{15}N-nitrates are obtained after enzymatic (nitrate reductase) pretreatment of the metabolite pool. The quantification by LC-MS/MS after DAN derivatization of this sample provides the cumulative concentration ② of free ^{15}N-nitrites + ^{15}N-nitrates (reduced into nitrites). The concentration in free ^{15}N-nitrates ③ is deduced from result ② by subtracting the concentration of free ^{15}N-nitrites ①. The concentration of RS^{15}NOs is obtained after the pretreatment of the metabolite pool with Hg^{2+}. The quantification by LC-MS/MS after DAN derivatization of this sample provides the cumulative concentration ④ of free ^{15}N-nitrites + GS^{15}NO (converted into nitrites, see reaction 2 in figure 1). The concentration of RS^{15}NO ⑤ is deduced from result ④ by subtracting the concentration of free ^{15}N-nitrites ①..104

2nd Chapter

1. Experimental paper in *Biochemical Pharmacology (155 (2018) 21–31)*:

2. Experimental paper *to be submitted* to *Drug Metabolism and Disposition*:

Abbreviations

Abbreviations	Full names
ACN	Acetonitrile
ADC	Arginine decarboxylase
ADMA	Asymmetric dimethylarginine
BCA	Bicinchoninic acid
BCS	Biopharmaceutical Classification System
BSA	Bovine serum albumin
CAD	Collision-activated dissociation
cAMP	Cyclic adenosine monophosphate
cCOx	Cytochrome C oxidase
CID	Collisionally induced dissociation
CL	Chemiluminescence
CNA	3-Carboxy-4-nitroanilide
CVDs	Cardiovascular diseases
Cys/Cu	Cysteine and $CuSO_4$
CysNO	*S*-nitrosocysteine
DAN	2,3-Diaminonaphthalene
DeoxyHb	Deoxygenated hemoglobin
DTNB	5,5′-Dithiobis(2-nitrobenzoic acid)
DTPA	Diethylene triamino pentaacetic acid
ECNICI	Electron-capture negative-ion chemical ionization
EDRF	Endothelium-derived relaxing factor
EDTA	Ethylene diaminotetraacetic acid
EMEM	Eagle’s Minimum Essential Medium
eNOS	Endothelial nitric oxide synthase

EPR	Electron paramagnetic resonance
ESI	Electrospray ionization
$Et_3O^+[BF_4^-]$	Triethyloxonium tetrafluoroborate
FAB	Fast atom bombardment
FAD	Flavin adenine dinucleotide
FBS	Fetal bovine serum
FL	Fluorescence
FMOCCI	9-Fluorenylmethyl chloroformate
FTIR	Fourier Transform InfraRed spectroscopy
FTIRM	FTIR Microscopy
GC	Gas chromatography
GGT	*γ*-glutamyltransferase
GIT	Gastrointestinal tract
Glygly	Glycylglycine
GCNA	*L*-*γ*-glutamyl-3-carboxy-4-nitroanilide
GSH	Reduced glutathione
GSNO	*S*-nitrosoglutathione
$GS^{15}NO$	^{15}N labeled *S*-nitrosoglutathione
GSSG	Glutathione disulphide
Hb	Hemoglobin
HbFeNO	Iron nitrosylhemoglobin
HbSNO	*S*-nitrosohemoglobin
HBSS	Hank's Balanced Salt Solution
HCD	Higher-energy Collision Dissociation
HILIC	Hydrophilic interaction liquid chromatography
LC	Liquid chromatography

LC-FL	LC coupled with fluorescence detection
IEC	Ion-exchange chromatography
iNOS	Inducible NO synthase
IS	Internal standard
ITMS	Ion Trap Mass Spectrometer
LC-MS	LC coupled with mass spectrometry
LC-ESI-MS/MS	Liquid chromatography-electrospray ionization-tandem mass spectrometry
LC-ESI-ITMS/MS	Liquid Chromatography-Electrospray Ionization -Ion Trap tandem Mass Spectrometry
LC-ITMS/MS	Liquid chromatography-tandem ion trap mass spectrometry
LC-MS/MS	Liquid chromatography-tandem mass spectrometry
LLOQ	Lower limit of quantification
LOD	Limit of detection
log P	Logarithmic value of partition coefficient
LOQ	Limit of quantification
MeOH	Methanol
MES	2-(*N*-morpholino)ethanesulfonic acid
MRM	Multiple-reaction monitoring
MS	Mass spectrometry
MS/MS	Tandem mass spectrometry
MTT	3(4,5-Dimethylthiazol-2-yl)-2,5-diphenyltetrazolium bromide
m/z	Mass-over-charge ratio
2-NA	2-Naphthylamine
NAC	*N*-acetyl-*L*-cysteine

NACNO	*S*-nitroso-*N*-acetyl-*L*-cysteine
$NAC^{15}NO$	^{15}N labeled *S*-nitroso-*N*-acetyl-*L*-cysteine
NADPH	Dihydronicotinamide-adenine dinucleotide phosphate
$Na^{15}NO_2$	^{15}N labeled sodium nitrite
$Na^{15}NO_3$	^{15}N labeled sodium nitrate
NAP	*N*-acetyl-D-penicillamine
NAT	2,3-Naphthotriazole
NDA	2,3-Naphthalene dicarboxyaldehyde
NED	*N*-(1-naphthyl)-ethylenediamine
NEM	*N*-ethylmaleimide
^{15}N-GDN	^{15}N labeled 1,2-glyceryl dinitrate
^{15}N-GTN	^{15}N labeled glyceryl trinitrate
$^{15}NH_4^+$	^{15}N labeled ammonium ion
^{15}N-NAT	^{15}N labeled 2,3-naphthotriazole
nNOS	Neuronal NO synthase
$^{15}NO_2^-$	^{15}N labeled nitrite ion
$^{15}NO_3^-$	^{15}N labeled nitrate ion
NOx	Nitrogen oxides
OCT	Organic Cation Transporters
OCTN	Zwitterion Transporters
$O^{15}NOO^-$	^{15}N labeled peroxynitrite ion
P_{app}	Apparent permeability coefficient
PDI	Protein Disulfide Isomerase
HePI-MS	Helium-plasma ionization mass spectrometry
PK	Pharmacokinetic
pKa	Negative logarithmic value of acid ionisation constant

PFBBr	Pentafluorobenzyl bromide
RNS	Reactive nitrogen species
RPLC	Reverse phase liquid chromatography
r^2	Coefficient of determination
RSD	Relative standard deviation
RSNOs	*S*-nitrosothiols
$RS^{15}NOs$	^{15}N labeled *S*-nitrosothiols
r.t.	Room temperature
SBC	Serine-borate complex
S/B	Signal-over-blank ratio
SD	Standard deviation
SDS	Sodium dodecyl sulfate
Sem	Standard error of the mean
SIM	Selected-ion monitoring
$S^{15}NACET$	^{15}N labeled *S*-nitroso-*N*-acetylcysteine ethyl ester
SNALB	*S*-nitrosoalbumin
$S^{15}NALB$	^{15}N labeled *S*-nitrosoalbumin
SNAP	*S*-nitroso-*N*-acetyl-*D*-penicillamine
$S^{15}NAP$	^{15}N labeled *S*-nitroso-*N*-acetyl-*D*-penicillamine
$S^{15}NC$	^{15}N labeled *S*-nitroso--*L*-cysteine
S/N	Signal-over-noise ratio
SRM	Selected-reaction monitoring
TEER	Transepithelial electrical resistance
UPLC	Ultra performance liquid chromatography
XO	Xanthine oxidase

General introduction

Titre:

Oral bioavailability studies of *S*-nitrosoglutathione using intestinal barrier models by liquid chromatography coupled with mass spectrometry after labeling with the isotope nitrogen 15

Etude de la biodisponibilité orale du *S*-nitrosoglutathion au moyen de modèles de la barrière intestinale par chromatographie en phase liquide couplée à la spectrométrie de masse après marquage par l'isotope 15 de l'azote

Introduction générale

Les maladies cardiovasculaires (MCV) représentent la première cause de mortalité dans le monde, en particulier dans les pays occidentaux du fait du vieillissement de la population, de suralimentation ou de mauvaise alimentation, ou encore d'un manque d'activité physique. En outre, le tabagisme et l'usage nocif de l'alcool sont des facteurs de risque aggravants. Il en résulte un réel enjeu sociétal et économique : maintenir une population vieillissante dans de bonnes conditions de vie et diminuer les dépenses de santé liées aux MCV.

L'athérosclérose intervient pour une part importante dans la physiopathologie des MCV, en particulier pour les syndromes coronariens aigus. Près de la moitié des décès mondiaux sont dus à un infarctus du myocarde ; un tiers résulte d'un accident vasculaire cérébral ; viennent ensuite l'hypertension artérielle ou d'autres MCV comme l'embolie pulmonaire et les causes d'insuffisance cardiaque.

La prise en charge des MCV (diagnostic, thérapeutique, chirurgie, hygiène de vie) s'améliore régulièrement mais elle nécessite de nouvelles avancées pour faire reculer la fréquence de celles-ci et leur corollaire en termes de morbidité. Les classes thérapeutiques des MCV sont nombreuses : bêtabloquants, inhibiteurs calciques, diurétiques, médicaments ciblant le système rénine angiotensine, dérivés nitrés, digitaliques, antiarythmiques, inhibiteurs de la phosphodiestérase, antagonistes des récepteurs à l'endothéline,…). Chacune de celles-ci bénéficie régulièrement de nouveaux développements. En outre, des combinaisons entre médicaments appartenant à différentes classes apportent des améliorations notables dans le traitement des MCV.

Parmi ces différentes classes thérapeutiques, les dérivés nitrés ou nitrates organiques constituent l'une des plus anciennes puisque Alfred Nobel (1833-1896), inventeur de la nitroglycérine, s'est administré celle-ci pour combattre l'angor dont il souffrait. La découverte de l'entité pharmacologique active, le monoxyde d'azote ou oxyde nitrique (NO), n'est intervenue que beaucoup plus tard. En effet, la nature chimique de l'EDRF (endothelium-derived relaxing factor ou facteur relaxant dérivé de l'endothélium) a été identifiée comme étant le NO en 1986 par Louis Ignarro, Ferid Murad et Salvador Moncada, récipiendaires du prix Nobel de physiologie et de médecine en 1998.

Depuis la découverte du NO en physiologie, les travaux qui lui sont consacrés

n'ont cessé de croître, permettant de mieux comprendre son rôle ubiquitaire au-delà de son action sur la relaxation des cellules musculaires lisses des vaisseaux sanguins : inhibition de l'agrégation plaquettaire, rôle dans les systèmes immunitaire et nerveux, etc... De plus, le NO, espèce radicalaire à demi-vie courte (de l'ordre de la seconde) et à l'état gazeux dans les conditions standards de température et de pression, appartient à la classe des gazotransmetteurs qui incluent le sulfure d'hydrogène (H_2S) et le monoxyde de carbone (CO). Ces gaz ont des propriétés physiologiques proches et les interactions entre eux (en particulier H_2S et NO) constituent un domaine d'investigation très récent et en plein essor.

Il est actuellement établi que la production endogène du NO diminue avec l'âge (Loo *et al.* 2000) et au cours des MCV du fait d'une détérioration des fonctions de l'endothélium (monocouche cellulaire recouvrant la paroi interne des vaisseaux sanguins). En effet, les cellules endothéliales produisent le NO *via* l'oxydation de l'arginine en citrulline catalysée par la NO synthase endothéliale (eNOS) ; le NO diffuse vers les cellules musculaires lisses sous-jacentes et active la guanylate cyclase soluble (sGC), ce qui va permettre la synthèse de monophosphate de guanosine cyclique (cGMP) induisant une vasodilatation. L'altération de l'endothélium résultant de l'apparition d'une plaque athéromateuse, d'une inflammation et d'un stress oxydant diminue l'activité de l'eNOS au profit de la production d'espèces réactives de l'azote délétères. Celles-ci résultent de l'expression de la NO synthase inductible (iNOS) qui mène à la production d'importantes quantités de NO réagissant avec l'anion superoxyde ($O_2^{\bullet -}$) également produit en grande quantité dans les conditions de stress oxydant. Il se forme ainsi l'anion peroxynitrite ($ONOO^-$) très réactif vis-à-vis des constituants cellulaires, en particulier par la nitration des résidus tyrosine des protéines.

Les travaux menés sur le NO en physiopathologie démontrent l'utilité d'une supplémentation en NO aussi bien dans des événements cardiovaculaires aigus ou chroniques. L'alimentation (eau de boisson, légumes,…) est une source importante d'ions nitrates qui sont réduits en ions nitrites par les bactéries du tube digestif, puis assimilés et réduits en NO dans l'organisme. Cette source ne permet cependant pas de compenser le manque de production de NO *in situ* au niveau du système cardiovasculaire.

La trinitrine, appellation pharmaceutique de la nitroglycérine, est toujours adaptée au traitement d'une crise d'angor, la voie d'administration sublinguale (spray)

ou perlinguale (comprimé à croquer) étant préférable pour obtenir des concentrations dans le compartiment sanguin efficaces en thérapeutique. Mais dans ce cas, la durée de l'effet est brève (demi-vie de l'ordre de 15 min). Dans le cas de traitements chroniques, la prise des dérivés nitrés par voie orale offre une biodisponibilité très faible (< 10 %), du fait d'un premier passage hépatique très important. Des formulations à libération prolongée permettent cependant d'obtenir un effet thérapeutique pendant 8 h (dinitrate d'isosorbide). La voie transdermique est également utilisée. Après application du dispositif « patch » sur la peau, la trinitrine pénètre directement dans la circulation sous forme active (pas d'effet de premier passage dans le foie). Les dérivés nitrés présentent cependant des effets secondaires notables : phénomène de tolérance, apparition d'un stress oxydant (consommation du pool de thiols en particulier du glutathion dans l'organisme). Ils s'administrent donc de façon discontinue (par exemple en retirant le patch durant la nuit), de manière à éviter tout échappement thérapeutique.

II apparait que les composés donneurs de NO actuellement disponibles ont des indications thérapeutiques restreintes et de nombreux inconvénients. Il est donc d'un intérêt majeur de développer de nouveaux donneurs de NO libérant celui-ci de façon prolongée et sans effets délétères.

Comment se positionnent mes travaux de thèse dans le projet scientifique de l'unité de recherche EA 3452 Cithefor dans laquelle j'ai réalisé ceux-ci, ainsi que dans la collaboration établie avec le Professeur Patrick Chaimbault (EA 4632 LCP-A2MC) ?

Le projet de l'EA 3452 Cithefor s'intitule «**Molécules et nanoformulations innovantes donneurs de NO à visée vasculaire**». Il est principalement axé sur les **thionitrites** ou ***S*-nitrosothiols (RSNOs)** capables de libérer NO sur de plus longues durées que les médicaments actuels sans présenter leurs inconvénients. Le principal mode d'obtention des RSNOs consiste à faire réagir un thiol avec les ions nitrites en milieu acide pour former une liaison S-NO. Les RSNOs utilisés au sein de l'EA Cithefor présentent soit un cœur cystéine (le *S*-nitrosoglutathion (GSNO), principal RSNOs endogène et la *S*-nitroso-*N*-acétylcystéine (NACNO)), soit un cœur pénicillamine (la *S*-nitroso-*N*-acétylpénicillamine (SNAP)). Une molécule originale, la *S,S'*-dinitrisobucillamine ($Buc(NO)_2$), possédant à la fois un cœur cystéine et

pénicillamine, a fait l'objet de travaux au sein de l'EA Cithefor (Dahboul *et al.* 2014)(Luo *et al.* 2016)(Bouressam *et al.* 2017). Ces molécules demeurent cependant sensibles aux conditions environnementales et elles nécessitent le développement de formulations adaptées réalisées au sein de l'EA Cithefor afin de limiter leur biotransformation et de faciliter leur diffusion vers les tissus vasculaires (Wu *et al.* 2016a).

La preuve du concept d'une libération prolongée de NO à partir de RSNOs formulés sous forme d'implants polymériques microparticulaires biodégradables sous-cutanés formés *in situ* a été apportée sur l'animal entier (rat), en observant à la fois la diminution de la pression artérielle par télémétrie, et l'effet antiagrégant plaquettaire, ceci sur plusieurs jours ; l'effet bénéfique du GSNO formulé en implants microparticulaires par rapport au GSNO libre a été démontré dans la récupération après un AVC. Il s'agit de la première étude de formulation retard de RSNOs testées *in vivo* dans des conditions physiologiques et pathologiques (modèle murin de thromboembolisme cérébral sans reperfusion (Parent *et al.* 2015).

En vue d'accroître le champ d'application des RSNOs en thérapeutique en particulier dans les traitements chroniques, il est nécessaire de privilégier la voie d'administration orale et par conséquent d'étudier le passage de la barrière intestinale par ceux-ci. Pour ce faire, les méthodologies analytiques couramment utilisées au sein de l'EA Cithefor reposent sur des techniques spectroscopiques conventionnelles décrites dans la littérature mais leur limite de quantification (LOQ) située entre 1 et 0,1 µM s'avère insuffisante. De plus, lors d'étude pharmacocinétique sur animal entier, il sera nécessaire de distinguer entre les différentes sources de NO : production endogène, alimentation et médicament. C'est en quoi les travaux de ma thèse doivent compléter le panel des méthodes bioanalytiques disponibles au sein de l'EA 3452 Cithefor. La collaboration avec le Professeur P Chaimbault est liée au choix de l'outil spectrométrie de masse (SM) pour remplir les objectifs en matière de méthodes sélectives présentant une limite de quantification (LOQ pour Limit Of Quantification) la plus faible possible.

Comment est organisé mon manuscrit de thèse ?

L'**introduction** porte sur les approches méthodologiques utilisées dans la littérature pour suivre spécifiquement un dérivé azoté marqué par l'isotope 15 de l'azote (^{15}N). Ce dernier étant de faible abondance naturelle (0,37%) et stable, le

marquage des ions nitrites et des RSNOs d'intérêt par celui-ci va représenter dans le cadre de nos études un excellent moyen de suivre le devenir de ceux-ci dans l'organisme, en particulier après administration orale. La méthodologie analytique de choix pour ce faire sera la spectrométrie de masse associée à une méthode séparative. Cette revue de la littérature a fait l'objet d'une publication intitulée "**Labeling nitrogen species with the stable isotope ^{15}N for their measurement by separative methods coupled with mass spectrometry: a review"** en cours de publication dans *Talanta (191 (2018) 491–503).*

Le **premier chapitre** est axé sur les développements méthodologiques analytiques. Le NO et ses métabolites inorganiques (ions nitrites et nitrates) ont des faibles valeurs de masse molaire et leurs ions m/z correspondants sont de détection difficile en SM. Le recours à des réactions de dérivation s'avère indispensable pour augmenter la masse molaire et faciliter leur rétention en chromatographie en phase liquide (CPL), leur détection au moyen d'une fragmentation appropriée (SM/SM). J'ai eu recours à des techniques analytiques existantes largement utilisées dans la littérature et complètement maîtrisées au sein de l'EA 3452 Cithefor. Il s'agit de :

- la méthode spectrophotocolorimétrique de Griess dans laquelle les ions nitrites réagissent successivement avec la sulfanilamide et la naphtylamine pour produire un adduit azoïque coloré ;
- une méthode spectrofluorimétrique dans laquelle les ions nitrites réagissent en milieu acide avec le 2,3-diaminonaphtalène (DAN) pour donner un adduit (2,3-naphtotriazole ; NAT) fluorescent en milieu alcalin.

Ces deux méthodes ont en commun l'avantage de permettre en plus de la mesure des ions nitrites, celle des ions nitrates (après réduction chimique ou enzymatique en ions nitrites) et des RSNOs (après clivage de la liaison S-NO par action des ions mercuriques). Les trois espèces (ions nitrates, nitrites et RSNOs) seront donc analysées par la même méthode finale.

La première partie de cette étude a concerné le choix entre ces deux méthodes de dérivation ; le principal critère de choix a été la LOQ atteinte par chacune des deux méthodes en examinant avec attention son mode de calcul. En effet, le calcul de la LOQ s'effectue classiquement par le rapport signal-sur-bruit (signal-over-noise ratio : S/N) ; mais il n'est pas approprié si on considère l'analyte « nitrite ». En effet, au cours des manipulations des échantillons et des réactifs au contact de l'air, il survient une contamination de toutes les solutions par les oxydes d'azote présents dans

l'atmosphère ainsi qu'une réduction des ions nitrates en nitrites par des bactéries contaminant les solutions. C'est pourquoi il lui sera préféré le rapport signal-sur-blanc (signal-over-blank ratio : S/B) pour calculer la LOQ.

Ces travaux ont fait l'objet d'une *short communication* intitulée « **Comparison between two derivatization methods of nitrite ion labeled with ^{15}N applied to liquid chromatography-tandem mass spectrometry**» soumise à *Analytical Methods (10 (2018) 3830–3836).*

La **seconde partie** de ce chapitre a consisté en un développement plus approfondi de la méthode reposant sur la dérivation des ions nitrites par le DAN sélectionnée en raison de la LOQ la plus faible qu'elle offre. Une optimisation des conditions opératoires a été suivie d'une validation complète de la méthode et d'une application de celle-ci à l'étude de la perméabilité intestinale de GSNO sur un modèle cellulaire.

Ces travaux ont fait l'objet d'un article intitulé «**Higher-energy Collision Dissociation for the quantification by liquid chromatography/tandem ion trap mass spectrometry of nitric oxide metabolites coming from *S*-nitrosoglutathione in an in vitro model of intestinal barrier** » soumis à *Rapid Communications in Mass Spectrometry* et actuellement en cours de révision.

Le **second chapitre** est consacré aux études de perméabilité intestinale menées sur le GSNO pris comme modèle de RSNOs. Un rapide rappel des nombreux modèles de barrière intestinale couramment utilisés pour évaluer la biodisponibilité orale des médicaments est réalisé en début de chapitre. En effet une revue très complète traitant ce sujet a été récemment publiée (Bilat *et al.* 2017). L'approche expérimentale s'est axée sur l'utilisation des deux modèles maîtrisés au niveau de l'EA Cithefor :

- un modèle *in vitro* utilisant la lignée cellulaire Caco-2 se différentiant en formant une mono-couche de cellules épithéliales;
- un modèle *ex vivo* consistant à isoler une partie de l'intestin de rat (ileum) dans une chambre de Ussing.

Les résultats obtenus sur le modèle cellulaire en plus des résultats purement analytiques présentés dans la publication soumis à *Rapid Communications in Mass Spectrometry*, ont fait l'objet d'un article intitulé **« Intestinal absorption of *S*-nitrosothiols: permeability and transport mechanisms »** et soumis à *Biochemical Pharmacology (155 (2018) 21–31)*. Les mesures de perméabilité

apparente (P_{app}) du GSNO ainsi que d'autres RSNOs ont permis de les positionner dans la classification de la perméabilité des médicaments. Des indications sur le type de mécanisme assurant le passage des RSNOs et de ses métabolites à travers cette barrière physiologique sont également données.

La place du GSNO dans la classification de la perméabilité des médicaments a été confirmée en utilisant le modèle ex vivo et la méthode de marquage à l'azote 15 associée à la technique LC-MS/MS. De plus, les principaux mécanismes, enzymatiques ou non, dénitrosant le GSNO ont été étudiés sur intestin isolé. Les résultats correspondants font l'objet d'un article intitulé «**Degradation of *S*-nitrosoglutathione in rat intestine: roles of denitrosating enzymatic and chemical factors on absorption and permeation**» en préparation pour soumission à *Drug Metabolism and Disposition.* La soumission de cet article ne pourra se faire qu'après des travaux complémentaires réalisés au sein de l'EA 3452 Cithefor.

Les **conclusions-perspectives** résument les points les plus remarquables obtenus au cours de mes travaux de thèse sur le plan bioanalytique et perméabilité intestinale du GSNO ainsi que les perspectives attendues dans le cadre du projet de l'EA 3452 Cithefor et au delà.

La **bibliographie** comprend l'ensemble des références (classées par ordre alphabétique) citées dans le texte du présent manuscrit de thèse ainsi que dans les publications incluses dans l'introduction et les deux chapitres.

Enfin, les **annexes** du présent manuscrit correspondent à 8 fiches techniques décrivant les principales méthodologies expérimentales développées au cours de ma thèse ou simplement adaptées à mes travaux. Elles pourront être aisément utilisées au sein de l'EA 3452 Cithefor.

Introduction

Nitric oxide (NO) is a radical molecule with a very short half-life playing important roles in physiology, pathophysiology and pharmacology. The detailed information can be easily found in numerous books and reviews such as: (Moncada, Palmer and Higgs 1991). *S*-nitrosothiols (RSNOs), such as *S*-nitrosoglutathione (GSNO), which can release NO without the drawbacks of NO donors present on the market (drug tolerance phenomenon and induction of oxidative stress), appear as promising candidate drugs. Related informations have been well detailed in the following reviews: (Richardson and Benjamin 2002)(Gaucher *et al.* 2013) and PhD thesis maunscripts (Wu 2015)(Belcastro 2016)(Ming 2017).

Administered RSNOs are converted to nitrite and nitrate ions, and other RSNOs through transnitrosation, in the body (Minamiyama, Takemura and Inoue 1997). All these NO species can be converted back into NO, and their concentrations are closely linked to physiology or pathology states. For example, NO in the range of pico to nanomolar, shows protective properties, while it becomes cytotoxic in the micromolar range (Mocellin, Bronte and Nitti 2007). Still, there are many unknown parts and challenges for these studies. For example, which method able to distinguish endogenous and exogenous NO sources can be used to analyze these NO species with a sufficient high specificity and the required sensitivity? Thus, the first step of our research is to find a selective and sensitive method, using nitrogen 15 (^{15}N) to label exogenous GSNO and taking advantage of MS to analyze ^{15}N labeled NO species. Related methods that have analyzed ^{15}N labeled NO species in the literature are summarized in the following review.

Review: “Labeling nitrogen species with the stable isotope ^{15}N for their measurement by separative methods coupled with mass spectrometry: a review” in *Talanta (191 (2018) 491–503)*

L'azote et ses nombreux dérivés hydrogénés et oxygénés sont d'une importance primordiale dans notre environnement et dans les cellules vivantes tant sur le plan qualitatif que quantitatif. Leur surveillance est nécessaire pour évaluer toutes les perturbations se produisant dans le cycle de l'azote et dans les événements physiopathologiques liés aux variations de la biodisponibilité de l'oxyde nitrique (NO). De nombreuses méthodes d'analyse sont consacrées à la mesure des espèces azotées, en particulier celles liées au NO, dans les domaines environnemental, biologique et pharmacologique. Elles ont déjà été compilées et discutées dans de nombreuses revues. Le marquage des espèces azotées avec l'isotope 15 (^{15}N) stable et à faible abondance naturelle associé à la spectrométrie de masse (MS) donne lieu à plus d'informations mécanistiques et à des performances analytiques supérieures aux méthodes conventionnelles. La présente revue est consacrée au marquage ^{15}N des espèces azotées apparentées pour suivre leur interconversion et leur métabolisme, aux différentes sondes chimiques utilisées pour leur dérivation et aux méthodes séparatives correspondantes couplées à la MS pour l'analyse des adduits obtenus. Le mode de fragmentation des différents adduits et la sélectivité et la sensibilité qui en résultent sont discutés.

Talanta 191 (2019) 491–503

Contents lists available at ScienceDirect

Talanta

journal homepage: www.elsevier.com/locate/talanta

Labeling nitrogen species with the stable isotope ^{15}N for their measurement by separative methods coupled with mass spectrometry: A review

Haiyan Yu[a], Patrick Chaimbault[b], Igor Clarot[a], Zilin Chen[c], Pierre Leroy[a,*]

[a] Université de Lorraine, CITHEFOR, F-54000 Nancy, France
[b] Université de Lorraine, LCP-A2MC, F-57000 Metz, France
[c] Wuhan University, School of Pharmaceutical Sciences, 430071, Wuhan, China

ARTICLE INFO

Keywords:
Stable nitrogen isotopes
Nitric oxide related species
^{15}N labeling
Derivatization methods
Separative methods
Mass spectrometry

ABSTRACT

Nitrogen and its numerous hydrogenated and oxygenated derivatives are of main importance in our environment and in living cells as well in both qualitative and quantitative aspects. Their monitoring is needed to evaluate all disturbances occurring in the nitrogen cycle and in pathophysiological events related to variations of nitric oxide (NO) bioavailability. Many analytical methods are devoted to the measurement of nitrogen species, especially those related to NO, in the environmental, biological and pharmacological fields, and they have already been compiled and discussed in numerous reviews. Nitrogen isotope (^{15}N) is stable and has a low level of natural abundance. Labeling nitrogen species with ^{15}N associated with mass spectrometry (MS) gives rise to more mechanistic information and improved analytical performances compared to conventional methods. The present review is dedicated to the ^{15}N labeling of related nitrogen species to monitor their interconversion and metabolism, the different chemical probes used for their derivatization and the corresponding separative methods coupled with MS for analyzing resulting adducts. The fragmentation mode of the different adducts and the resulting selectivity and sensitivity are discussed.

1. Introduction

Nitrogen is essential to the life on Earth. Proof of that, it is one of the four most abundant elements in living organisms (*i.e.* H, O, C and N), and therefore plays a significant biological role. Nitrogen is present in human body (2.5%, w/w) as a constituent of most life molecules, as well as in the earth atmosphere where it composes 78% of the air that we breathe [1]. Among 8 nitrogen isotopes, only 2 are stable and

Abbreviations: NO, Nitric oxide; eNOS, endothelial nitric oxide synthase; nNOS, neuronal NO synthases; iNOS, inducible NO synthase; CVDs, cardiovascular diseases; HbSNO, *S*-nitrosohemoglobin; GSNO, *S*-nitrosoglutathione; HbFeNO, iron nitrosylhemoglobin; SNALB, *S*-nitrosoalbumin; RSNOs, *S*-nitrosothiols; XO, xanthine oxidase; cCOx, cytochrome C oxidase; Hb, hemoglobin; DeoxyHb, deoxygenated hemoglobin; FAD, flavin adenine dinucleotide; NADPH, dihydronicotinamide-adenine dinucleotide phosphate; GSH, reduced glutathione; FL, fluorescence; CL, chemiluminescence; GC, gas chromatography; IEC, ion-exchange chromatography; HPLC, high performance liquid chromatography; UPLC, ultra performance liquid chromatography; MS, mass spectrometry; $^{15}NH_4^+$, ^{15}N labeled ammonium ion; $^{15}NO_2^-$, ^{15}N labeled nitrite ion; $^{15}NO_3^-$, ^{15}N labeled nitrate ion; ADMA, asymmetric dimethylarginine; ADC, arginine decarboxylase; cAMP, cyclic adenosine monophosphate; GIT, gastrointestinal tract; N_2O, Nitrous oxide; EPR, electron paramagnetic resonance; ^{15}N-GTN, ^{15}N labeled glyceryl trinitrate; ^{15}N-GDN, ^{15}N labeled 1,2-glyceryl dinitrate; S^{15}NALB, ^{15}N labeled *S*-nitrosoalbumin; GS^{15}NO, ^{15}N labeled *S*-nitrosoglutathione; S^{15}NC, ^{15}N labeled *S*-nitroso–*L*-cysteine; S^{15}NACET, ^{15}N labeled *S*-nitroso-*N*-acetylcysteine ethyl ester; S^{15}NAP, ^{15}N labeled *S*-nitroso-*N*-acetyl-*D*-penicillamine; NAC^{15}NO, ^{15}N labeled *S*-nitroso-*N*-acetyl-*L*-cysteine; MS/MS, tandem mass spectrometry; HNO_2, nitrous acid; SIM, selected-ion monitoring; CAD, collision-activated dissociation; SRM, selected-reaction monitoring; PFBBr, pentafluorobenzyl bromide; FMOCCI, 9-fluorenylmethyl chloroformate; $Et_3O^+[BF_4^-]$, triethyloxonium tetrafluoroborate; DAN, 2,3-diaminonaphthalene; GSH, reduced glutathione; Cys/Cu, cysteine and $CuSO_4$; RS^{15}NOs, ^{15}N labeled *S*-nitrosothiols; O^{15}NOO$^-$, ^{15}N labeled peroxynitrite ion; ^{15}N-NAT, ^{15}N labeled 2,3-naphthotriazole; MRM, multiple-reaction monitoring; RSD, relative standard deviation; NED, *N*-(1-naphthyl)-ethylenediamine; Griess reagents, sulfanilamide and NED; EDTA, ethylene diaminotetraacetic acid; DTPA, diethylene triamino pentaacetic acid; SBC, serine/borate complex; r.t., room temperature; HILIC, hydrophilic interaction liquid chromatography; RPLC, reverse phase liquid chromatography; ECNICI, electron-capture negative-ion chemical ionization; ESI, electrospray ionization; FAB, fast atom bombardment; HePI-MS, ambient pressure helium-plasma ionization mass spectrometry; m/z, mass charge ratio; LOD, limit of detection; LOQ, limit of quantification; LLOQ, lower limit of quantification; S/N, signal-over-noise ratio; S/B, signal-over-blank ratio; CID, collision induced dissociation; IS, internal standard; FTIR, Fourier Transform InfraRed spectroscopy; FTIRM, FTIR Microscopy

* Correspondence to: Université de Lorraine, CITHEFOR EA 3452, Faculté de Pharmacie, 5, rue Albert Lebrun, F-54001 Nancy, France.
E-mail address: pierre.leroy@univ-lorraine.fr (P. Leroy).

https://doi.org/10.1016/j.talanta.2018.09.011
Received 27 March 2018; Received in revised form 30 August 2018; Accepted 4 September 2018
Available online 05 September 2018
0039-9140/

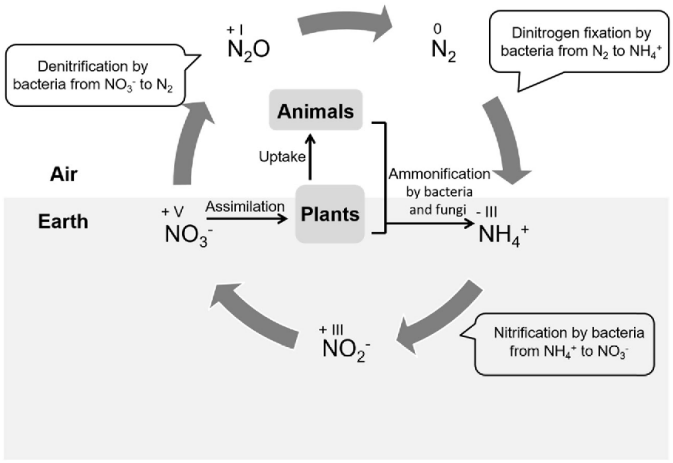

Fig. 1. Nitrogen cycle with pathways including dinitrogen fixation, ammonification, nitrification and denitrification (numbers upon each compound correspond to nitrogen oxidation state).

naturally occurring, *i.e.* ^{14}N and ^{15}N. ^{15}N is often used in scientific studies for labeling species, due to its very low natural abundance (0.37%) [1,2]. The majority of nitrogen comes from the atmosphere, and is converted to ammonium by microorganisms and eventually to nitrate ions. For these purposes, including dinitrogen fixation, ammonification and (de)nitrification, nitrogen plays important roles, resulting in nitrogen compounds with nine different oxidation states varying from –III (ammonium) to +V (nitrate) (Fig. 1).

Since the discovery of *"nitric oxide as a signaling molecule in the cardiovascular system"* [3–5] by Murad, Furchgott and Ignarro, awarded the Nobel Prize in 1998, the growing interest in this molecule have evolved it from the status of a mere noxious air pollutant to the one of a powerful signaling radical in the body. Nitric oxide (NO) is a highly reactive free radical with a very short half–life in the range of milliseconds to seconds [5]. In the body, NO reactivity manifests itself through three main reactions:

(i) **nitrosylation**, a reversible binding of NO to the metallic center (mainly ferrous) of metalloproteins, promoting their activation. For example, the soluble enzyme guanylate cyclase is activated by fixing NO, therefore cyclic guanosine monophosphate production is increased, leading to relaxation of blood vessels [6];
(ii) ***S*-nitrosation,** corresponding to the covalent binding of NO to the thiol group of cysteine residues of proteins and peptides, producing thionitrites, also called ***S*-nitrosothiols** (RSNOs). Furthermore, ***S*-transnitrosation** consists of the transfer of the NO moiety between a RSNO and a protein or peptide with a free cysteine thiol residue. These reversible processes change protein activity and function [7];
(iii) reaction with superoxide anion producing the very toxic **peroxynitrite anion**; eventually, this later can react with tyrosine residues of proteins through **nitration**, to form 3-nitrotyrosine, an indicator of cell oxidative damages and inflammation [8,9].

Thus, NO is considered as a very unique second messenger [10], and NO involved pathways are responsible for many physiological and pathophysiological processes, comprising inhibition of platelet aggregation, vasodilation, glucose metabolism and transport stimulation or immune system modulation [11].

Nitric oxide is generated from L-arginine in many types of cells and tissues. This process needs catalysis *via* a dihydronicotinamide adenine dinucleotide phosphate-dependent enzyme, which exists as three isoforms, *i.e.* endothelial and neuronal NO synthases (eNOS; nNOS) and inducible NO synthase (iNOS) [12]. Apart from the inhaled gas (nitrogen oxides), foods and drinks containing nitrite (NO_2^-) and nitrate (NO_3^-) ions are also a source of NO [13]. Inside the human body, NO is converted into more stable species, *i.e.* NO_2^-, NO_3^-, iron-nitrosyl complexes and *N*-, *O*-, *S*-nitroso compounds [14]. Meanwhile, these more stable NO species, except nitrates, are re-converted to NO by various chemical and enzymatic pathways. Thus, NO circulates in the human body by blood, is distributed into tissues, and finally is excreted in urine mainly as nitrite and nitrate (Fig. 2).

Nitric oxide production decreases with ageing and under various pathophysiological situations, especially in case of cardiovascular diseases (CVDs) (due to endothelial dysfunction and a following decrease of eNOS activity). Therefore, administration of NO donors [15] is essential to restore the NO pool for the treatment of CVDs related to endothelial dysfunction. Current marketed NO donors are sodium nitroprusside and organic nitrates. These drugs generate a tolerance phenomenon and oxidative stress when used as chronic treatments [16]. Thus, other classes without these side effects, like diazeniumdiolates and RSNOs, are under preclinical and clinical investigation (Fig. 3) [17].

Interestingly, NO demonstrates protective properties at low concentrations (pico to nanomolar range), while it becomes cytotoxic at higher levels (micromolar range) [18]. There is a great need for the development of appropriate analytical methods to study the bioavailability and biodistribution of NO-related compounds, from NO donors to their metabolites, and to apply for a wide range of concentrations [6,19,20]. Numerous analytical methods are available for the measurement of both environmental and biological levels of NO species, including colorimetric assay [21], methods based on derivatization associated with fluorescence (FL) [22], chemiluminescence (CL) [23], and electrochemistry [24]. Methods based on separative techniques such as gas chromatography (GC), ion-exchange chromatography (IEC), high performance liquid chromatography (HPLC) and capillary electrophoresis (CE) have also been reported. Liquid chromatographic methods are coupled with UV–visible spectrophotometry, FL, CL and mass spectrometry (MS) for detecting NO species either directly or after derivatization [25,26]. The choice of the method depends on the concentration range of the analytes to be measured in the studied matrices. For example, the colorimetric assay and separative methods with direct detection are commonly used for NO_3^- measurement in human blood, as

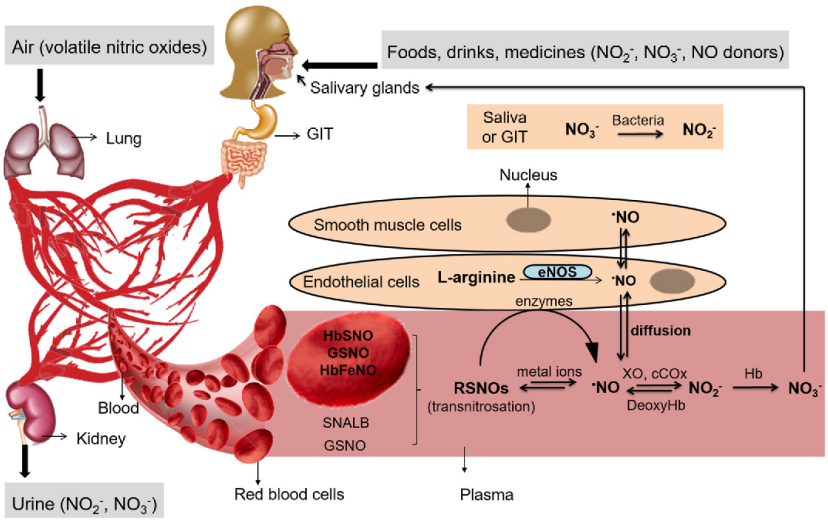

Fig. 2. The formation and circulation of NO species in the human body.

expected concentrations are of 10 μM or more [27]; FL detection associated with derivatization or CL is required for RSNOs measurement, because their concentration is under the micromolar [28], even in the nanomolar range in the case of *S*-nitrosoglutathione (GSNO) [29,30].

To specifically monitor NO species released from administered drugs, regardless of those coming from endogenous synthesis and/or diet intake, using MS after the labeling of the drug with ^{15}N appears the method of choice.

The present review will focus on the different methods of ^{15}N labeling of related nitrogen species associated with MS. It will mainly discuss: *(i)* associated interconversion and metabolism studies; *(ii)* methods devoted to the ^{15}N labeled NO species measurement with or without derivatization; *(iii)* specific operating conditions for the pre-analytical steps.

2. Stable nitrogen isotope (^{15}N) labeled nitrogen species and associated metabolic studies

All the ^{15}N labeling approaches used in environment, biochemistry and biomedicine fields are summarized in Table 1.

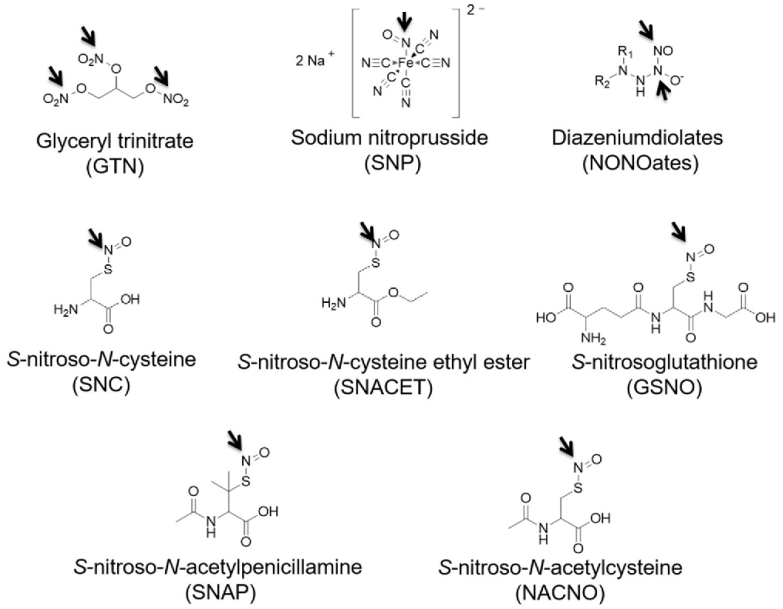

Fig. 3. Chemical structures of nitric oxide donors. Labeled nitrogen atom is indicated by arrows. For NONOates, R_1 and R_2 are alkyl groups, such as ethyl.

Table 1
Nitrogen 15 labeled compounds and their metabolic pathways or (bio)chemical conversion giving rise to related species.

Labeled species	Metabolites	Analytes	Matrix	Applications	References
$^{15}NH_4^+$	^{15}N labeled nitrogen species ($^{15}NH_4^+$, $^{15}NO_2^-$, $^{15}NO_3^-$, ...)	Sum of ^{15}N labeled species (by isotope ratio mass spectrometry)	Soil, plant, water and microbial biomass	As a tracer to study nitrogen cycling in ecosystems	[38–40]
^{15}N-glutamate, ^{15}N-alanine or amido-^{15}N-glutamine	^{15}N labeled amino acids	^{15}N labeled alanine, glycine, proline, serine, asparte and glutamate	Tissue culture medium	To study their metabolism in rat lens	[42]
L-[$^{15}N_2$]-arginine	$^{15}NO_2^-$, $^{15}NO_3^-$ and ^{15}N-citrulline	$^{15}NO_2^-$, $^{15}NO_3^-$	Plasma, human vascular endothelial cell culture medium and cell lysate	To measure nitric oxide synthase activity	[45,46]
$^{15}NO_2^-$, $^{15}NO_3^-$	^{15}N labeled nitrogen species	Sum of ^{15}N labeled species	Rat urine, feces and rat carcass	To study their fate after oral administration in rat	[52]
$^{15}NO_2^-$	^{15}N labeled NO species ($^{15}NO_2^-$, HbFe^{15}NO...)	HbFe^{15}NO	Rat blood	To investigate whether the NO_2^--derived NO can shift to the circulation from gastric cavity and act like nitric oxide synthase (NOS)-derived NO does in tissues	[53]
$^{15}NO_3^-$	^{15}N labeled nitrogen species	Sum of ^{15}N labeled species	Plants and soil	As a tracer to study nitrogen cycling process	[55,56]
^{15}N-GTN	^{15}N-GDN and ^{15}N labeled NO species	$^{15}NO_2^-$, $^{15}NO_3^-$	Cell culture medium	To study its bio-activation in a cell culture model of nitrate tolerance	[62]
^{15}N labeled diazeniumdiolates	^{15}N labeled NO species	$Et_2N[^{15}N(O)NO]Et_2NH_2$, $Et_2N[^{15}N(O)^{15}NO]Et_2Na$	–	To study their chemistry and aid in reaping their full potential in the area of rational drug design	[31]
$S^{15}NC$	^{15}N labeled NO species, cysteine	$GS^{15}NO$	Human erythrocyte lysate	To study its metabolism in human erythrocytes	[32]
$S^{15}NACET$	^{15}N labeled NO species, cysteine ethyl ester	$^{15}NO_2^-$, $^{15}NO_3^-$	Human urine	To study its inhibition potency on human dimethylarginine dimethylaminohydrolase activity after oral administration	[33]
$S^{15}NALB$	^{15}N labeled NO species, albumin	$S^{15}NALB$	Human blood	To study its metabolism in human blood	[34]
$GS^{15}NO$	^{15}N labeled NO species, reduced glutathione	$S^{15}NALB$	Rat plasma	To study *S*-transnitrosation	[65]
$S^{15}NAP$	^{15}N labeled NO species, *N*-acetylpenicillamine	$S^{15}NAP$, $^{14,15}N_2O$, $^{15,15}N_2O$, $^{14,15}N_2$, $^{15,15}N_2$	River sediment	To study nitric oxide turnover in permeable river sediment	[35]
$^{15}NO_2^-$, $^{15}NO_3^-$, $S^{15}NALB$, $GS^{15}NO$, $NAC^{15}NO$	–	$^{15}NO_2^-$, $^{15}NO_3^-$, $S^{15}NALB$, $GS^{15}NO$, $NAC^{15}NO$	Plasma or urine	As internal standards to study their metabolism in plasma or diagnose urinary tract infections	[30,34,65,68]

Sources of ^{15}N labeled species used in these different studies vary. The isotope ^{15}N is produced through explosive nucleosynthesis following a neutron bombardment of ^{18}F and alpha decay [36]. ^{15}N labeled ammonium, nitrite and nitrate salts, L-arginine, and glyceryl trinitrate are commercially available. The other ^{15}N labeled NO donors are easily obtained using conventional organic synthesis reactions. Namely, ^{15}NO reacts with diethylamine or diethylammonium salts to produce ^{15}N labeled diazeniumdiolates [31]. ^{15}N labeled RSNOs are obtained by reacting $^{15}NO_2^-$ in acidic medium with the corresponding thiols: ^{15}N labeled *S*-nitrosocysteine ($S^{15}NC$) [32], *S*-nitroso-*N*-acetylcysteine ethyl ester ($S^{15}NACET$) [33], *S*-nitrosoalbumin ($S^{15}NALB$) [34], *S*-nitrosoglutathione ($GS^{15}NO$) [32] and *S*-nitroso-*N*-acetylpenicillamine [35]. ^{15}NO is produced by reducing $Na^{15}NO_2$ with KI in presence of 67 mM H_2SO_4 [37].

2.1. ^{15}N labeled amino compounds

15N labeled ammonium ($^{15}NH_4^+$) has been used to understand the main process of soil/plant nitrogen cycle, by calculating the rates of total mineralization and nitrification and the plant nitrogen uptake, occurring as NH_4^+ and NO_3^- [38]. $^{15}NH_4^+$ has also been used as a tracer to study nitrogen cycling in a forest stream, after being added in early spring and measured in dominant biomass compartments of upstream and at several locations downstream [39]. Besides, $^{15}NH_4^+$ has also been added at the soil surface to describe the plant–microbial competition for nitrogen, through the evaluation of the $^{15}N/^{14}N$ ratio in plant and microbial biomass with an isotope ratio MS method [40].

^{15}N labeled amino acids are used to elucidate their metabolism [41]. For that purpose, rat lenses were incubated in a physiological medium containing ^{15}N-glutamate, ^{15}N-alanine or amido-^{15}N-glutamine, followed by the quantification of the amino acids by GC-MS [42]. To study effects of global warming and intensified forestry on nitrogen deposition, ^{15}N labeled glycine uptake by healthy plants and soil microbes has been investigated under elevated temperature, high CO_2 partial pressure and drought [43]. In addition, parameters of the whole-body protein metabolism are monitored in premature infants, using ^{15}N labeled yeast protein and its hydrolysate for kinetic studies to estimate protein turnover rates [44].

^{15}N labeled L-arginine is particularly interesting to study NOS activity. Indeed, the quantification of its produced metabolites, *i.e.* $^{15}NO_2^-$ and $^{15}NO_3^-$ indicate how the human body responds in health and disease. After intravenous (*i.v.*) injection of *L*-[$^{15}N_2$]-arginine in rat, $^{15}NO_2^-$ and $^{15}NO_3^-$ are measured in plasma, allowing the evaluation of the impact of various factors on NOS activity. As the main result, asymmetric dimethylarginine (ADMA) is the most potent enzyme inhibitor [45]. $^{15}NO_2^-$ content in human vascular endothelial cells has also been measured to elucidate L-arginine action [46]. Meanwhile, impaired conversion of $^{15}NO_3^-$ from *L*-[$^{15}N_2$]-arginine and increased ADMA are observed in hypercholesterolemic rabbits, proving that the mechanism most likely involves inhibition of NO synthase by ADMA [47]. Besides, ^{15}N labeled L-arginine has been used as a precursor to check whether isolated mitochondria from rat liver metabolize L-arginine into agmatine by arginine decarboxylase (ADC) catalysis. It was concluded that mitochondrial ADC is present in rat liver, and that cyclic adenosine monophosphate (cAMP) may stimulate the increase of produced agmatine through this pathway [48]. In addition, $^{15}NO_3^-$ is observed after *i.v.* administration of ^{15}N labeled L-arginine in children suffering from malaria and presenting the NOS2G-954C promoter polymorphism. This result confirms the idea that NOS2 genotype protects against severe malaria by increasing NO production during episodes of uncomplicated malaria compared to those without the polymorphism [49].

2.2. ^{15}N labeled nitrite, nitrate and peroxynitrite ions

Nitrous oxide (N_2O) plays an important role in global warming and stratospheric ozone depletion. Understanding the N_2O production pathways and their contribution to total greenhouse emissions is the key to effective mitigation of these processes. Using ^{15}N labeled N_2O, isotope ratio determinations in samples from atmosphere, ocean, fresh water and soils are useful parameters to understand the origin of this compound, the production-consumption mechanisms and their overall importance [50,51].

The use of ^{15}N labeled nitrite ions ($^{15}NO_2^-$) coupled to a specific quantification by MS directly highlights its outcome after an oral administration in rats. As a result, it has been shown that NO_2^- is excreted either unchanged or as its oxidized metabolite ($^{15}NO_3^-$) rather rapidly [52]. Furthermore, after oral administration of $^{15}NO_2^-$ in rats chronically treated with a NOS inhibitor, the ^{15}N labeled iron nitrosylhemoglobin (HbFeNO) has been quantified by electron paramagnetic resonance (EPR) spectroscopy, and the blood pressure has been measured. It has been concluded that the intake of NO_2^- (or NO_3^-)-rich foods such as vegetables and fruits, may alter the systemic HbFeNO dynamic, and decrease blood pressure, resulting in the improvement of CVDs [53]. NO_2^- plays a crucial role in physiology and therapeutics as it consists in both an inert metabolite of NO and an important alternative source of NO for the classical L-arginine-NO-synthase pathway [19]. Recently, rat aortic rings have been incubated with $^{15}NO_2^-$, with or without adding of NO_3^-. This latter ion does not affect the accumulation of $^{15}NO_2^-$ in aorta ring. This result suggests that the attenuation of the vascular responses to NO_2^- by NO_3^- is relevant to unknown mechanisms, instead of a competitive permeation process [54].

^{15}N labeled nitrate ion ($^{15}NO_3^-$) has also been used after oral administration in rats to show that it is excreted rapidly as $^{15}NO_2^-$ [52]. Besides, $^{15}NO_3^-$ has another important role as nitrogen source in the ecosystem. Thus, $^{15}NO_3^-$ is widely used to study the nitrogen cycle processes. For example, the addition of a nutrient solution containing$^{15}NO_3^-$ at the soil surface has been used to study the competition for its uptake by invasive and native strawberries. This competition has been evaluated by the plant biomass production, nitrogen content and assimilation according to the isotope ratio values [55]. Furthermore, to investigate the long-term fate of fertilizer-derived nitrogen in the plant-soil-water system, $^{15}NO_3^-$ was added to the soil fertilizers in 1982. Over three decades, only 8–12% of the $^{15}NO_3$-derived nitrogen have leaked towards the groundwater. As a prediction, it would take at least five decades for part of the remaining fertilizer nitrogen still residing in the soil to leak towards the groundwater [56]. In addition, $^{15}NO_3^-$ was added to the tropical forest floor to explore its influence on the C sequestration. It has been concluded that the anthropogenic N input in moderate levels may result in C sequestration enhancement and no significant long-term N loss to the environment exists [57]. $^{15}NO_3^-$ has also been used to identify possible errors in ^{15}N balance studies, which is due to the contamination through the foliar exchange of ^{15}N labeled atmospheric ammonia. As a result, the selection of appropriate controls for accurate ^{15}N determination should be taken into consideration [58]. At last, $^{15}NO_3^-$ together with glucose has been added to soil to evaluate the response of microbial communities. Both ^{14}N- and ^{15}N-containing target compounds (muramic acid and glucosamine) were quantified by GC-MS. It was concluded that the fungal cell wall residues helped the soil organic matter maintenance, while the bacterial cell wall components served as “capacitor” and provided N [59].

The use of ^{15}N labeled peroxynitrite ion ($O^{15}NOO^-$) as internal standard (IS) has been proposed for $ONOO^-$ quantification [60]. $^{13}C_6$-3-nitrotyrosine, $^{13}C_9$-3-nitrotyrosine have served as IS for monitoring nitration of tyrosine residues in proteins [61]. Thus, using $O^{15}NOO^-$ and measuring the resulting ^{15}N labeled 3-nitrotyrosine might be an alternative approach to evaluate oxidative damages.

2.3. ^{15}N labeled NO donors

The labeling of NO donors with ^{15}N is quite useful to study their bioavailability and metabolism.

2.3.1. ^{15}N labeled organic nitrates

^{15}N labeled glyceryl trinitrate (^{15}N-GTN) has been synthesized to investigate nitrate tolerance on human vascular endothelial cells. Cells were pretreated with GTN (20 μM) or without for 5 h, followed by a 1-h incubation with ^{15}N-GTN. ^{15}N-GTN-derived metabolites ($^{15}NO_2^-$ and $^{15}NO_3^-$) were measured. A smaller amount of $^{15}NO_2^-$ was produced in GTN-pretreated cells than in untreated ones. These findings suggest that the nitrate tolerance develops at the level of GTN bioactivation. It indicates that the enzymes that are responsible for GTN metabolism may be inactivated or deteriorated by continuous GTN treatment [62]. Meanwhile, ^{15}N-GTN has been used to study natural attenuation of propellant residues in anti-tank firing position, by quantifying produced $^{15}NO_3^-$ [63].

At that time, there is no report about labeling ^{15}N to study bioavailability of other marketed NO donors such as isosorbide mononitrate, isosorbide dinitrate and sodium nitroprusside. It might be interesting to investigate their metabolism in humans.

2.3.2. ^{15}N labeled diazeniumdiolates and S-nitrosothiols

^{15}N labeled diazeniumdiolates have only been used to characterize their chemistry and help in acquiring their full potential in the area of rational drug design [31]. ^{15}N labeled RSNOs have been synthesized to study their bioavailability.

^{15}N labeled *S*-nitrosocysteine ($S^{15}NC$) can operate *S*-transnitrosation with the thiol group of cysteine residues of proteins [64]. The study of $S^{15}NC$ metabolism in human erythrocytes has shown that one of the final products is the ^{15}N labeled *S*-nitrosoglutathione ($GS^{15}NO$) [32]. Furthermore, to study *S*-transnitrosation, $S^{15}NC$ given *i.v.* to rats is rapidly metabolized in blood, presumably by ^{15}NO release and *S*-transnitrosation of extra- and intra-cellular thiol groups. However, *S*-transnitrosation of albumin cysteine-34 occurs only marginally, suggesting that this reaction by endogenous SNC is not of physiological importance *in vivo*. In another word, *S*-transnitrosation of the only reduced cysteine moiety of albumin by endogenous SNC in blood does not represent an effective mechanism for the production of *S*-nitrosoalbumin (SNALB) [65].

^{15}N labeled *S*-nitroso-*N*-acetylcysteine ethyl ester ($S^{15}NACET$) has been prepared to verify its inhibiting potential on dimethylarginine dimethylaminohydrolase activity after oral administration in humans. The presence of quantifiable $S^{15}NACET$ catabolites, *i.e.* $^{15}NO_2^-$ and $^{15}NO_3^-$, in urine, ascertains its absorption [33].

The metabolism of ^{15}N labeled *S*-nitrosoalbumin ($S^{15}NALB$) has been studied in human blood *in vitro* [34]; $S^{15}NALB$ half-life calculated was found to be equal to 5.5 h.

S-nitrosoglutathione, one of the most abundant low-molecular-mass RSNOs in cells, has been labeled with ^{15}N to study *S*-transnitrosation. It appeared that it is rapidly metabolized in rat blood, and, just like $S^{15}NC$, it is not used for the formation of SNALB [65].

^{15}N labeled *S*-nitroso-*N*-acetylpenicillamine has been synthesized to describe the NO turnover in permeable river sediment. It confirms that N_2O is the major product obtained by denitrification, and N_2O reduction to N_2 is inhibited by NO excess [35].

^{15}N labeled *S*-nitroso-*N*-acetyl-*L*-cysteine ($NAC^{15}NO$) has only been used as IS to check whether NACNO is a circulating or an excreted NO metabolite in humans. As NACNO is undetectable in plasma and urine, it is concluded that it is not involved in the metabolic pathway [66].

3. Methods used for ^{15}N labeled NO species measurement

As mentioned above, ^{15}N labeled NO species are frequently used as IS to improve precision of unlabeled NO species measurement. For example, $S^{15}NALB$ is used as IS to measure SNALB in human plasma [67]. $^{15}NO_2^-$ and $^{15}NO_3^-$ are used as IS for unlabeled NO_2^- and NO_3^- quantification, thus a precise value of NO_2^-/NO_3^- ratio permits the diagnosis of urinary tract infections [68].

Mass spectrometry offers the advantages of high specificity and sensitivity when combined with separative methods for analyzing NO species in complex biological matrices. Among those methods, IEC is the most convenient mode for free NO_2^- and NO_3^- separation. But the applied fully aqueous mobile phases are not prone to MS ionization. In reversed phase partition mode, the retention of analytes on the non-polar stationary phase is obtained with a low organic solvent content in the mobile phase, leading to non-ideal conditions in MS. Thus, ion pairing chromatography by adding cationic surfactant (ion pairing agent), the derivatization of these ions leading to non-polar adducts and using hydrophilic interaction liquid chromatography (HILIC, characterized as normal-phase) appear to be the most convenient solutions. In this way, the adducts resulting from NO_2^- derivatization are eluted with a high organic solvent content, which is compatible with MS. Compared to HPLC, ultra performance liquid chromatography (UPLC) mode greatly reduces analysis time due to a shorter diffusion path between analytes and the stationary phase [69]. A UPLC-MS/MS based method was preferred to analyze GSNO in human plasma [30]. Usually, multiple processes are combined to improve the selectivity. For example, when analyzing NO_3^- in vegetables, sulfamic acid was added to remove NO_2^-, and $Et_3O^+[BF_4^-]$ was used to derivatize NO_3^- to the volatile Et-ONO_2, followed by GC-MS [70]. As reported by Chao et al., a solid phase extraction of the adduct result from NO_2^- derivatization coupled with LC-MS analysis was performed to quantify NO_2^- in urine (Table 3) [68].

We presently focus on the methods devoted to ^{15}N labeled NO species, mainly including $^{15}NO_2^-$, $^{15}NO_3^-$, and $RS^{15}NOs$, and relying upon a chromatographic technique coupled with MS or tandem mass spectrometry (MS/MS). Such an approach generally allows distinguishing a very low amplitude variation linked to an environmental, physiological or pathological event by easily highlighting this variation from the natural background.

The methods will be classified into two types: *(i)* direct quantification; *(ii)* quantification after derivatization of ^{15}N labeled NO species with different probes (Table 2). In most cases, direct methods are applied to simple matrices or for high analyte concentrations, while methods with derivatization offer higher selectivity, especially for the analysis of NO_2^-, NO_3^-, and RSNOs at low concentrations in complex matrices.

Usually, limits of detection (LOD) and quantification (LOQ) are determined according to the analyte signal-over-noise (S/N) ratio. In the case of NO derivatization, the samples as well as the standards and reagent solutions are often contaminated by atmospheric nitrogen oxides and by nitrate-reducing bacteria, leading to a signal corresponding to the adduct produced by these contaminants during the derivatization process [62,71]. This fact considerably increases blank values, consequently LOD and LOQ based on signal-over-blank (S/B) ratio, and it is not easy to limit this pollution by preventing air contact and inhibiting microbial growth. Freshly prepared solutions are the usual way to reduce the level of these interferences [72]. It will be indicated in this review how LOD and LOQ values of different methods are calculated (according to S/N or S/B) if mentioned by authors.

Noteworthy, the abundance of ^{15}N labeled NH_4^+, NO_2^- and NO_3^- needs to be quantified to understand nitrogen cycle in ecosystems. Usually, N-compounds are converted to gaseous N-species, followed by MS analysis. These indirect methods include the change of nitrogen redox state as follows: *(i)* reduction of NO_3^- to NH_3 by Devarda's alloy, reaching a LOQ of 5 μM after taking blank into consideration [73]; *(ii)* reduction of NO_3^- to N_2O by bacterial enzymes, with a LOQ of 1 μM based on S/B = 10 [74]; and *(iii)* oxidation of NH_4^+ to N_2 by NaOBr, reduction of NO_2^- to NO by KI, and NO_3^- to NO by VCl_3, with the LOD values of 140.0, 0.4 and 4.0 μM, respectively [75].

3.1. Direct quantification

^{15}N labeled nitrate ion ($^{15}NO_3^-$) has been directly analyzed by ambient pressure helium-plasma ionization mass spectrometry (HePI-MS).

Table 2
Probes used for derivatization of NO related species labeled with ^{15}N and corresponding chromatographic methods coupled with MS.

Probes	Analytes	Reaction conditions	Adducts	Purification before analysis	Analytical methods (detected fragments or transitions)	LOD or LOQ (nM)	Interference between unlabeled and labeled adducts due to isotopes (^{13}C, ^{15}N, ^{18}O…)	References
PFBBr	$^{15}NO_2^-$	60 min at 50 °C	PFB-$^{15}NO_2$	Toluene extraction	GC- ECNICI-MS (*m/z* 47 for $^{15}NO_2^-$)	LOD = 0.2 (S/N = 3)	No	[83]
	$^{15}NO_3^-$	60 min at 50 °C	PFB-$^{15}NO_3$		*m/z* 63 for $^{15}NO_3^-$;	LOD = 4.8 (S/N = 3)		[84]
	RS^{15}NOs	60 min at 50 °C after converting RS^{15}NOs to $^{15}NO_2^-$	PFB-$^{15}NO_2$		*m/z* 212 for [PFB-^{15}NO-H]$^-$)	LOD = 0.2 (S/N = 3)		[85]
	O^{15}NOO$^-$	2 min at r.t.	PFB-^{15}NO			Not indicated		[60]
FMOCCl	RS^{15}NOs	10 min at r.t.	FMOC-GS^{15}NO	RPLC purification	RPLC-FAB-MS (*m/z* 558 for [FMOC-GS^{15}NO-H]$^-$)	Not indicated	–	[88]
$Et_3O^+[BF_4^-]$	$^{15}NO_3^-$	30 min at r.t.	Et-O$^{15}NO_2$	No	GC-CI-MS (*m/z* 47 for $^{15}NO_2^-$)	LOD = 200 (S/N = 3)	–	[89]
DAN	$^{15}NO_2^-$	10–60 min at r.t.	^{15}N-NAT	No (except for $^{15}NO_2^-$ in cell lysate, protein precipitation after derivatization)	RPLC-EI-MS/MS	LLOQ = 4 (Cell lysate, S/B = 5) LLOQ = 1–4 (Incubation medium, S/B = 5)	No	[46,62]
	$^{15}NO_3^-$	10 min at r.t. after enzymatic reduction			(*m/z* 171 → 115)	LLOQ = 1 (Both water and cell culture medium, S/B = 5)		[62]
GSH	$^{15}NO_2^-$	5 min on ice	GS^{15}NO	No	HILIC-ESI-MS/MS	LOQ = 5 (human plasma ultrafiltrate)	11% (Theoretical value)	[90]
					(*m/z* 338 → 307)	LOQ = 0.5 (water) (LOQ: lower analytes concentration for calibration curve)		
Griess reagents	$^{15}NO_2^-$, $^{15}NO_3^-$	8 min at r.t	^{15}N labeled azo adduct	No	RPLC-EI-MS/MS (*m/z* 371 → 328)	LOQ = 1 (S/N = 10) LOQ = 100 (S/B = 5)	Around 20%	[92]

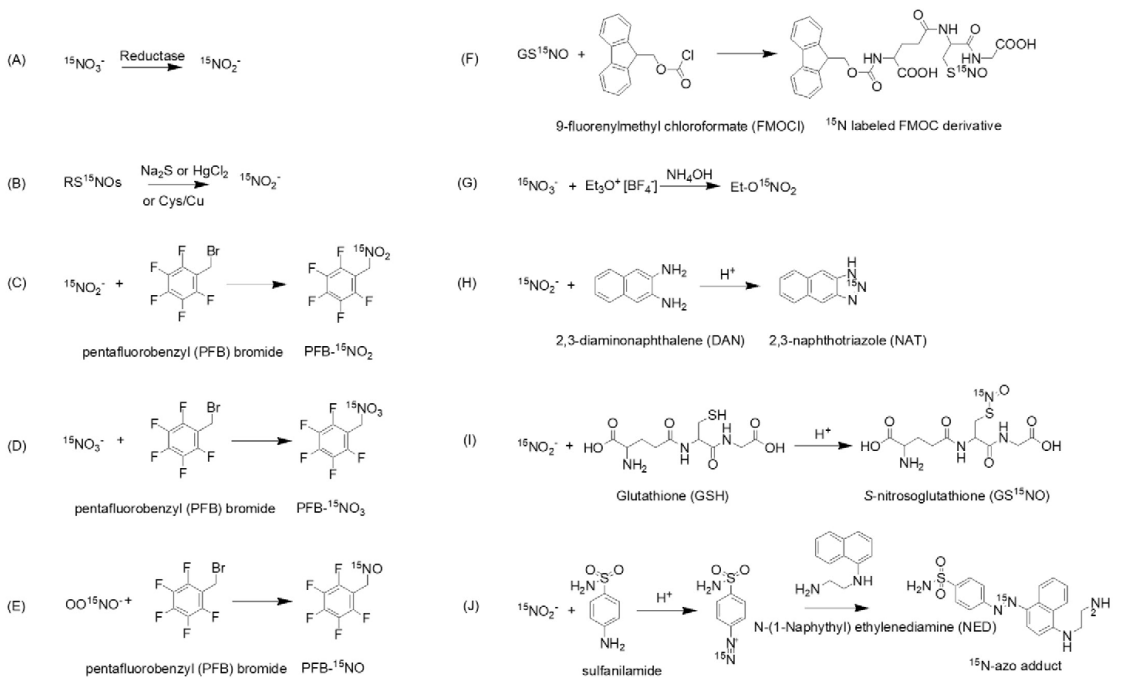

Fig. 4. Probes used for derivatization of NO related species labeled with ^{15}N: reaction of (A) $^{15}NO_3^-$ reduction to $^{15}NO_2^-$ (enzyme cofactors: FAD, NADPH), and (B) converting $RS^{15}NOs$ to $^{15}NO_2^-$; (C) $^{15}NO_2^-$, (D) $^{15}NO_3^-$ and (E) $O^{15}NOO^-$ derivatization by PFBBr; (F) $GS^{15}NO$ derivatization by FMOCCl; (G) $^{15}NO_3^-$ derivatization by $Et_3O^+[BF_4^-]$; $^{15}NO_2^-$ derivatization by (H) DAN, (I) GSH; and (J) Griess reagent.

Negative ionization and the selective-ion monitoring (SIM) of *m/z* 62 and 63 for $^{14}NO_3^-$ and $^{15}NO_3^-$ analysis were performed, with a LOD value of 0.1 nM for $^{15}NO_3^-$ [76].

The charged species NO_2^- and NO_3^- are non-volatile, thus they are adapted to GC-MS only after a derivatization step. However, Tsikas *et al.* report the analysis of $^{14}NO_2^-$ and $^{15}NO_2^-$ in urine directly by GC-MS [77]. This method is based on the acidification of NO_2^- in solution to form nitrous acid (HNO_2) followed by an organic solvent extraction (ethyl acetate) and finally its analysis by GC-MS. HNO_2 is stable in ethyl acetate for at least 24 h at room temperature (r.t.). Acetyl NO_2^- is produced inside the injector of the GC system at 300 °C, and the ions $^{14}NO_2^-$ and $^{15}NO_2^-$ (*m/z* 46 and 47, respectively) are formed under negative-ion chemical ionization (NICI). Their quantification is performed by selected-ion monitoring (SIM). $^{15}NO_2^-$ is used as IS and the LOQ of the method defined as the lowest concentration of the calibration curve in urine is 2 μM. It has to be noted that this method is not applicable for measuring NO_2^- in human plasma or serum, because HNO_2 reacts rapidly with endogenous constituents, such as thiols. As $^{15}NO_3^-$ is reduced to $^{15}NO_2^-$ by cadmium under acidic conditions [78,79], it would be also possible to quantify NO_3^- directly by GC-MS.

NO_2^- and NO_3^- can also be separated by reversed phase liquid chromatography (RPLC) using a Phenomenex Gemini C18 column, and detected by negative electrospray ionization MS. The data acquisition was obtained using a SIM mode, with *m/z* 46 and 47 for $^{14}NO_2^-$ and $^{15}NO_2^-$ analysis while *m/z* 62 and 63 for $^{14}NO_3^-$ and $^{15}NO_3^-$ analysis. Both $^{15}NO_2^-$ and $^{15}NO_3^-$ are used as IS, and water samples with different quality levels are analyzed [80]. Lab water refers to ultra-pure water (resistivity ≥ 18.25 MΩ cm) and other samples were contaminated by sulfate, chloride, carbonate, phosphate and nitrate salts. As a result, the LOD value of NO_3^- in contaminated lab water samples, based on acceptable recoveries (86–106%) is 10 times higher than the value found in ultra-pure water (0.01 μM).

^{15}N labeled RSNOs can also be directly quantified by GC-MS. $S^{15}NACET$ is extracted with ethylacetate, and quantified by GC-MS using electron-capture NICI (ECNICI) and SIM of *m/z* 47 for $^{15}NO_2^-$. Using either $S^{15}NACET$ as IS for SNACET measurement or SNACET as IS for d^3-$S^{15}NACET$ analysis, the LOQ value based on the lowest concentration of the calibration curve in plasma is 500 nM. The other $RS^{15}NOs$ are analyzed after conversion into $S^{15}NACET$ *via* *S*-transnitrosation [81].

In addition, $GS^{15}NO$ has been analyzed by LC-MS without *S*-transnitrosation. It has been measured by MS directly when monitoring the parent ion of *m/z* 338 under collision-activated dissociation (CAD) mode. A C18 column was used for GSNO purification before dilution with formic acid-containing acetonitrile and off-line ESI-MS analysis. No information related to the method validation is given [82]. A more recent method coupling HILIC and ESI-MS/MS has been reported [30]. Selected-reaction monitoring (SRM) of the specific mass transitions *m/z* 337 → 307 and *m/z* 338 → 307 for GSNO and $GS^{15}NO$, respectively, has been carried out. Using $GS^{15}NO$ as IS for GSNO quantification, the authors obtained a LOQ (defined as a S/N value equal to 10) of 2.8 nM in human plasma. Using HILIC rather than RPLC for $GS^{15}NO$ analysis improves the sensitivity. Because $GS^{15}NO$ is a polar analyte, a high content of acetonitrile in mobile phase is required for its elution favoring the ionization rate in ESI.

3.2. Derivatization of ^{15}N labeled NO species

Analytes of low molecular mass (≤ 50 u) are in most cases derivatized to allow their measurement in biological matrices. The reason is that it is difficult to reach such a low *m/z* value for many commercially available MS and the background noise is usually high for low mass

Table 3
Literature overview of 2,3-naphthotriazole adduct analysis resulting from derivatization of NO species with 2,3-diaminonaphthalene by using RPLC-MS/MS.

Analytes	Columns	Mobile phase components and elution mode	Ion source and mass analyzer (fragmentation modes and transitions)	IS	LOD or LOQ (nM)	Additional informations	Reference
NO_2^- and NO_3^-	C18, 5 μm, 33 × 2.1 mm	Mixture of methanol (from 49% to 75%) and ammonium acetate buffer	ESI; triple quadrupole (CID; m/z: 170 → 115)	$^{15}NO_2^-$	LOQ = 8 / 75 (NO_2^- / NO_3^-; S/N = 10)	2.2% interference between unlabeled and labeled adducts due to isotopes	[68]
$^{15}NO_2^-$ and $^{15}NO_3^-$	C18, 5 μm, 150 × 2.1 mm	Mixture of methanol (from 5% to 95%) and ammonium carbonate buffer	ESI; hybrid of triple quadrupole and linear ion trap (CID; m/z: 171 → 115)	No	LLOQ = 1 ($^{15}NO_2^-$ and $^{15}NO_3^-$; S/B = 5)	NO_2^- concentrations in ultrapure water and cell culture medium are 91 nM and 400 nM, respectively; NO_2^- in water is more than 100 nM	[62]
$^{15}NO_2^-$	C18, 5 μm, 50 × 2 mm	Mixture of acetonitrile (from 5% to 95%) and formic acid	ESI; triple quadrupole (CID; m/z: 171 → 115)	1H-naphth[2,3-d] imidazole	LLOQ = 40 (NO_2^-; S/B = 5) LLOQ = 4 ($^{15}NO_2^-$, S/B = 5)	–	[46]

values. The derivatization procedure also facilitates analysis either by GC (NO_2^- is transformed into a volatile derivative) or RPLC (NO_2^- is transformed into a more hydrophobic derivative increasing its retention on this kind of stationary phases).

^{15}N labeled NO species are analyzed by either GC-MS or LC-MS after derivatization, with use of the following probes: pentafluorobenzyl bromide (PFBBr), 9-fluorenylmethyl chloroformate (FMOCCl), triethyloxonium tetrafluoroborate ($Et_3O^+[BF_4^-]$), 2,3-diaminonaphthalene (DAN), reduced glutathione (GSH) and Griess reagents. All the reactions between these probes and the concerned analytes have a stoichiometric coefficient ratio equal to 1 (Fig. 4). Resulting adducts (PFB-derivatives, FMOC-derivative, 2,3-naphthotriazole (NAT) and azo adducts) are commonly detected according to their intrinsic spectroscopic properties by CL, FL and UV–vis, with LOQ ranging from nanomolar to micromolar concentrations. Their use in MS has been recently reported.

3.2.1. *Pentafluorobenzyl bromide (PFBBr)*

Pentafluorobenzyl bromide (PFBBr) reacts with $^{15}NO_2^-$ in aqueous acetone at 50 °C for 60 min to yield PFB-$^{15}NO_2$ (Fig. 4C). After cooling to r.t. and removing solvent under nitrogen protection, PFB-$^{15}NO_2$ is purified by toluene extraction, and analyzed by GC-MS, with ECNICI and SIM of *m/z* 47. As a result, a LOD value of 0.2 nM for $^{15}NO_2^-$ based on S/N of 3 is obtained [83]. PFBBr also reacts with $^{15}NO_3^-$ to produce PFB-$^{15}NO_3$ (Fig. 4D). After toluene extraction and GC-MS analysis with ECNICI and SIM of *m/z* 63, a LOD value of 4.8 nM for $^{15}NO_3^-$ is achieved [84]. Besides, PFBBr has been used to quantify RS^{15}NOs after they were converted into $^{15}NO_2^-$ by reacting with either aqueous Na_2S (S^{2-}) [85] or $HgCl_2$ [67] or a mixture of cysteine and $CuSO_4$ (Cys/Cu) (Fig. 4A) [86]. Among those reagents, $HgCl_2$ provides the highest conversion rate of RS^{15}Nos to $^{15}NO_2^-$ (> 90%), followed by Cys/Cu, whereas the Na_2S procedure seems to be less efficient [85]. For analyzing a mixture of different RSNOs, each RSNO is separated and identified by RPLC coupled with a UV–vis detector, followed by derivatization with PFBBr and quantification with GC-MS [32]. This GC-MS method simultaneously analyzes $^{15}NO_2^-$ and $^{15}NO_3^-$; $O^{15}NOO^-$ is also analyzed by formation of PFB-^{15}NO adduct (Fig. 4E), according to a similar process as described above for $^{15}NO_2^-$ and $^{15}NO_3^-$ analysis. In this case, the derivatization period lasts 2 min at r.t. and the fragment *m/z* 212 is monitored for its quantification [60]. No interference between unlabeled and labeled ^{15}N PFB derivatives is noted. PFB derivatives are thermally stable (up to 100 °C) for 30 min [87].

3.2.2. *9-fluorenylmethyl chloroformate (FMOCCl)*

9-fluorenylmethyl chloroformate (FMOCCl) reacts with GS^{15}NO in 1 M borate buffer at r.t. for 1 min to form FMOC-GS^{15}NO (Fig. 4F). After purification by RPLC, the FMOC derivative is analyzed by RPLC-MS with SIM of *m/z* 558 after Fast Atom Bombardment (FAB) ionization. Based on the lowest concentration of the calibration curve, LOQ value is *ca.* 100 nM in a 5% trifluoroacetic acid solution [88]. The derivative is stable for at least 2 months.

3.2.3. *Triethyloxonium tetrafluoroborate ($Et_3O^+[BF_4^-]$)*

Triethyloxonium tetrafluoroborate ($Et_3O^+[BF_4^-]$) reacts with NO_3^- in NH_4OH aqueous solution and in the dark at r.t. for at least 30 min to form Et-ONO_2 (Fig. 4G). The ethyl ester is analyzed by headspace GC-NICI-MS with SIM of *m/z* 46 and 47 for $^{14}NO_3^-$ and $^{15}NO_3^-$ analysis, respectively. In this method, $^{15}NO_3^-$ is used as IS for NO_3^- analysis. Based on S/N ratio of 3, a LOD value of 200 nM is obtained in seawater samples. When $Et_3O^+[BF_4^-]$ reacts with NO_2^-, ethyl nitrite is produced. After analysis by GC-NICI-MS, the resulting fragments do not show any nitrogen-containing ion, thus ^{15}N labeling appears not suitable for nitrite analysis by this method [89].

3.2.4. *2,3-diaminonaphthalene (DAN)*

2,3-diaminonaphthalene (DAN) reacts with $^{15}NO_2^-$ at r.t. for 10–60 min to produce ^{15}N labeled 2,3-naphthotriazole (^{15}N-NAT)

adduct (Fig. 4H). Without further purification, ^{15}N-NAT adduct is separated from DAN excess by RPLC using a gradient elution mode with mobile phases composed of methanol and a carbonate buffer or acetonitrile and a formic acid solution. MS detection is operated with either a triple quadrupole or a Q-trap instrument (operated as a triple quadrupole). ESI and multiple-reaction monitoring (MRM) of *m/z* 171 → 115 under collision induced dissociation mode are performed. The resulting lowest LOQ (LLOQ) value either in a cell (human vascular endothelial cell) lysate or in the incubation medium is 1–4 nM, based on a S/B value of 5, with relative standard deviation (RSD) less than 20% and an accuracy of 80–120%. According to the literature [46,62,68], description of the interference between ^{14}N-NAT and ^{15}N-NAT due to the natural presence of isotope ^{13}C in NAT is not consistent, as shown in Table 3. Theoretically, ^{13}C interferes at a *ca.* 2% level, and this might limit method sensitivity. In addition, DAN has also been used to quantify $^{15}NO_3^-$ after enzymatic reduction to $^{15}NO_2^-$ (Fig. 4A), with a LLOQ value in both water and cell culture medium of 1 nM [62].

It has been established that the NAT adduct is stable at r.t. for 24 h in alkaline medium [62], after storage at − 80 °C for 3 months, and after 2 freezing/thaw cycles.

3.2.5. Reduced glutathione (GSH)

Reduced glutathione (GSH) reacts with $^{15}NO_2^-$ on ice for 5 min to yield GS^{15}NO (Fig. 4I). With no further purification step, GS^{15}NO is injected into a HILIC column and detected by MS, with ESI and SRM of *m/z* 338 → 307. Finally, LOQ values for $^{15}NO_2^-$ are 0.5 and 5 nM in water and in human plasma ultra-filtrate, respectively, with a RSD value of 23% [90]. The theoretical contribution of GSNO to GS^{15}NO is about 11%, and the blank value depending on the matrices is not negligible. A major drawback of this probe is that the resulting GSNO adduct is very sensitive to light, temperature, dioxygen tension and pH [6] and appears less stable than adducts obtained with other probes. To date, no report uses GSH derivatization for $^{15}NO_3^-$ measurement after a reduction step.

3.2.6. Griess assay

The widely used Griess colorimetric assay is based on the derivatization of NO_2^- in two steps: sulfanilamide reacts with NO_2^- at r.t. for 3 min to yield a diazonium salt, followed by coupling with *N*-(1-naphthyl)ethylenediamine (NED) at r.t. for 5 min to form the corresponding azo adduct (Fig. 4J). More recently, the quantification of the azo adduct by RPLC coupled with visible detection has been reported leading to a LLOQ value of 67 nM in distilled water [91]. To the best of our knowledge, the analysis of the ^{15}N labeled azo adduct by LC-MS/MS has never been described. We have operated this labeling followed by MS/MS analysis, with ESI and MRM of the transition *m/z* 371 → 328. The LOQ value is about 100 nM based on a S/B ratio of 5, which means that this method is less sensitive than the one using DAN reaction [92]. As Griess method is capable to quantify NO_3^- after its reduction to NO_2^- by enzymes or metals, as well as RSNOs after conversion to NO_2^- by $HgCl_2$ (Fig. 4A) [93], this LC-MS/MS method should have a potential application for $^{15}NO_3^-$ and RS^{15}NOs analysis. The azo adduct is known to be stable under freezing at − 80 °C for at least one month and at r.t. for 1 h.

Obviously, the method using PFBBr for $^{15}NO_2^-$ and $^{15}NO_3^-$ derivatization affords lower LOQ values than other probes ($Et_3O^+[BF_4^-]$, DAN, GSH). But this method needs a liquid/liquid extraction of adducts and a GC-MS system equipped with a specific chemical ionization source. Employing GSH to derivatize $^{15}NO_2^-$ results in GSNO formation, which is very labile and sensitive to many factors such as temperature, light, metal ions and enzymes [6]. Finally, the storage of more and less stable derivatives until their analysis is a real challenge. Besides, the parameters used in LC-MS/MS are specific to quantify GSNO instead of different RSNOs. Using DAN as a probe for $^{15}NO_2^-$ derivatization produces NAT, which is more stable than GSNO. Griess assay uses cheap reagents, simple and fast derivatization process, but its LOQ is limited by a high blank value close to 100 nM [92].

As already mentioned at the beginning of third chapter concerning methods used for ^{15}N labeled NO species measurement, both direct and indirect methods (with or without derivatization) applied to quantify ^{15}N labeled NO species have their own advantages and limitations. Even though a direct GC-MS method has been reported to measure $^{14}NO_2^-$ and $^{15}NO_2^-$ in complex biological fluids [77], the "real ionized compounds" were acetyl $^{14}NO_2^-$ and acetyl $^{15}NO_2^-$, respectively. That is to say, the reported direct method still experienced a NO_2^- derivatization step. In addition, indirect methods contribute to using the same parameters in MS for different NO species quantification. For example, after NO_3^- reduction, the measurement procedure is the same as for NO_2^- [62].). In the future, improving indirect methods such as simplifying the derivatization process is a promising strategy to analyze NO species in biological media.

In short, using MS to analyze ^{15}N labeled NO species has a lower blank value than the one obtained with the unlabeled NO species, due to the low ^{15}N natural abundance. This results in improved LOQ of the method. However, interference between unlabeled and labeled adducts needs to be taken into consideration. Additionally, the contamination of reagent solutions by unlabeled NO species should be minimized by using high quality water and freshly prepared solutions for all operations.

4. Biological sample collection, storage and treatment

For both clinical and biological samples, the preanalytical steps are critical and necessary. Related operating conditions are usually the same for ^{15}N labeled NO species than for the unlabeled ones.

Nitroso/nitrosyl products are unstable [94], and NO_2^- is rapidly metabolized to different extents in various biological compartments by thiols and redox-active metals [95]. Thus a number of additives are commonly added to the samples to limit these processes. Ethylene diaminotetraacetic (EDTA) or diethylene triamino pentaacetic acid (DTPA) are added in order to chelate metallic ions [29]; serine/borate complex (SBC) added for inactivation of γ–glutamyltransferase limits specific degradation of GSNO; *N*-ethylmaleimide (NEM) blocks the thiol group for preventing transnitrosation reactions and thus limiting RSNOs and NO_2^- degradation [96]. Sample collection, storage and pretreatment are performed in reduced ambient light conditions and at low temperature (0–4 °C) before performing analysis [27]. Proteins which interfere with chromatographic steps are simply removed by ultrafiltration or precipitation with acetonitrile [25]. The operating conditions for dealing with ^{15}N labeled species are summarized below.

4.1. Blood and plasma

When collecting rat or human blood for the measurement of ^{15}N labeled NO species, plastic syringe or tube has to be used with additives such as EDTA and SBC [34,53,97]. Blood sampling is followed by immediate centrifugation to separate plasma from erythrocytes, because oxyhemoglobin can induce NO_2^- oxidation [30,65]. Usually, samples are maintained at 0–4 °C at the time of sampling and stored at − 80 °C until analysis [30,66].

4.2. Urine

Urine samples for ^{15}N labeled NO species measurement are maintained at 0–4 °C at the time of sampling and stored at − 20 °C before analysis. The two probes PFBBr and DAN have been used for derivatization, followed by purification with either liquid/ liquid extraction with toluene [33] or solid phase extraction [68].

4.3. Cultured cells and incubation medium

Cells containing ^{15}N labeled NO species are harvested with trypsin and lyzed with tensioactive agents; DAN has been used for

derivatization directly in the incubation medium and in the crude cell extracts, followed by protein precipitation and quantification with RPLC-MS/MS [46]. Cell culture medium samples containing derivatized ^{15}N labeled NO species are stored at − 80 °C until analysis [62].

4.4. Tissues

For ^{15}N labeled NO species measurement in tissues, liquid nitrogen [53] or freezer (− 20 °C) [52] is commonly used for samples storage. Kidney containing $HbFe^{15}NO$ is homogenized in a EPR quartz tubing by puncturing, followed by storage in liquid nitrogen before analysis [53]. Aorta rings containing $^{15}NO_2^-$ are powdered in liquid nitrogen, solubilized in water before derivatization with DAN. The produced ^{15}N-NAT is extracted with acetonitrile before LC-MS/MS analysis [54].

In summary, sample pretreatment is a necessary step to make reliable quantification of ^{15}N labeled NO species. Among this process, the stabilization of the analytes and their purification are the two main critical parts.

5. Conclusion-perspective

Concentrations of NO species range from nanomolar to millimolar values in environmental and biological matrices, and using MS to analyze ^{15}N labeled NO species improves sensitivity by decreasing blank values in all studied matrices. The present review demonstrates that ^{15}N labeling is a powerful tracer methodology for a better understanding of nitrogen cycle process and metabolism of nitrogen oxides. Further analytical developments can be foreseeing such as coupling CE with MS. CE offers the advantage of small sample volumes, and stacking process to concentrate analytes. It has already been used coupled with UV detection for nitrite and nitrate analysis in plasma [98]; GSNO degradation has been monitored by CE-MS [99], but to the best of our knowledge, no report concerns CE-MS applied to ^{15}N labeled NO species. Furthermore, both EPR spectroscopy [53] and Synchrotron Radiation FTIR Microscopy (FTIRM) [100] are capable of distinguishing and analyzing ^{15}N labeled and unlabeled species. Thus, it may be of interest to apply these methods for PK studies of both existing NO donors and newly developed ones.

Acknowledgements

Authors are grateful to the program of China Scholarship Council for the financial support of Ms. Haiyan YU's Ph.D. thesis (Grant no. 201506270166). Co-authors are grateful to Professor Alain Le Faou (EA CITHEFOR 3452, Université de Lorraine) for correcting the English style of the present manuscript.

References

[1] J. Emsley, Enriching the Earth: fritz Haber, Carl Bosch, and the transformation of world food, Nature 410 (2001) 633–634, https://doi.org/10.1038/35070632.
[2] J. Emsley, Chemistry of the Elements, 1st Edition - Greenwood,nn, Earnshaw,a, New Sci. 103 41–42, 1984.
[3] J. Braughler, C. Mittal, F. Murad, Effects of thiols, sugars, and proteins on nitric-oxide activation of guanylate-cyclase, J. Biol. Chem. 254 (1979) 2450–2454.
[4] L. Ignarro, H. Lippton, J. Edwards, W. Baricos, A. Hyman, P. Kadowitz, C. Gruetter, Mechanism of vascular smooth-muscle relaxation by organic nitrates, nitrites, nitroprusside and nitric-oxide - evidence for the involvement, J. Pharmacol. Exp. Ther. 218 (1981) 739–749.
[5] M. Akyuez, S. Ata, Determination of low level nitrite and nitrate in biological, food and environmental samples by gas chromatography-mass spectrometry and liquid chromatography with fluorescence detection, Talanta 79 (2009) 900–904, https://doi.org/10.1016/j.talanta.2009.05.016.
[6] C. Gaucher, A. Boudier, F. Dahboul, M. Parent, P. Leroy, S-nitrosation/denitrosation in cardiovascular pathologies: facts and concepts for the rational design of S-nitrosothiols, Curr. Pharm. Des. 19 (2013) 458–472.
[7] B.C. Smith, M.A. Marletta, Mechanisms of S-nitrosothiol formation and selectivity in nitric oxide signaling, Curr. Opin. Chem. Biol. 16 (2012) 498–506, https://doi.org/10.1016/j.cbpa.2012.10.016.
[8] J.S. Beckman, W.H. Koppenol, Nitric oxide, superoxide, and peroxynitrite: the good, the bad, and the ugly, Am. J. Physiol. -Cell Physiol. 271 (1996) C1424–C1437.
[9] S. Hekimi, J. Lapointe, Y. Wen, Taking a "good" look at free radicals in the aging process, Trends Cell Biol. 21 (2011) 569–576, https://doi.org/10.1016/j.tcb.2011.06.008.
[10] J.C. Toledo, O. Augusto, Connecting the chemical and biological properties of nitric oxide, Chem. Res. Toxicol. 25 (2012) 975–989, https://doi.org/10.1021/tx300042g.
[11] A.B. Levine, D. Punihaole, T.B. Levine, Characterization of the role of nitric oxide and its clinical applications, Cardiology 122 (2012) 55–68, https://doi.org/10.1159/000338150.
[12] P.J. Andrew, B. Mayer, Enzymatic function of nitric oxide synthases, Cardiovasc. Res. 43 (1999) 521–531, https://doi.org/10.1016/S0008-6363(99)00115-7.
[13] Y. Tang, H. Jiang, N.S. Bryan, Nitrite and nitrate: cardiovascular risk-benefit and metabolic effect, Curr. Opin. Lipidol. 22 (2011) 11–15, https://doi.org/10.1097/MOL.0b013e3283419 42c.
[14] Y. Minamiyama, S. Takemura, M. Inoue, Effect of thiol status on nitric oxide metabolism in the circulation, Arch. Biochem. Biophys. 341 (1997) 186–192, https://doi.org/10.1006/abbi.1997.9956.
[15] A.W. Carpenter, M.H. Schoenfisch, Nitric oxide release: part II. Therapeutic applications, Chem. Soc. Rev. 41 (2012) 3742–3752, https://doi.org/10.1039/c2cs15273h.
[16] J.C.B. Ferreira, D. Mochly-Rosen, Nitroglycerin use in myocardial infarction patients - risks and benefits, Circ. J. 76 (2012) 15–21, https://doi.org/10.1253/circj.CJ-11-1133.
[17] J. Lehmann, Nitric oxide donors - current trends in therapeutic applications, Expert Opin. Ther. Pat. 10 (2000) 559–574, https://doi.org/10.1517/13543776.10.5.559.
[18] S. Mocellin, V. Bronte, D. Nitti, Nitric oxide, a double edged sword in cancer biology: searching for therapeutic opportunities, Med. Res. Rev. 27 (2007) 317–352, https://doi.org/10.1002/med.20092.
[19] J.O. Lundberg, E. Weitzberg, M.T. Gladwin, The nitrate-nitrite-nitric oxide pathway in physiology and therapeutics, Nat. Rev. Drug Discov. 7 (2008) 156–167, https://doi.org/10.1038/nrd2466.
[20] K.A. Broniowska, A.R. Diers, N. Hogg, S-Nitrosoglutathione, Biochim. Biophys. Acta BBA - Gen. Subj. 1830 (2013) 3173–3181, https://doi.org/10.1016/j.bbagen.2013.02.004.
[21] R. Schaus, Griess nitrite test in diagnosis of urinary infection, Jama-J. Am. Med. Assoc. 161 (1956) 528–529, https://doi.org/10.1001/jama.1956.62970060009009d.
[22] Y. Mukai, H. Hara, H. Taniguchi, Fluorometric determinations of nitrite and amyl nitrite with 2,3-diaminonaphthalene, Bunseki Kagaku 40 (1991) 105–107.
[23] P.H. MacArthur, S. Shiva, M.T. Gladwin, Measurement of circulating nitrite and S-nitrosothiols by reductive chemiluminescence, J. Chromatogr. B-Anal. Technol. Biomed. Life Sci. 851 (2007) 93–105, https://doi.org/10.1016/j.jchromb.2006.12.012.
[24] C. Walters, P. Gillatt, R. Palmer, P. Smith, A rapid method for the determination of nitrate and nitrite by chemiluminescence, Food Addit. Contam. 4 (1987) 133–140.
[25] A. Wu, T. Duan, D. Tang, Z. Zheng, J. Zhu, R. Wang, B. He, H. Cheng, L. Feng, Q. Zhu, Review the application of chromatography in the analysis of nitric oxide-derived nitrite and nitrate ions in biological fluids, Curr. Anal. Chem. 10 (2014) 609–621.
[26] S.M. Helmke, M.W. Duncan, Measurement of the NO metabolites, nitrite and nitrate, in human biological fluids by GC-MS, J. Chromatogr. B-Anal. Technol. Biomed. Life Sci. 851 (2007) 83–92, https://doi.org/10.1016/j.jchromb.2006.09.047.
[27] W.S. Jobgen, S.C. Jobgen, H. Li, C.J. Meininger, G. Wu, Analysis of nitrite and nitrate in biological samples using high-performance liquid chromatography, J. Chromatogr. B. 851 (2007) 71–82, https://doi.org/10.1016/j.jchromb.2006.07.018.
[28] D. Giustarini, A. Milzani, I. Dalle-Donne, R. Rossi, Detection of S-nitrosothiols in biological fluids: a comparison among the most widely applied methodologies, J. Chromatogr. B Anal. Technol. Biomed. Life Sci. 851 (2007) 124–139, https://doi.org/10.1016/j.jchromb.2006.09.031.
[29] E. Bramanti, V. Angeli, Z. Mester, A. Pompella, A. Paolicchi, A. D'Ulivo, Determination of S-nitrosoglutathione in plasma: comparison of two methods, Talanta 81 (2010) 1295–1299, https://doi.org/10.1016/j.talanta.2010.02.024.
[30] D. Tsikas, M. Schmidt, A. Böhmer, A.A. Zoerner, F.-M. Gutzki, J. Jordan, UPLC–MS/MS measurement of S-nitrosoglutathione (GSNO) in human plasma solves the S-nitrosothiol concentration enigma, J. Chromatogr. B 927 (2013) 147–157, https://doi.org/10.1016/j.jchromb.2013.01.023.
[31] L.K. Keefer, J.L. Flippen-Anderson, C. George, A.P. Shanklin, T.A. Dunams, D. Christodoulou, J.E. Saavedra, E.S. Sagan, D.S. Bohle, Chemistry of the diazeniumdiolates − 1. Structural and spectral characteristics of the [N(O)NO](-) functional group, Nitric Oxide-Biol. Chem. 5 (2001) 377–394, https://doi.org/10.1006/niox.2001.0359.
[32] D. Tsikas, J. Sandmann, S. Rossa, F.-M. Gutzki, J.C. Frölich, Gas chromatographic–mass spectrometric detection of S-Nitroso-cysteine and S-Nitroso-glutathione, Anal. Biochem. 272 (1999) 117–122, https://doi.org/10.1006/abio.1999.4177.
[33] K. Chobanyan, T. Thum, M.-T. Suchy, B. Zhu, A. Mitschke, F.-M. Gutzki, B. Beckmann, D.O. Stichtenoth, D. Tsikas, GC-MS assay for hepatic DDAH activity in diabetic and non-diabetic rats by measuring dimethylamine (DMA) formed from asymmetric dimethylarginine (ADMA): evaluation of the importance of S-nitrosothiols as inhibitors of DDAH activity in vitro and in vivo in humans, J. Chromatogr. B-Anal. Technol. Biomed. Life Sci. 858 (2007) 32–41, https://doi.org/10.1016/j.jchromb.2007.08.002.
[34] D. Tsikas, J. Sandmann, S. Rossa, F.M. Gutzki, J.C. Frolich, Measurement of S-nitrosoalbumin by gas chromatography mass spectrometry - I. Preparation,

purification, isolation, characterization and metabolism of S-[N-15]nitrosoalbumin in human blood in vitro, J. Chromatogr. B 726 (1999) 1–12, https://doi.org/10.1016/S0378-4347(99)00011-0.
[35] F. Schreiber, P. Stief, M.M.M. Kuypers, D. de Beer, Nitric oxide turnover in permeable river sediment, Limnol. Oceanogr. 59 (2014) 1310–1320, https://doi.org/10.4319/lo.2014.59.4.1310.
[36] M. Bojazi, B.S. Meyer, Explosive nucleosynthesis of N 15 in a massive-star model, Phys. Rev. C. 89 (2014), https://doi.org/10.1103/PhysRevC.89.025807.
[37] E. Aerssens, J. Tiedje, B. Averill, Isotope labeling studies on the mechanism of N-N Bond formation in denitrification, J. Biol. Chem. 261 (1986) 9652–9656.
[38] D. Barraclough, The use of mean pool abundances to interpret N-15 tracer experiments. 1. Theory, Plant Soil. 131 (1991) 89–96, https://doi.org/10.1007/BF00010423.
[39] P.J. Mulholland, J.L. Tank, D.M. Sanzone, W.M. Wollheim, B.J. Peterson, J.R. Webster, J.L. Meyer, Nitrogen cycling in a forest stream determined by a N-15 tracer addition, Ecol. Monogr. 70 (2000) 471–493, https://doi.org/10.1890/0012-9615(2000)070[0471:NCIAFS]2.0.CO;2.
[40] Y. Kuzyakov, X. Xu, Competition between roots and microorganisms for nitrogen: mechanisms and ecological relevance, New Phytol. 198 (2013) 656–669, https://doi.org/10.1111/nph.12235.
[41] N. Ohkouchi, Y. Chikaraishi, H.G. Close, B. Fry, T. Larsen, D.J. Madigan, M.D. McCarthy, K.W. McMahon, T. Nagata, Y.I. Naito, N.O. Ogawa, B.N. Popp, S. Steffan, Y. Takano, I. Tayasu, A.S.J. Wyatt, Y.T. Yamaguchi, Y. Yokoyama, Advances in the application of amino acid nitrogen isotopic analysis in ecological and biogeochemical studies, Org. Geochem. 113 (2017) 150–174, https://doi.org/10.1016/j.orggeochem.2017.07.009.
[42] H. Jernigan, Metabolism of N-15-labeled amino-acids in rat lens, Exp. Eye Res. 37 (1983) 77–84, https://doi.org/10.1016/0014-4835(83)90151-3.
[43] L.C. Andresen, A. Michelsen, S. Jonasson, C. Beier, P. Ambus, Glycine uptake in heath plants and soil microbes responds to elevated temperature, CO_2 and drought, Acta Oecologica-Int. J. Ecol. 35 (2009) 786–796, https://doi.org/10.1016/j.actao.2009.08.010.
[44] K.D. Wutzke, Development and application of N-15-tracer substances for measuring the whole-body protein turnover rates in the human, especially in neonates: a review, Isot. Environ. Health Stud. 48 (2012) 239–258, https://doi.org/10.1080/10256016.2012.662971.
[45] D. Tsikas, J. Sandmann, A. Savva, P. Luessen, R.H. Boger, F.M. Gutzki, B. Mayer, J.C. Frolich, Assessment of nitric oxide synthase activity in vitro and in vivo by gas chromatography-mass spectrometry, J. Chromatogr. B. 742 (2000) 143–153, https://doi.org/10.1016/S0378-4347(00)00142-0.
[46] S. Shin, H.-L. Fung, Evaluation of an LC–MS/MS assay for 15N-nitrite for cellular studies of L-arginine action, J. Pharm. Biomed. Anal. 56 (2011) 1127–1131, https://doi.org/10.1016/j.jpba.2011.08.017.
[47] R.H. Boger, D. Tsikas, S.M. Bode-Boger, L. Phivthong-ngam, E. Schwedhelm, J.C. Frolich, Hypercholesterolemia impairs basal nitric oxide synthase turnover rate: a study investigating the conversion of L-[guanidino-15N(2)]-arginine to N-15-labeled nitrate by gas chromatography-mass spectrometry, Nitric Oxide-Biol. Chem. 11 (2004) 1–8, https://doi.org/10.1016/j.niox.2004.07.008.
[48] O. Horyn, B. Luhovyy, A. Lazarow, Y. Daikhin, I. Nissim, M. Yudkoff, I. Nissim, Biosynthesis of agmatine in isolated mitochondria and perfused rat liver: studies with 15N-labelled arginine, Biochem. J. 388 (2005) 419–425, https://doi.org/10.1042/BJ20041260.
[49] T. Planche, D.C. Macallan, T. Sobande, S. Borrmann, J.F.J. Kun, S. Krishna, P.G. Kremsner, Nitric oxide generation in children with malaria and the NOS2G-954C promoter polymorphism, Am. J. Physiol. -Regul. Integr. Comp. Physiol. 299 (2010) R1248–R1253, https://doi.org/10.1152/ajpregu.00390.2010.
[50] S. Toyoda, N. Yoshida, K. Koba, Isotopocule analysis of biologically produced nitrous oxide in various environments, Mass Spectrom. Rev. 36 (2017) 135–160, https://doi.org/10.1002/mas.21459.
[51] H. Duan, L. Ye, D. Erler, B.-J. Ni, Z. Yuan, Quantifying nitrous oxide production pathways in wastewater treatment systems using isotope technology - a critical review, Water Res. 122 (2017) 96–113, https://doi.org/10.1016/j.watres.2017.05.054.
[52] C. Wang, R. Cassens, W. Hoekstra, Fate of Ingested 15n-Labeled Nitrate and Nitrite in the Rat, J. Food Sci. 46 (1981) 745–748, https://doi.org/10.1111/j.1365-2621.1981.tb15340.x.
[53] K. Tsuchiya, Y. Takiguchi, M. Okamoto, Y. Izawa, Y. Kanematsu, M. Yoshizumi, T. Tamaki, Malfunction of vascular control in lifestyle-related diseases: formation of systemic hemoglobin-nitric oxide complex (HbNO) from dietary nitrite, J. Pharmacol. Sci. 96 (2004) 395–400, https://doi.org/10.1254/jphs.FMJ04006X3.
[54] C. Damacena-Angelis, G.H. Oliveira-Paula, L.C. Pinheiro, E.J. Crevelin, R.L. Portella, L.A.B. Moraes, J.E. Tanus-Santos, Nitrate decreases xanthine oxidoreductase-mediated nitrite reductase activity and attenuates vascular and blood pressure responses to nitrite, Redox Biol. 12 (2017) 291–299, https://doi.org/10.1016/j.redox.2017.03.003.
[55] J. Littschwager, M. Lauerer, E. Blagodatskaya, Y. Kuzyakov, Nitrogen uptake and utilisation as a competition factor between invasive Duchesnea indica and native Fragaria vesca, Plant Soil. 331 (2010) 105–114, https://doi.org/10.1007/s11104-009-0236-2.
[56] M. Sebilo, B. Mayer, B. Nicolardot, G. Pinay, A. Mariotti, Long-term fate of nitrate fertilizer in agricultural soils, Proc. Natl. Acad. Sci. USA 110 (2013) 18185–18189, https://doi.org/10.1073/pnas.1305372110.
[57] A. Wang, W. Zhu, P. Gundersen, O.L. Phillips, D. Chen, Y. Fang, Fates of atmospheric deposited nitrogen in an Asian tropical primary forest, For. Ecol. Manag. 411 (2018) 213–222, https://doi.org/10.1016/j.foreco.2018.01.029.
[58] H. Janzen, C. Gilbertson, Exchange of N-15 among plants in controlled environment studies, Can. J. Soil Sci. 74 (1994) 109–110, https://doi.org/10.4141/cjss94-014.
[59] H.B. He, X.B. Li, W. Zhang, X.D. Zhang, Differentiating the dynamics of native and newly immobilized amino sugars in soil frequently amended with inorganic nitrogen and glucose, Eur. J. Soil Sci., vol. 62, n.d., pp. 144–151. doi:⟨http://dx.doi.org/10.1111/j.1365-2389.2010.01324.x⟩.
[60] D. Tsikas, GC-MS and HPLC methods for peroxynitrite (ONOO- and (ONOO-)-N-15) analysis: a study on stability, decomposition to nitrite and nitrate, laboratory synthesis, and formation of peroxynitrite from S-nitrosoglutathione (GSNO) and KO2, Analyst 136 (2011) 979–987, https://doi.org/10.1039/c0an00625d.
[61] D. Tsikas, M.W. Duncan, Mass spectrometry and 3-nitrotyrosine: strategies, controversies, and our current perspective, Mass Spectrom. Rev. 33 (2014) 237–276, https://doi.org/10.1002/mas.21396.
[62] E.R. Axton, E.A. Hardardt, J.F. Stevens, Stable isotope-assisted LC–MS/MS monitoring of glyceryl trinitrate bioactivation in a cell culture model of nitrate tolerance, J. Chromatogr. B 1019 (2016) 156–163, https://doi.org/10.1016/j.jchromb.2015.12.010.
[63] G. Bordeleau, M.M. Savard, R. Martel, A. Smirnoff, G. Ampleman, S. Thiboutot, Stable isotopes of nitrate reflect natural attenuation of propellant residues on military training ranges, Environ. Sci. Technol. 47 (2013) 8265–8272, https://doi.org/10.1021/es4004526.
[64] K. Okada, B.-T. Zhu, S-nitrosylation of the IGF-1 receptor disrupts the cell proliferative action of IGF-1, Biochem. Biophys. Res. Commun. 491 (2017) 870–875, https://doi.org/10.1016/j.bbrc.2017.06.177.
[65] A. Warnecke, P. Luessen, J. Sandmann, M. Ikic, S. Rossa, F.-M. Gutzki, D.O. Stichtenoth, D. Tsikas, Application of a stable-isotope dilution technique to study the pharmacokinetics of human N-15-labelled S-nitrosoalbumin in the rat: possible mechanistic and biological implications, J. Chromatogr. B-Anal. Technol. Biomed. Life Sci. 877 (2009) 1375–1387, https://doi.org/10.1016/j.jchromb.2008.11.035.
[66] D. Tsikas, S. Rossa, D.O. Stichtenoth, M. Raida, F.-M. Gutzki, J.C. Frölich, Is S-Nitroso-N-acetyl-L-cysteine a circulating or an excretory metabolite of nitric oxide (NO) in man? Assessment by gas chromatography–mass spectrometry, Biochem. Biophys. Res. Commun. 220 (1996) 939–944, https://doi.org/10.1006/bbrc.1996.0510.
[67] D. Tsikas, J. Sandmann, F.-M. Gutzki, D.O. Stichtenoth, J.C. Frölich, Measurement of S-nitrosoalbumin by gas chromatography–mass spectrometry: ii. Quantitative determination of S-nitrosoalbumin in human plasma using S-[15N]nitrosoalbumin as internal standard, J. Chromatogr. B Biomed. Sci. Appl. 726 (1999) 13–24, https://doi.org/10.1016/S0378-4347(99)00058-4.
[68] M.-R. Chao, Y.-M. Shih, Y.-W. Hsu, H.-H. Liu, Y.-J. Chang, B.-H. Lin, C.-W. Hu, Urinary nitrite/nitrate ratio measured by isotope-dilution LC–MS/MS as a tool to screen for urinary tract infections, Free Radic. Biol. Med. 93 (2016) 77–83, https://doi.org/10.1016/j.freeradbiomed.2016.01.025.
[69] M.E. Swartz, UPLC (TM): an introduction and review, J. Liq. Chromatogr. Relat. Technol. 28 (2005) 1253–1263, https://doi.org/10.1081/JLC-200053046.
[70] B. Campanella, M. Onor, E. Pagliano, Rapid determination of nitrate in vegetables by gas chromatography mass spectrometry, Anal. Chim. Acta 980 (2017) 33–40, https://doi.org/10.1016/j.aca.2017.04.053.
[71] D. Chen, P. Chalk, External-source contamination during extraction distillation in isotope-ratio analysis of soil inorganic nitrogen, Anal. Chim. Acta 245 (1991) 49–55, https://doi.org/10.1016/S0003-2670(00)80200-7.
[72] H. Kabuto, M. Yamamoto, I. Yokoi, N. Ogawa, The source of nitrate and nitrite contamination that interferes with their accurate estimation in blood, Clin. Chim. Acta 266 (1997) 199–200.
[73] D.M. Sigman, M.A. Altabet, R. Michener, D.C. McCorkle, B. Fry, R.M. Holmes, Natural abundance-level measurement of the nitrogen isotopic composition of oceanic nitrate: an adaptation of the ammonia diffusion method, Mar. Chem. 57 (1997) 227–242, https://doi.org/10.1016/S0304-4203(97)00009-1.
[74] D.M. Sigman, K.L. Casciotti, M. Andreani, C. Barford, M. Galanter, J.K. Bohlke, A bacterial method for the nitrogen isotopic analysis of nitrate in seawater and freshwater, Anal. Chem. 73 (2001) 4145–4153, https://doi.org/10.1021/ac010088e.
[75] C.F. Stange, O. Spott, B. Apelt, R.W.B. Russow, Automated and rapid online determination of 15N abundance and concentration of ammonium, nitrite, or nitrate in aqueous samples by the SPINMAS technique, Isot. Environ. Health Stud. 43 (2007) 227–236, https://doi.org/10.1080/10256010701550658.
[76] J. Pavlov, A.B. Attygalle, Direct detection of inorganic nitrate salts by ambient pressure helium-plasma ionization mass spectrometry, Anal. Chem. 85 (2013) 278–282, https://doi.org/10.1021/ac3026916.
[77] D. Tsikas, A. Boehmer, A. Mitschke, Gas chromatography-mass spectrometry analysis of nitrite in biological fluids without derivatization, Anal. Chem. 82 (2010) 5384–5390, https://doi.org/10.1021/ac1008354.
[78] D. Tsikas, R. Boger, S. Bodeboger, F. Gutzki, J. Frolich, Quantification of nitrite and nitrate in human urine and plasma as pentafluorobenzyl derivatives by gas-chromatography mass-spectrometry using their N-15-labeled analogs, J. Chromatogr. B-Biomed. Appl. 661 (1994) 185–191, https://doi.org/10.1016/0378-4347(94)00374-2.
[79] D. Tsikas, F.-M. Gutzki, S. Rossa, H. Bauer, C. Neumann, K. Dockendorff, J. Sandmann, J.C. Frölich, Measurement of nitrite and nitrate in biological fluids by gas chromatography–mass spectrometry and by the griess assay: problems with the griess assay—solutions by gas chromatography–mass spectrometry, Anal. Biochem. 244 (1997) 208–220, https://doi.org/10.1006/abio.1996.9880.
[80] Y. Li, J.S. Whitaker, C.L. McCarty, Reversed-phase liquid chromatography/electrospray ionization/mass spectrometry with isotope dilution for the analysis of nitrate and nitrite in water, J. Chromatogr. A 1218 (2011) 476–483, https://doi.org/10.1016/j.chroma.2010.11.073.

[81] D. Tsikas, S. Dehnert, K. Urban, A. Surdacki, H.H. Meyer, GC–MS analysis of S-nitrosothiols after conversion to S-nitroso-N-acetyl cysteine ethyl ester and in-in-jector nitrosation of ethyl acetate, J. Chromatogr. B 877 (2009) 3442–3455, https://doi.org/10.1016/j.jchromb.2009.06.032.
[82] D. Tsikas, M. Raida, J. Sandmann, S. Rossa, W.-G. Forssmann, J.C. Frölich, Electrospray ionization mass spectrometry of low-molecular-mass S-nitroso compounds and their thiols, J. Chromatogr. B Biomed. Sci. Appl. 742 (2000) 99–108, https://doi.org/10.1016/S0378-4347(00)00141-9.
[83] E. Hanff, M.F. Eisenga, B. Beckmann, S.J.L. Bakker, D. Tsikas, Simultaneous pentafluorobenzyl derivatization and GC-ECNICI-MS measurement of nitrite and malondialdehyde in human urine: close positive correlation between these disparate oxidative stress biomarkers, J. Chromatogr. B-Anal. Technol. Biomed. Life Sci. 1043 (2017) 167–175, https://doi.org/10.1016/j.jchromb.2016.07.027.
[84] E. Hanff, M. Luetzow, A.A. Kayacelebi, A. Finkel, M. Maassen, G.R. Yancheva, A. Haghikia, U. Bavendiek, A. Bucke, T. Luecke, N. Maassen, D. Tsikas, Simultaneous GC-ECNICI-MS measurement of nitrite, nitrate and creatinine in human urine and plasma in clinical settings, J. Chromatogr. B-Anal. Technol. Biomed. Life Sci. 1047 (2017) 207–214, https://doi.org/10.1016/j.jchromb.2016.03.034.
[85] D. Tsikas, M. Schmidt, E. Hanff, A. Boehmer, GC-ECNICI-MS analysis of S-nitrosothiols and nitroprusside after treatment with aqueous sulphide (S2-) and derivatization with pentafluorobenzyl bromide: evidence of S-transnitrosylation and formation of nitrite and nitrate, J. Chromatogr. B-Anal. Technol. Biomed. Life Sci. 1043 (2017) 209–218, https://doi.org/10.1016/j.jchromb.2016.09.002.
[86] D. Tsikas, J. Sandmann, J.C. Frolich, Measurement of S-nitrosoalbumin by gas chromatography - mass spectrometry III. Quantitative determination in human plasma after specific conversion of the S-nitroso group to nitrite by cysteine and CU2+ via intermediate formation of S-nitrosocysteine and nitric oxide, J. Chromatogr. B-Anal. Technol. Biomed. Life Sci. 772 (2002) 335–346, https://doi.org/10.1016/S1570-0232(02)00121-6.
[87] X. Yang, C.P. Bondonno, A. Indrawan, J.M. Hodgson, K.D. Croft, An improved mass spectrometry-based measurement of NO metabolites in biological fluids, Free Radic. Biol. Med. 56 (2013) 1–8, https://doi.org/10.1016/j.freeradbiomed.2012.12.002.
[88] I. Kluge, U. GutteckAmsler, M. Zollinger, K.Q. Do, J. Neurochem. 69 (1997) 2599–2607.
[89] E. Pagliano, J. Meija, R.E. Sturgeon, Z. Mester, A. D'Ulivo, Negative chemical ionization GC/MS determination of nitrite and nitrate in seawater using exact matching double spike isotope dilution and derivatization with triethyloxonium tetrafluoroborate, Anal. Chem. 84 (2012) 2592–2596, https://doi.org/10.1021/ac2030128.
[90] E. Hanff, A. Boehmer, J. Jordan, D. Tsikas, Stable-isotope dilution LC-MS/MS measurement of nitrite in human plasma after its conversion to S-nitrosoglutathione, J. Chromatogr. B-Anal. Technol. Biomed. Life Sci. 970 (2014) 44–52, https://doi.org/10.1016/j.jchromb.2014.08.041.
[91] J. Bai, H. Gao, R. Xiao, J. Wang, C. Huang, A review of soil nitrogen mineralization as affected by water and salt in Coastal Wetlands: issues and methods, Clean.-Soil Air Water 40 (2012) 1099–1105, https://doi.org/10.1002/clen.201200055.
[92] H. Yu, R. Schmitt, A. Sapin, P. Chaimbault, P. Leroy, Comparison between two derivatization methods of nitrite ion labeled with 15N applied to liquid chromatography-tandem mass spectrometry, Anal. Methods 10 (2018) 3830–3836, https://doi.org/10.1039/C8AY01206G.
[93] M. Marzinzig, A.K. Nussler, J. Stadler, E. Marzinzig, W. Barthlen, N.C. Nussler, H.G. Beger, S.M. Morris Jr., U.B. Brückner, Improved methods to measure end products of nitric oxide in biological fluids: nitrite, nitrate, andS-Nitrosothiols, Nitric Oxide 1 (1997) 177–189, https://doi.org/10.1006/niox.1997.0116.
[94] N.S. Bryan, T. Rassaf, R.E. Maloney, C.M. Rodriguez, F. Saijo, J.R. Rodriguez, M. Feelisch, Cellular targets and mechanisms of nitros(yl)ation: an insight into their nature and kinetics in vivo, Proc. Natl. Acad. Sci. USA 101 (2004) 4308–4313, https://doi.org/10.1073/pnas.0306706101.
[95] N.S. Bryan, B.O. Fernandez, S.M. Bauer, M.F. Gauria-Saura, A.B. Milsom, T. Rassaf, R.E. Maloney, A. Bharti, J. Rodriguez, M. Feelisch, Nitrite is a signaling molecule and regulator of gene expression in mammalian tissues, Nat. Chem. Biol. 1 (2005) 290–297, https://doi.org/10.1038/nchembio734.
[96] N.S. Bryan, M.B. Grisham, Methods to detect nitric oxide and its metabolites in biological samples, Free Radic. Biol. Med. 43 (2007) 645–657, https://doi.org/10.1016/j.freeradbiomed.2007.04.026.
[97] E. Bramanti, V. Angeli, A. Paolicchi, A. Pompella, The determination of S-nitrosothiols in biological samples-Procedures, problems and precautions, Life Sci. 88 (2011) 126–129, https://doi.org/10.1016/j.lfs.2010.10.024.
[98] G.K. Glantzounis, S.A. Rocks, H. Sheth, I. Knight, H.J. Salacinski, B.R. Davidson, P.G. Winyard, A.M. Selfalian, Formation and role of plasma S-nitrosothiols in liver ischemia-reperfusion injury, Free Radic. Biol. Med. 42 (2007) 882–892, https://doi.org/10.1016/j.freeradbiomed.2006.12.020.
[99] A. Ismail, F. d'Orlye, S. Griveau, J.A. Fracassi da Silva, F. Bedioui, A. Varenne, Capillary electrophoresis with mass spectrometric detection for separation of S-nitrosoglutathione and its decomposition products: a deeper insight into the decomposition pathways, Anal. Bioanal. Chem. 407 (2015) 6221–6226, https://doi.org/10.1007/s00216-015-8786-z.
[100] E. Mitri, L. Barbieri, L. Vaccari, E. Luchinat, 15 N isotopic labelling for in-cell protein studies by NMR spectroscopy and single-cell IR synchrotron radiation FTIR microscopy: a correlative study, Analyst 143 (2018) 1171–1181, https://doi.org/10.1039/c7an01464c.

1st Chapter: Development and validation of bioanalytical methods dedicated to the measurement of NO species labeled with the stable nitrogen isotope 15

Lors de la quantification de composés d'intérêt biologique dans les milieux complexes, quelle que soit leur origine, il est communément admis que le couplage de méthodes séparatives à la spectrométrie de masse en tandem (MS/MS ou MS²) est la plus performante des méthodes pour atteindre l'état de trace. En effet, outre sa haute sensibilité, cette technique de détection permet même souvent de s'affranchir d'une préparation d'échantillons compliquée grâce à sa plus grande spécificité au regard de la détection UV-Vis, voire fluorescence. Par ailleurs, la MS permet aussi de distinguer des compositions isotopiques différentes pour une même molécule, que cette composition soit naturelle (exemple ^{13}C naturellement présent à hauteur de 1,1% sur Terre) ou issue de synthèses par enrichissement isotopique pour des études de mécanisme de fragmentation, pour son utilisation en tant qu'étalon interne en quantification ou encore pour le suivi de flux métaboliques dans les organismes vivants (fluxomique).

Dans ce travail, l'utilisation de la MS/MS (ou MS²) fait la synthèse d'un grand nombre de ces avantages puisque nous allons utiliser sa spécificité de détection pour nous affranchir au maximum de l'effet de matrice complexe, sa grande sensibilité de détection pour atteindre une détection des métabolites d'intérêt à des concentrations de l'ordre du nanomolaire, et enfin le marquage isotopique qui nous permettra de distinguer les sources naturelles de NO possédant l'isotope ^{14}N de celle du médicament étudié, marqué spécifiquement par synthèse avec l'isotope ^{15}N.

La plupart du temps, les quantifications de composés d'intérêt à l'aide des techniques couplées à la MS/MS utilisent des spectromètres triple quadripôles (QqQ, Figure 1 A), ces derniers étant les plus performants dans la quantification à l'état de trace. Dans ce cas, l'ion moléculaire (radicalaire, protonné ou déprotonné selon le mode d'ionisation et la source utilisée) est sélectionné après filtrage par un premier quadripôle (Q_1) qui ne laisse passer que l'ion de rapport m/z désiré. Cet ion (dit précurseur) pénètre dans un deuxième quadripôle (Q_2) qui sert de cellule de collision où il percute plus ou moins violemment (selon l'énergie cinétique communiquée par l'expérimentateur) un gaz inerte (N_2 ou Ar). Il en résulte un accroissement d'énergie interne de l'ion moléculaire qui se fragmente en ions plus petits (les fragments neutres ne seront pas observables). Les ions fragments qui sortent de la cellule de collisions sont alors analysés par un troisième quadripôle (Q_3). Lorsqu'un seul de ces ions fragments (dits produits) est sélectionné pour atteindre l'analyseur, on est en mode de détection MRM (pour Multiple Reaction Monitoring).

On appelle « transition », le couple des rapports m/z suivis en $Q_1 \rightarrow Q_3$. L'utilisation typique de ce mode de fonctionnement est le dosage à l'état de trace. La technique de fragmentation induite par collision décrite s'appelle CID pour « Collision ou Collisionally Induced Dissociation ». C'est la technique classiquement utilisée sur des spectromètres QqQ. Le mode MRM issu d'une CID peut aussi être utilisé sur des spectromètres de type trappe d'ions (ITMS pour IonTrap Mass Spectrometer). Ces spectromètres, plus intéressants pour des approches structurales sont un peu moins performants en termes de limite de quantification que leurs homologue QqQ. Dans le cas d'un ITMS, l'analyseur IT permet à la fois la sélection de l'ion moléculaire, sa fragmentation et l'analyse des fragments générés.

Si cette description un peu longue vient d'être faite, c'est que pour bien comprendre le travail qui va suivre, il faut expliquer maintenant l'originalité du spectromètre de masse dont nous disposons. Il s'agît d'un appareil ITMS que le constructeur a doté de plusieurs techniques de fragmentation dont le CID bien entendu mais aussi de la technique dite HCD pour « Higher-energy Collision Dissociation ». Cette dernière fait l'originalité de la technique de dosage par chromatographie en phase liquide (LC) que nous avons couplée à notre spectromètre de masse à trappe d'ion en mode tandem (ITMS/MS). L'ionisation des composés à la sortie de la colonne chromatographique aura lieu par électronébulisation (ESI) comme les travaux déjà publiés dans le domaine (McAlister *et al.* 2011). Il convient donc maintenant de décrire le fonctionnement des ces deux modes sur notre appareil dont la conception est présentée à la figure 1 B.

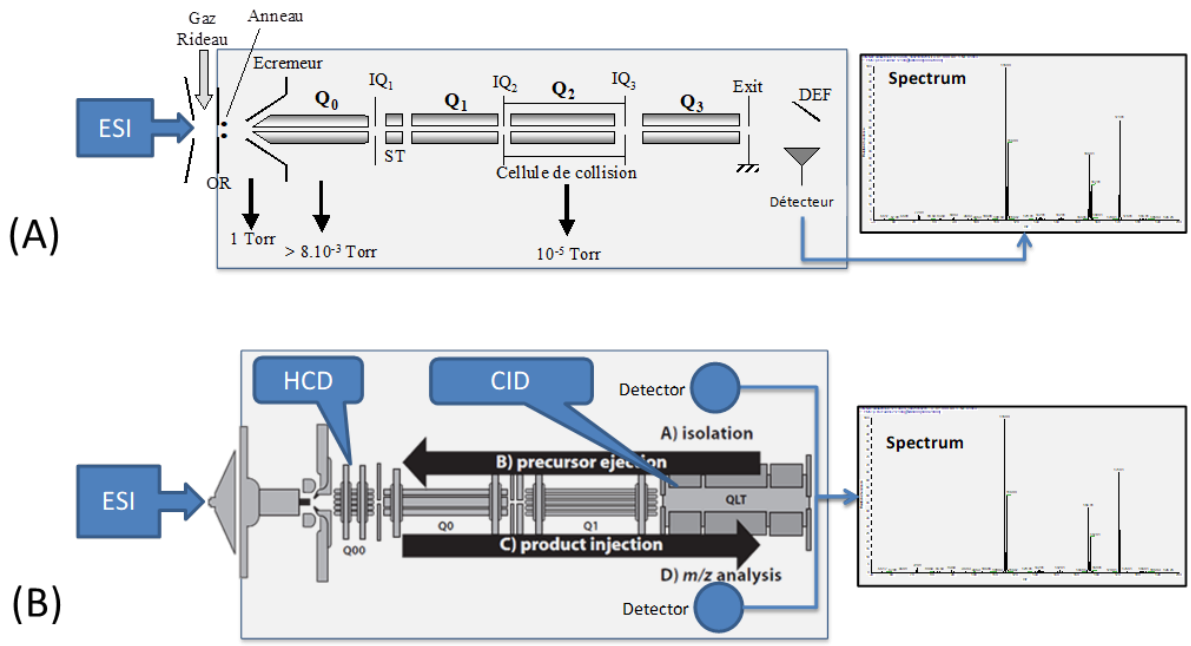

Figure 1. (A) : Schéma d'un spectromètre de type triple quadripôle QqQ. Le quadripôle Q_0 et les lentilles IQ_i servent de système de focalisation des ions. OR = orifice, lentille par laquelle les ions provenant de la source Electrospray (à pression atmosphérique) pénètrent dans le vide du spectromètre de masse pour y être analysés selon leur rapport masse sur charge (m/z). Le quadripôle Q_2 sert de cellule de collision (souvent notée « q ») en mode de fragmentation soit pour un suivi des ions produits, précurseurs ou des pertes de neutres en fonction de l'utilisation des quadripôles Q_1 et Q_3. En Mode MRM (dosage), les quadripôles Q_1 et Q_3 sont réglés sur les rapports m/z de l'ion moléculaire et d'un fragment respectivement pour une plus grande spécificité et sensibilité de détection. (B) : Schéma du spectromètre LTQ Velos Pro (Thermo Scientific). Les quadripôles Q_{00}, Q_0 et Q_1 servent de système de focalisation des ions provenant de la source Electrospray (à pression atmosphérique) après leur entrée dans le vide du spectromètre de masse et du système d'acheminement vers l'analyseur de type trappe linéaire (QLT pour Quadrupole Linear Trap). En mode CID, la fragmentation de l'ion moléculaire a lieu dans la trappe alors qu'en mode HCD, l'ion moléculaire sélectionné dans la trappe (étape A) est renvoyé en arrière pour être fragmenté dans la région du Q_{00} (étape B). Les fragments reviennent dans la trappe (étape C) pour être analysés selon leur rapport m/z (étape D). D'après (McAlister *et al.* 2011).

Le spectromètre LTQ Velos Pro (Thermo Scientific) est conçu de manière à proposer plusieurs techniques de fragmentation dont la technique CID. Dans ce cas,

celui-ci procède comme sur les autres appareils de type trappe d'ions. Après avoir été ionisés dans la source, les composés pénètrent dans le spectromètre pour y rejoindre l'analyseur sous l'effet d'un gradient de vide et de tension. Ces ions rejoignent la trappe qui sur l'appareil est de type linéaire, d'où son nom « LTQ » pour Linear Quadrupole Trap (on trouve aussi l'abréviation QTL selon les sources). La trappe linéaire a une capacité de piégeage des ions plus élevée que les trappes classiques (circulaires) qui leur confèrent de meilleures limites de détection. En spectrométrie de masse tandem, l'ion moléculaire est d'abord isolé dans la trappe (on élimine tout les autres) puis fragmenté par excitation dans la trappe (collision avec de l'hélium généralement toujours présent même en spectrométrie de masse simple) puis après un certain temps de génération, les fragments sont à leur tour analysés par la trappe. En mode MRM, pour le dosage, comme pour un QqQ, on suivra une transition mais les ions auront été générés dans le même analyseur. Sur ce spectromètre de masse, nous disposons également d'un mode HCD qui est en règle générale utilisé dans l'analyse des protéines et peptides pour générer des informations structurales complémentaires au mode CID. Le mode de fonctionnement de l'appareil est alors complètement différent. L'étape d'isolement (A de la figure 1 B) de l'ion moléculaire reste cependant la même mais la génération des fragments ne se fait plus dans la trappe. L'ion moléculaire est éjecté de la trappe pour un retour en arrière dans la région de l'interface Q00 (étape B de la figure 1 B) pour y être fragmenté et les ions fragments sont réinjectés vers la trappe (étape C de la figure 1 B) pour y être analysés (étape D de la figure 1 B). En mode MRM, on suivra toujours une transition, mais alors, d'où provient l'intérêt d'utiliser ce mode dans notre travail ? Comme il sera possible de le découvrir dans la deuxième partie de ce chapitre intitulée "Higher-energy Collision Dissociation for the quantification by liquid chromatography/tandem ion trap mass spectrometry of nitric oxide metabolites coming from *S*-nitrosoglutathione in an *in vitro* model of intestinal barrier" produite dans *Rapid Communications in Mass Spectrometry*, la différence entre CID et HCD peut être de taille. En effet, au fur et à mesure qu'on pénètre à l'intérieur du spectromètre, l'atmosphère de la source fait rapidement place au vide et dans la trappe, la collision en CID se fait avec un gaz inerte (hélium), *a priori* sans autre réaction qu'une simple fragmentation. Il n'en va pas de même avec le mode HCD pour lequel, le retour en arrière de l'ion s'accompagne de collisions avec les vapeurs de solvants issus de la source et principalement les solvants composant la phase

mobile chromatographique. Ces molécules de solvants, plus grosses communiquent plus d'énergie aux ions moléculaires à fragmenter mais ce n'est pas tout... Elles n'ont pas du tout la même inertie chimique et peuvent éventuellement réagir avec l'ion moléculaire en phase gazeuse provoquant des mécanismes de fragmentation originaux comme nous en avons été témoins lors de ce travail.

1. Experimental paper: "Comparison between two derivatization methods of nitrite ion labeled with ^{15}N applied to liquid chromatography-tandem mass spectrometry" in *Analytical Methods (10 (2018) 3830–3836)*

Detailed procedures used for experiments in this article are present in protocols (see appendices) entitled "Purification of azo adduct and 2,3-naphthotriazole adduct by LC coupled with UV/Vis detection", "Measurement of nitrite, nitrate ions and S-nitrosothiols using the 2,3-diaminonaphthalene assay by LC coupled with tandem mass spectrometry" and "Permeability studies of *S*-nitrosothiols in isolated rat intestine using Ussing chamber".

Analytical Methods

COMMUNICATION

View Article Online
View Journal

Cite this: DOI: 10.1039/c8ay01206g

Received 28th May 2018
Accepted 19th July 2018

DOI: 10.1039/c8ay01206g

rsc.li/methods

Comparison between two derivatization methods of nitrite ion labeled with ^{15}N applied to liquid chromatography-tandem mass spectrometry†

Yu Haiyan,[a] Schmitt Romain,[a] Sapin Anne,[a] Chaimbault Patrick[b] and Leroy Pierre*[a]

The fragmentations of the adducts resulting from the derivatization of nitrite ion by Griess method (formation of an azo compound) and 2,3-diaminonaphthalene (formation of 2,3-naphthotriazole (NAT)) were studied by tandem mass spectrometry (MS/MS). The transition used for quantification was selected according to the highest value of the signal-over-blank ratio (S/B) obtained from each adduct fragmentation. When derivatizing nitrite ion labeled with the stable ^{15}N isotope, followed by liquid chromatography (LC)-MS/MS measurement, the lowest limit of quantification obtained was 5 nM with NAT. The method was applied to study the intestinal permeability of *S*-nitrosoglutathione, a drug candidate for the chronic treatment of cardiovascular disease. This compound was labeled with ^{15}N and its permeability was studied in an *ex vivo* rat intestine model using an Ussing chamber.

1. Introduction

Nitrogen derivatives especially oxides play important roles in the environment[1] and in living organisms.[2] For example, nitric oxide (NO) is a crucial actor of vascular tone homeostasis. Its endogenous production in the endothelial cell layer of vessels decreases with ageing and in cardiovascular diseases related to endothelial dysfunction.[3] The monitoring of NO and related species (nitrite and nitrate ions, *S*-nitrosothiols (RSNOs)) in the body is of main importance to evaluate the bioavailability of NO donors recently developed and proposed as drug candidates, such as *S*-nitrosoglutathione (GSNO).[4]

Because of the low molecular mass of NO (30 u), it has to be derivatized to allow its measurement by MS at low concentration levels in biological fluids. The samples, the standards and the reagent solutions are most of the time spoiled by nitrogen oxides from the atmosphere and by bacteria reducing nitrate to nitrite through a specific reductase. Consequently, this natural contamination leads to a signal which interferes with the NO coming from the drugs during the derivatization process.[5] The reduction of this pollution by suppressing air contact and microbial growth is not so obvious. Preparing fresh solutions in ultra-pure water is the usual way to limit the level of this phenomenon,[6] but significant interferences are still observed in the blank. Consequently, the limit of quantification (LOQ) increases as it is calculated on the basis of the signal-over-blank (S/B) rather than the signal-over-noise ratio (S/N).

The advantages of using nitrite ion labeled by the stable ^{15}N isotope (exhibiting a very low natural abundance, *i.e.* 0.37%),[7] derivatization with various probes, *e.g.* pentafluorobenzyl bromide,[8–10] 2,3-diaminonaphthalene (DAN)[5,11,12] and reduced glutathione (GSH),[13] followed by gas or liquid chromatography coupled with MS have already been reported to improve sensitivity.

Presently, we selected two derivatization methods of nitrite ion which are the most commonly used in the literature for unlabeled NO species analysis (Fig. 1): the first one is based on a two-step reaction of nitrite ion with sulfanilamide and *N*-(1-naphthyl)ethylenediamine (NED) to form an azo adduct followed by a spectrophotocolorimetric measurement (Griess assay); the second way consists in the reaction between the fluorogenic probe DAN and nitrite ion in acidic medium giving rise to 2,3-naphthotriazole (NAT), followed by spectrofluorimetric measurement in alkaline medium (DAN assay). The LOQ values are 1 and 0.2 μM for Griess and DAN assays,[14,15] respectively. The advantage of both methods is the possible quantification of nitrate ions after chemical or enzymatic reduction, and RSNOs after cleavage of the S–NO bond with mercuric ions. Moreover, they have been adapted to HPLC with their corresponding detection mode: visible spectrophotometry for Griess[16] and fluorescence for DAN assay.[17] DAN derivatization has been previously used in LC-MS/MS after labeling NO species with ^{15}N.[5,11,12] But to the best of our knowledge, it is the first report of ^{15}N labeled azo adduct resulting from Griess reaction. The present work consists in a comparison of the fragmentation modes of the two adducts, azo compound and

[a]Université de Lorraine, CITHEFOR EA 3452, Faculté de Pharmacie, 5, Rue Albert Lebrun, F-54001, Nancy, France. E-mail: pierre.leroy@univ-lorraine.fr
[b]Université de Lorraine, LCP-A2MC, F-57000 Metz, France

† Electronic supplementary information (ESI) available. See DOI: 10.1039/c8ay01206g

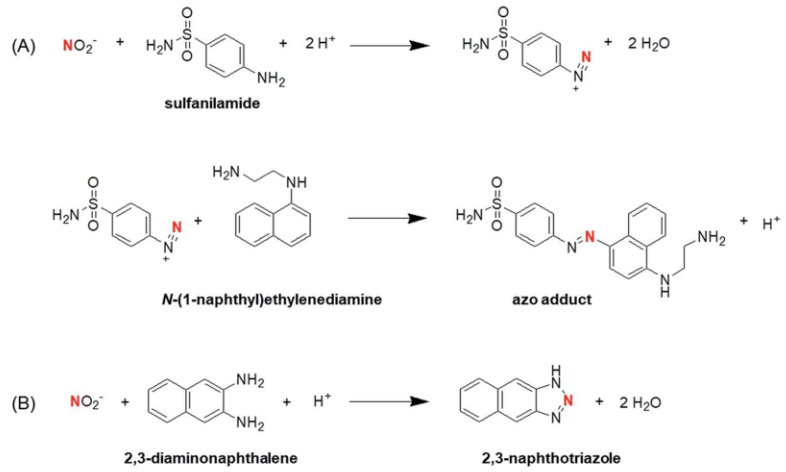

Fig. 1 Reaction between nitrite ion and (A) Griess reagents (sulfanilamide and *N*-(1-naphthyl)ethylenediamine (NED)) to form the azo adduct; (B) 2,3-diaminonaphthalene (DAN) leading to 2,3-naphthotriazole (NAT). "N" in red is labeled with nitrogen 15.

NAT, and consequent analytical performances by using LC coupled to Electrospray-Ion Trap tandem Mass Spectrometry (LC-ESI-ITMS/MS). The LOQ calculation was based on both S/N and S/B values. For the studies of the S/B value, the azo and NAT adducts were first purified by a semi-preparative LC system. The selected method offering the lowest LOQ was applied to the intestinal permeability studies of *S*-nitrosoglutathione labeled with ^{15}N ($GS^{15}NO$) by using isolated and oriented rat intestine in an Ussing chamber system. This latter *ex vivo* model appears more correlated to *in vivo* conditions than simpler cell models, *e.g.* Caco-2 cell monolayer.[18]

2. Material and methods

2.1. Chemicals

All reagents and standards were of analytical grade. All solutions were daily prepared in fresh ultrapure water (>18.2 MΩ × cm). Sodium ^{15}N-nitrite ($Na^{15}NO_2$) was supplied by Cambridge Isotope Laboratories (Tewksbury, MA, USA) and ^{14}N-NAT by Chemodex (St. Gallen, Switzerland). $Na^{15}NO_3$ was provided by Sigma-Aldrich (Saint-Quentin-Fallavier, France) and $GS^{15}NO$ was synthesized according to the method previously reported for unlabeled GSNO.[14]

2.2. Derivatization of ^{15}N labeled nitrite ion

For Griess assay, one mL of 0.001 M of $Na^{15}NO_2$ in 1.575 M acetate buffer pH 2.5 were mixed with 200 μL of 0.035 M sulfanilamide in 0.4 M HCl; the reaction mixture was incubated at room temperature in the dark for 3 min. Then, 50 μL of 0.017 M NED in 0.3 M HCl were added, and the resulting mixture was incubated for 5 min. For DAN assay, 300 μL of 0.005 M $Na^{15}NO_2$ in ultrapure water were mixed with 600 μL of 3.16 mM DAN in 0.6 M HCl and the resulting mixture was incubated at room temperature in the dark for 10 min. Next, 310 μL of 1.2 M NaOH were added. The resulting azo adduct and NAT solutions were stored at 4 °C for a maximum period of 5 h until LC purification.

2.3. Purification of adducts

Both adducts were purified from their reaction mixture by a LC system incorporating a Nucleosil C-18 column (4.6 × 250 mm ID, 5 μm, Macherey Nagel, Darmstadt, Germany). For azo adduct purification, the mobile phase was an acetonitrile–water–trifluoroacetic acid (25 : 75 : 0.1, v/v/v) mixture used at a flow rate of 1.2 mL min^{-1} and at a column temperature of 40 °C, followed by UV detection at λ = 220 nm (diode array detector (DAD), UV 6000 LP, Thermo, Les Ulis, France or UV/VIS-155 model, Gilson, Middleton, WI, USA). The fraction with peak corresponding to the azo adduct (retention time: *ca.* 12 min) was collected and stored at −80 °C for maximum one month. For NAT purification, the mobile phase was acetonitrile–0.01 M ammonium acetate buffer pH 7.2 (28 : 72, v/v) at a flow rate of 0.8 mL min^{-1} and at 40 °C, followed by UV detection at λ = 330 nm. The fraction with peak corresponding to NAT (retention time: *ca.* 12 min) was collected and stored at −80 °C for maximum 3 months. In both cases, the loop volume was 100 μL and the derivatization mixture (see 2.2) was directly injected into the corresponding LC system. The adduct concentrations in the collected fractions were measured by using the respective conventional techniques (Griess[14] and DAN[15] assays) and they were in the range of 60 to 120 μM.

2.4. Analysis of adducts with LC-ESI-ITMS/MS

Both purified adducts (50-fold diluted in the corresponding mobile phase) and derivatization mixtures in Krebs solution (6.90 g L^{-1} NaCl, 0.35 g L^{-1} KCl, 1.80 g L^{-1} glucose, 0.16 g L^{-1} KH_2PO_4, 2.02 g L^{-1} $NaHCO_3$, 0.14 g L^{-1} $MgSO_4$, 0.35 g L^{-1}

$CaCl_2 \cdot 2H_2O$, pH 7.4) were injected (20 μL loop) into the LC-ESI-ITMS/MS system (Dionex, Ultimate 3000, coupled with LTQ Velos Pro, Thermo Scientific, San José, CA, USA). The Acclaim 120 C-18 column (2.1 × 150 mm ID, 3 μm, Thermo) was eluted at a flow rate of 0.2 mL min^{-1} and at 25 °C with (i) methanol–water–acetic acid (49 : 51 : 0.1, v/v/v) for the azo adduct analysis, and (ii) with a gradient mobile phase consisting of acetonitrile and 0.01 M acetic acid mixtures for NAT analysis. In the latter case, the content of acetonitrile was increased from 40 to 80% between 1.5 and 5 min, then held at 80% for 2.5 min. A switching valve was used to discard the mobile phase eluting from the column during the first 3 min-period of each chromatographic run. The source voltage applied was 5.00 kV; a MS scan and a multiple reaction monitoring (MRM) of transitions were realized. The LOQ values based on both S/N and S/B for purified and unpurified adducts were calculated.

2.5. Intestinal permeability studies

The intestinal permeability of $GS^{15}NO$ was studied in an *ex vivo* model according to a previously reported procedure.[19] This system offers the possibility to maintain *ex vivo* tissue viability for 2 hours in specific experimental conditions (using Krebs buffer at 37 °C with continuous O_2–CO_2 (95 : 5, v/v) mixture bubbling). All experiments were performed in accordance with the European Parliament guidelines (2010/63/EU) for the use of experimental animals and the respect of the 3 Rs' requirements for Animal Welfare. Briefly, intact isolated intestine (ileum, 100 ± 5 mg) of Wistar rat was mounted in Ussing chamber (EM-CSYS-6, Physiologic Instrument Inc, San Diego, CA, USA). Two compartments were separated by the vertical and oriented tissue (isolated rat intestine with mucosa part mimicking intestinal lumen toward donor compartment and serosa toward acceptor compartment). 2.5 mL of Krebs solution were added into each compartment. Tissue samples exhibiting a *trans*-epithelial electrical resistance (TEER) value less than 30 Ω cm^2, translating a loss of intestine barrier integrity, were discarded. Next, 250 nanomoles of $GS^{15}NO$ were deposited in the donor compartment, and samples (250 μL) were harvested from the acceptor compartment after incubation at 37 °C with O_2–CO_2 (95 : 5, v/v) mixture bubbling for 2 h. $RS^{15}NOs$ and ^{15}N-nitrate ions were converted to ^{15}N-nitrite ions by using mercuric ions and nitrate reductase associated with corresponding cofactors, respectively, as previously described.[15] For the method validation, five point calibration curves were built by spiking the physiological medium used in the Ussing chamber, *i.e.* Krebs solution, with $Na^{15}NO_2$, $GS^{15}NO$ and $Na^{15}NO_3$. Accuracy, intra- and inter-day precision were evaluated with quality control points of $Na^{15}NO_2$ and $GS^{15}NO$ (15, 50 and 180 nM), and $Na^{15}NO_3$ (120, 1000 and 1600 nM) prepared in Krebs solution. Standards and real samples were derivatized as described in 2.2, except that 60 μL of 0.105 mM DAN instead of 600 μL were used. After incubation (room temperature, 10 min), 36 μL of 1 M NaOH together with 4 μL of 0.0001 M NaOH were added to adjust pH close to 8. Finally, these derivatives were stored at −80 °C until analysis. 10 μL of 0.02 mM naphthylamine solution as the internal standard (IS) were added just before injection into the LC system as described in 2.4.

The apparent permeability coefficient (P_{app}) values were calculated using the following equation:

$$P_{app} = \frac{dQ}{dt} \times \frac{1}{A \times C_0}$$

dQ/dt (mol s^{-1}) refers to the quantity of permeated NO related species (dQ) in the acceptor compartment at the time of quantification (dt), "A" refers to the membrane diffusion area (0.25 cm^2), and C_0 refers to the initial concentration of $GS^{15}NO$ in the donor compartment.

3. Results and discussion

^{15}N labeled adducts were purified by semi-preparative LC (Fig. S1†). The selected wavelength of the DAD allowed the simultaneous detection of reagent excess and adduct. A baseline resolution between adduct and reagents was obtained in both cases. Collected fractions containing purified adducts were injected into the LC-ESI-ITMS/MS system for studying their fragmentation pattern. The main transitions obtained for the ^{15}N-azo adduct were m/z 371 → 354 and m/z 371 → 328 under Collisionally Induced Dissociation (CID) mode with optimized collision energy of 35 eV (Fig. 2A). For the ^{15}N-NAT adduct, different transitions were observed: m/z 171 → 115 and m/z 171 → 156 depending the collision mode (Fig. 2B and C). The main transition m/z 171 → 115 observed under CID at 35 eV (Fig. 2B) led to the highest sensitivity. This result was in good agreement with the literature.[5] Although this transition gave also the highest signal in Higher-energy Collision Dissociation (HCD) at 50 eV, the sensitivity was found lower than for the new original transition, m/z 171 → 156, only observed in HCD mode. Even if the absolute abundance of the transition m/z 171 → 156 is lower than for m/z 171 → 115 under HCD mode, the highest sensitivity is due a lowest background noise at m/z 171 → 156.

The LOQ values corresponding to the selected transitions for each adduct are indicated in Table 1: (i) a LOQ value of 1 nM (based on S/N = 10) was reached using the best transitions for Griess and DAN adducts; (ii) the percentage of interference due to the natural presence of ^{13}C in the unlabeled azo adduct (coming from ^{14}NO in the atmospheric or/and bacterial pollution) on the signal of the ^{15}N-labeled adduct (coming from the drug) is 20% whereas it is only 2% for the NAT adduct; (iii) the LOQ (*ca.* 5 nM, S/B = 5) using DAN assay based on HCD mode is consequently lower than the one obtained with the Griess derivative (100 nM). As mentioned above, the blank values of Griess and DAN assays for ^{14}N-nitrite ion analysis were not negligible due to unavoidable contaminations (around 100 and 50 nM, respectively). Consequently, the LOQ values of Griess and DAN assays for ^{14}N–NO_2 analysis were regarded as 500 and 250 nM, respectively, based on S/B = 5. Meanwhile, ^{13}C interference levels were in accordance with theoretical calculation. As a result, blank values of Griess and DAN assays for ^{15}N-nitrite ion analysis were 20 and 1 nM, respectively. Clearly, the reason why LOQ value of DAN assay is 20-fold lower than in Griess assay, is due to a lower blank value.

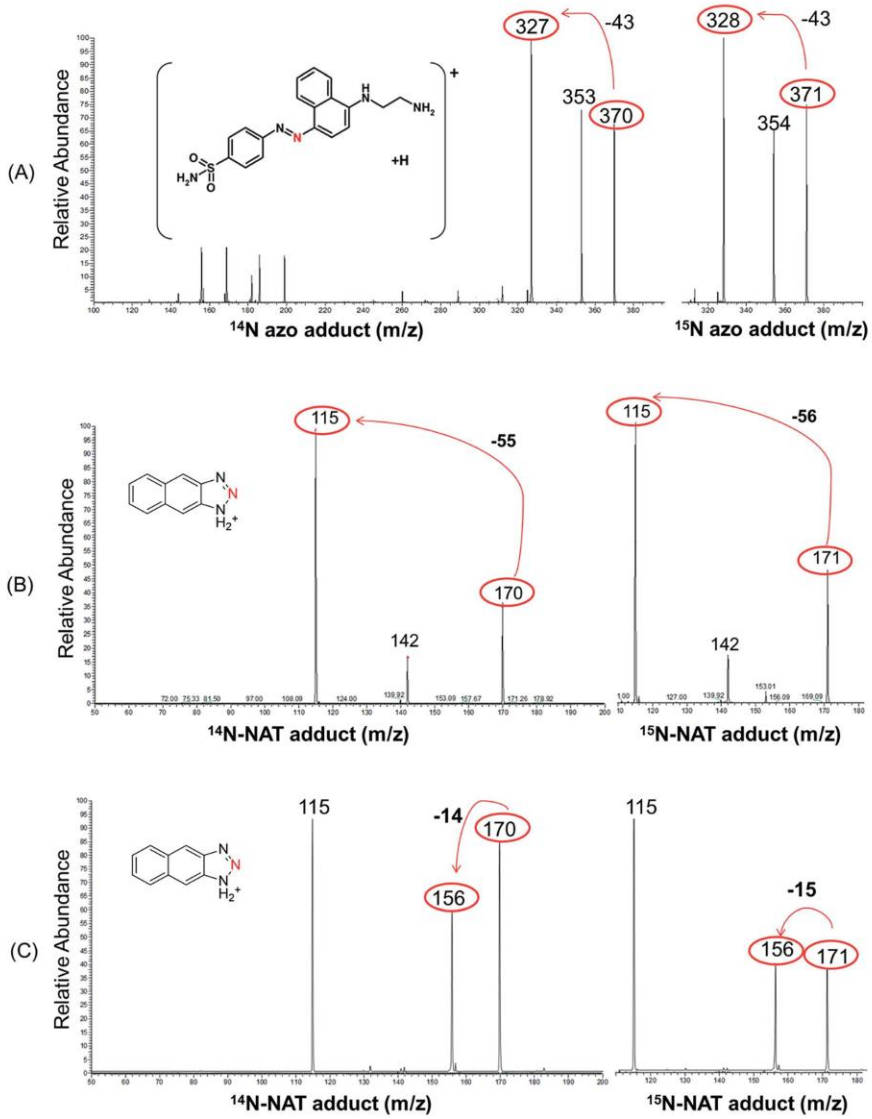

Fig. 2 Fragmentation studies of (A) azo adduct under Collision Induced Dissociation (CID) mode; (B) 2,3-naphthotriazole (NAT) adduct under CID mode; and (C) NAT adduct under Higher-energy Collisional Dissociation (HCD) mode by liquid chromatography coupled to Electrospray-Ion Trap tandem Mass Spectrometry, with both isotopes ($^{14}N - [M + H]^+$ – on the left, and $^{15}N - [M + H + 1]^+$ – on the right side of the figure). The red nitrogen in protonated adducts comes from nitric oxide.

The selectivity has been tested by comparing purified adducts and the derivatization mixtures. As a result, no matrix (Krebs solution) effect was observed. The retention times of sulfanilamide, azo adduct and NED in the LC-MS/MS system were 2.1, 3.6 and 4.2 min, respectively. The retention times of DAN and NAT were 4.2 and 5.5 min, respectively. Regarding the Griess method, a baseline resolution between peaks corresponding to sulfanilamide and azo adduct was obtained, which precluded reagent interference in the MS source. Concerning the DAN assay, a baseline resolution between peaks corresponding to DAN and NAT adduct was achieved. Moreover, discarding the mobile phase at the beginning of each run avoided any contamination of the MS source by polar products contained in the real samples.

Noteworthy, the blank values obtained for both methods decreased after labeling NO_2^- with ^{15}N despite the ^{13}C

Table 1 Comparison of performances between derivatization of nitrite ion with Griess and 2,3-diaminonaphthalene (DAN) methods followed by LC-ESI-ITMS/MS analysis (CID: Collisionally Induced Dissociation; HCD: Higher-energy Collision Dissociation; LOQ: limit of quantification; S/N: signal-over-noise; S/B: signal-over-blank)

Assay		Griess	DAN	
Collision modes		CID (35 eV)	CID (35 eV)	HCD (50 eV)
Selected transitions m/z	^{14}N-adduct	370 → 327 (370 → 353)	170 → 115	170 → 156
	^{15}N-adduct	371 → 328 (371 → 354)	171 → 115	171 → 156
Adduct retention time/total analysis time/reequilibration time (min)		5.7/8/No (isocratic condition)	4.5/7.0/10	4.5/7.0/10
LOQ (S/N = 10)	^{14}N-adduct and ^{15}N-adduct	1 nM	20 nM	1 nM
LOQ (S/B = 5; the blank (B) corresponds to the derivatization mixture)	^{14}N-adduct	500 nM	250 nM	250 nM
	^{15}N-adduct	100 nM	20 nM	5 nM
Interferences in blank samples (due to ^{14}N-adduct because of ^{13}C)		*ca.* 20%	*ca.* 2%	*ca.* 2%

interference. Finally, LOQ based on S/B = 5 was improved: 100 *vs.* 500 nM for Griess assay, 5 *vs.* 250 nM for DAN assay. In the present work, the product ions kept the ^{15}N during fragmentation of the protonated azo adduct, while the fragments lost it for NAT (Fig. 2). Usually, the transition keeping the labeled atom shows a higher specificity. However, DAN assay led to the most interesting method for further experiments, because its LOQ was 20-fold lower than for Griess assay with MS and 50-fold lower than DAN assay with spectrofluorimetric detection.

Obviously, the DAN method provides more advantages than Griess one to analyze ^{15}N labeled NO species, especially by decreasing LOQ value based on S/B, as discussed above. The DAN method has also to be compared with other probes already reported in the literature. First, the use of PFBBr for derivatizing ^{15}N labeled nitrite and nitrate ions[9,10] affords low LOD values based on a S/N value equal to 3 (0.2 and 4.8 nM for nitrite and nitrate, respectively), but an additional preanalytical step consisting in a liquid/liquid extraction of the adducts and a GC-MS system equipped with a specific chemical ionization source is required; at last, the LOQ value based on a S/B value is not provided by the literature. Employing GSH as a probe to derivatize ^{15}N labeled nitrite[13] leads to GSNO formation, which is a very fragile compound sensitive to many environmental factors such as light, temperature, metal ions and biological pathways (degradation through gamma-glutamyltransferase and redoxin catalysis, transnitrosation with other endogenous thiols). Thus the storage of derivatized samples until analysis could become a real challenge. DAN method has already been reported in the literature to derivatize ^{15}N labeled nitrite with subsequent analysis by LC-ESI-MS/MS. The produced NAT adduct is stable at r.t. for 24 h, and at −80 °C for 3 months with 2 freezing/thaw cycles (data not shown). As a triple quadrupole or Q-trap mass spectrometer was used in the literature, the presently used ion trap mass spectrometer operated in HCD offers parallel capacity to analyze ^{15}N labeled NO species, with a novel sensitive transition m/z 171 → 156 for ^{15}N labeled NAT adduct. Besides, the present method is to the best of our knowledge the first report of analysis of GS^{15}NO by DAN method.

The labeling efficiency of both methods has been evaluated. For Griess method, as the pure adduct is not available, the purified azo adduct contained in the fraction collected in the LC-UV system was titrated by using the molar absorbance reported in the literature, *i.e.* 38 000 M^{-1} cm^{-1}.[20] Next, the absorbance of adduct produced in the reaction medium was compared to the titrated adduct. For NAT method, the MS signal of the pure adduct which is commercially available, was compared to the signal obtained at the same theoretical molar

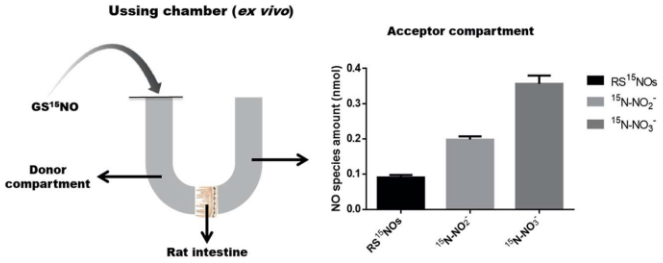

Fig. 3 Permeation of 250 nanomoles of ^{15}N labeled *S*-nitrosoglutathione (GS^{15}NO) through an *ex vivo* model of intestinal barrier (isolated rat intestine with mucosa toward donor compartment, and serosa toward acceptor compartment) after incubation at 37 °C with O_2–CO_2 (95 : 5, v/v) mixture bubbling for 2 h. GS^{15}NO metabolites (nitric oxide (NO) species amount) were quantified in the acceptor compartment, $n = 3$. Results are expressed as mean ± sem.

concentration of nitrite ion reacted with DAN according to the operating conditions described in paragraph 2.2. Resulting labeling efficiencies were 94.2 ± 5.8% and 93.0 ± 8.4% ($n = 3$) for azo and NAT adduct, respectively.

The quantification of NO species (^{15}N-nitrite ion, RS^{15}NOs and ^{15}N-nitrate ion) was realized by an IS calculation mode (the retention time of IS in the LC system is 6.6 min and the measured transition is 144 → 117). Linearity was observed in the concentration range of 5–200 nM for ^{15}N-nitrite ion and RS^{15}NOs, and 100–2000 nM for ^{15}N-nitrate ion, with the coefficient of determination (R^2) values more than 0.995. Accuracy ranged from 90.6 to 109.4%. Intra- and inter-day precision expressed as RSD % was between 8.8 and 11.6, and 11.2 and 12.9%, respectively. All these values comply with FDA rules ($R^2 \geq 0.99$; 85% ≤ recovery ≤ 115%; RSD % ≤ 15%).[21]

Intestinal permeability of GS^{15}NO was evaluated by determining the permeated concentrations of its metabolites, *i.e.* RS^{15}NOs, ^{15}N-nitrite and ^{15}N-nitrate ions, after a 2 h incubation measured by DAN derivatization and LC-ESI-ITMS/MS. Previous measurements carried out in spectrofluorimetry after DAN derivatization failed to give data, because the concentrations of all quantified metabolites in the sample were lower than LOQ (250 nM, S/B = 5). As shown in Fig. 3, less than 1% of initial GS^{15}NO was permeated through intact isolated rat intestine (around 0.04%, 0.08% and 0.15% of RS^{15}NOs, ^{15}N-nitrite and ^{15}N-nitrate ions, respectively). Based on calculation of P_{app} values (1.00 ± 0.11, 2.18 ± 0.15 and 3.93 ± 0.37 × 10^{-6} cm s^{-1} for RS^{15}NOs, ^{15}N-nitrite and ^{15}N-nitrate ions, respectively), it can be concluded that GSNO belongs to the medium permeability class according to FDA guidelines with P_{app} value of (7.12 ± 0.62) × 10^{-6} cm s^{-1}, which is in the range of 10^{-6} to 10^{-5} cm s^{-1}. In the Biopharmaceutics Classification System,[16] an excellent candidate drug for oral administration to treat chronic diseases should be highly soluble and permeable. GSNO is a soluble compound with medium permeability, thus it can be considered for oral administration.

Conclusion

Both Griess and DAN assays based on use of ^{15}N labeling of nitrite ion and LC-ESI-ITMS/MS succeeded in improving LOQ. Noteworthy, the blank value is still not neglected due to interferences between isotopes. The DAN assay under HCD mode provides a lower LOQ (*ca.* 5 nM) than the Griess one (100 nM). Thus, DAN assay under HCD mode for NAT fragmentation has been further applied for GSNO intestinal permeability studies. This method has the advantage of monitoring NO species released from GS^{15}NO in the nanomolar range, and differentiating them from other sources (endogenous synthesis and diet). Preliminary data presently obtained about GSNO intestinal permeability offer the perspective to use it as an oral drug candidate in CVDs chronic treatment. To evaluate its bioavailability more deeply, the development and validation of this method in a more complex matrix (such as plasma) should be performed to conduct further pharmacokinetic study.

Conflicts of interest

There are no conflicts to declare.

Acknowledgements

Authors are grateful to the program of China Scholarship Council for the financial support of Ms Haiyan Yu's PhD thesis (grant No. 201506270166). Authors also thank Dr Philippe Giummelly (CITHEFOR, Université de Lorraine) for realizing the synthesis of GS^{15}NO.

References

1 S. S. Gill, M. Hasanuzzaman, K. Nahar, A. Macovei and N. Tuteja, *Plant Physiol. Biochem.*, 2013, **63**, 254–261.
2 S. Moncada, R. M. Palmer and E. A. Higgs, *Pharmacol. Rev.*, 1991, **43**, 109–142.
3 B. van der Loo, R. Labugger, J. N. Skepper, M. Bachschmid, J. Kilo, J. M. Powell, M. Palacios-Callender, J. D. Erusalimsky, T. Quaschning, T. Malinski, D. Gygi, V. Ullrich and T. F. Lüscher, *J. Exp. Med.*, 2000, **192**, 1731–1744.
4 C. Gaucher, A. Boudier, F. Dahboul, M. Parent and P. Leroy, *Curr. Pharm. Des.*, 2013, **19**, 458–472.
5 E. R. Axton, E. A. Hardardt and J. F. Stevens, *J. Chromatogr. B*, 2016, **1019**, 156–163.
6 H. Kabuto, M. Yamamoto, I. Yokoi and N. Ogawa, *Clin. Chim. Acta*, 1997, **266**, 199–200.
7 J. Emsley, *New Sci.*, 1984, **103**, 41–42.
8 D. Tsikas, J. Sandmann, F.-M. Gutzki, D. O. Stichtenoth and J. C. Frölich, *J. Chromatogr. B*, 1999, **726**, 13–24.
9 E. Hanff, M. F. Eisenga, B. Beckmann, S. J. L. Bakker and D. Tsikas, *J. Chromatogr. B*, 2017, **1043**, 167–175.
10 E. Hanff, M. Luetzow, A. A. Kayacelebi, A. Finkel, M. Maassen, G. R. Yancheva, A. Haghikia, U. Bavendiek, A. Bucke, T. Luecke, N. Maassen and D. Tsikas, *J. Chromatogr. B*, 2017, **1047**, 207–214.
11 S. Shin and H.-L. Fung, *J. Pharm. Biomed. Anal.*, 2011, **56**, 1127–1131.
12 M.-R. Chao, Y.-M. Shih, Y.-W. Hsu, H.-H. Liu, Y.-J. Chang, B.-H. Lin and C.-W. Hu, *Free Radic. Biol. Med.*, 2016, **93**, 77–83.
13 E. Hanff, A. Boehmer, J. Jordan and D. Tsikas, *J. Chromatogr. B*, 2014, **970**, 44–52.
14 M. Parent, F. Dahboul, R. Schneider, I. Clarot, P. Maincent, P. Leroy and A. Boudier, *Curr. Pharm. Anal.*, 2013, **9**, 31–42.
15 W. Wu, C. Gaucher, R. Diab, I. Fries, Y.-L. Xiao, X.-M. Hu, P. Maincent and A. Sapin-Minet, *Eur. J. Pharm. Biopharm.*, 2015, **89**, 1–8.
16 M. Marzinzig, A. K. Nussler, J. Stadler, E. Marzinzig, W. Barthlen, N. C. Nussler, H. G. Beger, S. M. Morris Jr and U. B. Brückner, *Nitric Oxide*, 1997, **1**, 177–189.
17 W. S. Jobgen, S. C. Jobgen, H. Li, C. J. Meininger and G. Wu, *J. Chromatogr. B*, 2007, **851**, 71–82.

18 P.-A. Bilat, E. Roger, S. Faure and F. Lagarce, *Drug Discov. Today*, 2017, **22**, 761–775.
19 E. Neirinckx, C. Vervaet, J. Michiels, S. de Smet, W. van den Broeck, J. P. Remon, P. de Backer and S. Croubels, *J. Vet. Pharmacol. Therapeut.*, 2011, **34**, 290–297.
20 E. Sawicki, T. W. Stanley, J. Pfaff and A. D'Amico, *Talanta*, 1963, **10**, 641–655.
21 V. P. Shah, K. K. Midha, J. W. Findlay, H. M. Hill, J. D. Hulse, I. J. McGilveray, G. McKay, K. J. Miller, R. N. Patnaik, M. L. Powell, A. Tonelli, C. T. Viswanathan and A. Yacobi, *Pharm. Res.*, 2000, **17**, 1551–1557.

2. Experimental paper: "Higher-energy Collision Dissociation for the quantification by liquid chromatography/tandem ion trap mass spectrometry of nitric oxide metabolites coming from S-nitrosoglutathione in an in vitro model of intestinal barrier" in *Rapid Communications in Mass Spectrometry (under minor revision)*

Detailed procedures used for experiments in this article are present in protocols (see appendices) entitled "Measurement of nitrite, nitrate ions and S-nitrosothiols using the 2,3-diaminonaphthalene assay by LC coupled with tandem mass spectrometry" and "Intestinal permeability studies of S-nitrosothiols using a Caco-2 cell monolayer model".

Higher-energy Collision Dissociation for the quantification by liquid chromatography-tandem ion trap mass spectrometry of nitric oxide metabolites coming from *S*-nitrosoglutathione in an *in vitro* model of intestinal barrier

Yu Haiyan[1], Bonetti Justine[1], Gaucher Caroline[1], Fries Isabelle[1], Vernex-Loset Lionel[2], Leroy Pierre[1], Chaimbault Patrick[2,*]

[1] Université de Lorraine, CITHEFOR, F-54000 Nancy, France

[2] Université de Lorraine, LCP-A2MC, F-57000 Metz, France

* Correspondence to: Chaimbault Patrick, SRSMC UMR 7565, ICPM, 1 boulevard Arago, 57070 Metz, France

E-mail: patrick.chaimbault@univ-lorraine.fr

Abstract

RATIONALE: The potency of *S*-nitrosoglutathione (GSNO) as a nitric oxide (NO) donor to treat cardiovascular diseases (CVDs) has been highlighted in numerous studies. In order to study its bioavailability after oral administration, which represents the most convenient route for the chronic treatment of CVDs, it is essential to develop an analytical method permitting *(i)* the simultaneous measurement of GSNO metabolites, *i.e.* nitrite, *S*-nitrosothiols (RSNOs) and nitrate and *(ii)* them to be distinguished from other sources (endogenous synthesis and diet).

METHODS: Exogenous GSNO was labeled with ^{15}N, and the $GS^{15}NO$ metabolites after conversion to nitrite ion were derivatized with 2,3-diaminonaphthalene. The resulting 2,3-naphthotriazole was quantified by liquid chromatography-tandem ion trap mass spectrometry (LC/ITMS/MS) in multiple reaction monitoring mode after Higher-energy Collision Dissociation (HCD). Finally, the validated method was

applied to an *in vitro* model of intestinal barrier (monolayer of Caco-2 cells) to study $GS^{15}NO$ intestinal permeability.

RESULTS: A LC/ITMS/MS method based on an original transition (*m/z* 171 → 156) for sodium ^{15}N-nitrite, $GS^{15}NO$ and sodium ^{15}N-nitrate measurements was validated, with recovery of 100.8 ± 3.8, 98.0 ± 2.7 and 104.1 ± 3.3 %, respectively. Intra- and inter-day variabilities were below 13.4 and 12.6 %, and the limit of quantification reached 5 nM (signal over blank = 4). The permeability of labeled $GS^{15}NO$ (10-100 µM) was evaluated by calculating its apparent permeability coefficient (P_{app}).

CONCLUSIONS: A quantitative LC-ITMS/MS method using HCD was developed for the first time to selectively monitor $GS^{15}NO$ metabolites. The assay allowed evaluating $GS^{15}NO$ intestinal permeability and situated this drug candidate within the middle permeability class according to FDA guidelines. In addition, the present method has opened the perspective of a more fundamental work aiming at studying the fragmentation mechanism leading to the ion at *m/z* 156 in HCD tandem mass spectrometry in the presence of acetonitrile.

Key words: ^{15}N-nitrite, ^{15}N-nitrate, ^{15}N-*S*-nitrosoglutathione, 2,3-diaminonaphthalene, LC-ITMS/MS

INTRODUCTION

Nitric oxide (NO) is a gaseous messenger playing an important role in the vascular system homeostasis[1]. Its origin includes both endogenous (catabolism of arginine catalyzed by endothelial NO synthase)[2,3] and exogenous (intake of drinking water and food)[4] sources. The endogenous production of NO decreases with ageing[5] and cardiovascular diseases (CVDs) related to endothelial dysfunction. In this case, an exogenous supply of NO is necessary. Currently, drugs used as NO donors have major drawbacks such as oxidative stress induction and tolerance phenomenon[6,7]. Many studies highlight the potency of *S*-nitrosothiols (RSNOs) as NO donors, especially *S*-nitrosoglutathione (GSNO)[8], because they do not exhibit the side effects previously cited[9]. However, very few reports have been focused on their bioavailability after oral administration[10], which is their most convenient route for the chronic treatment of CVDs. The small intestine is the major barrier for the efficient absorption of orally administered therapeutics[11,12]. Caco-2 trans-epithelial permeability assay (monolayer of differentiated Caco-2 cells) is commonly used for intestinal absorption studies of drugs [13,14]. Thus, using this Caco-2 cell monolayer model to evaluate the intestinal permeability of GSNO is the first step to study its oral bioavailability.

In a biological environment, GSNO is easily decomposed by metal ions, reductants, enzymes or light, resulting in a release of NO[9]. This reactive species is then rapidly oxidized into nitrite and nitrate ions[4]. Moreover, GSNO undergoes a transnitrosation process corresponding to NO moieties exchange with a cysteine residue of peptides and proteins, resulting in a formation of RSNOs[8]. The different GSNO metabolites, *i.e.* nitrite, nitrate ions and RSNOs, represent a NO reservoir[9]. *S*-nitrosation of proteins is also a post-translational pathway playing a key role in many physiopathological processes[8,9,15]. GSNO metabolites should be measured together because they give complementary information[4,8,9]. Thus, there is a great need to

develop appropriate assays in this field. Actually, very few assays allow the determination of all cited NO species using the same method[16,17,18].

Mass spectrometry is a widespread technique used for the quantification of metabolites of interest in biological samples because of its high specificity of detection (multiple reaction monitoring (MRM) mode) and its sensitivity for trace level measurement. Because of its low molecular mass, NO (30 u) has to be derivatized to allow its measurement in cells or biological fluids (urine, plasma, etc). Indeed, it is not possible for many commercially available mass spectrometers to reach such a low *m/z* value and the background noise is usually high at low masses. As mentioned above, NO is rapidly converted into nitrite and nitrate ions, which are the real derivatized compounds. For pharmacology studies, there is a need to quantify NO species coming from administered NO donor drugs regardless of whether they come from endogenous synthesis or diet intake. Mass spectrometry allows distinguishing NO species coming from administered NO donors and those from endogenous synthesis and diet intake, thanks to the incorporation of the stable nitrogen isotope ^{15}N into the NO donor (presently GS^{15}NO). Indeed, the ^{15}N isotope is stable and its natural abundance level represents 0.37% of all nitrogen isotopes[19]. Thus, it is possible to monitor specifically adducts labeled either with ^{14}N (corresponding to the endogenous production and the diet uptake) or with ^{15}N (corresponding to the drug uptake).

In addition to the increase in molecular mass, the derivatization procedure facilitates nitrite and nitrate ions analysis either by gas chromatography (the nitrite ion is transformed into a volatile derivative) or by Reversed Phase Liquid Chromatography (nitrite ion is transformed into a more hydrophobic derivative increasing the retention on this kind of stationary phases). The GC-CI-MS method developed by Tsikas *et al* uses pentafluorobenzyl bromide (PFBBr) for ^{15}N-nitrite and ^{15}N-nitrate derivatization. It has the benefit of measuring derivatized nitrite and nitrate ions in the same chromatographic run[20]. The method in liquid chromatography-

tandem mass spectrometry (LC-MS/MS) reported by Hanff and coworkers uses reduced *L*-glutathione (GSH) for ^{15}N-nitrite derivatization and simultaneously analyzes nitrite ion and GSNO[21]. This assay relies upon the *S*-nitrosation reaction between GSH as a probe and the nitrite ion to yield GSNO. 2,3-diaminonaphthalene (DAN) is a fluorogenic probe which reacts with nitrite ion to yield 2,3-naphthotriazole (NAT) adduct[22] (Figure 1A). It has been widely used with spectrofluorimetric direct detection[23] or coupled with LC[22] and even LC-MS/MS associated with ^{15}N-nitrite derivatization and ^{15}N-nitrate after reduction *via* enzymatic catalysis[24,25,26] (Figure 1C). Currently, there is no report of using LC-MS/MS to measure RSNOs after DAN derivatization. For RSNOs, mercuric ions are commonly used to cleave the *S*-NO bond with further analysis of released nitrite ion[27] (Figure 1B).

This paper presents the development of a DAN-based LC-MS/MS assay for selectively monitoring all NO species metabolized from ^{15}N-labeled GSNO (nitrite, nitrate ions and RSNOs). For the first time, all these NO species will be quantified using the same analytical approach, providing a significant contribution to understanding the mechanism of GSNO metabolism. Currently, the publications related to a DAN-based LC-MS/MS assay[24,25,26] involve either a triple quadrupole mass spectrometer or a Q-trap instrument (operated as a triple quadrupole). This is easily understandable as triple quadrupole apparatus are well known to be the most sensitive tandem mass spectrometers for quantification when they are operated in MRM mode. However, this kind of spectrometer is not always available in the laboratory, and here we evaluated the sensitivity of Ion Trap Mass Spectrometry (ITMS) for the quantification of NO traces associated to the potential benefit of the Higher-energy Collision Dissociation (HCD) mode in this field. This original fragmentation method which cannot be used with a triple quadrupole mass spectrometer was compared with the traditional Collisionally Induced Dissociation (CID) available on both ion trap and triple quadrupole mass spectrometers. Thus, the

presented method involves liquid chromatography coupled to tandem ion trap mass spectrometry (LC-ITMS/MS) for the selective quantification of NO species metabolized from $GS^{15}NO$. DAN will be used for the derivatization of free ^{15}N-nitrites and ^{15}N-nitrites coming from ^{15}N-nitrates and $RS^{15}NO$ species. The resulting adduct will be further analyzed by LC-ITMS/MS. Finally, the method will be validated and applied to study the intestinal permeability of $GS^{15}NO$ with use of an *in vitro* model.

EXPERIMENTAL

Chemicals and reagents

All reagents and standards are analytical grade and used without further purification. DAN, GSH, sodium ^{15}N-nitrate ($Na^{15}NO_3$), 2-naphthylamine (2-NA) and mercuric chloride ($HgCl_2$) were obtained from Sigma-Aldrich (Saint-Quentin-Fallavier, France); sodium ^{15}N-nitrite ($Na^{15}NO_2$) was from Cambridge Isotope Laboratories (Tewksbury, MA, USA) and ^{14}N-NAT from Chemodex (St. Gallen, Switzerland). Ultrapure deionized water (> 18.2 MΩ·cm) was used for the preparation of all solutions.

S-nitrosoglutathione ($GS^{15}NO$) synthesis

$GS^{15}NO$ was synthesized as already described[28] for $GS^{14}NO$: 20 mM GSH was incubated with 20 mM $Na^{15}NO_2$ in 500 mM HCl at 4°C in the dark for 1 h. The reaction was stopped by neutralization with NaOH (40%) and the reaction mixture was further two-fold diluted with 500 mM phosphate buffer, pH 7.4. The final concentration was determined by UV spectrophotometry at a wavelength of 334 nm (ε = 922 $L \cdot mol^{-1} \cdot cm^{-1}$).

2,3-Diaminonaphthalene (DAN) derivatization

Different GS^{15}NO metabolites (^{15}N-nitrites, ^{15}N-nitrates and RS^{15}NO) generated during the *in vitro* study were quantified using the same LC-ITMS/MS approach after DAN derivatization. This strategy of analysis is depicted in Figure 2.

^{15}N-nitrite standard solutions were prepared daily in Hank's Balanced Salt Solution (HBSS; NaCl, KCl, glucose, KH_2PO_4, Na_2HPO_4, $CaCl_2$, $MgSO_4$, pH 7.4). Three hundred µL of standard solutions were mixed with 60 µL of 0.105 mM DAN in 0.6 M HCl, incubated at 37°C for 10 min (Figure 1A). The addition of 36 µL of 1 M NaOH and 4 µL of 0.1 mM NaOH stopped the reaction. The real samples were similarly treated and their analysis provided the concentration of free ^{15}N-nitrites in the *in vitro* model (①).

^{15}N-nitrate was enzymatically converted into ^{15}N-nitrite by using Nitrate/Nitrite Fluorometric Assay Kit (Cayman Chemical, Ann Arbor, MI, USA) with some modifications (Figure 1C). Briefly, 40 µL of ^{15}N-nitrate standard solutions were diluted with 120 µL of assay buffer (Item N0. 780022). The resulting mixture was incubated at room temperature for 60 min after adding 20 µL of enzyme cofactor (Item N0. 780012) and 20 µL of nitrate reductase (Item N0. 780010). To continue the derivatization reaction, the mixture was immediately processed as described for the nitrite ion by adding 40 µL of 0.105 mM DAN and incubating at 37°C for 10 min, followed by the addition of 24 µL of 1 M NaOH and 3 µL of 0.1 mM NaOH. The real samples were similarly treated and their analysis provided the cumulative concentration of free ^{15}N-nitrites and ^{15}N-nitrates (②) in the *in vitro* model. The ^{15}N-nitrate concentration in the *in vivo* model (③) was then obtained by subtracting the concentration of free nitrites (③=②-①).

The quantification of RS^{15}NOs is carried out using a calibration curve built with GS^{15}NO in presence of mercuric ions: 300 µL of GS^{15}NO standard solution were incubated with 60 µL of 0.105mM DAN solution containing 1.05 mM $HgCl_2$ in 0.6 M HCl at 37 °C for 10 min. The addition of 36 µL of 1 M NaOH and 4 µL of 0.1 mM

NaOH stopped the reaction. The real samples were similarly treated to provide the cumulative concentration of free ^{15}N-nitrites and RS^{15}NO (④) in the *in vitro* model. The RS^{15}NO concentration in the *in vivo* model (⑤) was then obtained by subtracting the concentration of free nitrites (⑤=④-①).

All resulting solutions were frozen at −80 °C for a maximum period of 3 months, until analysis by LC-ITMS/MS.

2-Naphthylamine (2-NA) was used as internal standard (IS). For quantitative analysis, each sample was spiked with 10 µL of a 0.02 mM solution of 2-NA prepared in acetonitrile-water (50/50, v/v).

Analysis of 2,3-naphthotriazole (NAT) by LC-ITMS/MS

A Dionex Ultimate 3000 liquid chromatograph (Dionex, Sunnyvale, CA, USA) was coupled with an ion trap mass spectrometer (LTQ Velos Pro, Thermo Scientific, San Jose, CA, USA) fitted with the HESI-II probe (electrospray) operated in positive ion mode. Data were collected and analyzed with Tune Plus software (Thermo Scientific). The injection volume was 20 µL. The separation was carried out on a Thermo Scientific Extend-C18 (2.1 × 150 mm ID, 3 µm) column at a temperature of 25 °C. The mobile phase was composed of A: 0.01 M acetic acid and B: acetonitrile, delivered at 200 µL·min^{-1} in a gradient mode. The column was first equilibrated at 40% B. When the sample was injected, the percentage of B increased to 80% over 3.5 min and held for 2.5 min. The column was re-equilibrated for 10 min between two sample runs. In these chromatographic conditions, NAT is eluted from the column in 5.5 min and 2-NA in 6.6 min (Figure 3). In addition, during the first 3 min, the mobile phase was directed to waste using a switching valve in order to limit the contamination of the mass spectrometer by the matrix.

The electrospray voltage was +5.0 kV. The ion source and capillary temperatures were 280 and 250 °C, respectively. The sheath, auxiliary and sweep gas flows were set at 10, 5 and 0 (arbitrary units) respectively. For quantification, the best MS/MS conditions were reached by optimizing the collision energy for each analyte in order

to obtain the highest signal. The selected reaction monitoring (SRM) method recorded the following transitions for the analytes: *m/z* 171 → 156 for ^{15}N-NAT or *m/z* 170 →156 for ^{14}N-NAT (the choice of these transitions will be discussed later on in the result and discussion section) obtained in HCD at 50 eV and *m/z* 144 → 117 for the IS (2-NA) in CID at 35 eV. The activation Q value was 0.250 and the isolation window was 1u for each transition.

Samples were randomized to prevent batch effect, paired and run in sequence.

Method validation and quality control

A six-point calibration curve (blank, 5, 10, 20, 50, 100, 200 nM) for $Na^{15}NO_2$ and $GS^{15}NO$, and a five-point calibration curve (blank, 250, 500, 1250, 2500, 5000 nM) for $Na^{15}NO_3$ were made in HBSS. They were used to calculate the limits of quantification (LOQ), to check the linear range and to determine the percentage of recovery. Background levels of ^{15}N-nitrite, $GS^{15}NO$ and ^{15}N-nitrate in HBSS corresponding to blanks were measured and subtracted from all quantification values. Three concentrations (15, 50 and 180 nM) of $Na^{15}NO_2$ and $GS^{15}NO$ and (300, 2500 and 4000 nM) of $Na^{15}NO_3$ in HBSS were analyzed six times to determine the intra-day precision and accuracy. The number of replicates for the inter-day validation was also six. The inter-day statistics were determined from three independent analytical runs, each containing the calibration standards and two QC samples at low, medium and high concentration levels. A six-point calibration curve of $Na^{15}NO_2$ in HBSS was daily run to assess instrument performances.

Permeability studies of $GS^{15}NO$ on Caco-2 cell monolayer model

The permeability of $GS^{15}NO$ across the Caco-2 monolayer was evaluated in the apical-to-basolateral direction in HBSS buffer containing Ca^{2+} and Mg^{2+} as previously described[10]. Briefly, 2×10^6 cells·cm^{-2} were seeded on cell culture inserts (Transwell®, Corning, NY, USA) with 0.4 µm pore size disposed in a 12-wells plate. The medium was replaced every two days during the first week and daily during the final days, until the differentiated cell monolayer was formed (14-18 days, transepithelial

electrical resistance (TEER) > 500 Ω·cm^{-2}). TEER was measured with a Millicell®-Electrical Resistance System (Millipore, Billerica, MA, USA).

For permeation experiments, 500 µL of HBSS containing 10, 25, 50 or 100 µM of GS^{15}NO were introduced into the apical (donor) compartment. The basolateral (receptor) compartment was filled with 1.5 mL of HBSS. After 1 h of permeation at 37°C, both compartments were harvested and diluted with HBSS to fit the ranges of calibration curves for ^{15}N-nitrite, GS^{15}NO and ^{15}N-nitrate analysis. The resulting dilutions were immediately derivatized with DAN and stored at -80 °C until analysis by LC/ITMS/MS. After each permeation study, the integrity of the Caco-2 cell monolayer was evaluated by TEER measurement and sodium fluorescein (5 µM) permeability assessment.

The cumulative amounts of GS^{15}NO permeated through the Caco-2 cell monolayer were calculated from the concentrations measured in the basolateral compartment. The apparent permeability coefficient (P_{app}) values were calculated using the following equation:

$$P_{app} = \frac{dQ}{dt} \times \frac{1}{A \times C_0}$$

dQ/dt (mol·s^{-1}) refers to the quantity of permeated ^{15}NO species (dQ) in the basolateral compartment at the time of quantification (dt), A refers to membrane diffusion area (1.12 cm^2), and C_0 refers to the initial concentration of GS^{15}NO in the apical compartment (from 1.10^{-5} to 1.10^{-4} M).

For each concentration level evaluated (incubation with 10, 25, 50 and 100 µM of GS^{15}NO), the permeation experiments were carried out 3 times.

Statistical analysis

All results are expressed as the means ± standard deviation. The Student's t-test was used to determine significant differences ($p < 0.05$).

RESULTS AND DISCUSSION

Nitric oxide is very unstable and turns rapidly into nitrite ion (NO_2^-) which is the real measured compound. .In the field of LC, nitrites are often derivatized by the 2,3-diaminonaphthalene (DAN) (Figure 1). The resulting 2,3-naphthotriazole (NAT) derivative allows its detection by fluorescence. The DAN-based fluorescence LC method is particularly appreciated for the analysis of nitrites (and nitrates after enzymatic reduction) in all biological samples because of its simplicity of use, the rapidity of the sample preparation, and the easy automation[29]. However, the fluorescence detection does not allow the distinction of isotope labeling and the quantification of NO metabolites in the nM range (LOQ is around 100 nM with DAN-based fluorescence HPLC).

Currently, there are three publications related to DAN-based LC-MS/MS assays found in the literature[24,25,26]. All these experiments were carried out either with a triple quadrupole or with a Q-trap instrument (operated as a triple quadrupole) using the CID fragmentation mode. In 2011, Shin *et al.*[26] reached a LOQ of 4nM and their method was only validated for the measurement of NO_2^-. In 2016, Chao *et al.*[24] published the quantification of NO_2^- and of NO_3^- in urine by DAN-based LC-MS/MS after on-line solid phase extraction. For the first time, the interference on the ^{15}N-labeled NAT due to the natural presence of ^{13}C is evoked and estimated to be 2.2% (in good agreement with the theoretical value) of the contribution of the followed transition for this derivative. The same year, Axton *et al.*[25] reached a LOQ of 1nM in water and in the Dulbecco's Modified Eagle Medium (DMEM). However, the values of interferences in the blank samples were not discussed whereas they were 91 and 339 nM for ^{14}N-nitrites in water and DMEM respectively. Thus, the interference due to ^{13}C on the signal of ^{15}N-nitrite derivative in the blank samples should be around 2 nM in water and 7.5 nM in DMEM. These interference levels have to be considered to appreciate the LOQ in the real samples.

In this paper, we evaluated the sensitivity of an Ion Trap Mass Spectrometer associated to the HCD mode for the quantification of NO metabolite traces. To achieve this goal, we compared the performance of the HCD mode with the traditionally used CID mode, and the blank values were also discussed to provide the LOQ in the real samples. The method developed and validated in this paper was also tested to monitor NO freed from GSNO.

Optimization of the LC-ITMS/MS detection - Comparison between CID and HCD

The NAT adduct resulting from the derivatization of nitrite ion with DAN was quantified by LC/ITMS/MS. Its quantification at trace level supposed the optimization of the whole analytical pathway. Among the existing literatures on NAT analysis by reversed phase LC/MS/MS, acetonitrile (ACN) and methanol (MeOH) have been used as organic modifiers in the mobile phase in combination with various acidic buffers. In our study, the most intense MS signal was obtained with a 10 mM acetic acid solution combined with ACN in gradient elution (see experimental section for details). Acetonitrile improved the sensitivity of NAT detection by a factor of 10 compared with MeOH. The analysis took 7 min with a re-equilibration time of 10 min between two injections. The gradient helped to reduce peak widths and thus improved the sensitivity.

Acetonitrile also showed another interesting effect when we compared the two modes of fragmentation with the LTQ Velos Pro ion trap instrument: the commonly used CID and HCD. The CID mode led to the same fragmentation pathway already published when using a triple quadrupole instrument[24,25,26] (Figure 4A). The protonated ^{14}N-NAT (m/z 170) yielded two product ions at *m/z* 142 (loss of N_2) and *m/z* 115 (the indene ion $[C_9H_7]^+$ derived from *m/z* 142 and comprising the rest of the naphthyl ring after the loss of HCN)[25].

The fragmentation in HCD was slightly different from that in CID (Figure 4B). When *m/z* 170 is isolated and MS/MS experiments are carried out on this ion, the ultimate product ion at *m/z* 115 remained the same but the intermediate product ion was now observed at *m/z* 156. Thus, there is a difference of 14 u between this product ion and its precursor ion. This difference, which cannot obviously be assigned to a loss of a single nitrogen atom (N) or a methylene group (CH_2), has another complex origin which has been resolved through several complementary experiments detailed below (Figures 4C and 4D, and Table 1):

- When MeOH replaced ACN in the mobile phase, both the CID and HCD spectra showed the same transition. In both cases, the precursor ion $[^{14}N\text{-NAT+H}]^+$ produced two transitions *m/z* 170 → 142 and *m/z* 170 → 115. Thus, the presence of ACN is responsible of the original fragment at m/z 156.
- In this work, ^{15}N-NAT is quantified in order to monitor NO coming from the parent drug. Its corresponding HCD MS/MS spectrum is provided in Figure 4D. The precursor ion $[^{15}N\text{-NAT+H}]^+$ produced two transitions: *m/z* 171 → 156 and *m/z* 171 → 115. The observed fragments are the same as for $[^{14}N\text{-NAT+H}]^+$. The conclusion is that ^{15}N is lost during the fragmentation *m/z* 171 → 156.
- In order to understand what happened in the HCD cell with ACN during the fragmentation, the ^{14}N- and ^{15}N-labeled NAT were infused using the LC mobile phase containing either ACN or d_3-ACN. The results are displayed in Table 1, and Figures 4C and 4D. The hypothesis was the formation of a $[NAT+H+ACN]^+$ adduct, confirmed by the presence of a peak at *m/z* 211 for ^{14}N-NAT in ACN and *m/z* 214 in d_3-ACN. This adduct underwent a rearrangement during fragmentation leading to *m/z* 183 by N_2 loss (*m/z* 186 with d_3-ACN). Then, an additional HCN loss led to *m/z* 156 from *m/z* 183 or *m/z* 159 from *m/z* 186 with d_3-ACN. All these ions were perfectly visible on the mass spectra (even if some of them exhibited a very low intensity). The values of *m/z* observed for each ion were consistent with this explanation whatever the derivative (^{14}N or ^{15}N-NAT) and the solvent

condition (ACN or d_3-ACN), as illustrated in Table 1 and Figure 4. From these last experiments, we concluded that ACN probably strongly interacted with the $[NAT+H]^+$ ion in the HCD cell. This is probably due to the specific position of the HCD cell in the LTQ Velos Pro mass spectrometer (see supplementary data, Figure S1), which is located upstream of the CID trap. In this particular design, the parent ion is first isolated in the linear ion trap, then ejected back to the Q_{00} region where its fragmentation occurs. Next, the generated fragments are directed toward the linear ion trap where they are analyzed. In this process, it is easy to understand that the solvent vapors can enter the HCD cell making the possible reaction between $[NAT+H]^+$ and ACN to produce this original fragmentation pathway. The fragmentation pathway can be summarized as follows ($[^{14}N\text{-}NAT+H]^+$ is taken as example):

- In CID, *m/z* 170 losses N_2 to give m/z 142 which in turn loses HCN to give *m/z* 115. This pathway was checked by MS^3 which allows the observation of the transition *m/z* 142 → 115.
- In HCD, *m/z* 170 reacts or interacts with ACN to give m/z 211 ($[^{14}N\text{-}NAT+H+ACN]^+$). Then m/z 211 undergoes two consecutive fragmentations, one loss of N_2 (m/z 183) and one loss of HCN, to give the original *m/z* 156. Unfortunately, the signal intensities of *m/z* 211 and 183 are too weak to check this pathway by MS^3. But interestingly, these neutral losses are precisely the same (and in the same order) as observed from m/z 170 in CID. The last step consists in the loss of the solvent molecule from *m/z* 156 to restore m/z 115 also observed in CID. This final pathway was checked by an MS^3 experiment in CID at 35 eV, which allows the observation of the transition *m/z* 156 → 115. The ion *m/z* 156 can be somehow described as the ACN adduct of m/z 115 $[C_9H_7+ACN]^+$, then *m/z* 183 is corresponding to the ACN adduct of m/z 142 (in CID) but the precursor of these fragment ion *m/z* 211 ($[^{14}N\text{-}NAT+H+ACN]^+$) is

not observed in the source (see supplementary data, Figure S2) meaning that the ACN adduct is only formed thank to the HCD process.

The reaction mechanism remains unclear at this time and its elucidation would deserve future investigation, but the combination of ACN in the mobile phase and the HCD mode allowed us to reach a limit of quantification of 1 nM for the NAT adduct, by following the new SRM transition (i.e. *m/z* 171 → 156 for ^{15}N-NAT). For the transition *m/z* 171 → 115, the LOQ was 10 nM in HCD mode and only 20 nM in CID (best achievable results in CID). This value was within the same range as in previous studies for the measurement of ^{15}N-nitrite by LC-MS/MS[25,26]. The chosen transitions for each compound (including the IS, i.e. the 2-naphthylamine) are reported in the experimental section. The method was then validated to monitor with accuracy the NO species freed from GSNO in an *in vitro* model of intestinal barrier at trace levels.

Interferences in blank samples and working LOQ

The final objective of this study is to assess the permeability of GSNO across the intestinal barrier by means of an *in vitro* model (Caco-2 monolayer). During the incubation, Caco-2 cells secreted many metabolites into the buffer, including unlabeled NO species. Thus, the incubation medium turned into a complex biological matrix, which required a high specific or selective method of analysis. In this field, LC-MS/MS has become the standard technique, being much more specific, selective and even much more sensitive than most other conventional spectroscopic techniques (UV and even fluorescence). The selectivity has been tested by analyzing corresponding blanks (untreated cells).

When developing a reliable quantitative analysis of ^{15}N-nitrite, there is a clear risk of interference between ^{15}N-NAT and ^{14}N-NAT containing one ^{13}C atom (due to its natural abundance of 1.1%). Chao *et al*[24] showed a 2.2%-interference due to ^{13}C, which was in good agreement with what is theoretically expected. We did not observe any interference when the quantification was performed using fresh reactants and

culture medium. Thus, a LOQ of 1 nM was obtained LC-ITMS/MS which is comparable to the LOQ obtained by Axton *et al.* on their Q-Trap[25]. However, ambient nitrogen oxides (NOx) are rapidly able to dissolve into them, leading to an interference in the experimental blanks (Figure 5). This interference was estimated to be around 50 to 60 nM in ^{14}NOx (using the transition *m/z* 170 → 156), which is equivalent to the signal of 1 nM of ^{15}N-NAT for the corresponding transition (m/z 171 → 156). Consequently, the working LOQ was set at 5 nM for the validation step, taking in account the signal-over-blank ratio rather than the signal-over-noise one. Nevertheless, this concentration level is satisfactory enough for the accurate quantification of nitrites in the real samples.

Method validation

The next step of this study was the investigation of the linearity range, reproducibility, accuracy, precision, interferences, percent recovery, and carryover of the developed LC-ITMS/MS method.

The linearity range and the LOQ were determined from 3 standard curves of nitrite ions. The LOQ was limited to 5 nM, as described in the previous section. The calibration curve of ^{15}N-NAT adduct was linear between 5 and 200 nM for $Na^{15}NO_2$ and $GS^{15}NO$ and between 250 and 5000 nM for $Na^{15}NO_3$, with the coefficient of determination (r^2) higher than 0.9956. The intra- and inter-day variabilities of the method were evaluated by using quality control samples and the results are summarized in Table 2. Three concentrations of $Na^{15}NO_2$ and $GS^{15}NO$ (15, 50, 180 nM), and of $Na^{15}NO_3$ (300, 2500, 4000 nM) were spiked into HBSS (n = 6), and the concentration was calculated by using a six-point calibration curve for $Na^{15}NO_2$ and $GS^{15}NO$ (5, 10, 20, 50, 100, 200 nM), and for $Na^{15}NO_3$ (250, 500, 1250, 2500, 5000 nM). The accuracy was determined as the deviation (%) of the calculated concentrations from the nominal concentrations. The precision was determined as the

relative standard deviation (RSD) of the six measurements. Satisfactory accuracies were obtained with intra- and inter-day bias lower than 5.2 % and 5.3 % for $Na^{15}NO_2$, 1.9 % and 6.7 % for $GS^{15}NO$, and 7.7 % and 9.4 % for $Na^{15}NO_3$, respectively, over the studied concentration ranges. The intra- and inter-day precision ranged from 3.0 to 7.1 % for $Na^{15}NO_2$, from 7.7 to 13.4 % for $GS^{15}NO$ and from 5.6 to 8.7 % for $Na^{15}NO_3$ in HBSS. These ranges were within the criteria stated in the FDA guidance on bioanalytical method validation (Table 2).

Additionally, the product NAT was found stable after storage at -80 °C for 3 months and freezing/thaw for 2 cycles (data not shown).

Intestinal permeability of $GS^{15}NO$ *in vitro*

To evaluate the intestinal permeability of nitrate, nitrite and RSNOs, we needed to determine their concentration in the apical and basolateral compartments after incubation (Figure 6). To the best of our knowledge, for the first time, one single derivatization technique is used to determine the three considered analytes. In our approach, all GSNO metabolites, nitrites, nitrates and RSNOs, were derivatized to the same compound (NAT) and then quantified by LC-ITMS/MS. Free nitrites were measured first. The nitrate concentration was then determined after enzymatic reduction of nitrate ions subtracting the concentration of free nitrites. Similarly, RSNOs concentrations are calculated by subtracting the concentration of free nitrites from the sum "RSNOs + nitrites" measured after the S-NO bond cleavage with mercuric ions. In the apical compartment, the decomposition of GSNO into nitrites and nitrates was also checked by direct HPLC-UV as proposed by Parent *et al* for concentrations in the micromolar range[30]. GSNO was found to be stable under the present operating conditions (data not shown). Nevertheless, in the basolateral compartment, GSNO degradation could not be investigated by HPLC-UV because of the very low measured concentrations (nanomolar range). In this compartment, the transfer of the NO moiety of GSNO on cysteine residues of peptides and proteins is

possible, resulting in a formation of other RSNOs. That is the reason why, in the basolateral compartment, it is preferable to use the term RSNOs rather than GSNO to take into account all possible compounds reacting with mercuric ions. Nevertheless, whatever the GS^{15}NO fate in the basolateral compartment, it is clear that the ^{15}N-labeled species analyzed by our LC-ITMS/MS method originates from this drug.

The TEER values measured before and after 1 h of GS^{15}NO permeation through the Caco-2 cell monolayer was higher than 500 $\Omega \cdot cm^{-2}$. Meanwhile, the permeability percentage of the sodium fluorescein was less than 5 %. These results indicated a confluent and unalterated monolayer.

In the Biopharmaceutics Classification System[31], drugs are assigned within four classes depending on their aqueous solubility and intestinal permeability. Three classes of intestinal permeability are defined according to drug P_{app} value: high permeability compounds such as propranolol show P_{app} value higher than 10^{-5} $cm \cdot s^{-1}$, while low permeability compounds such as furosemide show P_{app} value less than $1 \cdot 10^{-6}$ $cm \cdot s^{-1}$ [32]. Intermediate values correspond to "middle permeability" drugs. It was found that ^{15}N-nitrite has a P_{app} value in the range of $(0.32 - 0.47) \times 10^{-6}$ $cm \cdot s^{-1}$, RS^{15}NOs in the range of $(0.16 - 0.35) \times 10^{-6}$ $cm \cdot s^{-1}$, while ^{15}N-nitrate is in the range of $(1.65 - 1.79) \times 10^{-6}$ $cm \cdot s^{-1}$, which demonstrated that GS^{15}NO belongs to the class of middle permeability compounds. In addition, GSNO showed concentration-dependent distribution in both compartments in the tested concentration range (10-100 µM) (Figure 6), and concentration-independent permeability. Noteworthy, the present LC/ITMS/MS method allows us to reach the low concentrations of NO-related species in the basolateral compartment, even at the lowest dose of GSNO applied to the cellular barrier model (10 µM). Applying fluorescence with the same derivatization process (DAN) limits the permeability studies to the highest concentration of GSNO (100 µM). High levels of NO species (nitrite, nitrate and RSNOs) in the blank demonstrate the necessity of using isotope labeling to improve the method LOQ, and sample dilution contributes to a lower risk of matrix

interference.

CONCLUSIONS

We have developed and validated a LC-ITMS/MS method capable of selectively monitoring NO species metabolized from ^{15}N labeled GSNO as NAT adducts using an Ion Trap Mass Spectrometer. Compared with other published approaches, this method combines several original features such as (i) the use of a single derivatization technique for the three considered analytes (nitrites, nitrates and RSNOs), (ii) a new described fragmentation pattern that is at least as sensitive as (sometime even more sensitive than) the previously described methods (in the nM range)[24,25,26] on triple quadrupole mass spectrometers, and (iii) the first report of a ^{15}N labeling method applied to an intestinal barrier model.

The IT mass spectrometer enables us to reach a very satisfying sensitivity thanks to an original MS/MS transition (*m/z* 171 → 156) obtained in HCD mode with a limit of quantification of 1 nM on ^{15}NO freed from GS^{15}NO. The working LOQ was set at 5 nM to overcome interferences produced by ^{14}NO present in the real samples. The assay, applied to the study of the intestinal permeability of GS^{15}NO with an *in vitro* model of this physiological barrier, classifies the S-nitrosoglutathione in the middle permeability class according to FDA guidelines.

The work was the preamble of future assays of NO species metabolized from labeled GS^{15}NO or other NO donors in the cells or tissues. It also opens the perspective of a more fundamental work such as the study of the reactivity of the ion $[NAT+H]^+$ in HCD tandem mass spectrometry in the presence of acetonitrile.

Furthermore, the use of *in vitro* models of intestinal permeability is of key importance to evaluate the drug (GSNO) bioavailability after oral administration. To the best of our knowledge, this work provides the first report of a ^{15}N-labeled drug using an intestinal permeability model. In the future, the transposition of our approach to other biological matrices (plasma, tissues, organs like aorta) using sample

preparation protocols already described[33,34] constitutes a natural extension of the fields of application.

Acknowledgements

Authors are grateful to the program of China Scholarship Council for the financial support of Ms Haiyan Yu's PhD thesis (grant NO. 201506270166). Authors also thank Dr Philippe Giummelly (CITHEFOR, Université de Lorraine) for the synthesis of $GS^{15}NO$.

REFERENCES

1 Moncada S, Palmer RM, Higgs EA. Nitric oxide: physiology, pathophysiology, and pharmacology. *Pharmacol Rev.* 1991;43(2):109–142.

2 Cooke JP, Dzau VJ. Nitric oxide synthase: Role in the genesis of vascular disease. *Annu Rev Med.* 1997;48:489–509.

3 Vallance P, Leone A, Calver A, Collier J, Moncada S. Accumulation of an Endogenous Inhibitor of Nitric-Oxide Synthesis in Chronic-Renal-Failure. *Lancet.* 1992;339(8793):572–575.

4 Lundberg JO, Weitzberg E, Gladwin MT. The nitrate-nitrite-nitric oxide pathway in physiology and therapeutics. *Nat Rev Drug Discov.* 2008;7(2):156–167. Doi: 10.1038/nrd2466.

5 Loo B, Labugger R, Skepper JN, et al. Enhanced Peroxynitrite Formation Is Associated with Vascular Aging. *J Exp Med.* 2000;192(12):1731–1744. Doi: 10.1084/jem.192.12.1731.

6 Münzel T, Steven S, Daiber A. Organic nitrates: Update on mechanisms underlying vasodilation, tolerance and endothelial dysfunction. *Vascul Pharmacol.* 2014;63(3):105–113. Doi: 10.1016/j.vph.2014.09.002.

7 Csont T, Ferdinandy P. Cardioprotective effects of glyceryl trinitrate: beyond vascular nitrate tolerance. *Pharmacol Ther.* 2005;105(1):57–68. Doi: 10.1016/j.pharmthera.2004.10.001.

8 Broniowska KA, Diers AR, Hogg N. S-Nitrosoglutathione. *Biochim Biophys Acta. BBA - Gen Subj.* 2013;1830(5):3173–3181. Doi: 10.1016/j.bbagen.2013.02.004.

9 Gaucher C, Boudier A, Dahboul F, Parent M, Leroy P. S-nitrosation/Denitrosation in Cardiovascular Pathologies: Facts and Concepts for the Rational Design of S-nitrosothiols. *Curr Pharm Des.* 2013;19(3):458–472.

10 Wu W, Perrin-Sarrado C, Ming H, et al. Polymer nanocomposites enhance S-nitrosoglutathione intestinal absorption and promote the formation of releasable nitric oxide stores in rat aorta. *Nanomedicine-Nanotechnol Biol Med.* 2016;12(7):1795–1803. Doi: 10.1016/j.nano.2016.05.006.

11 Chan OH, Stewart BH. Physicochemical and drug-delivery considerations for oral drug bioavailability. *Drug Discov Today.* 1996;1(11):461–473.

12 Badhan R, Penny J, Galetin A, Houston IB. Methodology for Development of a Physiological Model Incorporating CYP3A and P-Glycoprotein for the Prediction of Intestinal Drug Absorption. *J Pharm Sci.* 2009;98(6):2180–2197. Doi: 10.1002/jps.21572.

13 Artursson P. Cell-Cultures as Models for Drug Absorption Across the Intestinal-Mucosa. *Crit Rev Ther Drug Carrier Syst.* 1991;**8**(4):305–330.

14 Alqahtani S, Mohamed LA, Kaddoumi A. Experimental models for predicting drug absorption and metabolism. *Expert Opin Drug Metab Toxicol.* 2013;9(10):1241–1254. Doi: 10.1517/17425255.2013.802772.

15 Miersch S, Mutus B. Protein S-nitrosation: Biochemistry and characterization of protein thiol–NO interactions as cellular signals. *Clin Biochem.* 2005;38(9):777–791. Doi: 10.1016/j.clinbiochem.2005.05.014.

16 Bryan NS, Grisham MB. Methods to detect nitric oxide and its metabolites in biological samples. *Free Radic Biol Med.* 2007;43(5):645–657. Doi: 10.1016/j.freeradbiomed.2007.04.026.

17 Marzinzig M, Nussler AK, Stadler J, et al. Improved Methods to Measure End Products of Nitric Oxide in Biological Fluids: Nitrite, Nitrate, andS-Nitrosothiols. *Nitric Oxide.* 1997;1(2):177–189. Doi: 10.1006/niox.1997.0116.

18 Tsikas D. Methods of quantitative analysis of the nitric oxide metabolites nitrite and nitrate in human biological fluids. *Free Radic Res.* 2005;39(8):797–815. Doi: 10.1080/10715760500053651.

19 Schmidt TC, Zwank L, Elsner M, Berg M, Meckenstock RU, Haderlein SB. Compound-specific stable isotope analysis of organic contaminants in natural environments: a critical review of the state of the art, prospects, and future challenges. *Anal Bioanal Chem.* 2004;378(2):283–300. Doi: 10.1007/s00216-003-2350-y.

20 Tsikas D. Pentafluorobenzyl bromide—A versatile derivatization agent in chromatography and mass spectrometry: I. Analysis of inorganic anions and organophosphates. *J Chromatogr B.* 2017;1043:187–201. Doi: 10.1016/j.jchromb.2016.08.015.

21 Hanff E, Boehmer A, Jordan J, Tsikas D. Stable-isotope dilution LC-MS/MS measurement of nitrite in human plasma after its conversion to S-nitrosoglutathione. *J Chromatogr B-Anal Technol Biomed Life Sci.* 2014;970:44–52. Doi: 10.1016/j.jchromb.2014.08.041.

22 Li H, Meininger CJ, Wu G. Rapid determination of nitrite by reversed-phase high-performance liquid chromatography with fluorescence detection. *J Chromatogr B Biomed Sci App.* 2000;746(2):199–207. Doi: 10.1016/S0378-4347(00)00328-5.

23 Marzinzig M, Nussler AK, Stadler J, et al. Improved methods to measure end products of nitric oxide in biological fluids: Nitrite, nitrate, and S-nitrosothiols. *Nitric Oxide-Biol Chem.* 1997;1(2):177–189. Doi: 10.1006/niox.1997.0116.

24 Chao MR, Shih YM, Hsu YW, et al. Urinary nitrite/nitrate ratio measured by isotope-dilution LC–MS/MS as a tool to screen for urinary tract infections. *Free Radic Biol Med.* 2016;93:77–83. Doi: 10.1016/j.freeradbiomed.2016.01.025.

25 Axton ER, Hardardt EA, Stevens JF. Stable isotope-assisted LC–MS/MS monitoring of glyceryl trinitrate bioactivation in a cell culture model of nitrate tolerance. *J Chromatogr B.* 2016;1019:156–163. Doi: 10.1016/j.jchromb.2015.12.010.

26 Shin S, Fung HL. Evaluation of an LC–MS/MS assay for 15N-nitrite for cellular studies of l-arginine action. *J Pharm Biomed Anal.* 2011;56(5):1127–1131. Doi: 10.1016/j.jpba.2011.08.017.

27 Saville B. A scheme for the colorimetric determination of microgram amounts of thiols. *Analyst.* 1958;83(993):670–2. Doi: 10.1039/AN9588300670.

28 Parent M, Dahboul F, Schneider R, et al. A Complete Physicochemical Identity Card of S-nitrosoglutathione. *Curr Pharm Anal.* 2013;9(1):31–42.

29 Jobgen WS, Jobgen SC, Li H, Meininger CJ, Wu G. Analysis of nitrite and nitrate in biological samples using high-performance liquid chromatography. *J Chromatogr B.* 2007;851(1-2):71–82. Doi: 10.1016/j.jchromb.2006.07.018.

30 Parent M, Dahboul F, Schneider R, Clarot C, Maincent P, Leroy P, Boudier A. A Complete Physicochemical Identity Card of S-Nitrosoglutathione. *Current Pharmaceutical Analysis.* 2013;9:31–42.

31 U.S. Department of Health and Human Services Food and Drug Administration Center for Drug Evaluation and Research (CDER). Waiver of in vivo bioavailability and bioequivalence studies for immediate-release solid oral dosage forms based on a biopharmaceutics classification system. *Biopharmaceutics.* 2015.

32 Peng Y, Yadava P, Heikkinen AT, Parrott N, Railkar A. Applications of a 7-day Caco-2 cell model in drug discovery and development. *Eur J Pharm Sci.* 2014;56:120–130. Doi: 10.1016/j.ejps.2014.02.008.

33 Warnecke A, Luessen P, Sandmann J, et al. Application of a stable-isotope dilution technique to study the pharmacokinetics of human N-15-labelled S-nitrosoalbumin in the rat: Possible mechanistic and biological implications. *J Chromatogr B-Anal Technol Biomed Life Sci.* 2009;877(13):1375–1387. Doi: 10.1016/j.jchromb.2008.11.035.

34 Damacena-Angelis C, Oliveira-Paula GH, Pinheiro LC, et al. Nitrate decreases xanthine oxidoreductase-mediated nitrite reductase activity and attenuates vascular and blood pressure responses to nitrite. *Redox Biol.* 2017;12:291–299. Doi: 10.1016/j.redox.2017.03.003.

Table 1: Ion composition of the MS/MS spectra of the ^{14}N-NAT or ^{15}N-NAT adduct in CID (35 eV) and HCD (50 eV) depending on the organic modifier composing the chromatographic mobile phase (solvent S). The NAT adduct was infused in a mixture of a 10 mM-acetic acid aqueous solution containing 40% of the solvent S. The relative abundance (%) of each ion is indicated in parentheses. Nd: not detected

Labeling	MS/MS	Solv. S[a]	Observed *m/z* for $[NAT+H]^+$ precursor ion					
			$[NAT+H]^+$	$[NAT-N_2+H]^+$	$[C_9H_7]^+$[b]	$[NAT+H+S]^+$	$[NAT-N_2+H+S]^+$	$[NAT-N_2-HCN+H+S]^+$
^{14}N-NAT	CID (35eV)	MeOH	$170_{(38)}$	$142_{(19)}$	$115_{(100)}$	Nd	Nd	Nd
		ACN	$170_{(36)}$	$142_{(18)}$	$115_{(100)}$	Nd	Nd	Nd
	HCD (50eV)	ACN	$170_{(46)}$	Nd	$115_{(100)}$	$211_{(0.1)}$	$183_{(1.1)}$	$156_{(46)}$
		d_3-ACN	$170_{(45)}$	Nd	$115_{(100)}$	$214_{(0.1)}$	$186_{(1.1)}$	$159_{(45)}$
^{15}N-NAT	CID (35eV)	MeOH	$171_{(38)}$	$142_{(19)}$[c]	$115_{(100)}$	Nd	Nd	Nd
		ACN	$171_{(36)}$	$142_{(15)}$[c]	$115_{(100)}$	Nd	Nd	Nd
	HCD (50eV)	ACN	$171_{(45)}$	Nd	$115_{(100)}$	$212_{(0.1)}$	$183_{(1.1)}$[c]	$156_{(40)}$[c]
		d_3-ACN	$171_{(46)}$	Nd	$115_{(100)}$	$215_{(0.2)}$	$186_{(1.0)}$[c]	$159_{(42)}$[c]

Remarks:
a: The NAT adduct is infused in a mixture of a 10 mM-acetic acid aqueous solution containing 40% of solvent S (MeOH, ACN or d_3-ACN)
b: This ion is also corresponding to $[NAT-N_2-HCN+H]^+$ (see also Axton *et al*[25] and also Shin *et al*[26])
c: For these ions, the loss is 29 u because N_2 is containing the labeled nitrogen (^{15}N).

Table 2. Inter-day and intra-day variability of quality control samples for ^{15}N-nitrite *S*-nitrosoglutathione (GS^{15}NO) and ^{15}N-nitrate analysis with IS. ^{15}N-nitrite, GS^{15}NO and ^{15}N-nitrate were spiked into HBSS buffer (n = 6), and the concentration was calculated by using related six-point calibration curve (5, 10, 20, 50, 100, 200 nM) of ^{15}N-nitrite and *S*-nitrosoglutathione (GS^{15}NO), and five-point calibration curve (250, 500, 1250, 2500, 5000 nM) of ^{15}N-nitrite. Accuracy was determined as the deviation (%) of calculated concentrations from the nominal concentrations. Precision was determined as the relative standard deviation (RSD) of the 6 measurements.

NO species	Concentration (nM)	Intra-day		Inter-day	
		Accuracy (%)	Precision (%)	Accuracy (%)	Precision (%)
^{15}N-nitrite	15	105.2±6.4	6.1	104.7±7.0	6.7
	50	99.0±6.8	6.9	94.7±2.8	3.0
	180	98.6±5.3	5.4	102.7±7.3	7.1
GS^{15}NO	15	98.1±13.1	13.4	93.3±11.8	12.6
	50	99.1±10.9	11.0	96.0±7.4	7.7
	180	100.0±12.7	12.7	101.5±11.4	11.3
^{15}N-nitrate	300	103.0±6.9	6.7	103.0±7.0	6.8
	2500	100.8±5.6	5.6	100.6±8.7	8.7
	4000	107.7±8.5	7.9	109.4±8.8	8.1

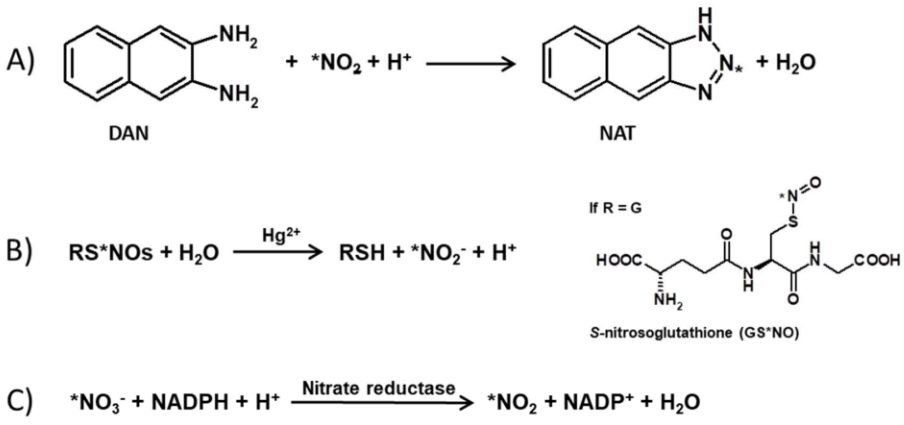

Figure 1. Principal reactions involved in this study. A) Derivatization of nitrite ion with 2,3-diaminonaphthalene (DAN) leading to a 2,3-naphthotriazole (NAT) derivative. The nitrogen transferred from the nitrite ion is indicated with an asterisk (*); B) Release of nitrites from the *S*-nitrosoglutathione (GSNO) catalyzed by mercuric ions and C) Reaction of nitrate conversion into to nitrite ion catalyzed by a nitrate reductase in presence of cofactor (here NADPH = nicotinamide adenine dinucleotide phosphate).

GS^{15}NO metabolites determination by LC-MS/MS

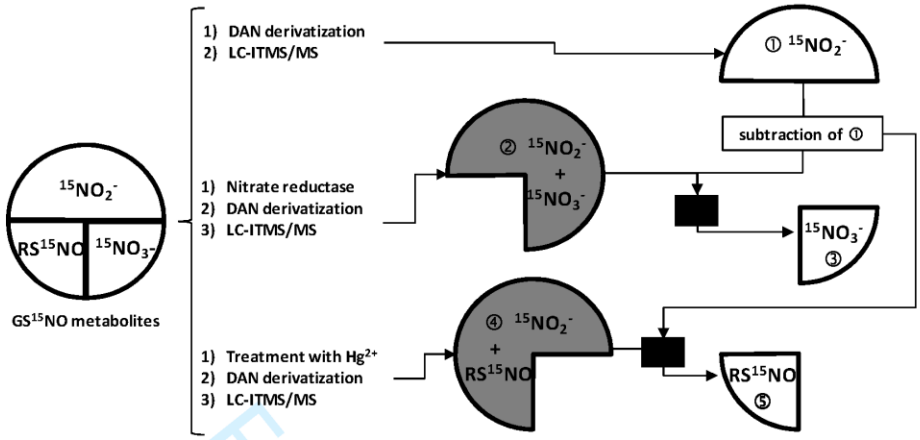

Figure 2. Strategy of analysis of the different GS^{15}NO metabolites obtained during the *in vitro* study using the same LC-ITMS/MS approach. The concentration of free ^{15}N-nitrites ① after incubation is directly obtained after DAN derivatization followed by LC-ITMS/MS. Free ^{15}N-nitrates are obtained after enzymatic (nitrate reductase) pretreatment of the metabolite pool. The quantification by LC-MS/MS after DAN derivatization of this sample provides the cumulative concentration ② of free ^{15}N-nitrites + ^{15}N-nitrates (reduced into nitrites). The concentration in free ^{15}N-nitrates ③ is deduced from result ② by subtracting the concentration of free ^{15}N-nitrites ①. The concentration of RS^{15}NOs is obtained after the pretreatment of the metabolite pool with Hg^{2+}. The quantification by LC-MS/MS after DAN derivatization of this sample provides the cumulative concentration ④ of free ^{15}N-nitrites + GS^{15}NO (converted into nitrites, see reaction 2 in figure 1). The concentration of RS^{15}NO ⑤ is deduced from result ④ by subtracting the concentration of free ^{15}N-nitrites ①.

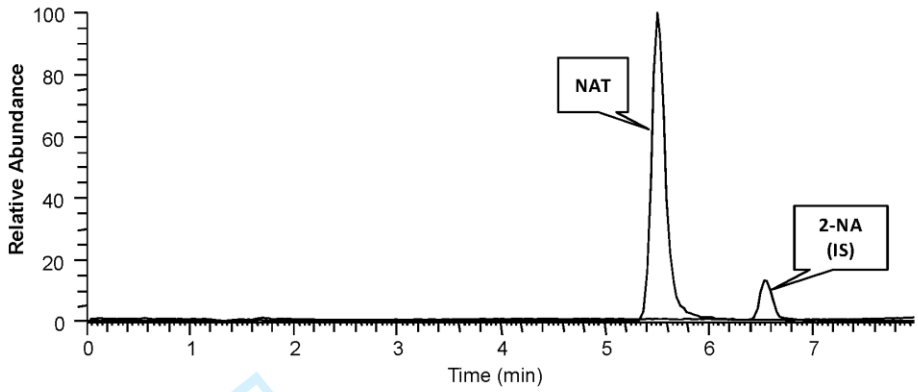

Figure 3. Representative LC-ESI-ITMS/MS chromatogram (conditions given in the experimental section) of the 2,3-naphthotriazole (NAT) derivative and the internal standard (IS, 2-naphthylamine (2-NA)).

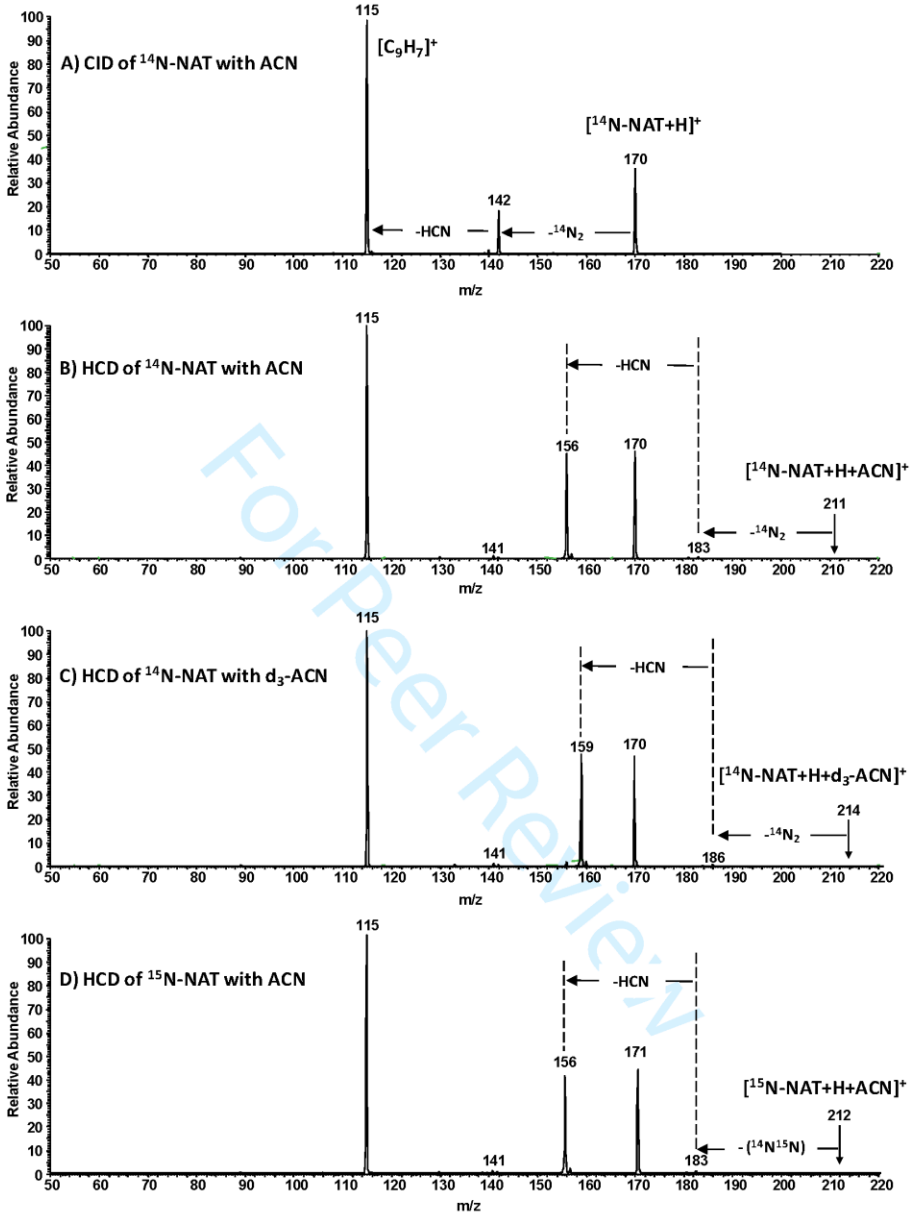

Figure 4. Fragmentation of the protonated molecular ion of NAT diluted at 2 µM in the chromatographic mobile phase. A) CID at 35 eV of $[^{14}N\text{-NAT+H}]^+$ (m/z 170) using acetonitrile (ACN), B) HCD at 50 eV of $[^{14}N\text{-NAT+H}]^+$ using ACN, C) HCD at 50 eV of $[^{14}N\text{-NAT+H}]^+$ using deuterated acetonitrile (d_3-ACN) and D) HCD at 50 eV of $[^{15}N\text{-NAT+H}]^+$ (m/z 171) using ACN. See also Table 1 for complementary information.

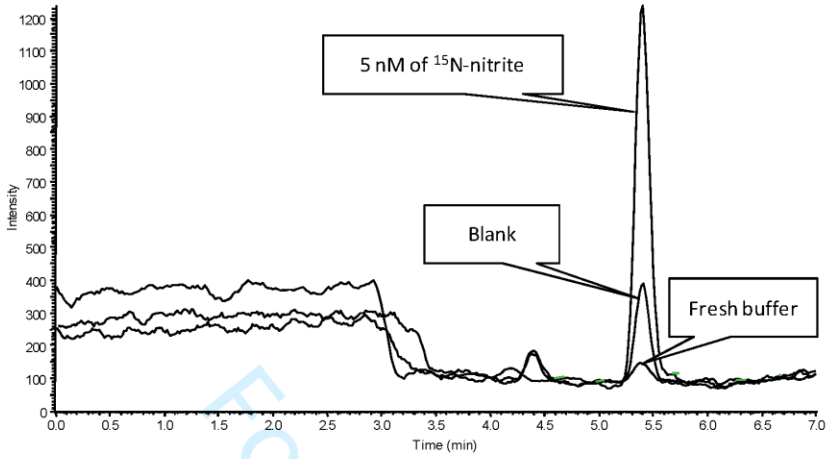

Figure 5. Representative ion chromatograms under multiple reaction monitoring (MRM) transition of m/z 171 → 115, corresponding to derivatization of 5 nM ^{15}N-nitrite in HBSS buffer, blank of the *in vitro* study and freshly prepared HBSS buffer.

GS^{15}NO metabolites determination by LC-MS/MS

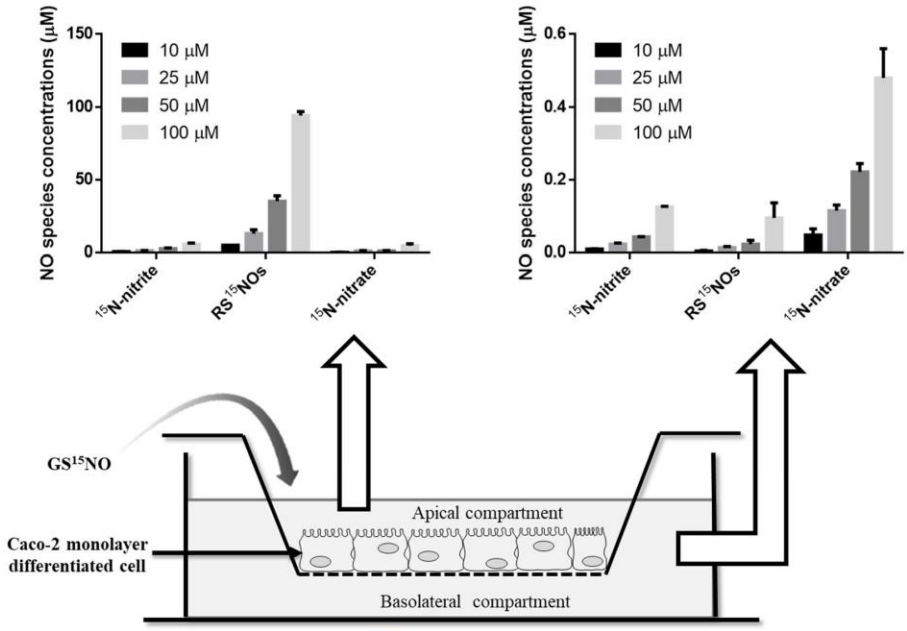

Figure 6. Permeation of 10, 25, 50 or 100 µM of ^{15}N labeled *S*-nitrosoglutathione (GS^{15}NO) through an *in vitro* model of intestinal barrier (differentiated Caco-2 cell monolayer) during 1 h at 37 °C. GS^{15}NO metabolites (nitric oxide (NO) species concentrations) were quantified in both compartments, n = 3. Results are expressed as mean ± SD.

GS^{15}NO metabolites determination by LC-MS/MS

Supplementary data

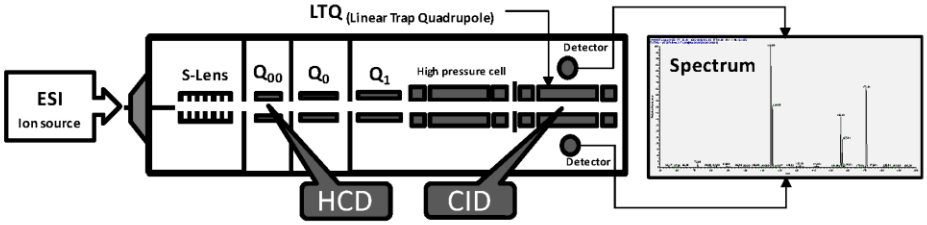

Figure S1. Simplified scheme of the LTQ Velos Pro showing where the fragmentation occurs in the 2 different fragmentation modes evaluated in this publication. In CID (Collisionally Induced Dissociation), the parent ion is isolated and fragmented in the LTQ (Linear Trap Quadrupole or Linear Ion Trap). The fragments are then analyzed by the LTQ. In HCD (Higher-energy Collision Dissociation), the parent ion is first isolated in the LTQ then ejected back to the Q_{00} region where its fragmentation occurs. Then the generated fragments are directed toward the LTQ where they are analyzed.

GS^{15}NO metabolites determination by LC-MS/MS

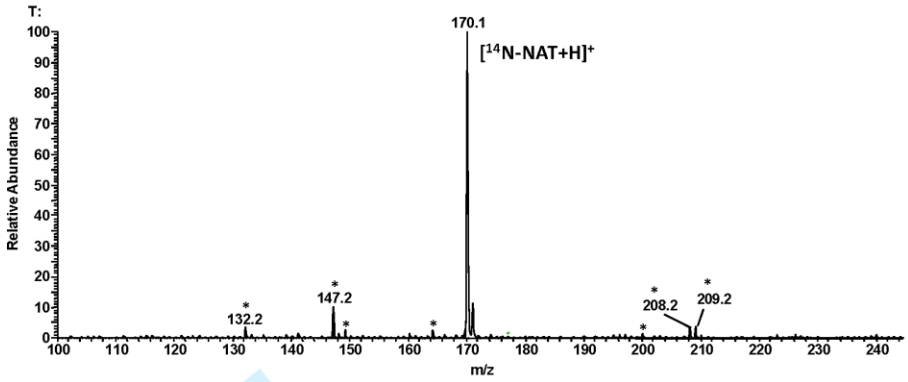

Figure S2. Mass spectrum in positive ion mode of the 2,3-naphthotriazole (^{14}NAT) at 2 µM infused at 10 µL·min^{-1}. The ^{14}NAT is solubilized in a mixture of water containing 0.01 M acetic acid and acetonitrile (20/80 v/v). The asterisks are corresponding to ions present in the background noise of the mobile phase

In conclusion, DAN derivatization of nitrite ions coupled with LC-ITMS/MS in HCD mode shows a lower LOQ value for the quantification of ^{15}N labeled NO species than with the Griess method. Consequently, preliminary experiments of GSNO permeability in intestinal barrier models (Caco-2 cell monolayer and isolated rat intestine in Ussing chamber) have been carried out using this method. They allowed concluding that GSNO belongs to medium permeability class of drugs according to BCS rules (Peng *et al.* 2014). Intestinal permeability of RSNOs has been more deeply studied by using both models in the following chapter.

2nd Chapter: Intestinal permeability studies of *S*-nitrosothiols using two models

Oral formulations are widely used as they are convenient for drug delivery, especially for CVDs which need chronic treatments. According to the Biopharmaceutical Classification System (BCS) (Amidon *et al.* 1995), a drug suitable for oral administration should possess high solubility and permeability (Figure 1). The RSNOs such as GSNO and *S*-nitroso-*N*-acetyl-*D*-penicillamine (SNAP), are known to have high solubility, but their intestinal permeability is not yet reported.

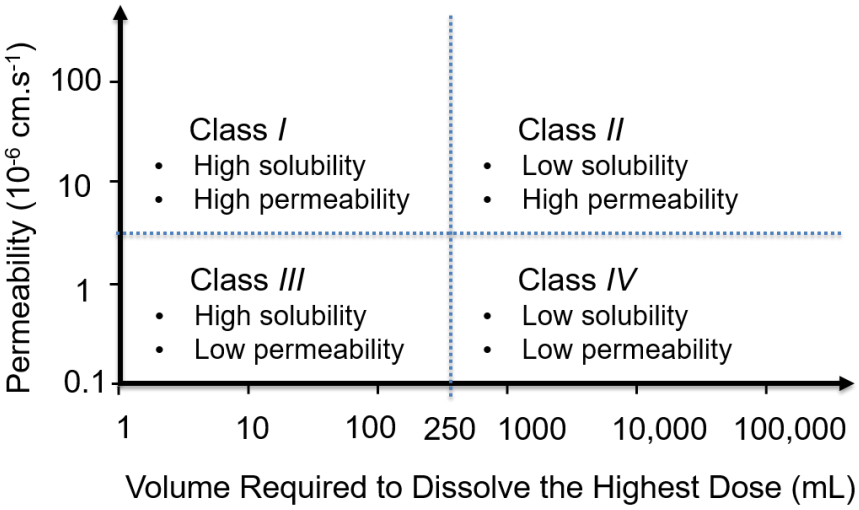

Figure 1. Scheme of Biopharmaceutical Classification System.

The main absorption part is small intestine (Figure 2 C). Interestingly, parts of small intestine differ with their physicological characteristics (Table 1) (Bilat *et al.* 2017).

Table 1. Comparison of the physiological parameters in different parts of the gut (Bilat *et al.* 2017)

Region	Average length (m)	Absorbing surface area (m^2)	pH	Residence time	Mucus thickness[a]	Bacterial cells (cells/mL)
Duodenum	0.25-0.30	0.09	5.7-6.8	≈ 40 min	FAL: 16 ± 3 LAL: 154 ± 39	10^1–10^4 Aerobes and facultative anaerobes
Jejunum	3	60	6.6-7.0	2-3 h	FAL: 15 ± 2 LAL: 108 ± 5	10^4–10^8 Facultative anaerobes and aerobes
Ileum	3	60	7.0-7.3	3-4 h	FAL: 29 ± 8 LAL: 447 ± 47	10^4–10^8 Facultative anaerobes and aerobes
Colon	1.5	0.3	5.7(caecum) to 6.6	16.6-19.0 h	FAL: 116 ± 51 LAL: 714 ± 109	10^{10}–10^{12} Facultative aerobes to strict anaerobic bacteria (mainly Clostridia)

Abbreviations: LAL, loosely adherent layer; FAL, firmly attached layer.

[a] Study performed in rats.

Usually, there are three steps to study intestinal permeability of drugs. The first step is to use an *in vitro* model, such as a monolayer of epithelial cells. This model is simple but does not fully correspond to the real conditions in the body; it can be improved by co-culturing colon cell lines HT-29-H or HT-29-MTX producing mucus (Bilat *et al.* 2017). Noteworthy, the commonly used Caco-2 cell monolayer model needs two to three weekes to form the cell monolayer. The second step is to use an *ex vivo* model, taking advantage of the isolated tissue. Usually, O_2-CO_2 (95:5, V/V) mixture bubbling is needed for tissue viability. This model is more relevant to the final real conditions than the *in vitro* model. The last step is performing experiments *in vivo*, but they are still suffering of drawbacks because of variations between animals and humans, and in human genotype and phenotype (Bilat *et al.* 2017).

To study RSNOs intestinal permeability, two models mastered at the EA 3452 Cithefor level have been presently used:

- an *in vitro* model with a monolayer of the differentiated epithelial cells (Caco-2) (Figure 2 A);

- an *ex vivo* model using “intact” isolated intestine (ileum) of rat placed in Ussing chamber (Figure 2 B). Previous studies have been realized in the lab with “stripped” isolated rat intestine in Ussing chamber (Shah *et al.* 2015)(Shah *et al.* 2016) . As the model offers poor reproducibility, “intact” intestine was preferred.

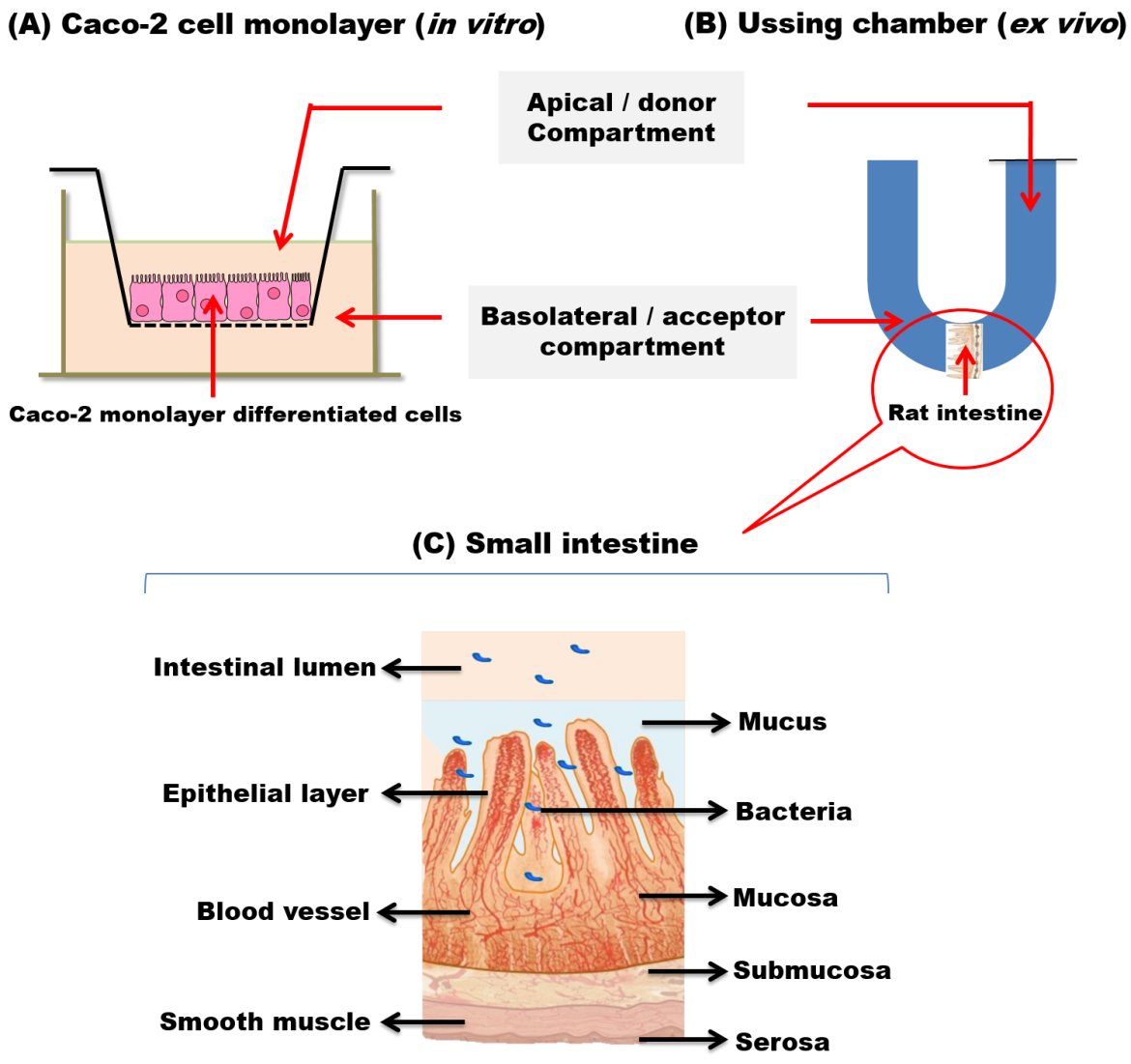

Figure 2. Scheme of (A) Caco-2 cell monolayer model, (B) intact isolated intestine model in Ussing chamber (oriented with mucosa toward donor compartment and serosa toward acceptor compartment) and (C) small intestine.

First, RSNOs (GSNO, SNAP and NACNO) permeability and corresponding pathway (passive or active) were studied by using the *in vitro* model. In addition, their permeability in different parts of rat intestine were explored, by measuring permeability values at different pH values (pH = 6.4, jejunum; pH = 7.4, ileum). The resulting data and conclusions are described in the following experimental paper entitled "**Intestinal absorption of *S*-nitrosothiols: permeability and transport mechanisms**".

Then, the classification of GSNO permeability was confirmed by using $GS^{15}NO$ in the *ex vivo* model and quantifying the permeated labeled NO species by LC-MS/MS (Yu *et al.* 2018).

In addition, the roles of denitrosating enzyme *γ*–glutamyltransferase (GGT; EC 2.3.2.2) and other reagents of GSNO degradation (*e.g.* thiols) were studied. All related data are reported in the article draft "**Degradation of *S*-nitrosoglutathione in rat intestine: roles of denitrosating enzymatic and chemical factors on absorption and permeation".** All experimental parts currently missing during manuscript deposit are indicated.

1. Experimental paper: “Intestinal absorption of *S*-nitrosothiols: permeability and transport mechanisms” in *Biochemical Pharmacology (155 (2018) 21–31)*

Detailed procedures used for experiments in this article are present in protocols (see appendices) entitled “Measurement of nitrite, nitrate ions and S-nitrosothiols using the 2,3-diaminonaphthalene assay by spectrofluorometry” and “Intestinal permeability studies of S-nitrosothiols using a Caco-2 cell monolayer model”.

Biochemical Pharmacology 155 (2018) 21–31

Contents lists available at ScienceDirect

Biochemical Pharmacology

journal homepage: www.elsevier.com/locate/biochempharm

Intestinal absorption of *S*-nitrosothiols: Permeability and transport mechanisms

Justine Bonetti[1], Yi Zhou[1], Marianne Parent, Igor Clarot, Haiyan Yu, Isabelle Fries-Raeth, Pierre Leroy, Isabelle Lartaud, Caroline Gaucher*

Université de Lorraine, CITHEFOR, F-54000 Nancy, France

ARTICLE INFO

Keywords:
S-Nitrosothiols
Nitric oxide
Intestinal permeability
Caco-2 cells
Passive diffusion

ABSTRACT

S-Nitrosothiols, a class of NO donors, demonstrate potential benefits for cardiovascular diseases. Drugs for such chronic diseases require long term administration preferentially through the oral route. However, the absorption of *S*-nitrosothiols by the intestine, which is the first limiting barrier for their vascular bioavailability, is rarely evaluated. Using an *in vitro* model of intestinal barrier, based on human cells, the present work aimed at elucidating the mechanisms of intestinal transport (passive or active, paracellular or transcellular pathway) and at predicting the absorption site of three *S*-nitrosothiols: *S*-nitrosoglutathione (GSNO), *S*-nitroso-*N*-acetyl-L-cysteine (NACNO) and *S*-nitroso-*N*-acetyl-D-penicillamine (SNAP). These *S*-nitrosothiols include different skeletons carrying the nitroso group, which confer different physico-chemical characteristics and biological activities (antioxidant and anti-inflammatory). According to the values of apparent permeability coefficient, the three *S*-nitrosothiols belong to the medium class of permeability. The evaluation of the bidirectional apparent permeability demonstrated a passive diffusion of the three *S*-nitrosothiols. GSNO and NACNO preferentially cross the intestinal barrier though the transcellular pathway, while SNAP followed both the trans- and paracellular pathways. Finally, the permeability of NACNO was favoured at pH 6.4, which is close to the pH of the jejunal part of the intestine. Through this study, we determined the absorption mechanisms of *S*-nitrosothiols and postulated that they can be administrated through the oral route.

1. Introduction

Nitric oxide (NO) is a gaseous mediator with a short half-life (less than 5 s [1]). Due to its radical nature and oxidative activity, NO is involved in various signalling pathways among different cellular types and physiological systems. NO is continuously synthesised by oxydoreductases, *i.e.* the three endothelial, inducible or neuronal isoforms of NO synthases. The decrease in NO bioavailability, linked to vascular endothelium dysfunction and oxidative stress, plays a major role in ageing and cardiovascular chronic diseases like atherosclerosis, angina pectoris and stroke. As a result, the restoration of NO bioavailability, using among NO donors the physiologically occurring *S*-nitrosothiols, is a therapeutic key to treat cardiovascular diseases [2–7]. *S*-Nitrosothiols are formed by *S*-nitrosation – *i.e.* formation of a covalent bond between NO and a reduced thiol function of a cysteine residue belonging to high or low molecular weight proteins or peptides. *In vivo*, *S*-nitrosothiols like *S*-nitrosoalbumin, *S*-nitrosohemoglobin and *S*-nitrosoglutathione (GSNO) are the physiological forms of NO storage and transport [8]. Indeed, the formation of the *S*-NO bond extends NO half-life from 45 min up to several hours [9–10] and limits the oxidative/nitrosative stress induced by NO oxidation into peroxynitrite ions ($ONOO^-$) [11]. Despite the therapeutic potential of *S*-nitrosothiols, their half-life linked to their physico-chemical instability (heat, light, metallic cations,…) and/or enzymatic (redoxines or, for GSNO only, γ-glutamyltransferase) degradation, is too short for chronic diseases treatment [12].

Nowadays, many preclinical studies focused on cardiovascular therapeutics using *S*-nitrosothiols [6,13–17]. For example, daily intraperitoneal administration of *S*-nitroso-*N*-acetyl-L-cysteine (NACNO) for two weeks shows anti-atherosclerotic effects in mice [13]. However, compared to the oral route, the intraperitoneal administration is less suitable for chronic treatments. GSNO administration through the oral route in a context of stroke [14] results in neuroprotective effects: GSNO maintains the blood-brain barrier integrity, reduces peroxynitrite formation and stabilises several deleterious factors *via* *S*-nitrosation [13–16]. Despite such beneficial effects following oral administration, to the best of our knowledge, no study evaluated the mechanisms of

* Corresponding author at: Université de Lorraine, CITHEFOR EA 3452, Faculté de Pharmacie, BP 80403, F-54001 Nancy Cedex, France.
E-mail address: caroline.gaucher@univ-lorraine.fr (C. Gaucher).
[1] Both authors contributed equally to this work.

https://doi.org/10.1016/j.bcp.2018.06.018
Received 12 April 2018; Accepted 19 June 2018
Available online 21 June 2018
0006-2952/

intestinal absorption of GSNO and other *S*-nitrosothiols. Only Pinheiro et al. [17] demonstrated that oral administration of nitrite and nitrate ions (stable NO derived species) to rats increased the concentration of circulating *S*-nitrosothiols, thus produced antihypertensive effects. This study indirectly proves the intestinal absorption of *S*-nitrosothiols without elucidated the underlying mechanisms. However, the understanding of the intestinal absorption mechanisms of *S*-nitrosothiols is a prerequisite to control the dose and the kinetic of NO reaching its action sites.

To predict the intestinal absorption of drugs, the Biopharmaceutical Classification System (BCS) [18] defines four classes based on the physico-chemical properties (solubility) and intestinal permeability of drugs. The intestinal permeability of a drug is characterised, using *in vitro* or *ex vivo* models, by apparent permeability coefficient (Papp) from low permeability ($< 1 \times 10^{-6}$ cm.s^{-1}) to high permeability ($\geq 10 \times 10^{-6}$ cm.s^{-1}) including also a medium permeability class [19]. Thus far, only one of our studies was interested in the improvement and the prolongation of GSNO intestinal absorption by proposing alginate/chitosan nanocomposite formulation [20]. Using an *in vitro* intestinal barrier model of differentiated Caco-2 cells, we showed low intestinal permeability for GSNO with a Papp of 0.83×10^{-7} cm.s^{-1}. The nanocomposite formulation delayed GSNO absorption up to 24 h (1 h for free GSNO) and multiplied by four the Papp value (3.41×10^{-7} cm.s^{-1}) even if GSNO stayed in the low class of permeability [20]. This study showed the ability for GSNO to cross the intestinal barrier model and the possibility to modulate its kinetics of absorption. This opens new therapeutic applications in the treatment of chronic pathologies linked to a decrease of NO bioavailability.

Intestinal absorption of low molecular weight molecules is mainly driven by their physico-chemical properties such as lipophilicity, correlated with the octanol/water partition coefficient, expressed as a logarithmic value (log P), and the ionisation constant (pKa). For *S*-nitrosothiols, the log P value is driven by the skeleton carrying NO. GSNO, NACNO and *S*-nitroso-*N*-acetyl-D-penicillamine (SNAP), the three main *S*-nitrosothiols described in the literature, are characterised by calculated log P value of −2.70, −0.47 and 1.08, respectively [2]. The skeleton carrying NO presents also different therapeutic properties linked with its chemical structure. GSNO is a physiological *S*-nitrosothiol [21], present in the cytosol at a high concentration especially in erythrocytes [22], platelets and cerebral tissue. Its reduced glutathione (GSH) skeleton shows an antioxidant chemical structure thanks to its thiol functional group and forms, with the glutathione disulphide (GSSG), the intracellular redox buffer. NACNO and SNAP are synthetic *S*-nitrosothiols. NACNO with its *N*-acetyl-L-cysteine (NAC) skeleton possesses also an antioxidant activity in accordance with its chemical structure (thiol function). Furthermore, NAC is already used in human medicine as a mucolytic agent (oral administration) or as the antidote in acetaminophen intoxication [23]. SNAP shows in addition to its antioxidant properties (thiol function), an anti-inflammatory skeleton, *N*-acetyl-D-penicillamine (NAP) is used in the treatment of Wilson's disease (Trolovol®) and rheumatoid arthritis.

In this study, using an *in vitro* cell model of intestinal barrier, we propose to elucidate the intestinal transport mechanisms of *S*-nitrosothiols and NO in relation to their physico-chemical properties. Three different conditions were studied, i) permeability from the apical to the basolateral compartment, ii) permeability from the basolateral to the apical compartment to highlight an active transport such as drug influx/efflux, or a passive diffusion, and iii) permeability from an acidified apical compartment, mimicking the luminal intestinal pH of the jejunum, the major site of amino acid absorption [24].

2. Material and methods

2.1. Material and reagents

Eagle's Minimum Essential Medium (EMEM), foetal bovine serum (FBS), sodium pyruvate, penicillin 10 000 U.mL^{-1} and streptomycin 10 mg.mL^{-1} mix, trypsin, non-essential amino acids, glutamine, Hank's Balanced Salt Solution (HBSS Ca^{2+}/Mg^{2+}), sodium nitrate ($NaNO_3$), 2,3-diaminonaphthalene (DAN), 1.0 M hydrochloric acid (HCl) solution, propranolol hydrochloride, furosemide salt, triethylamine, 2-(*N*-morpholino)ethanesulfonic acid (MES), Trisma base (Tris), sodium chloride (NaCl), Igepal CA-630, sodium dodecyl sulfate (SDS), ethylenediaminetetraacetic acid (EDTA), neocuproine and *N*-ethylmaleimide (NEM) were purchased from Sigma, France. Mercuric chloride ($HgCl_2$), orthophosphoric acid and sodium tetraborate were purchased from Prolabo (VWR). Sodium nitrite ($NaNO_2$) from Merck, sodium hydroxide (NaOH) from VWR Chemicals, methanol from Carlo Erba Reagents and acetonitrile was from Biosolve. Nitrite/nitrate fluorimetric kit was purchased from Cayman Chemical (Ref. 780051).

2.2. S-Nitrosothiols synthesis

GSNO, NACNO and SNAP were synthesised according to a previously described method [25]. Briefly, GSH, NAC or NAP were incubated with one equivalent of sodium nitrite under acidic condition. Then, the pH was shifted to 7.4 using a phosphate buffered saline (PBS 0.148 M) solution. The final concentration was assessed by UV–Vis. spectrophotometry (Shimadzu; UV-spectrophotometer; UV-1800) using the specific molar absorbance of the *S*-NO bond at 334 nm for GSNO and NACNO ($\varepsilon_{GSNO} = 922\ M^{-1}\ cm^{-1}$; $\varepsilon_{NACNO} = 900\ M^{-1}\ cm^{-1}$) and at 340 nm for SNAP ($\varepsilon_{SNAP} = 1020\ M^{-1}\ cm^{-1}$).

2.3. Caco-2 cells culture and cytocompatibility

Intestinal Caco-2 cells (ATCC® HTB-37™) from passage 36 to 45 were grown in complete medium consisting of EMEM supplemented with 10% (v/v) of FBS, 4 mM of glutamine, 100 U/mL of penicillin, 100 U/mL of streptomycin, 1% (v/v) of non-essential amino acids. Cells were cultivated at 37 °C under 5% CO_2 (v/v) in a humidified incubator. Caco-2 cells were seeded in 96-wells plates at 2×10^4 cells/well 24 h before experiment. They were then exposed to each *S*-nitrosothiol (from 10 to 100 µM) for 24 h at 37 °C, complete medium being used as control. Cytocompatibility was assessed through metabolic activity with the 3(4,5-dimethylthiazol-2-yl)-2,5-diphenyltetrazolium bromide (MTT) assay. The absorbance of extracted formazan crystals was read at 570 nm with a reference at 630 nm (EL 800 microplate reader, Bio-TEK Instrument, Inc®, France). Metabolic activity in control condition was considered as 100%.

2.4. Intestinal permeability of reference molecules and S-nitrosothiols

Caco-2 cells were seeded at 2×10^6 cell/cm^2 on cell culture inserts (Transwell®, Corning, USA, membrane with 0.4 µm pore size, 1.12 cm^2 area or 4.97 cm^2) disposed in a 12-wells or 6-wells plate, respectively. The complete medium was replaced every two days during the first week of cell proliferation. During the second week, the medium was replaced every day until the differentiated cell monolayer was formed (14–15 days). The formation of the barrier was followed by transepithelial electrical resistance (TEER) measurement using a Millicell®-Electrical Resistance system (Millipore, USA) and validated for TEER values higher than 500 Ω.cm^2.

The bidirectional permeability of each *S*-nitrosothiol across the Caco-2 monolayer was evaluated from the apical to basolateral (A-B) compartment, mimicking physiological permeability conditions (intestinal lumen to blood compartment), and from the basolateral to the apical (B-A) (Fig. 1) compartment in HBSS at pH 7.4 to evaluate possible efflux mechanisms. A third condition evaluates the importance of the influence of luminal pH adjusted to 6.4 with 0.5 M MES solution in the apical compartment to determine the intestinal site of absorption (intestinal segment).

The concentration of *S*-nitrosothiols used to study the permeability

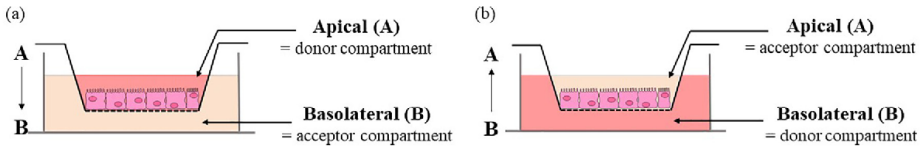

Fig. 1. Schematic representation of the bidirectional permeability of *S*-nitrosothiols across the Caco-2 monolayer. (a) From the apical (intestinal lumen) to the basolateral (bloodstream) compartment (on the left, A → B) to study physiological intestinal permeability, (b) from the basolateral to the apical compartment (on the right, B → A) to study S-nitrosothiol efflux.

in each direction was the same (100 µM). Since the apical and the basolateral compartments have different volumes (0.5 and 1.5 mL, respectively), the initial amounts of *S*-nitrosothiol for A-B and for B-A permeability studies were 50 and 150 nmol, respectively. $NaNO_2$ treatment (100 µM) was used as a positive control for nitrite ions permeability. The bidirectional permeability of propranolol (50 µM) and furosemide (100 µM), two reference molecules belonging to the high and low permeability class, respectively, was also assessed to surround the permeability of *S*-nitrosothiols [26,27] and to validate our model faced to the literature.

Permeability tests were conducted during 4 h under orbital shaking (500 rpm) at 37 °C. In the acceptor compartment, *S*-nitrosothiols were considered as RSNO because the R skeleton carrying NO cannot be identified by the methodology of quantification used. Reference molecules as well as NOx species (RSNO, nitrite ions and nitrate ions) were quantified after 1 h (entire volume of acceptor compartment removed) in the acceptor compartment and after 4 h in both compartments (for methodologies, see Sections 2.5. and 2.6.). RSNO and nitrite ions were also quantified inside the cells after 1 h and 4 h of permeability study.

At the end of the study, the integrity of the intestinal cell monolayer was checked by measuring the TEER value and the permeability of sodium fluorescein (5 µM), a marker of low paracellular permeability. A TEER value higher than 300 $\Omega.cm^2$ as well as a 5% of fluorescein permeability validated the integrity of the intestinal monolayer at the end of the experiment [28,29].

2.5. Quantification of S-nitrosothiols, nitrite and nitrate ions

S-Nitrosothiols and nitrite ions were immediately quantified using a fluorimetric method [30] with standard curves of GSNO and sodium nitrite, respectively (Table 1). Briefly, N_2O_3 generated from acidified nitrite ions reacts with DAN in the presence (for RSNO) or absence (for nitrite ions) of $HgCl_2$ producing 2,3-naphthotriazole that emits fluorescence at 415 nm after excitation at 375 nm (JASCO FP-8300, France). Nitrate ions quantification, using a standard curve of sodium nitrate included a reduction step to nitrite ions by reacting with nitrate reductase and its cofactors before the addition of DAN reagent (fluorimetric kit nitrite/nitrate Cayman Chemical) (Table 1). The concentration of nitrite ions (DAN assay) was subtracted from the value obtained by DAN-Hg^{2+} quantification to obtain the RSNO concentration and from the nitrate reductase quantification to obtain the nitrate ions concentration. The cumulative amounts of RSNO, NO_2^- and NO_3^- crossing the Caco-2 monolayer were calculated from the concentrations measured at 1 h and 4 h of the permeability studies in the acceptor compartment.

For intracellular quantifications, cells were lysed in 50 mM Tris buffer pH 6.8 added with 150 mM of NaCl, 1% of Igepal CA-630 (v/v), 0.1% of SDS (v/v), 1 mM of EDTA, 0.1 mM of neocuproine, 20 mM of sodium tetraborate and 10 mM of NEM.

2.6. Quantification of furosemide and propranolol

This procedure was adapted from [31–33] for propranolol and from [34] for furosemide. Briefly, the separation was performed on a C18 analytical column (Macherey-Nagel LiChrospher RP 18e; 5 µm; 125 × 4 mm) eluted with a mobile phase composed of acetonitrile added with 14 mM triethylamine in water buffered with orthophosphoric acid, pH 2.5 (30/70; v/v) at a flow rate of 1.0 $mL.min^{-1}$ and with a column temperature of 40 °C. The injection volume was 20 µL. Propranolol and furosemide were detected using a spectrofluorometric detector (model Jasco FP-920) set at λ_{ex} = 230 nm/λ_{em} = 340 nm, and λ_{ex} = 235 nm/λ_{em} = 402 nm, respectively. Standard curves of propranolol and furosemide were established between 0.5 and 10.0 µM and 62.5 nM to 2.0 µM, respectively.

2.7. Calculation of apparent permeability coefficients and recovery rates

2.7.1. Apparent permeability coefficient

The apparent permeability coefficient (Papp) values were calculated using the following equation (Eq. (1)):

$$Papp = \frac{dQ}{dt} \times \frac{1}{A \times C_0} \quad (1)$$

dQ/dt (mol.s^{-1}) refers to the permeability rate of reference molecules, RSNO or NOx species (mol) in the acceptor compartment at the time (s) of quantification, A (cm^2) refers to membrane diffusion area, and C_0 (mol.mL-1 or mol.cm^{-3}) refers to the initial concentration in the donor compartment.

2.7.2. Recovery rate

Mass balance was calculated as the addition of the amount of drug recovered in the acceptor compartment after each interval and in the donor compartment at the end of the experiment.

2.8. Statistical analysis

Results are shown as mean ± standard deviation (SD), based on 3 or 4 independent experiments in duplicate. Values were compared with

Table 1
Standard curves validation parameters for *S*-nitrosothiols (RSNO), nitrite ions (NO_2^-) and nitrate ions (NO_3^-) in HBSS with Ca^{2+}/Mg^{2+}. Mean ± SD; n = 3.

	Concentration range (µM)	Standard curves equation	Relative standard deviation (%)	R^2
RSNO	0.1–2.0	y = (1451 ± 236)x + (399 ± 98)	0.1 µM: 12.3 2 µM: 1.2	0.99
NO_2^-		y = (1527 ± 96)x + (435 ± 89)	0.1 µM: 4.3 2 µM: 3.2	
NO_3^-	0.01–3.75	y = (264 ± 22)x + (1719 ± 116)	0.01 µM: 8.4 3.75 µM: 5.1	

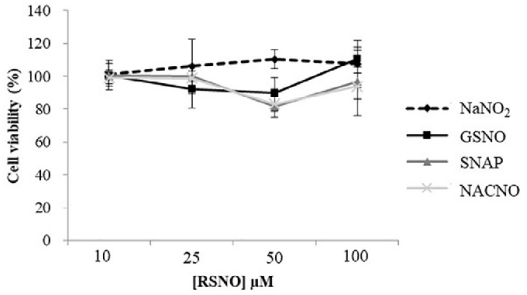

Fig. 2. Cytocompatibility of *S*-nitrosothiols with Caco-2 cells. Cell activity was assessed with the MTT test, 24 h after incubation with different *S*-nitrosothiols or $NaNO_2$. Values are expressed as mean ± SD of three independent experiments done in duplicate.

one-way ANOVA (treatments) or two-way ANOVA (treatment and time) followed by a Bonferroni's post-test using the Graphpad Prism 5 software; $p < 0.05$ was considered as statistically significant. Statistics are analysed excluding $NaNO_2$ treatments, which too high permeability values interfered with the statistical comparison of *S*-nitrosothiols.

3. Results

3.1. Cytocompatibility

Cell viability was not affected by any of the *S*-nitrosothiols presently tested and $NaNO_2$, with more 80% of viability independently of the concentration used (Fig. 2). For all the forthcoming experiments, a concentration of 100 µM of each *S*-nitrosothiol will be safely used.

Table 2
Values of apparent permeability coefficient (Papp) for NOx species ($RSNO + NO_2^- + NO_3^-$) and the RSNO molecular form after 4 h of permeation from the apical to the basolateral compartment. nd: not determined, LOQ: Limit of quantification. Mean ± SD of four independent experiments done in duplicate.

Treatments	NOx Papp ($\times 10^{-6}$ cm.s^{-1})	RSNO Papp ($\times 10^{-6}$ cm.s^{-1})
GSNO	2.6 ± 0.9	0.2 ± 0.1
NACNO	5.0 ± 2.1	0.21 ± 0.08
SNAP	3.3 ± 1.6	0.13 ± 0.09
$NaNO_2$	12.3 ± 3.2	Under LOQ
Propranolol	24.4 ± 1	nd
Furosemide	0.3 ± 0.1	nd

3.2. S-Nitrosothiols permeability from the apical to the basolateral compartment

S-Nitrosothiols permeation through the intestinal barrier model, evaluated in the A-B direction, showed the same profile for each treatment (GSNO, NACNO and SNAP) (Fig. 3). Each *S*-nitrosothiol (treatment) was permeated under three different chemical species. The RSNO form (Fig. 3A) was less permeated (0.50% ± 0.14% of the initial amount deposited in the donor compartment) than the NO_2^- (the first stable oxidation degree of NO in aqueous media) and NO_3^- ionic forms (4.8% ± 1.9% and 7.9% ± 2.4% of the initial amount, respectively). The NACNO treatment led to a higher permeation under the RSNO form than the GSNO and SNAP treatments (Fig. 3A). The duration of the study has no impact on the permeability of each treatment under the RSNO form while the permeability under the nitrite ions and nitrate ions (the oxidation product of nitrite ions) forms depended on time (Fig. 3B and 3C, $p_{time} < 0.05$) and on the treatment. Indeed, the NACNO treatment induced a higher absorption of NO_2^- (and NO_3^-) ionic forms than the GSNO and the SNAP treatments

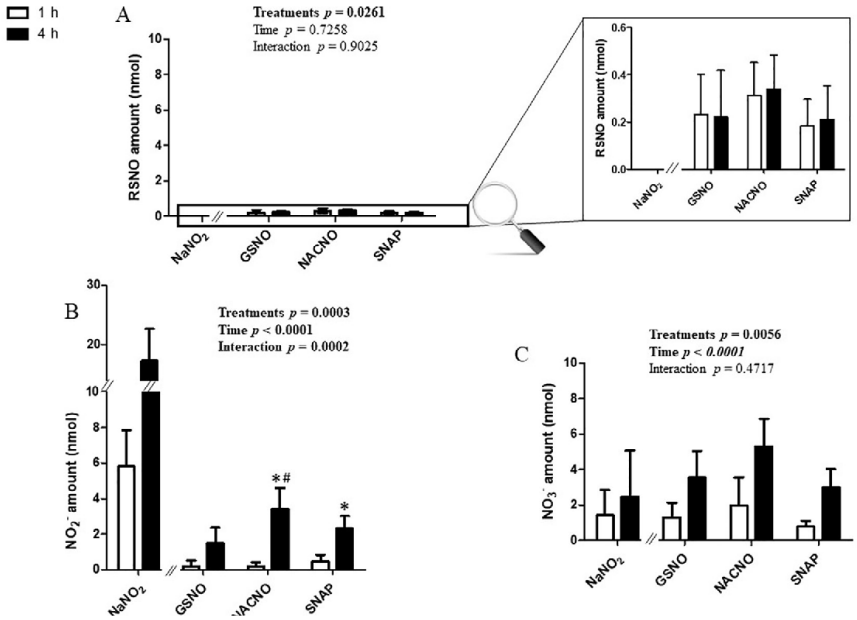

Fig. 3. Apical (pH 7.4) to basolateral compartment – Quantification in the basolateral compartment of permeated (A) RSNO, (B) NO_2^- and (C) NO_3^- after 1 h and 4 h of exposure to 50 nmol of each treatment. Results are shown as mean ± SD of four independent experiments done in duplicate and are compared using two-way ANOVA ($p_{treatment}$ (GSNO, NACNO, SNAP; excluding $NaNO_2$), p_{time} (1h, 4 h) and $p_{interaction}$). * *vs.* GSNO; # *vs.* SNAP at the same time; $p < 0.05$ (Bonferroni's multiple comparisons test).

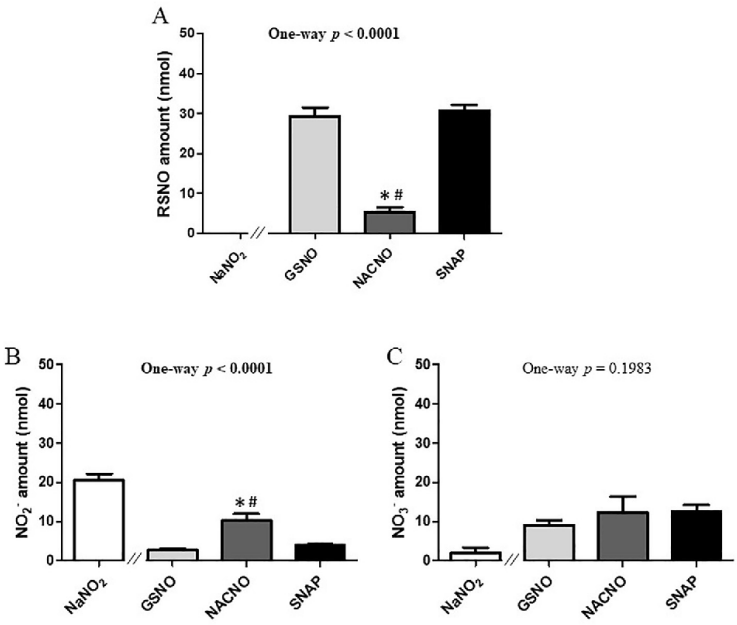

Fig. 4. Apical (pH 7.4) o basolateral compartment – Quantification in the apical compartment of remaining (A) RSNO, (B) NO_2^- and (C) NO_3^- and 4 h of exposure to 50 nmol of each treatment. Results are shown as mean ± SD of four independent experiments done in duplicate and are compared using one-way ANOVA (excluding $NaNO_2$) Bonferroni post-test. * *vs.* GSNO; # *vs.* SNAP at the same time; $p < 0.05$.

Table 3
Mass balance for each treatment (initial amount: 50 nmol) after 4 h of permeation from the apical to the basolateral compartment. Mean ± SD of four independent experiments done in duplicate.

Treatments	Amount (nmol)	Percentage of initial amount
GSNO	46 ± 4	92 ± 8
NACNO	38 ± 6	77 ± 12
SNAP	53 ± 7	106 ± 13
$NaNO_2$	41 ± 8	83 ± 16

($p_{treatment} = 0.0003$ and $p_{interaction}$ 0.0002), especially after 4 h ($p_{time} < 0.0001$) (Fig. 3B).

The $NaNO_2$ treatment led to the permeability of the two ionic species only (Fig. 3). The permeability under the NO_2^- form was time dependent and 30% higher than the permeability of each *S*-nitrosothiol treatment under NO_2^- form (Fig. 3B). The permeability under the nitrate ionic form (Fig. 3C), representing 5% of the initial amount, supposes a spontaneous oxidation of nitrite ions into nitrate ions within our experimental conditions (presence of dioxygen).

The Papp values for the NOx species (addition of RSNO, NO_2^- and NO_3^-) were situated within the medium class of permeability (BCS definition) for each *S*-nitrosothiol treatment and surrounded by the Papp values of the reference drugs, propranolol and furosemide (Table 2). The permeability of *S*-nitrosothiols under the RSNO form was 25–40 times lower (Papp ≈ 0.17×10^{-6} cm.s^{-1}) than that of NOx species, confirming the higher absorption of *S*-nitrosothiols under the NO_2^- and NO_3^- ionic forms. The $NaNO_2$ treatment allowed to define a high permeability under the NO_2^- ionic form.

After 4 h of permeability, 60% of the initial amount (50 nmol) of *S*-

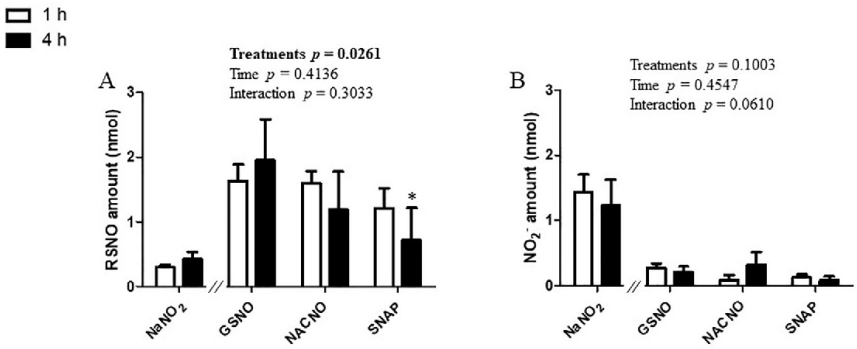

Fig. 5. Apical (pH 7.4) to basolateral permeability – Intracellular quantifications of (A) RSNO, (B) NO_2^-, (subtracted from the control cells) after 1 h and 4 h of exposure to 50 nmol of each treatment. Results are shown as mean ± SD of four independent experiments done in duplicate and are compared using two-way ANOVA ($p_{treatment}$ (GSNO, NACNO, SNAP; excluding $NaNO_2$), p_{time} (1h, 4 h) and $p_{interaction}$). * *vs.* GSNO at the same time; $p < 0.05$ (Bonferroni's multiple comparisons test).

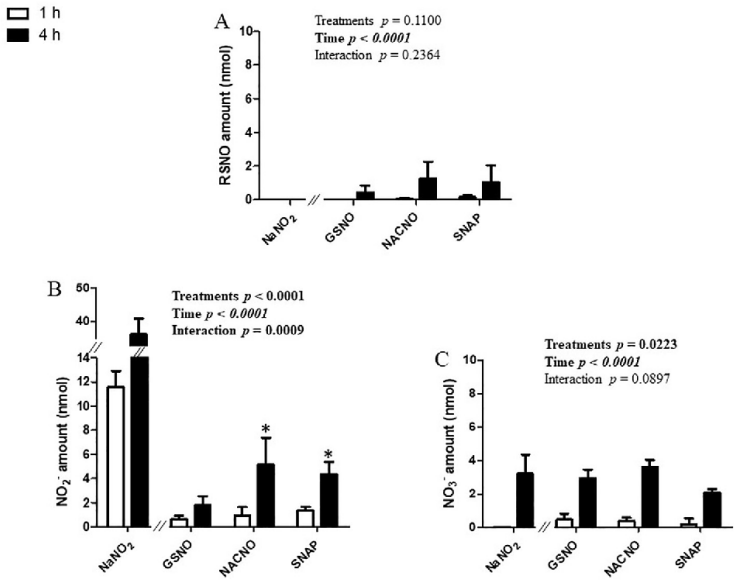

Fig. 6. Basolateral to Apical permeability – Quantification in the apical compartment of permeated (A) RSNO, (B) NO_2^- and (C) NO_3^- after 1 h and 4 h from 150 nmol of each treatment. Results are shown as mean ± SD of four independent experiments done in duplicate and are compared using two-way ANOVA ($p_{treatment}$ (GSNO, NACNO, SNAP; excluding $NaNO_2$), p_{time} (1h, 4 h) and $p_{interaction}$). * *vs.* GSNO at the same time; $p < 0.05$ (Bonferroni's multiple comparisons test).

Table 4
Values of apparent permeability coefficient (Papp) for NOx species (RSNO + NO_2^- + NO_3^-) and the RSNO form after 4 h of permeation from basolateral to apical compartment. nd: not determined, LOQ: Limit of quantification. Mean ± SD of four independent experiments done in duplicate.

Treatments	NOx Papp ($\times 10^{-6}$ cm.s^{-1})	RSNO Papp ($\times 10^{-6}$ cm.s^{-1})
GSNO	2.8 ± 1.2	0.3 ± 0.2
NACNO	4.5 ± 1.5	0.6 ± 0.6
SNAP	4.1 ± 0.7	0.5 ± 0.5
$NaNO_2$	97.5 ± 16.4	Under LOQ
Propranolol	33.1 ± 0.8	nd
Furosemide	15.2 ± 0.8	nd

nitrosothiols remained in the apical compartment for the GSNO and SNAP treatments, and only 10% for the NACNO treatment (Fig. 4A). Furthermore, the NACNO treatment led to a higher amount of nitrite ions remaining in the apical compartment compared to the GSNO and SNAP treatments (Fig. 4B), suggesting a higher degradation of NACNO into NO_2^-. Non-permeated nitrate ions amounts were around 23% for each treatment (Fig. 4C). The $NaNO_2$ treatment was still presenting 41% of non-permeated nitrite ions after 4 h (Fig. 4B) and lower spontaneous oxidation into nitrate ions (4%) within the apical compartment compared to *S*-nitrosothiol treatments (Fig. 4C).

Finally, the calculation of the mass balance (addition of all species quantified in the two compartments) after 4 h of permeability study, showed 83 ± 16% to 106 ± 13% of recovery for GSNO, SNAP and $NaNO_2$ (Table 3). Nevertheless, the NACNO treatment showed a loss of 23% of the initial amount deposited in the apical compartment. This missing can be trapped inside the cell monolayer, so cells were lysed and only RSNO and nitrite ions were quantified. Indeed, due to intracellular reducing power [35], the nitrate ions cannot exist inside cells. Quantities of RSNO found inside the cells were higher for *S*-nitrosothiol treatments than for the $NaNO_2$ treatment (Fig. 5A). This was the opposite for the NO_2^- intake (Fig. 5B). For each *S*-nitrosothiol treatment, the intracellular incorporation of the RSNO form was higher than the nitrite ions form. Intracellular quantity of the RSNO form depended on the *S*-nitrosothiol chemical structure ($p_{treatment} < 0.05$) with the lowest incorporation obtained for the SNAP treatment (< 2% of the initial amount) (Fig. 5A). Intracellular incorporation of nitrite ions was independent on time and treatments (Fig. 5B).

For intracellular quantification, the surface area of cells was increased 4.17 times (from 1.12 to 4.67 cm^2) in order to be able to quantify NOx species inside the cells. So, the intracellular amounts of RSNO and NO_2^- form were divided by 4.17 to calculate the mass balance (Table 2). The intracellular incorporation of RSNO and NO_2^- represented only 1.1%, 1.0% and 0.4% of the initial amount, for the GSNO, NACNO and SNAP treatments, respectively. Therefore, 22% of the initial amount are still missing for the NACNO treatment.

3.3. *S*-Nitrosothiols permeability from the basolateral to apical compartment

In order to determine the permeability modality (passive *vs.* active) for each *S*-nitrosothiol, the study was carried out in the opposite direction, from the basolateral to the apical compartment.

In this condition, the permeability of the RSNO form (Fig. 6A) was only dependent on time for each *S*-nitrosothiol treatment. The permeability of the NO_2^- and NO_3^- ionic forms was dependent on time and treatment (Fig. 6B and 6C). Higher amounts were permeated under the NO_2^- ionic form for the NACNO and SNAP treatments (≈ 3% of initial amounts) compared to the GSNO treatment (1.2% of initial amount, Fig. 6B). As in the experiments performed from the apical to the basolateral compartment (Section 3.2), NO_2^- and NO_3^- were the major permeated species.

For each *S*-nitrosothiol treatment, the Papp values in both directions (apical to basolateral versus basolateral to apical) were equivalent (Tables 2 and 4), the *S*-nitrosothiols intestinal permeability can be postulated as a passive diffusion [36]. This postulate is also based on the validation of our intestinal barrier model comparing the Papp values of reference molecules with the literature [19]. Propranolol with equivalent bidirectional Papp values follows a passive diffusion whereas furosemide with a higher Papp value from basolateral to apical than from apical to basolateral, follows an active efflux transport.

After 4 h of permeability study, 95% of the initial amount (150 nmol) of each *S*-nitrosothiol treatment remained unpermeated

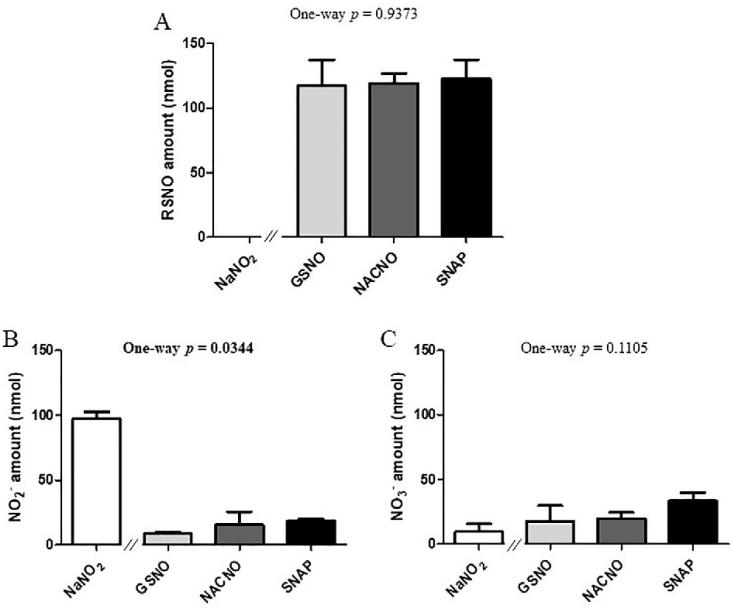

Fig. 7. Basolateral to apical permeability – Quantification in the basolateral compartment of remaining (A) RSNO, (B) NO_2^- and (C) NO_3^- after 4 h of exposure to 150 nmol of each treatment. Results are shown as mean ± SD of four independent experiments done in duplicate and are compared using one-way ANOVA (excluding $NaNO_2$).

Table 5
Mass balance for each tested treatment (initial amount 150 nmol) after 4 h of permeability from the basolateral to the apical compartment. Mean ± SD of four independent experiments done in duplicate.

Treatments	Amount (nmol)	Percentage of the initial amount
GSNO	169 ± 40	113 ± 36
NACNO	159 ± 24	106 ± 21
SNAP	162 ± 49	108 ± 44
$NaNO_2$	155 ± 18	103 ± 17

(Fig. 7). The amounts of unpermeated NO_2^- ions (Fig. 7B) were the only form that depended on *S*-nitrosothiol chemical structure ($p_{treatment} = 0.0344$). As *S*-nitrosothiols are separated from cells by the porous membrane of the device, they cannot be metabolised by cell membrane enzymes showing the great importance of *S*-nitrosothiol metabolism in their permeability. Furthermore, the high amount of remaining RSNO form (Fig. 7A) attested from the stability of each *S*-nitrosothiol in our operating conditions.

This also showed that the degradation of *S*-nitrosothiols into ionic forms observed in the apical to basolateral permeability study (Fig. 4) was due to cell membrane enzymes activity. Finally, the study of *S*-nitrosothiols permeability from the basolateral to the apical compartment showed a mass balance of 100% for each *S*-nitrosothiol treatment (Table 5).

3.4. Influence of the apical pH on S-nitrosothiols permeability

The principal site of absorption of small molecules including peptides and amino acids is the jejunum part of the intestine, which physiological pH ranges from 6 to 7. In order to study the permeability of *S*-nitrosothiols close to physiological conditions, the pH of the apical compartment mimicking the intestinal lumen was shifted of one log from pH 7.4 to pH 6.4. pH acidification has no impact on propranolol and furosemide permeability [27], so the experiment was not performed.

At pH 6.4, the permeability of each *S*-nitrosothiol under the RSNO and the ionic forms (Fig. 8) followed the same profile than at pH 7.4 (Fig. 3). However, the NACNO treatment showed a 7 times increase of permeability under the RSNO form (Fig. 8A) compared to pH 7.4. The $NaNO_2$ treatment showed a permeability under the RSNO form (Fig. 8A) and a large (10 times at 1 h and 20 times at 4 h) increase of the permeability under the NO_3^- form (Fig. 8C). So, at pH 6.4, the Papp values of NOx species and RSNO form rose for the $NaNO_2$ treatment (Table 6) compared to pH 7.4 (Table 2).

The Papp values at pH 6.4 (Table 6) maintained each *S*-nitrosothiol in the medium class of permeability for NOx species and in the low permeability class for the RSNO form. However, the Papp value of the NACNO treatment under the RSNO form increased from $0.21 \pm 0.08 \times 10^{-6}$ cm.s^{-1} (Table 2) at pH 7.4 to $0.9 \pm 0.7 \times 10^{-6}$ cm.s^{-1} at pH 6.4, bringing NACNO close to the medium permeability class (from 1 to 10×10^{-6} cm.s^{-1}, [19]).

The distribution of non-permeated species remaining in the apical compartment after 4 h of permeability at pH 6.4 (Fig. 9) was similar to that at pH 7.4 (Fig. 4).

The absorption of *S*-nitrosothiols from the apical compartment at pH 6.4 to the basolateral compartment at pH 7.4 presented a mass balance from 58% to 78% of the initial amount (Table 7).

4. Discussion

The human intestinal barrier model based on Caco-2 cells is widely used in the pharmaceutical industry to determine the parameters of intestinal permeability of new drugs. The results obtained depend mainly on cell culture parameters (time, medium and age [29]). In the present study, we validated our conditions using two reference molecules, *i.e.* propranolol and furosemide, in comparison with already published Papp values. These Papp values, as well as TEER values (> 500 Ω.cm^2), are quality guaranties of our model and results. From the literature, propranolol, with a Papp value between 3.30×10^{-6} and 41.90×10^{-6} cm.s^{-1} [26,27] belongs to the high permeability class, and furosemide, with a Papp value varying from 0.04×10^{-6} to 0.11×10^{-6} cm.s^{-1} [26,37] belongs to the low permeability class. Such a low permeability for furosemide was attributed to an efflux

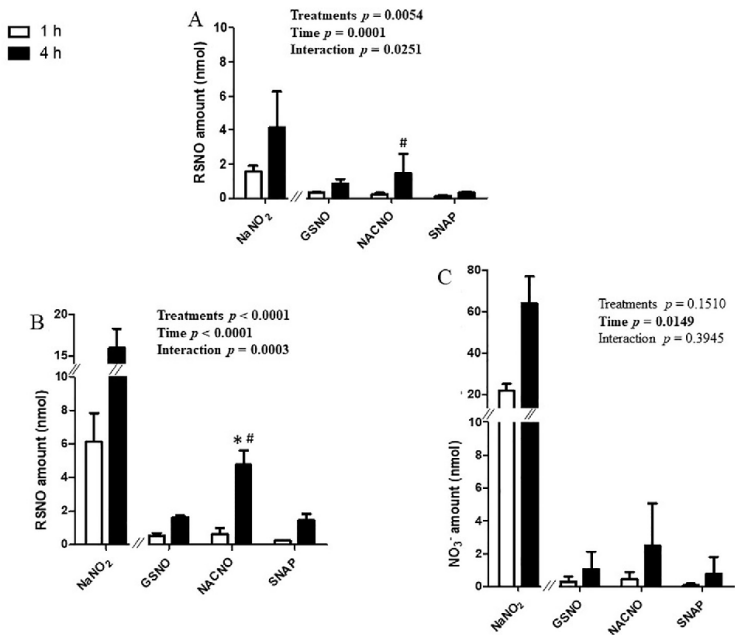

Fig. 8. Apical pH 6.4 to Basolateral permeability – Quantification in the basolateral compartment of remaining (A) RSNO, (B) NO_2^- and (C) NO_3^- after 1 h and 4 h of exposure to 50 nmol of each treatment. Results are shown as mean ± SD of three independent experiments done in duplicate and are compared using two-way ANOVA ($p_{treatment}$ (GSNO, NACNO, SNAP; excluding $NaNO_2$), p_{time} (1h, 4 h) and $p_{interaction}$). * *vs.* GSNO; # *vs.* SNAP at the same time; $p < 0.05$ (Bonferroni's multiple comparisons test).

Table 6
Values of apparent permeability coefficient (Papp) for NOx species (RSNO + NO_2^- + NO_3^-) and the RSNO form after 4 h of permeability study from the apical compartment (pH 6.4) to the basolateral compartment (pH 7.4). Mean ± SD of three independent experiments done in duplicate.

Treatments	NOx Papp ($\times 10^{-6}$ cm.s^{-1})	RSNO Papp ($\times 10^{-6}$ cm.s^{-1})
GSNO	1.9 ± 0.6	0.5 ± 0.2
NACNO	4.8 ± 2.4	0.9 ± 0.7
SNAP	1.4 ± 0.8	0.20 ± 0.05
$NaNO_2$	207.0 ± 37.9	7.7 ± 6.5

driven by the intestinal P-glycoprotein to the luminal direction [38]. The Papp values for propranolol (24.4×10^{-6} cm.s^{-1}) and furosemide (0.3×10^{-6} cm.s^{-1}) obtained using our intestinal barrier model confirm the already published values and probably attest for the presence and activity of the P-glycoprotein in this model.

S-Nitrosothiols are NO donors allowing the release of NO with a relative short half-life (within a few hours) [2]. Thereby, in aqueous medium, NO is spontaneously and quickly oxidized into nitrite and nitrate ions. So, it is mandatory to study the intestinal permeability of these ionic species as well as the permeability of the RSNO form to evaluate the bioavailability of NO in the blood stream after oral administration. In the present study, each *S*-nitrosothiol increased their permeability following time, in each of the three proposed conditions (apical to basolateral compartments at pH 7.4 direction, opposite direction, apical compartment at pH 6.4 to basolateral compartment at pH 7.4).

The study of *S*-nitrosothiols permeability from the compartment mimicking the intestinal lumen (apical compartment) to the compartment mimicking the lumen of blood vessels (basolateral compartment) revealed a weak absorption of each *S*-nitrosothiol treatment under the RSNO form compared to the ionic species, which are the major absorbed species (Fig. 10A). In a general point of view, the ionic species are more absorbed by the intestine than the neutral molecules. Indeed, specific ionic transporters such as the Organic Cation Transporters (OCT) and the Zwitterion Transporters (OCTN), implied in the absorption of Na^+ and Ca^{2+}, are expressed within the intestinal tissue and Caco-2 cells [39,40].

The Papp values of all permeated species placed each *S*-nitrosothiol studied within the medium permeability class for NOx species, class that was surrounded by our two reference molecules (propranolol and furosemide). The Papp value was the same for each *S*-nitrosothiol even if they presented different physico-chemical properties with a higher hydrophilicity for GSNO than SNAP [2]. In this way, the physico-chemical properties of the skeleton (R) carrying the nitroso group are not prevalent for the intestinal permeability of the *S*-nitrosothiols. The mass balance within both compartments allowed a recovery of 100% of the initial amount deposited for the SNAP treatment. The small missing amount for the GSNO treatment was recovered by the intracellular quantification, rising the mass balance to almost 100%. However, the NACNO treatment showed a mass balance of 75%, which was not completed to 100% after intracellular quantification.

The amount of NOx species found inside the cells was higher for the GSNO treatment than for the SNAP treatment, with the NACNO treatment situated between each other. SNAP promotes drug intestinal absorption [41] by opening tight junctions without affecting barrier integrity. Indeed, SNAP increases insulin rectal absorption, transepithelial transport of fluorescein sulfonic acid (low absorbable molecule) [41,42] and macromolecules absorption through the intestine by the reversible opening of tight junctions [41,43,44] and a thickening of ileal mucosal membrane [45]. So, in our study, paracellular absorption of SNAP can be speculated. GSNO and NACNO were partially absorbed *via* a transcellular pathway. The mass imbalance observed for the NACNO treatment can be attributed to its higher metabolism within the apical compartment. Moreover, the metabolism of each *S*-nitrosothiol was abolished in the donor compartment when studying the permeability from the basolateral to the apical compartments. This phenomenon is a proof of the intestinal barrier orientation with a brush border including metabolic enzymes like redoxins and gamma-glutamyl transferase [46], faced to the apical compartment, and a basal lamina without any metabolic activity faced to the basolateral compartment.

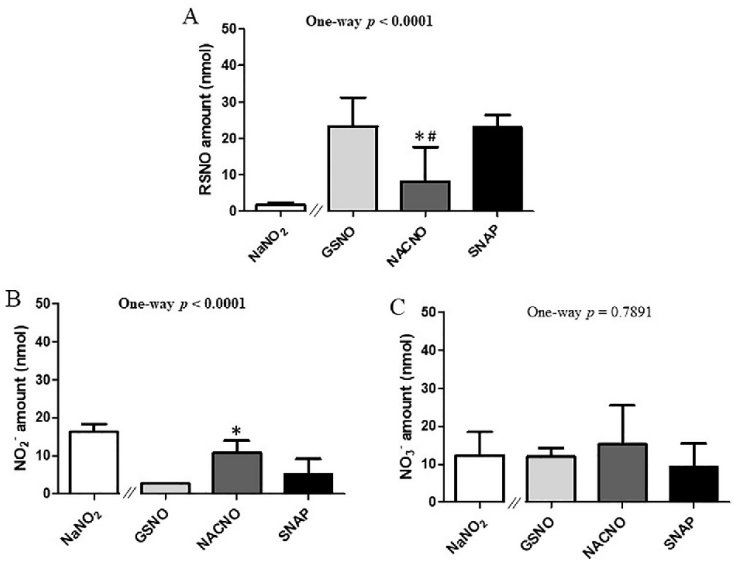

Fig. 9. Apical (pH 6.4) to basolateral compartment – Quantification in the apical compartment of remaining (A) RSNO, (B) NO_2^- and (C) NO_3^- after 1 h and 4 h of exposure to 50 nmol of each treatment. Results are shown as mean ± SD of three independent experiments done in duplicate and are compared using one-way ANOVA (excluding $NaNO_2$). * *vs.* GSNO; # *vs.* SNAP at the same time; $p < 0.05$ (Bonferroni post-test).

Table 7
Mass balance for all tested treatments (initial amount 50 nmol) after 4 h of permeability from the apical compartment at pH 6.4 to the basolateral compartment at pH 7.4. Mean ± SD of three independent experiments done in duplicate.

Treatments	Amount (nmol)	Percentage of the initial amount
GSNO	34 ± 10	68 ± 20
NACNO	37 ± 10	78 ± 20
SNAP	31 ± 5	58 ± 8
$NaNO_2$	114 ± 18	227 ± 35

The equal Papp values obtained permeability studies from the apical to the basolateral compartments and permeability studies from the basolateral to the apical compartments revealed that the absorption of *S*-nitrosothiols is driven by a passive diffusion through the intestinal barrier (Fig. 10B). This transport modality excluded the participation of all transport systems and energy consumption in the permeability of *S*-nitrosothiols [47]. In that way, *S*-nitrosothiols permeability may be improved using pharmaceutical formulations, which are aimed at opening tight junctions and increasing the local concentration and the residence time of the molecule.

Finally, the acidification (pH 6.4) of the apical compartment to mimic the physiological condition of the jejunum part of the intestine (Fig. 10C) showed a permeability dependent on the *S*-nitrosothiol treatment. The very low permeability of the RSNO form for the NACNO treatment at pH 7.4 was multiplied by ten at pH 6.4. However, this favoured permeability of NACNO seemed to be related neither to the lipophilic balance – as NACNO showed a log P intermediate between GSNO and SNAP – nor to the ionization state – as the isoelectric point (pI) of NACNO is intermediate (3.24) between GSNO and SNAP (4.8 and 4.85, respectively) and far away from the studied pHs. As the thiol functions are blocked by NO, their pKa values are not involved in the pI of the *S*-nitrosothiols. However, it may be involved in the stability of the S-NO bound, *e.g* the *S*-nitrosocysteine (cysNO) is less stable than GSNO due to a lower pKa of the thiol function of the cysteine residue. The permeability of the RSNO form for the $NaNO_2$ treatment suggested that pH 6.4 favoured the formation of RSNO starting from NO_2^-. This can also be postulated for all the experiments where permeability of the RSNO forms was observed. However, the formation of RSNO following the $NaNO_2$ treatment should certainly occur thanks to intracellular thiols, which are the only available source of thiol in the experimental system. This phenomenon will lead to cell thiol depletion, which will induce tolerance at it was already seen in clinics for organic nitrate treatments [48]. However, our experiments showed that *S*-nitrosothiol treatments bringing the thiol function itself, won't induce thiol depletion neither tolerance phenomenon. Furthermore, Pinheiro and coworkers demonstrated that oral administration of nitrite ions allowed the formation of RSNO in the stomach leading to an increased plasma RSNO concentration [17]. Our work precises that the formation of RSNO may also occur in the jejunum part of the intestine at acidic pH.

Finally, according to the BCS, *S*-nitrosothiols can be classified between class I and class III, regarding their high solubility and medium permeability. From Le Ferrec et al. [49], the result obtained *in vitro* with high permeability molecules (class I and class II) can be easily transposed to *in vivo* intestinal absorption unlike results obtained for low permeability molecules (class III and class IV). So, the *S*-nitrosothiols included in the medium class of permeability can be considered as drugs suitable for oral administration. Thereafter, it would be interesting to study the permeability of *S*-nitrosothiols in the presence of albumin in the basolateral compartment to mimic the blood stream compartment [50]. Furthermore, albumin including a free reduced cysteine residue in position 34 will increase the amount of RSNO found in the basolateral compartment through *S*-nitrosation process.

In conclusion, our study suggested that *S*-nitrosothiols can be administrated by the oral route to be absorbed at the intestinal level, mainly in the jejunum part. The passive diffusion of *S*-nitrosothiols under three different kinds of species such as nitrite and nitrate ions and the RSNO form was demonstrated using a model of human intestinal barrier. The permeation of the RSNO species will improve the interest for *S*-nitrosothiols oral administration compared to nitrite ions. Indeed, *S*-nitrosothiols would not deplete the intracellular stock of reduced thiols. Even if *S*-nitrosothiols are good candidates for NO oral supplementation, they will need appropriate protection from enzymatic degradation using nanotechnologies [20,51–53].

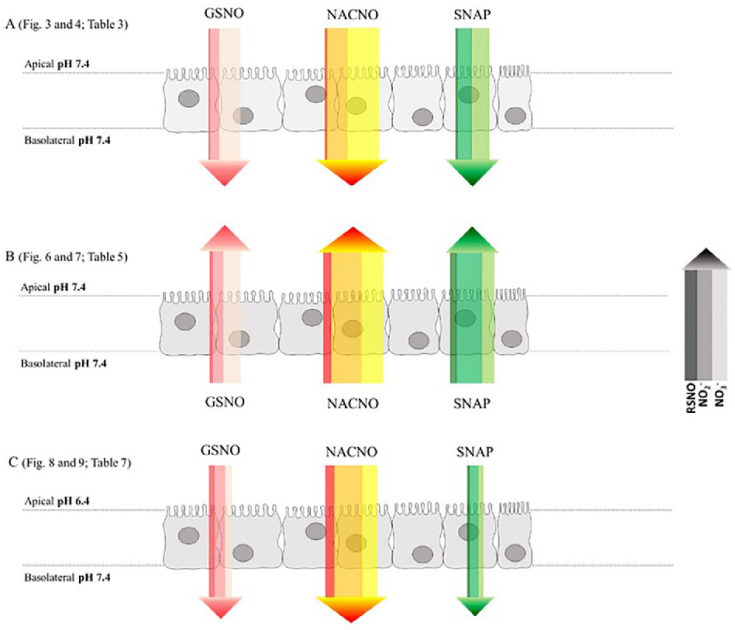

Fig. 10. Summary of NOx species permeability for each *S*-nitrosothiol treatment. The colour code of each arrow from the left to the right is the amount (width) of RSNO, NO_2^- and NO_3^-. The 4 h-permeability for each treatment is represented from (A) apical to basolateral compartment, (B) basolateral to apical compartment and (C) apical (pH 6.4) to basolateral compartment (pH 7.4).

Acknowledgments

The authors acknowledge Dr Wen WU for her help in preliminary experiment settings. The CITHEFOR EA3452 lab was supported by the "Impact Biomolecules" project of the "*Lorraine Université d'Excellence*" (*Investissements d'avenir – ANR*).

References

[1] T.S. Hakim, K. Sugimori, E.M. Camporesi, G. Anderson, Half-life of nitric oxide in aqueous solutions with and without haemoglobin, Physiol. Meas. 17 (1996) 267–277.

[2] C. Gaucher, A. Boudier, F. Dahboul, M. Parent, P. Leroy, S-nitrosation/denitrosation in cardiovascular pathologies: facts and concepts for the rational design of S-nitrosothiols, Curr. Pharm. Des. 19 (2013) 458–472.

[3] Z. Kaposzta, P.A. Baskerville, D. Madge, S. Fraser, J.F. Martin, H.S. Markus, L-Arginine and S-nitrosoglutathione reduce embolization in humans, Circulation 103 (2001) 2371–2375.

[4] Z. Kaposzta, A. Clifton, J. Molloy, J.F. Martin, H.S. Markus, S-nitrosoglutathione reduces asymptomatic embolization after carotid angioplasty, Circulation 106 (2002) 3057–3062.

[5] Z. Kaposzta, J.F. Martin, H.S. Markus, Switching off embolization from symptomatic carotid plaque using S-nitrosoglutathione, Circulation 105 (2002) 1480–1484.

[6] T. Rassaf, P. Kleinbongard, M. Preik, A. Dejam, P. Gharini, T. Lauer, J. Erckenbrecht, A. Duschin, R. Schulz, G. Heusch, M. Feelisch, M. Kelm, Plasma nitrosothiols contribute to the systemic vasodilator effects of intravenously applied NO: experimental and clinical Study on the fate of NO in human blood, Circ. Res. 91 (2002) 470–477.

[7] T. Rassaf, L.W. Poll, P. Brouzos, T. Lauer, M. Totzeck, P. Kleinbongard, P. Gharini, K. Andersen, R. Schulz, G. Heusch, U. Mödder, M. Kelm, Positive effects of nitric oxide on left ventricular function in humans, Eur. Heart J. 27 (2006) 1699–1705, http://dx.doi.org/10.1093/eurheartj/ehl096.

[8] S. Moncada, A. Higgs, The L-arginine-nitric oxide pathway, N. Engl. J. Med. 329 (1993) 2002–2012, http://dx.doi.org/10.1056/NEJM199312303292706.

[9] B. Meyer, A. Genoni, A. Boudier, P. Leroy, M.F. Ruiz-Lopez, Structure and stability studies of pharmacologically relevant S-nitrosothiols: a theoretical approach, J. Phys. Chem. A 120 (2016) 4191–4200, http://dx.doi.org/10.1021/acs.jpca.6b02230.

[10] B.A. Maron, S.-S. Tang, J. Loscalzo, S-nitrosothiols and the S-nitrosoproteome of the cardiovascular system, Antioxid. Redox Signal. 18 (2013) 270–287, http://dx.doi.org/10.1089/ars.2012.4744.

[11] E. Belcastro, W. Wu, I. Fries-Raeth, A. Corti, A. Pompella, P. Leroy, I. Lartaud, C. Gaucher, Oxidative stress enhances and modulates protein S-nitrosation in smooth muscle cells exposed to S-nitrosoglutathione, Nitric Oxide Biol. Chem. 69 (2017) 10–21, http://dx.doi.org/10.1016/j.niox.2017.07.004.

[12] F. Dahboul, P. Leroy, K. Maguin Gate, A. Boudier, C. Gaucher, P. Liminana, I. Lartaud, A. Pompella, C. Perrin-Sarrado, Endothelial γ-glutamyltransferase contributes to the vasorelaxant effect of S-nitrosoglutathione in rat aorta, PloS One 7 (2012) e43190, , http://dx.doi.org/10.1371/journal.pone.0043190.

[13] M.H. Krieger, K.F.R. Santos, S.M. Shishido, A.C.B.A. Wanschel, H.F.G. Estrela, L. Santos, M.G. De Oliveira, K.G. Franchini, R.C. Spadari-Bratfisch, F.R.M. Laurindo, Antiatherogenic effects of S-nitroso-N-acetylcysteine in hypercholesterolemic LDL receptor knockout mice, Nitric Oxide Biol. Chem. 14 (2006) 12–20, http://dx.doi.org/10.1016/j.niox.2005.07.011.

[14] M. Khan, B. Sekhon, S. Giri, M. Jatana, A.G. Gilg, K. Ayasolla, C. Elango, A.K. Singh, I. Singh, S-Nitrosoglutathione reduces inflammation and protects brain against focal cerebral ischemia in a rat model of experimental stroke, J. Cereb. Blood Flow Metab. Off. J. Int. Soc. Cereb. Blood Flow Metab. 25 (2005) 177–192, http://dx.doi.org/10.1038/sj.jcbfm.9600012.

[15] M. Khan, M. Jatana, C. Elango, A.S. Paintlia, A.K. Singh, I. Singh, Cerebrovascular protection by various nitric oxide donors in rats after experimental stroke, Nitric Oxide Biol. Chem. 15 (2006) 114–124, http://dx.doi.org/10.1016/j.niox.2006.01.008.

[16] M. Khan, T.S. Dhammu, M. Baarine, J. Kim, M.K. Paintlia, I. Singh, A.K. Singh, GSNO promotes functional recovery in experimental TBI by stabilizing HIF-1α, Behav. Brain Res. 340 (2018) 63–70, http://dx.doi.org/10.1016/j.bbr.2016.10.037.

[17] L.C. Pinheiro, J.H. Amaral, G.C. Ferreira, R.L. Portella, C.S. Ceron, M.F. Montenegro, J.C. Toledo, J.E. Tanus-Santos, Gastric S-nitrosothiol formation drives the antihypertensive effects of oral sodium nitrite and nitrate in a rat model of renovascular hypertension, Free Radic. Biol. Med. 87 (2015) 252–262, http://dx.doi.org/10.1016/j.freeradbiomed.2015.06.038.

[18] M. Levin (Ed.), Pharm. Process Scale-Up, Informa Healthcare, 2001, , http://dx.doi.org/10.1201/9780824741969.axh.

[19] Y. Peng, P. Yadava, A.T. Heikkinen, N. Parrott, A. Railkar, Applications of a 7-day Caco-2 cell model in drug discovery and development, Eur. J. Pharm. Sci. Off. J. Eur. Fed. Pharm. Sci. 56 (2014) 120–130, http://dx.doi.org/10.1016/j.ejps.2014.02.008.

[20] W. Wu, C. Perrin-Sarrado, H. Ming, I. Lartaud, P. Maincent, X.-M. Hu, A. Sapin-Minet, C. Gaucher, Polymer nanocomposites enhance S-nitrosoglutathione intestinal absorption and promote the formation of releasable nitric oxide stores in rat aorta, Nanomed. Nanotechnol. Biol. Med. 12 (2016) 1795–1803, http://dx.doi.org/10.1016/j.nano.2016.05.006.

[21] K.A. Broniowska, A.R. Diers, N. Hogg, S-nitrosoglutathione, Biochim. Biophys. Acta. 2013 (1830) 3173–3181, http://dx.doi.org/10.1016/j.bbagen.2013.02.004.

[22] P. Teixeira, P. Napoleão, C. Saldanha, S-nitrosoglutathione efflux in the erythrocyte, Clin. Hemorheol. Microcirc. 60 (2015) 397–404, http://dx.doi.org/10.3233/CH-141855.

[23] L.F. Prescott, R.N. Illingworth, J.A. Critchley, M.J. Stewart, R.D. Adam, A.T. Proudfoot, Intravenous N-acetylcystine: the treatment of choice for paracetamol poisoning, Br. Med. J. 2 (1979) 1097–1100.

[24] Y. Wang, J. Cao, X. Wang, S. Zeng, Stereoselective transport and uptake of propranolol across human intestinal Caco-2 cell monolayers, Chirality 22 (2010) 361–368, http://dx.doi.org/10.1002/chir.20753.

[25] M. Parent, A. Boudier, F. Dupuis, C. Nouvel, A. Sapin, I. Lartaud, J.-L. Six, P. Leroy, P. Maincent, Are in situ formulations the keys for the therapeutic future of S-nitrosothiols? Eur. J. Pharm. Biopharm. Off. J. Arbeitsgemeinschaft Pharm. Verfahrenstechnik EV 85 (2013) 640–649, http://dx.doi.org/10.1016/j.ejpb.2013.08.005.

[26] E.H. Kerns, L. Di, S. Petusky, M. Farris, R. Ley, P. Jupp, Combined application of parallel artificial membrane permeability assay and Caco-2 permeability assays in drug discovery, J. Pharm. Sci. 93 (2004) 1440–1453, http://dx.doi.org/10.1002/jps.20075.

[27] C. Zhu, L. Jiang, T.-M. Chen, K.-K. Hwang, A comparative study of artificial membrane permeability assay for high throughput profiling of drug absorption potential, Eur. J. Med. Chem. 37 (2002) 399–407.

[28] S.I. Khan, E.A. Abourashed, I.A. Khan, L.A. Walker, Transport of harman alkaloids across Caco-2 cell monolayers, Chem. Pharm. Bull. (Tokyo) 52 (2004) 394–397.

[29] B. Srinivasan, A.R. Kolli, M.B. Esch, H.E. Abaci, M.L. Shuler, J.J. Hickman, TEER measurement techniques for in vitro barrier model systems, J. Lab. Autom. 20 (2015) 107–126, http://dx.doi.org/10.1177/2211068214561025.

[30] W.S. Jobgen, S.C. Jobgen, H. Li, C.J. Meininger, G. Wu, Analysis of nitrite and nitrate in biological samples using high-performance liquid chromatography, J. Chromatogr. B Analyt. Technol. Biomed. Life. Sci. 851 (2007) 71–82, http://dx.doi.org/10.1016/j.jchromb.2006.07.018.

[31] H.K. Kim, J.H. Hong, M.S. Park, J.S. Kang, M.H. Lee, Determination of propranolol concentration in small volume of rat plasma by HPLC with fluorometric detection, Biomed. Chromatogr. BMC 15 (2001) 539–545, http://dx.doi.org/10.1002/bmc.110.

[32] G.S. Rekhi, S.S. Jambhekar, P.F. Souney, D.A. Williams, A fluorimetric liquid chromatographic method for the determination of propranolol in human serum/plasma, J. Pharm. Biomed. Anal. 13 (1995) 1499–1505.

[33] J.M. Ryu, S.J. Chung, M.H. Lee, C.K. Kim, C.K. Shim, Increased bioavailability of propranolol in rats by retaining thermally gelling liquid suppositories in the rectum, J. Control. Release Off. J. Control. Release Soc. 59 (1999) 163–172.

[34] T. Galaon, S. Udrescu, I. Sora, V. David, A. Medvedovici, High-throughput liquid-chromatography method with fluorescence detection for reciprocal determination of furosemide or norfloxacin in human plasma, Biomed. Chromatogr. 21 (2007) 40–47, http://dx.doi.org/10.1002/bmc.715.

[35] O. Parodi, R. De Maria, E. Roubina, Redox state, oxidative stress and endothelial dysfunction in heart failure: the puzzle of nitrate-thiol interaction, J. Cardiovasc. Med. 8 (2007) 765–774, http://dx.doi.org/10.2459/JCM.0b013e32801194d4.

[36] E.C. Sherer, A. Verras, M. Madeira, W.K. Hagmann, R.P. Sheridan, D. Roberts, K. Bleasby, W.D. Cornell, QSAR prediction of passive permeability in the LLC-PK1 cell line: trends in molecular properties and cross-prediction of Caco-2 permeabilities, Mol. Inform. 31 (2012) 231–245, http://dx.doi.org/10.1002/minf.201100157.

[37] S. Yamashita, T. Furubayashi, M. Kataoka, T. Sakane, H. Sezaki, H. Tokuda, Optimized conditions for prediction of intestinal drug permeability using Caco-2 cells, Eur. J. Pharm. Sci. Off. J. Eur. Fed. Pharm. Sci. 10 (2000) 195–204.

[38] P.-A. Billat, E. Roger, S. Faure, F. Lagarce, Models for drug absorption from the small intestine: where are we and where are we going? Drug Discov. Today. 22 (2017) 761–775, http://dx.doi.org/10.1016/j.drudis.2017.01.007.

[39] T. Han, R.S. Everett, W.R. Proctor, C.M. Ng, C.L. Costales, K.L.R. Brouwer, D.R. Thakker, Organic cation transporter 1 (OCT1/mOct1) is localized in the apical membrane of caco-2 cell monolayers and enterocytes, Mol. Pharmacol. 84 (2013) 182–189, http://dx.doi.org/10.1124/mol.112.084517.

[40] T. Hirano, S. Yasuda, Y. Osaka, M. Kobayashi, S. Itagaki, K. Iseki, Mechanism of the inhibitory effect of zwitterionic drugs (levofloxacin and grepafloxacin) on carnitine transporter (OCTN2) in Caco-2 cells, Biochim. Biophys. Acta BBA – Biomembr. 1758 (2006) 1743–1750, http://dx.doi.org/10.1016/j.bbamem.2006.07.002.

[41] G. Fetih, F. Habib, H. Katsumi, N. Okada, T. Fujita, M. Attia, A. Yamamoto, Excellent absorption enhancing characteristics of NO donors for improving the intestinal absorption of poorly absorbable compound compared with conventional absorption enhancers, Drug Metab. Pharmacokinet. 21 (2006) 222–229.

[42] A. Yamamoto, H. Tatsumi, M. Maruyama, T. Uchiyama, N. Okada, T. Fujita, Modulation of intestinal permeability by nitric oxide donors: implications in intestinal delivery of poorly absorbable, Drugs 7 (2018).

[43] A.L. Salzman, M.J. Menconi, N. Unno, R.M. Ezzell, D.M. Casey, P.K. Gonzalez, M.P. Fink, Nitric oxide dilates tight junctions and depletes ATP in cultured Caco-2BBe intestinal epithelial monolayers, Am. J. Physiol. 268 (1995) G361–373, http://dx.doi.org/10.1152/ajpgi.1995.268.2.G361.

[44] N. Numata, K. Takahashi, N. Mizuno, N. Utoguchi, Y. Watanabe, M. Matsumoto, T. Mayumi, Improvement of intestinal absorption of macromolecules by nitric oxide donor, J. Pharm. Sci. 89 (2000) 1296–1304.

[45] D.-Z. Xu, Q. Lu, E.A. Deitch, Nitric oxide directly impairs intestinal barrier function, Shock Augusta Ga 17 (2002) 139–145.

[46] N. Hogg, R.J. Singh, E. Konorev, J. Joseph, B. Kalyanaraman, S-Nitrosoglutathione as a substrate for gamma-glutamyl transpeptidase, Biochem. J. 323 (Pt 2) (1997) 477–481.

[47] B. Alberts, A. Johnson, J. Lewis, M. Raff, K. Roberts, P. Walter, Carrier Proteins and Active Membrane Transport, 2002. https://www.ncbi.nlm.nih.gov/books/NBK26896/ (accessed January 23, 2018).

[48] A. Daiber, T. Münzel, Organic nitrate therapy, nitrate tolerance, and nitrate-induced endothelial dysfunction: emphasis on redox biology and oxidative stress, Antioxid. Redox Signal. 23 (2015) 899–942, http://dx.doi.org/10.1089/ars.2015.6376.

[49] E. Le Ferrec, C. Chesne, P. Artusson, D. Brayden, G. Fabre, P. Gires, F. Guillou, M. Rousset, W. Rubas, M.L. Scarino, In vitro Models of the Intestinal Barrier. The Report and Recommendations of ECVAM Workshop 46, European Centre for the Validation of Alternative methods, Altern. Lab. Anim. ATLA, 2001, pp. 649–668.

[50] J.E. Gonçalves, M. Ballerini Fernandes, C. Chiann, M.N. Gai, J. De Souza, S. Storpirtis, Effect of pH, mucin and bovine serum on rifampicin permeability through Caco-2 cells, Biopharm. Drug Dispos. 33 (2012) 316–323, http://dx.doi.org/10.1002/bdd.1802.

[51] W. Wu, C. Gaucher, R. Diab, I. Fries, Y.-L. Xiao, X.-M. Hu, P. Maincent, A. Sapin-Minet, Time lasting S-nitrosoglutathione polymeric nanoparticles delay cellular protein S-nitrosation, Eur. J. Pharm. Biopharm. Off. J. Arbeitsgemeinschaft Pharm. Verfahrenstechnik EV 89 (2015) 1–8, http://dx.doi.org/10.1016/j.ejpb.2014.11.005.

[52] W. Wu, C. Gaucher, I. Fries, X.-M. Hu, P. Maincent, A. Sapin-Minet, Polymer nanocomposite particles of S-nitrosoglutathione: a suitable formulation for protection and sustained oral delivery, Int. J. Pharm. 495 (2015) 354–361, http://dx.doi.org/10.1016/j.ijpharm.2015.08.074.

[53] K.U. Shah, S.U. Shah, N. Dilawar, G.M. Khan, S. Gibaud, Thiomers and their potential applications in drug delivery, Expert Opin. Drug Deliv. 14 (2017) 601–610, http://dx.doi.org/10.1080/17425247.2016.1227787.

2. Experimental paper: "Degradation of *S*-nitrosoglutathione in rat intestine: roles of denitrosating enzymatic and chemical factors on absorption and permeation" to be submitted in *Drug Metabolism and Disposition* after completion of additional experiments

Detailed procedures used for experiments in this article are present in protocols (see appendices) entitled "Measurement of nitrite, nitrate ions and S-nitrosothiols using the 2,3-diaminonaphthalene assay by spectrofluorometry", "Measurement of nitrite, nitrate ions and *S*-nitrosothiols using the 2,3-diaminonaphthalene assay by LC coupled with tandem mass spectrometry", "Measurement of nitrite, nitrate ions and S-nitrosothiols using the 2,3-diaminonaphthalene assay by LC coupled with tandem mass spectrometry", "Measurement of *γ*-glutamyltransferase activity by spectrophotocolorimetry" and "Permeability studies of *S*-nitrosothiols in isolated rat intestine using Ussing chamber".

Detailed procedures used for the experiment concerning identification of protein disulfide isomerase (PDI) in rat intestine are present in protocols (see appendices) entitled "Western blot for protein disulfide isomerase identification in tissues".

Degradation of *S*-nitrosoglutathione in rat intestine: roles of denitrosating enzymatic and chemical factors on absorption and permeation

Yu Haiyan[1,*], Schmitt Romain[1,*], Leroy Pierre[1], Gaucher Caroline[1], Fries Isabelle[1], Chaimbault Patrick[2], Sapin Anne[1,**]

[1]Université de Lorraine, CITHEFOR, F-54000 Nancy, France

[2]Université de Lorraine, LCP-A2MC, F-570 00 Metz, France

*Equal contribution to the present work

**Correspondence to: Sapin Anne, Université de Lorraine, CITHEFOR EA 3452, Faculté de Pharmacie, 5, rue Albert Lebrun, F-54001, NANCY, France

(To be submitted to *Drug Metabolism and Disposition* (IF: 3.64) when the experimental part will be completed by other researchers of the lab)

Abstract

Background: *S*-nitrosoglutathione (GSNO) is a promising nitric oxide (NO) donor in comparison with presently marketed drugs in the field of cardiovascular diseases (CVDs). Oral delivery of GSNO is an ideal route to treat chronic CVDs related to endothelial dysfunction. GSNO is a highly soluble molecule with medium permeability as already demonstrated by using two intestinal barrier models: Caco-2 cell monolayer (Bonetti *et al.*, 2018) and isolated rat intestine (Yu *et al.*, 2018). A passive transportation mechanism was demonstrated in the Caco-2 cell monolayer model (Bonetti *et al.*, 2018). However, little is known about its degradation in the intestine and how the corresponding involved enzymatic and chemical processes can modify its absorption.

Aims: The present work will focus on GSNO degradation and absorption in isolated rat intestine. The main factors already identified to be involved in the degradation of GSNO and leading to NO release in the aorta, *i.e.* γ-glutamyltransferase (GGT) and thiols including protein disulfide isomerase (PDI) (Dahboul *et al.*, 2012)(Dahboul *et al.*, 2014) will be studied.

Methods: First, GGT activity and thiol content were measured in isolated rat intestine samples using various substrates. Namely, GSNO and inhibitors (serine-borate complex, SBC) were added for GGT measurement; Ellman's reagents and the thiol blocker (*N*-ethylmaleimide, NEM) were used for thiol quantification. *GGT has to be localized in intestine samples through histological staining. Moreover, mucus, bacteria and epithelium visualization has to be performed by microscopy to understand whether denitrosating processes are localized on epithelial layer and/or on microbiota.* The addition of glycylglycine, a cosubstrate of GGT, and Mg^{2+} (glygly-Mg^{2+}) is needed to accelerate the transferase activity. Next, GSNO degradation and absorption in isolated rat intestine were evaluated. For this purpose, GSNO metabolites (*S*-nitrosothiols (RSNOs), nitrite and nitrate ions) were quantified by spectrophotometry and LC-FL, respectively, in presence or not of glygly-Mg^{2+}, SBC and NEM. At last, the absorption of GSNO and its metabolites with or without glygly-Mg^{2+} and glygly-Mg^{2+} coupled with SBC and NEM was studied with an *ex vivo* model based on isolated rat intestine placed in an Ussing chamber using LC coupled to Electrospray-Ion Trap tandem Mass Spectrometry (LC-ESI-ITMS/MS). The permeability of labeled $GS^{15}NO$ was evaluated by calculating its apparent permeability coefficient (P_{app}).

Results: The specific GGT activity measured in isolated rat intestine in presence of glygly-Mg^{2+} was 6.8 ± 0.8 nmol of 3-carboxy-4-nitroanilide $min^{-1}.mg^{-1}$ of proteins. *Histological studies showed that GGT was localized in epithelial layer/mucus (microbiota) of the intestine (to be done).* 26.5 ± 1.2 nmol of thiol $.mg^{-1}$ of proteins were detected with Ellman's reagents. When incubating GSNO with glygly-Mg^{2+} for 60 min, a degradation rate of 0.9 ± 0.1 nmol of GSNO $min^{-1}.mg^{-1}$ of proteins was observed. This degradation rate was lowered in presence of SBC and NEM. After incubating GSNO with intestine in absence and presence of activators (glygly-Mg^{2+}) or inhibitors (SBC and NEM) for 60 min, both inside and outside Ussing chamber, less than 1 % of initial GSNO was absorbed in the intestine tissue. Compared to incubating GSNO alone with isolated rat intestine in Ussing chamber, more nitrite ions (NO_2^-) was permeated through intestine (0.7 *vs.* 0.2 nmol) when GGT activators were added, and more RSNOs were permeated (0.5 *vs.* 0.1 nmol) when GGT inhibitor and thiol blocker were added. Conventional spectrofluorometry can not be used to quantify permeated NO species through intestine in Ussing chamber, due to its poor limit of

quantification (LOQ, 100 nM).

Conclusion: GGT and thiols in isolated rat intestine are involved in GSNO metabolism. Extra adding glygly-Mg^{2+} appears to reduce GSNO absorption in intestine but promotes permeation of NO_2^- through intestine, while extra addition of SBC and NEM contributes to higher permeation of RSNOs. Method using LC-ESI-ITMS/MS is needed to study GSNO with low concentration (*e.g.* 100 µM). Other enzymes are maybe involved in GSNO metabolism, such as redoxin (*i.e*. protein disulfide isomerase). As NO plays important roles in the intestinal physiology, it could be also interesting to further investigate the GSNO impact in a pathological model of intestine, and to explore a possible modification of its metabolism. In addition, degradation/absorption of GSNO formulations or other RSNOs in intestine could be tested to improve its permeability after oral administration; method using liquid chromatography/tandem ion trap mass spectrometry can be adapted to GSNO labeled with ^{15}N and its metabolites measurement in the intestine tissue.

Keywords: *S*-nitrosoglutathione, *γ*-glutamyltransferase, thiols, rat intestine, intestinal metabolism

1. Introduction

In the case of vascular endothelium dysfunction resulting from aging and cardiovascular diseases (CVDs), the activity of the endothelial nitric oxide (NO) synthases decreases and consequently NO is produced at a low level. Meanwhile, inducible NO production increases, and oxidative stress emerges (Loo *et al.*, 2000). *S*-nitrosoglutathione (GSNO) as a physiological NO reservoir shows high potency to treat CVDs, as it does not present drawbacks of presently marketed NO donors, especially tolerance phenomenon and induction of oxidative stress (Gaucher *et al.*, 2013). Since most of CVDs are chronic, oral administration of GSNO appears to be the most practical route. Noteworthy, a drug suitable for oral administration should possess a good solubility and permeability according to the Biopharmaceutical Classification System (Amidon *et al.*, 1995). Solubility depends on the physico-chemical properties of the drug while permeability is determined by the absorption through the gastrointestinal tract (GIT).

The main drug absorption part in GIT is the small intestine, which consists of duodenum, jejunum and ileum. Jejunum and ileum are often considered for research, because their length is 10-fold more than duodenum (3 *vs* 0.25-0.3 m) (Kararli, 1995). Interestingly, ileum shows better absorption than jejunum, due to a longer residence time and a heavier mucus thickness (3-4 *vs* 2-3 h, 476 *vs* 123 µm, respectively) (Fallingborg *et al.*, 1989)(Atuma *et al.*, 2001). In addition, mucus is not tightly attached to mucosa. This may contribute to poor reproducibility of related experiments, due to its partial loss. It is situated between intestinal lumen and epithelial layer, where a lot of bacteria coexist.

Apart from transporters that should be taken into consideration, enzymes also play vital roles in drug absorption process. In biological environment, *γ*–glutamyltransferase (GGT) is a specific denitrosating enzyme of GSNO. It is primarily found on the cell surface in secretory or absorptive tissues such as kidney, liver, seminal vesicles/prostate, small intestine, and it specially exists in epithelial cells, according to previous immunohistochemical studies (Hanigan and Frierson, 1996). Actually, GGT is well-known for its anti-oxidant and pro-oxidant activities, because its most abundant physiological substrates are reduced *L*-glutathione (GSH) and glutathione disulfide (GSSG), which can reflect cell oxidation state by their ratio (Schafer and Buettner, 2001)(Jones, 2002)(Wickham *et al.*, 2011). Besides, GGT is also a predictor of CVDs, due to its higher serum level observed with the progression of atherosclerosis and related complications (Pompella *et al.*, 2004). In addition, it induces GSNO breakdown with first the release of *S*-nitrosocysteinylglycine, then rapidly liberating NO in the presence of metal ions (Me^{n+}), such as Fe^{2+} and Cu^{2+} (Broniowska *et al.*, 2013) (Figure 1 A). The role of GGT in the release of NO from GSNO and in the vasodilation has already been investigated in an *ex vivo* model (isolated rat aorta)(Dahboul *et al.*, 2012). Its activity can be reversibly inhibited by serine-borate complex (SBC) (Tate and Meister, 1978).

In a biological environment, GSNO undergoes transnitrosation reaction (Figure 1 B) and decomposes as a consequence of many impacting factors such as thiols (Figure 1 C), reductants and enzymes, resulting in formation of NO and corresponding by-products, *e.g.* GSSG (Al-Sa'doni *et al.*, 2000). Consequently, SBC to reversibly inhibit GGT and *N*-ethylmaleimide (NEM) for thiol blockage (Bryan and Grisham, 2007) are usually used to stabilize GSNO during sample pre-treatment steps before

analytical measurement.

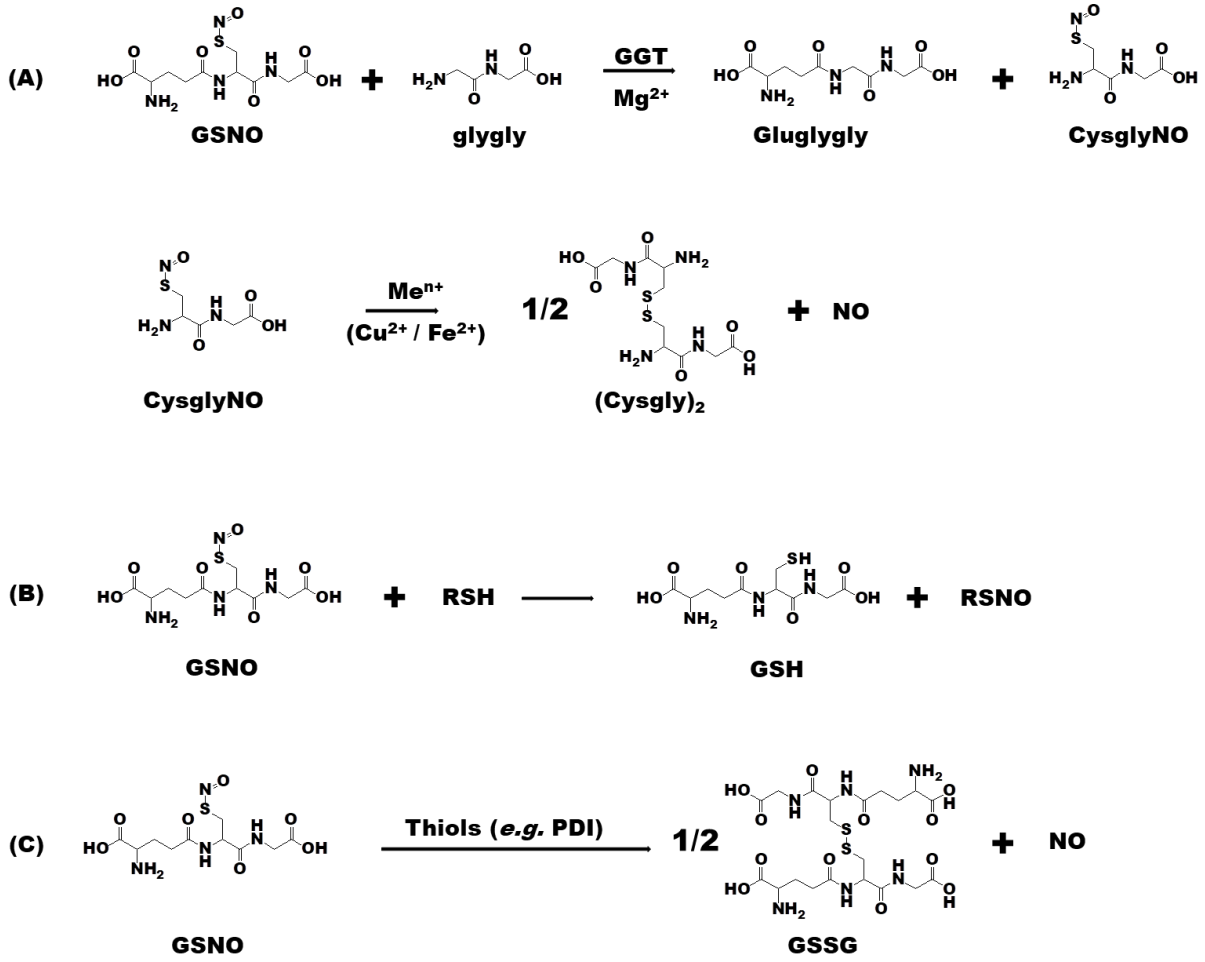

Figure 1. Scheme of *S*-nitrosoglutathione (GSNO) metabolism by (A) *γ*-glutamyltransferase (GGT); (B) thiols (RSH) through transnitrosation reaction; and (C) some thiols (*e.g.* PDI) (glygly：glycylglycine; GSSG: glutathione disulfide; PDI: protein disulfide isomerase).

To study drug intestinal permeability, numerous models exist, but it is difficult to achieve a simple and relevant model (Bilat *et al.*, 2017). Three kinds of models are commonly used: *(i)* an *in vitro* model consisting of two compartments separated by intestinal cells, such as Caco-2 cell monolayer; it is usually for preliminary study; *(ii)* an *ex vivo* model such as isolated animal intestine in Ussing chamber: this is often applied for complementary information, due to a better correlation with *in vivo* studies than *in vitro* experiments; and *(iii)* an *in vivo* model using rodents for pre-clinical evaluation of drugs, such as pharmacokinetic studies (PK), which is one of the indispensable parts of drug discovery, to explore actively transported drug.

According to the literature, the conversion of nitrate (NO_3^-) to nitrite (NO_2^-) in the GIT through microorganism action is well known (Benjamin *et al.*, 1994); the formation of RSNOs in stomach and their chemical decomposition have also already been reported (Pinheiro *et al.*, 2015). Several reports conclude on the efficiency of GSNO after oral administration in rats: *(i)* GSNO either as a free molecule (Khan *et al.*, 2011) or formulated (Parent *et al., 2015*) improves the therapeutic score in a stroke rat model; *(ii)* Wu *et al.* used GSNO encapsulated nano-composite particles and showed that the NO storage increased in vessels (Wu *et al.,* 2016). In addition, GSNO is a highly soluble molecule with medium permeability through both intestinal cell (Caco-2) monolayer (Bonetti *et al.*, 2018) and isolated rat intestine (Yu *et al.*, 2018). It has passive transportation mechanism in Caco-2 cell monolayer model, based on our previous study (Bonetti *et al.*, 2018). However, little is known about its intestinal absorption, not to mention the involved factors of transferring GSNO from GIT to blood vessel. The present work aims at studying GSNO degradation and absorption in isolated rat intestine.

2. Methods

2.1. Material and Reagents

All reagents were of analytical or chromatographic grade and used without further purification. Reduced *L*-glutathione (GSH), glutathione disulfide (GSSG), *γ*-glutamyltransferase (GGT) (bovine kidney, EC 2.3.2.2), *L*-*γ*-glutamyl-3-carboxy-4-nitroanilide (GCNA), glycylglycine (glygly), *L*-serine, sodium borate, *N*-ethylmaleimide (NEM), 2,3-diaminonaphthalene (DAN), mercuric chloride ($HgCl_2$) and 5,5′-dithiobis(2-nitrobenzoic acid) (DTNB) were obtained from Sigma-Aldrich (Saint-Quentin Fallavier, France). Sodium ^{15}N-nitrite ($Na^{15}NO_2$) was supplied by Cambridge Isotope Laboratories (Tewksbury, MA, USA). Nitrate/Nitrite fluorometric assay kit (ref. 780051) was obtained from Cayman Chemical (Michigan, USA)

S-nitrosoglutathione (GSNO) was synthesized according to a method previously described (Parent *et al.*, 2013). Briefly, 20 mM GSH was incubated with 20 mM $NaNO_2$ in 500 mM HCl at 4°C in the dark for 60 min. The reaction was stopped by neutralization with NaOH (40%) and was further 2-fold diluted with 500 mM phosphate buffer, pH 7.4. The final GSNO concentration was determined by UV

spectrophotometry (UV-1800, Shimadzu, Lognes, France) at a wavelength of 334 nm (ε = 922 $M^{-1}\times cm^{-1}$). $GS^{15}NO$ was synthesized as above but using $Na^{15}NO_2$.

All experiments and assays involving GSNO were conducted under conditions of subdued light.

2.2. Isolation of rat intestine

All experiments were performed in accordance with the European Community guidelines (2010/63/EU) for the use of experimental animals in the respect of the 3 Rs' requirements for Animal Welfare. The protocols and procedures were approved by the advisory regional ethical committee on animal experiments: Comité d'Ethique Lorrain en Matière d'Expérimentation Animale, CELMEA protocol agreement N◦ 02420.03. Animals were kept under standard conditions (temperature: 21 ± 1 °C, hygrometry 60 ± 10%, light on from 6 am to 6 pm) and had free access to standard diet (A04, Safe, Villemoisson-sur-Orge, France) and water (reverse osmosis system, Culligan, Brussells, Belgium). Wistar rats (350 g, 8 weeks old, males, Janvier Laboratories, Le Genest Saint Isle, France) were used for the present experiments. Isolated rat intestine (ileum, weight: 100 ± 5 mg) was obtained after sacrifice (anesthetized with sodium pentobarbitone (60 $mg.kg^{-1}$, intraperitoneal injection, Sanofi Santé Nutrition Animale, Libourne, France), administrated with heparin (1000 $IU.kg^{-1}$ heparin Choay, penis vein) and sacrificed by exsanguination). The fat tissue along the mesenteric attachment was removed and the intestine was longitudinally opened, followed by quick rinsing with 1 mL of PBS for 2 times.

2.3. Evaluation of GGT activity

γ-Glutamyltransferase (GGT) activity was determined using a specific chromogenic substrate, *i.e.* GCNA (Schiele *et al.*, 1981). Briefly, isolated rat intestine prepared in section 2.2 was incubated with 1 mM GCNA, 20 mM glygly and 10 mM $MgCl_2$ (glygly-Mg^{2+}) in presence or absence of 20 mM SBC (20 mM serine-20 mM sodium borate) in 5 mL of 100 mM Tris buffer (pH 7.4) at 37°C under rotation (35 rpm, CAT Roller RM5-40, Dordrecht, Netherlands). Every 10 min during 30 min, the absorbance was read at 405 nm (ε (3-carboxy-4-nitroanilide) = 9 500 $M^{-1}\times cm^{-1}$).

Protein concentrations were quantified using the bicinchoninic acid (BCA) method (Pierce Protein Assay Kit), with Bovine Serum Albumin as the standard. Proteins were extracted from isolated rat intestine samples as follows: the rat intestine sample was frozen with liquid nitrogen (N_2), next smashed into powder in liquid N_2

with a pestle in a mortar; then, 100 mg of intestine powder was mixed with 400 µL of lysis buffer (0.05 M Tris-HCl, 0.15 M NaCl, 0.1 % sodium dodecyl sulfate (SDS), and 1 % pure Triton X-100), and incubated at 4°C in the dark for 10 min; next, the supernatants were collected after centrifugation at 15,000 x *g* at 4°C for 15 min, and proteins were precipitated by adding 3.3 mL of acetone and centrifugated at 3000 × *g* at 4°C for 10 min; at last, 200 µL of lysis buffer were used to resuspend the proteins in the pellet before storage at -80 °C and quantification. GGT specific activity was expressed in nmol of obtained product per min per mg of proteins.

2.4. Quantification of thiols

The thiol content was measured using the DTNB (Ellman's reagent) method. Briefly, 750 µL of 1 mM DTNB in Tris buffer (0.1 M, pH 7.4) were incubated with intestine at room temperature (r.t.) in the dark under rotation (35 rpm, CAT Roller RM5-40) for 10 min. Then, 200 µL of medium were transferred to a 96-well microplate and the absorbance was read at 405 nm (EL800 Microplate Reader, BioTek Instruments). The efficiency of NEM to block all thiols including those of cysteine residues in active sites of redoxins like protein disulfide isomerase (PDI) was also assessed. First, intestine was pre-incubated with 5 mL of 10 mM NEM in Tris buffer (0.1 M, pH = 7.4) at 37 °C under rotation for 10 min. Then, intestine was rinsed with 5 mL of PBS for 3 times, Next, DTNB was added to quantify remaining active thiols with procedures described above.

2.5. Degradation of GSNO in isolated rat intestine

50 µM GSNO in 5 mL of Tris buffer (0.1 M, pH 7.4) was incubated with isolated rat intestine placed in a 15-mL polypropylene tube at 37°C under rotation (35 rpm, CAT Roller RM5-40), in the absence and in the presence of *i*) glygly-Mg^{2+}, or *ii*) 20 mM glygly,10 mM $MgCl_2$ and 20 mM SBC (glygly-Mg^{2+}-SBC), or *iii*) 20 mM glygly, 10 mM $MgCl_2$, 20 mM SBC and 10 mM NEM (glygly-Mg^{2+}-SBC-NEM). Every 10 min during 60 min, 25 µL of reaction medium were collected and diluted 25 times in PBS for GSNO quantification using the DAN–Hg^{2+} assay (Wu *et al.*, 2015) (measurements in triplicate). In parallel, the stability of GSNO in oxygenated Krebs solution in the absence of intestine was evaluated.

Briefly, 100 µL of each standard (concentration range: 0.1 – 2 µM) or sample (in triplicate) were mixed with 20 µL of 0.105 mM DAN solution in 0.6 M HCl. The mixture was shaken at 500 rpm (Heidolph, VIBRAMAX 110) at r.t. for 1 min, followed by

incubation at 37 °C in the dark for 10 min. Then, 20 µL of 2.1 M NaOH were added. The mixture was then shaken for another 5-min period, before measuring fluorescence intensity (spectrofluorometer model: FP-8300iRM, JASCO, Tokyo, Japan) coupled with FMP micro-well plate reader. The excitation and emission wavelengths were 375 and 415 nm, respectively. For RSNOs and (RSNOs + NO_2^-) measurements, DAN reagent was replaced by DAN-$HgCl_2$ reagent.

The concentrations of NO_3^- and (NO_2^- + NO_3^-) were measured using the Nitrate/Nitrite Fluorometric Assay Kit (Kayman, (ref. 780051). Twenty µL of each standard (concentration range: 0.75 – 25 µM) or sample (in triplicate) were derivatized according to the manufacturer protocol and fluorescence intensity was measured.

2.6. Absorption of GSNO in isolated rat intestine

Method for quantifying (NO_2^-) and RSNOs in rat intestine samples was first validated, and applied to study GSNO absorption inside intestine.

2.6.1. Method validation for quantification of NO species in intestine

Three five-point concentration curves of $NaNO_2$ and GSNO standards (blank, 6.25, 12.5, 25, 37.5, 50 nM) for three different days were built according to the literature (Damacena-Angelis *et al.*, 2017)(Shin and Fung, 2011). Resulting 2,3-naphthotriazole (NAT) was extracted with acetonitrile and analyzed by reversed phase liquid chromatography coupled with fluorescence detection (LC-FL). Briefly, the rat intestine was frozen with liquid N_2, next smashed into powder in liquid N_2 with a pestle in a mortar; 20 ± 2 mg intestine powder were spiked with 20 µL of $NaNO_2$ or GSNO standard solutions. Next, 600 µL DAN or DAN/Hg^{2+} in 0.6 M HCl were added, followed by vortex for 30 s. The mixture was then incubated at 37 °C for 10 min under rotation (80 rpm, MX-RD-E Classic Rotator, Labtech, Cernusco, Italy). 40 µL of 10 M NaOH were added, and mixed by vortex for 10 s. Finally, 600 µL acetonitrile were added, followed by centrifugation at 18,000 x *g* at 4 °C for 15 min. The supernatant was collected and stored at 4 °C for a maximum period of 24 h before analysis by LC-FL. A ZORBAX SB-Aq C18 column (4.6 X 150 mm, 3.5 µm, Agilent) eluted with CH_3CN-0.01 M ammonium acetate pH 7.2 (28:72, v/v), and a spectrofluorometric detector (RF-10A XL model, Shimadzu, Kyoto, Japan) with excitation and emission wavelengths set at 375 and 415 nm, respectively, were used. Background levels of $NaNO_2$ and RSNOs in Tris buffer and intestine without GSNO treatment corresponding to blanks were measured and subtracted from all values.

2.6.2. Quantification of nitrite ions and RSNOs in intestine

The nitrite ions (NO_2^-) and RSNOs concentrations were measured after incubating intestine samples with 5 mL of *i*) 25 or *ii*) 50 or *iii*) 100 µM GSNO in a 15-mL tube at 37°C for 60 min under rotation (35 rpm, CAT Roller RM5-40). Intestine was rinsed with 5 mL of cold PBS for 3 times, and frozen in liquid N_2. Then, RSNOs in intestine tissue were quantified with the LC-FL method described above.

In parallel, NO_2^- and RSNOs concentrations in isolated rat intestine were also measured after incubating intestine with 5 mL of *i*) 100 µM GSNO alone or *ii*) 100 µM GSNO in presence of glygly-Mg^{2+} or *iii*) 100 µM GSNO with glygly-Mg^{2+}-SBC-NEM, in a 15-mL tube at 37°C for 60 min under rotation; further steps for quantification were similar to operating conditions described above.

2.7. Metabolism of GS15NO in isolated rat intestine in Ussing chamber

Before studying the role of intestinal GGT and thiols in GSNO degradation and permeation through isolated rat intestine in Using chamber, the potential influence of the different additives tested (glygly-Mg^{2+}, SBC and NEM) was checked on intestine integrity by measuring transepithelial electrical resistance (TEER) value over 2-h, using an adapted Millicell® ERS ohm-meter (Millipore).

The intestinal permeability of 100 µM $GS^{15}NO$ with and without glygly-Mg^{2+}, and glygly-Mg^{2+}-SBC-NEM in Ussing chamber was carried out with the same procedure described before (Yu *et al.*, 2018). In parallel, the same experiments using Ussing chamber but without isolated rat intestine were carried out to evaluate GSNO stability at 37°C with O_2-CO_2 (95:5, V/V) mixture bubbling.

2.7.1. Quantification of NO species in donor, intestine and acceptor compartments

After a 2-h incubation, NO species in the donor compartment were quantified as described in 2.5, NO_2^-/RSNOs in isolated rat intestine were quantified as in 2.6.2, and ^{15}N-NO species in the acceptor compartment were quantified using LC coupled to Electrospray-Ion Trap tandem Mass Spectrometry (LC-ESI-ITMS/MS) as described before (Yu *et al.*, 2018). Briefly, permeated ^{15}N-NO species were derivatized and injected (20-µL loop) into a LC-ESI-ITMS/MS system (Dionex, Ultimate 3000, coupled with LTQ Velos Pro, Thermo Scientific, San José, CA, USA). An Acclaim 120 C-18 column (2.1 × 150 mm ID, 3 µm, Thermo) was eluted with a gradient mobile phase consisting of acetonitrile (from 40 to 80 %) and 0.01 M acetic acid solution. An ion trap

mass spectrometer (LTQ Velos Pro, Thermo Scientific, San Jose, CA, USA) fitted with the HESI-II probe (electrospray) was coupled to monitor transitions of *m/z* 171 to 156 for ^{15}N-NAT quantification (HCD fragmentation mode). The apparent permeability coefficient (P_{app}) values were calculated using the following equation:

$$\mathrm{Papp} = \frac{\mathrm{dQ}}{\mathrm{dt}} \times \frac{1}{\mathrm{A} \times \mathrm{C0}}$$

dQ/dt (mol.s^{-1}) refers to the quantity of permeated NO related species (dQ) in the acceptor compartment at the time of quantification (dt), “A” refers to the membrane diffusion area (0.25 cm^2), and C_0 refers to the initial concentration of GS^{15}NO in the donor compartment.

2.8. Histological studies

[Operating conditions to be inserted when developed]

2.9. Statistical tests

All results were expressed as mean ± standard deviation (SD) or mean ± standard error of the mean (sem). Values were analyzed with one-way ANOVA, followed by a Bonferroni’s post-test using the Graphpad Prism 5 software; $p < 0.05$ was considered as statistically significant.

3. Results and discussion

3.1. Measurement of GGT activity and thiol content in isolated rat intestine

The specific GGT activity in the presence of glygly-Mg^{2+} was 6.8 ± 0.8 nmol of 3-carboxy-4-nitroanilide.min^{-1}.mg^{-1} of proteins, which was abolished by adding SBC (values were under the limit of detection) (Table 1). In the literature (Carter *et al.*, 1997), the specific GGT activity was 24 700 nmol of 4-nitroanilide.min^{-1}.mg^{-1} of proteins in small intestine of female mice; thus, it was around 3600-times higher than the one observed in our experiment using isolated ileum. This huge difference has two possible explanations: *(i)* a lot of GGT comes from bacteria in GIT, but most of these bacteria were lost during our washing steps realized for intestine treatment; *(ii)* there is an inter-species or gender variation of GGT activity between female mice and male (Lash *et al.*, 1998). In addition, the specific GGT activity presently measured in rat ileum is higher than the one in rat aorta (0.3 ± 0.01 nmol of 3-carboxy-4-nitroanilide.min^{-1}.mg^{-1} of proteins) (Dahboul *et al.*, 2012) and differentiated Caco-2 cells (1.9 ± 0.3 nmol of 3-carboxy-4-nitroanilide.min^{-1}.mg^{-1} of

proteins) (data not shown). This may result from the different structures between ileum, aorta and Caco-2 cells, and only ileum contains a lot of bacteria with high GGT expression.

[Histology results to be inserted when related experiments be done]

The intact isolated rat intestine showed around 26.5 ± 1.2 nmol of thiols.mg^{-1} of proteins, and 93.0 ± 0.7 % of these thiols were blocked by NEM (Table 1).

Table 1. Specific activity of *γ* -glutamyltransferase (GGT) and thiol content in isolated rat intestine. ($ND^{\#}$: not detected, under limit of detection; -: undone; GCNA: *L*-*γ*-glutamyl-3-carboxy-4-nitroanilide; CNA: 3-carboxy-4-nitroanilide; SBC: serine-borate complex; DTNB: 5,5′-dithiobis(2-nitrobenzoic acid); NEM: *N*-ethylmaleimide))

Incubating with isolated rat intestine	GGT activity (nmol of CNA $min^{-1}.mg^{-1}$ of proteins)	Thiol content (nmol of thiol mg^{-1} of proteins)
Substrates (GCNA + glygly-Mg^{2+} or DTNB)	6.8 ± 0.8 (n = 9)	26.5 ± 1.2 (n = 3)
Substrates + inhibitors (GCNA + glygly-Mg^{2+} + SBC or DTNB + NEM)	$ND^{\#}$ (n = 3)	1.9 ± 0.1 (n = 3)

3.2. Degradation of GSNO in isolated rat intestine

GSNO in Tris buffer (50 µM) under conditions (fast rotation) providing high oxygenation rate at 37°C was stable in the absence of intestine for at least 60 min. In the presence of intestine, around 40 % of GSNO (250 nmol as starting amount) were degraded within 60 min corresponding to a degradation rate of 0.5 ± 0.1 nmol of GSNO $min^{-1}.mg^{-1}$ of proteins. This degradation was stimulated by adding glygly-Mg^{2+} (around 80 % of GSNO loss), rising the degradation rate to 0.9 ± 0.1 nmol of GSNO $min^{-1}.mg^{-1}$ of proteins. 100 % of GSNO catabolism was inhibited by SBC-NEM (GGT inhibitor and thiol blocker) (Figure 2 A). Most of the initial amount of GSNO was converted to NO_3^- ions (Figure 2 B). Perhaps, GGT does not catalyze GSNO degradation without adding co-substrates (glygly-Mg^{2+}). Or there is other factors protecting GSNO from degradation, and SBC could block this process. In summary, intestine GGT and thiols play a significant role in GSNO metabolism.

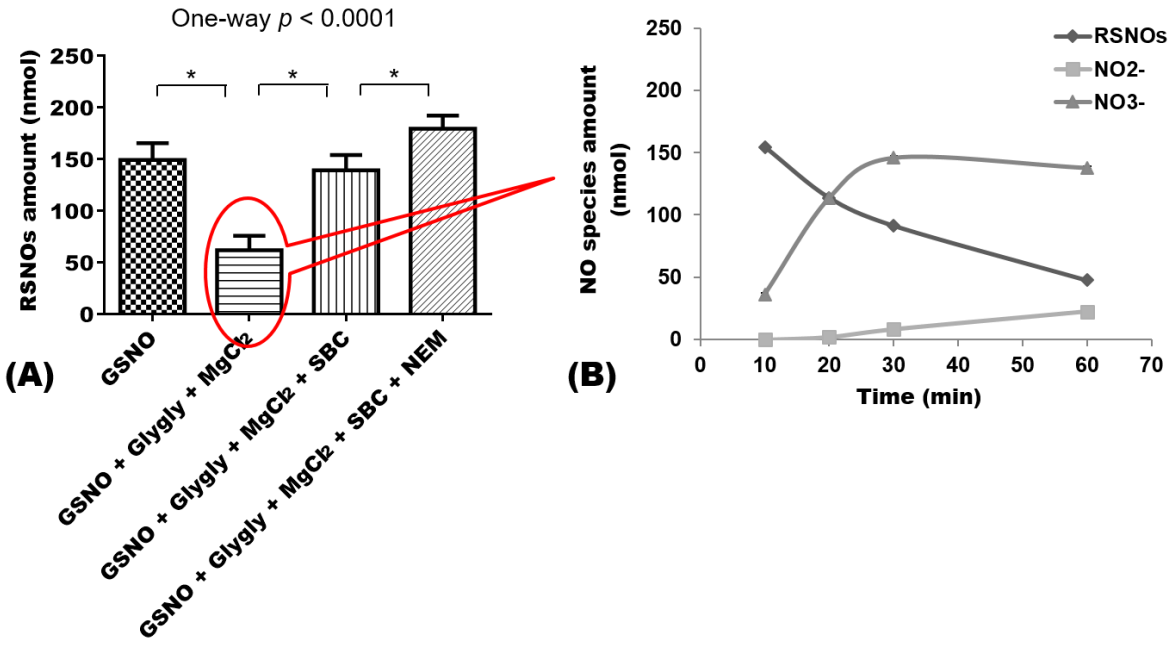

Figure 2. Remaining amounts of (A) *S*-nitrosothiols (RSNOs) (250 nmol of *S*-nitrosoglutathione (GSNO) as starting amount) after 60 min of incubation with different additives in presence or absence of rat intestine; (B) NO species (RSNOs, nitrite and nitrate ions) repartition when rat intestine is incubating with GSNO in the presence of glycylglycine (Glygly) and $MgCl_2$. Data are shown as mean ± sem, n = 3. *P value (One-way ANOVA,* Bonferroni's post-test): *$p < 0.05$ (additives: glygly, magnesium chloride ($MgCl_2$), serine-borate complex (SBC) and *N*-ethylmaleimide (NEM)).

3.3. Method validation with LC-FL for quantification of NO species in intestine

To quantify NO species in the intestine tissue, the conventional fluorometric assay relying upon DAN derivatization (Wu *et al.*, 2015) did not exhibit enough selectivity. Thus a LC-FL method was presently developed for NO_2^- and RSNOs quantification in the rat intestine tissue has a linear range of 0.3 – 2.2 nmol.mg^{-1} of proteins, with a determination coefficient (r^2) higher than 0.995. The accuracy as the deviation (%) of calculated concentrations from the nominal concentrations was in the range of 97.0 -113.3 %. Satisfactory precisions were obtained with intra- and inter-day bias less than 8.2 % and 11.9 %, respectively, over the concentration ranges studied. These ranges were within the criteria stated in the FDA guidance on bioanalytical method validation (Shah *et al.*, 2000) (Table 2). NO_3^- concentrations were not

measured as it was already shown that the intracellular reducing power of cells enables their existence (Parodi *et al.*, 2007).

Table 2. Standard curves validation parameters for *S*-nitrosoglutathione (GSNO) and nitrite ions (NO_2^-). Mean ± SD; n ≥ 3.

NO species	Linearity (6.25 – 50 µM) Slope (a); intercept (b); determination coefficient (r^2)	Concentration (µM)	Accuracy (%)	Precision (%)	
				Intra-day	Inter-day
GSNO	a: 15308 ± 1160 b: -51365 ± 56834 r^2: 0.996 ± 0.005	6.25	113.3	0.7	10.2
		12.5	97.0	8.2	11.9
		25	98.6	6.4	5.7
		37.5	104.0	4.6	4.3
		50	100.3	4.5	5.6
NO_2^-	a: 16572 ± 218 b: -40458 ± 29394 r^2: 0.995 ± 0.005	6.25	99.9	2.9	11.3
		12.5	100.2	0.4	2.0
		25	112.9	3.8	7.9
		37.5	101.8	2.1	7.9
		50	98.4	6.5	4.7

3.4. Absorption of GSNO in isolated rat intestine

A concentration-dependent absorption of RSNOs in intestine was observed, but no significant difference for NO_2^- and RSNOs absorption in intestine between 25 and 100 µM GSNO (initial concentrations used for incubation) was observed (Figure 3 A). Finally, 100 µM GSNO was chosen as working concentration for further experiment. Method with a lower limit of quantification (LOQ) should be applied to study GSNO with lower concentrations (*i.e.* less than 25 µM).

The presence of the different additives (glygly-Mg^{2+}, SBC and NEM) showed no significant differences for NO_2^- and RSNOs absorption in intestine between each group (Figure 3 B). **[Histology discussion]** *This may due to the low reproducibility of experiments (is it linked to the loss of mucus during washing steps of tissue preparation? Histological studies are needed to visualize mucus, bacteria and epithelium.*

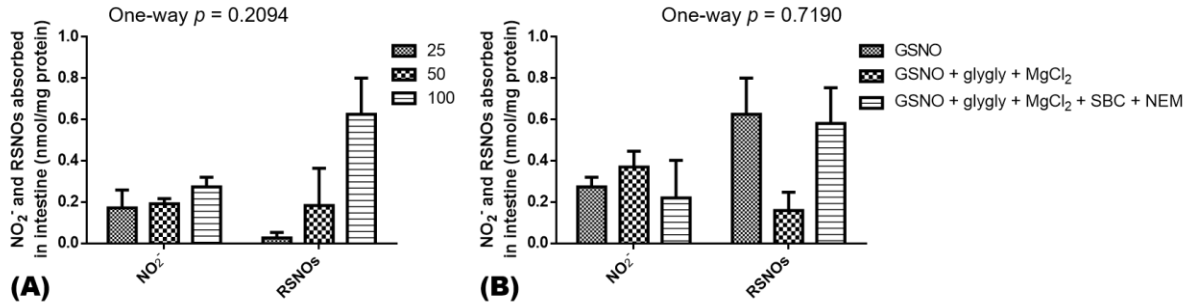

Figure 3. Amounts of nitrite ions and *S*-nitrosothiols (RSNOs) quantified inside the isolated rat intestine, after incubation with (A) 25, 50 and 100 µM (equal to 125, 250 and 500 nmol, respectively) of *S*-nitrosoglutathione (GSNO) in Tris buffer (0.1 M, pH 7.4) for 60 min; (B) 100 µM (equal to 500 nmol) GSNO in the presence of different additives. Data are shown as mean ± sem, n = 3. *P value (One-way ANOVA,* Bonferroni's post-test): **p* < 0.05 (additives: glycylglycine (glygly), magnesium chloride ($MgCl_2$), serine-borate complex (SBC), *N*-ethylmaleimide (NEM)).

3.5. Intestinal permeability of GSNO and implication of denitrosating enzymes

Transepithelial electrical resistance (TEER) values were respectively of 24.3 ± 3.4, 21.5 ± 2.4 and 47.1 ± 5.0 ohm×cm². There is not impact of glygly-Mg^{2+} or SBC on intestine integrity, but an increase of TEER due to the presence of NEM.

In absence of intestine, 100 µM GSNO with extra addition (or not) of glygly-Mg^{2+} or SBC-NEM was stable in Ussing chamber's operating conditions. However, only 29.4 % of initial GSNO amount were remaining in the donor compartment as the intact form, 12.7 % were converted to NO_2^- and 23.2 % to NO_3^- after a 2-h incubation with intestine. With extra addition of GGT activator (glygly-Mg^{2+}), there was no significant difference of remaining RSNOs in donor compartment (30.5 % *vs.* 29.4 %), but significant increases of released NO_2^- (23.4 % vs. 12.7 %) and NO_3^- (40.5 % vs. 23.2 %) were observed. This proves that GGT activator stimulates GSNO degradation in presence of rat intestine. When extra GGT inhibitor (SBC) and thiol blocker (NEM) were added, there were more remaining RSNOs (57.6 % *vs.* 29.4 %), but no difference for released NO_2^- and NO_3^- in the donor compartment (12.5 % and 23.2 %, respectively), as shown in Figure 4. Indeed, SBC and NEM protect GSNO from degradation.

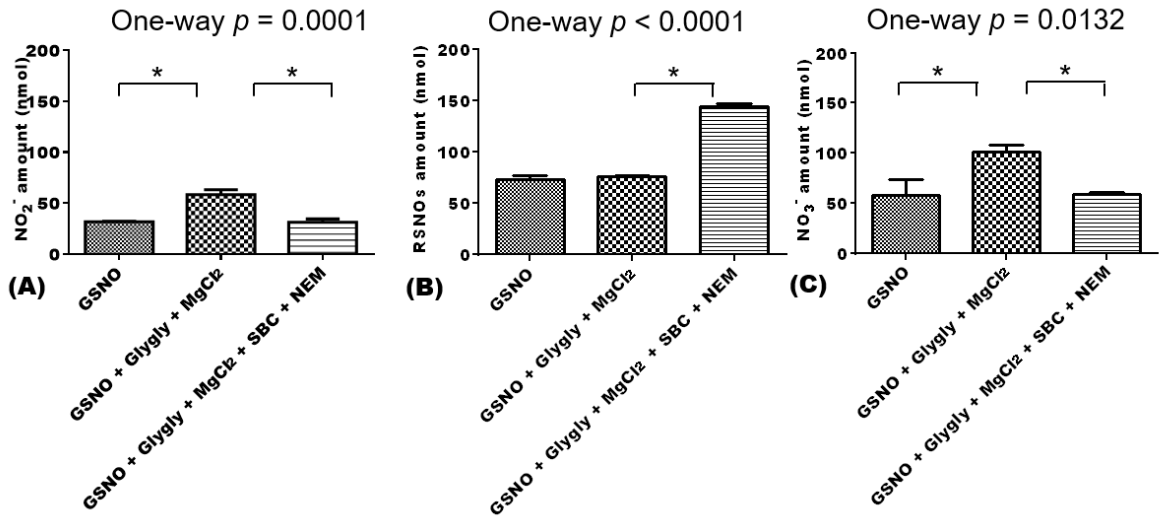

Figure 4. Remaining amounts of (A) nitrite ions (NO_2^-), (B) *S*-nitrosothiols (RSNOs) and (C) nitrate ions (NO_3^-) in the donor compartment of the Ussing chamber after incubating intact intestine with 100 µM (equal to 250 nmol) of *S*-nitrosoglutathione (GSNO) together with or without glygly-$MgCl_2$ and SBC-NEM. Data are shown as mean ± sem, n = 3. *P value (One-way ANOVA,* Bonferroni's post-test): *$p < 0.05$.

In the acceptor compartment, a higher amount of permeated NO_2^- (0.7 vs. 0.2 nmol) was observed (in comparison to incubation with GSNO alone), but the stimulation of GSNO degradation by adding GGT activator do not showed significant increase of NO_3^-. Besides, the permeated RSNOs amount was less than 0.01 nmol, and the corresponding concentration was under LOQ of the analytical method using DAN coupled with LC-ESI-ITMS/MS. With extra addition of SBC-NEM, more RSNOs (0.5 *vs.* 0.1 nmol) were permeated through intestine, but there was no difference for NO_2^- permeation, and NO_3^- was hardly detected, shown in Figure 5.

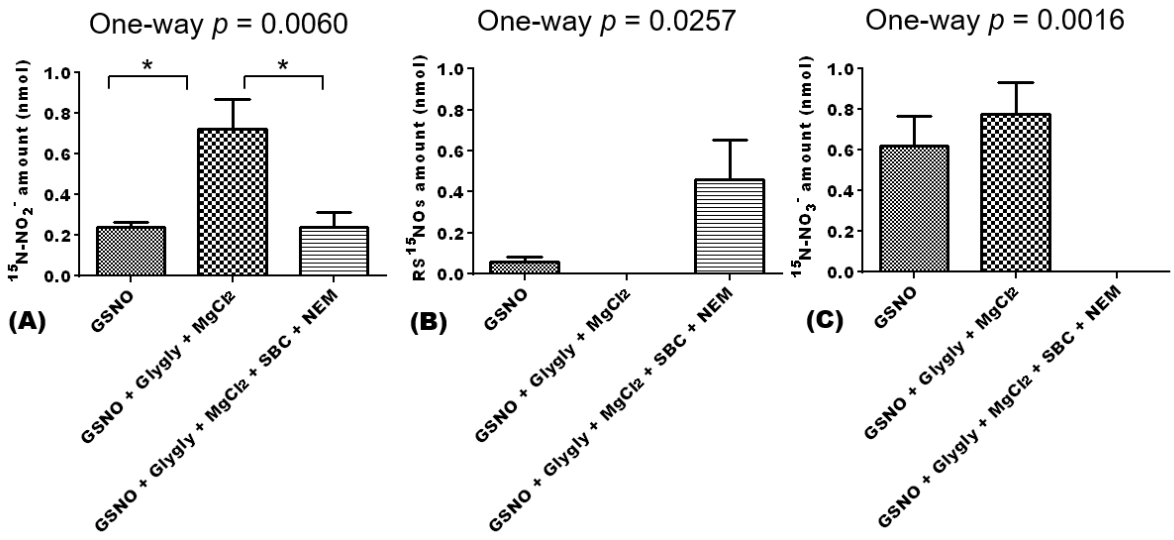

Figure 5. Permeated amounts of (A) nitrite ions (NO_2^-), (B) *S*-nitrosothiols (RSNOs) and (C) nitrate ions (NO_3^-) in the acceptor compartment of the Ussing chamber after a 2-h incubation of 100 µM (equal to 250 nmol) *S*-nitrosoglutathione (GSNO) with intact intestine in the presence or absence of glygly-$MgCl_2$ and SBC-NEM. Data are shown as mean ± sem, n = 3. *P value (One-way ANOVA,* Bonferroni's post-test) : **p* < 0.05.

No matter adding extra GGT activator (glygly-Mg^{2+}) or GGT inhibitor-thiol blocker (SBC-NEM) or not, both the absorbed NO species amount inside intestine and the permeated ones through intestine were less than 1%. Also, the final recovery of NO species was calculated by the sum of amounts in donor, acceptor compartments, and rinsing solutions over the initial GSNO amount; the ratio found is 97 ± 12 %, which validates both model and methods (Table 3). Moreover, adding the activator did not change the permeation rate of NO species from GSNO, but has increased NO_2^- permeation rate. Meanwhile, adding the inhibitor has increased RSNOs permeation rate, but did not change the permeation rate of NO species. Consequently, the drug classification of GSNO remains the same (medium permeability class), whatever adding GSNO activator or inhibitor (Table 3).

Table 3. Values of apparent permeability coefficient (P_{app}) for NOx species (RSNOs + NO_2^- + NO_3^-), NO_2^-, RSNOs and NO_3^- molecular forms after 2 h of permeation through rat intestine; and recovery of NO species in Ussing chamber. nd: not determined. Mean ± sem of three independent experiments done in duplicate (GSNO: *S*-nitrosoglutathione; RSNOs: *S*-nitrosothiols; Glygly: glycylglycine; SBC: serine-borate complex; NEM: *N*-ethylmaleimide).

Treatments	P_{app} (x 10^{-6} cm.s^{-1})				Recovery
	NOx	NO_2^-	RSNOs	NO_3^-	(%)
GSNO	5.3 ± 0.8	1.4 ± 0.2	0.3 ± 0.1	3.5 ± 0.8	96 ± 26
GSNO + Glygly + $MgCl_2$	6.4 ± 1.7	4.0 ± 0.8	nd	2.4 ± 1.0	97 ± 18
GSNO + Glygly + $MgCl_2$ + SBC + NEM	3.4 ± 0.9	0.9 ± 0.3	2.4 ± 1.1	nd	97 ± 18

Noteworthy, method using LC-ESI-ITMS/MS is needed to quantify permeated NO species, due to poor LOQ of conventional spectrofluorometry. Since LOQ of both methods are limited by blank, labeling drug candidate of GSNO with ^{15}N not only contributes to distinguish NO species from exo- and endo-genous RSNOs, but also results in studying GSNO with low concentration (*e.g.* 100 μM).

4. Conclusions and perspectives

GGT and thiol groups in rat intestine are the main factors involved in GSNO degradation. The GGT activator (glygly-Mg^{2+}) contributes to GSNO degradation and increases NO_2^- permeation through intestine, while GGT inhibitor and thiol blocker (SBC-NEM) protect GSNO from degradation, and leads to a higher RSNOs permeation. Other enzymes are maybe involved in GSNO metabolism, such as redoxin (*i.e*. Protein Disulfide Isomerase, PDI). Actually, PDI in the intestine was identified by western blot (data not shown). In addition, method using LC-ESI-ITMS/MS is needed to study GSNO with low concentration (*e.g.* 100 μM).

As NO plays important roles in the intestinal homeostatis, it could be interesting (i) to investigate GSNO impact on a pathological model, and to explore a possible modification of the drug metabolism; *(ii)* to adapt the analytical method using liquid chromatography/tandem ion trap mass spectrometry to measure GSNO labeled with ^{15}N and its metabolites in biological tissues (*i.e.* intestine, aorta, …); *(iii)* to test degradation/absorption of GSNO formulations or other RSNOs in intestine.

Acknowledgments

The authors acknowledge the program of China Scholarship Council. The authors also thank Dr Philippe Giummelly (CITHEFOR, Université de Lorraine) for the synthesis of $GS^{15}NO$. The funders had no role in study design, data collection and analysis, decision to publish, or preparation of the present manuscript.

References

Al-Sa'doni HH, Khan IY, Poston L, Fisher I, and Ferro A (2000) A novel family of S-nitrosothiols: chemical synthesis and biological actions. *Nitric Oxide Biol Chem Off J Nitric Oxide Soc* **4**:550–560.

Amidon G, Lennernas H, Shah V, and Crison J (1995) A Theoretical Basis for a Biopharmaceutic Drug Classification - the Correlation of in-Vitro Drug Product Dissolution and in-Vivo Bioavailability. *Pharm Res* **12**:413–420.

Atuma C, Strugala V, Allen A, and Holm L (2001) The adherent gastrointestinal mucus gel layer: thickness and physical state in vivo. *Am J Physiol-Gastrointest Liver Physiol* **280**:G922–G929.

Benjamin N, Odriscoll F, Dougall H, Duncan C, Smith L, Golden M, and Mckenzie H (1994) Stomach No Synthesis. *Nature* **368**:502–502.

Bilat P-A, Roger E, Faure S, and Lagarce F (2017) Models for drug absorbtion from the small intestine: where are we and where are we going? *Drug Discov Today* **22**:761–775.

Bonetti J, Zhou Y, Parent M, Clarot I, Yu H, Fries-Raeth I, Leroy P, Lartaud I, and Gaucher C (2018) Intestinal absorption of S -nitrosothiols: permeability and transport mechanisms. *Biochem Pharmacol*, doi: 10.1016/j.bcp.2018.06.018.

Broniowska KA, Diers AR, and Hogg N (2013) S-Nitrosoglutathione. *Biochim Biophys Acta BBA - Gen Subj* **1830**:3173–3181.

Bryan NS, and Grisham MB (2007) Methods to detect nitric oxide and its metabolites in biological samples. *Free Radic Biol Med* **43**:645–657.

Carter BZ, Wiseman AL, Orkiszewski R, Ballard KD, Ou CN, and Lieberman MW (1997) Metabolism of leukotriene C-4 in gamma-glutamyl transpeptidase-deficient mice. *J Biol Chem* **272**:12305–12310.

Dahboul F, Leroy P, Gate KM, Boudier A, Gaucher C, Liminana P, Lartaud I, Pompella A, and Perrin-Sarrado C (2012) Endothelial γ-Glutamyltransferase

Contributes to the Vasorelaxant Effect of S -Nitrosoglutathione in Rat Aorta. *PLOS ONE* **7**:e43190.

Dahboul F, Perrin-Sarrado C, Boudier A, Lartaud I, Schneider R, and Leroy P (2014) S,S′-dinitrosobucillamine, a new nitric oxide donor, induces a better vasorelaxation than other S-nitrosothiols. *Eur J Pharmacol* **730**:171–179.

Damacena-Angelis C, Oliveira-Paula GH, Pinheiro LC, Crevelin EJ, Portella RL, Moraes LAB, and Tanus-Santos JE (2017) Nitrate decreases xanthine oxidoreductase-mediated nitrite reductase activity and attenuates vascular and blood pressure responses to nitrite. *Redox Biol* **12**:291–299.

Fallingborg J, Christensen L, Ingemannielsen M, Jacobsen B, Abildgaard K, and Rasmussen H (1989) Ph-Profile and Regional Transit Times of the Normal Gut Measured by a Radiotelemetry Device. *Aliment Pharmacol Ther* **3**:605–613.

Gaucher C, Boudier A, Dahboul F, Parent M, and Leroy P (2013) S-nitrosation/Denitrosation in Cardiovascular Pathologies: Facts and Concepts for the Rational Design of S-nitrosothiols. *Curr Pharm Des* **19**:458–472.

Hanigan MH, and Frierson HF (1996) Immunohistochemical detection of gamma-glutamyl transpeptidase in normal human tissue. *J Histochem Cytochem* **44**:1101–1108.

Jones DP (2002) Redox potential of GSH/GSSG couple: Assay and biological significance. *Protein Sens React Oxyg Species Pt B Thiol Enzym Proteins* **348**:93–112.

Kararli T (1995) Comparison of the Gastrointestinal Anatomy, Physiology, and Biochemistry. *Biopharm Drug Dispos* **16**:351–380.

Khan M, Sakakima H, Dhammu TS, Shunmugavel A, Im Y-B, Gilg AG, Singh AK, and Singh I (2011) S-Nitrosoglutathione reduces oxidative injury and promotes mechanisms of neurorepair following traumatic brain injury in rats. *J Neuroinflammation* **8**:78.

Lash LH, Qian W, Putt DA, Jacobs K, Elfarra AA, Krause RJ, and Parker JC (1998) Glutathione conjugation of trichloroethylene in rats and mice: Sex-, species-, and tissue-dependent differences. *Drug Metab Dispos* **26**:12–19.

Loo B van der, Labugger R, Skepper JN, Bachschmid M, Kilo J, Powell JM, Palacios-Callender M, Erusalimsky JD, Quaschning T, Malinski T, Gygi D, Ullrich V, and Lüscher TF (2000) Enhanced Peroxynitrite Formation Is Associated with Vascular Aging. *J Exp Med* **192**:1731–1744.

Parent M, Dahboul F, Schneider R, Clarot I, Maincent P, Leroy P, and Boudier A (2013) A Complete Physicochemical Identity Card of S-nitrosoglutathione. *Curr Pharm Anal* **9**:31–42.

Parodi O, De Maria R, and Roubina E (2007) Redox state, oxidative stress and endothelial dysfunction in heart failure: the puzzle of nitrate-thiol interaction. *J Cardiovasc Med* **8**:765–774.

Pinheiro LC, Amaral JH, Ferreira GC, Portella RL, Ceron CS, Montenegro MF, Toledo JC, and Tanus-Santos JE (2015) Gastric S-nitrosothiol formation drives the antihypertensive effects of oral sodium nitrite and nitrate in a rat model of renovascular hypertension. *Free Radic Biol Med* **87**:252–262.

Pompella A, Emdin M, Passino C, and Paolicchi A (2004) The significance of serum gamma-glutamyltransferase in cardiovascular diseases. *Clin Chem Lab Med* **42**:1085–1091.

Schafer FQ, and Buettner GR (2001) Redox environment of the cell as viewed through the redox state of the glutathione disulfide/glutathione couple. *Free Radic Biol Med* **30**:1191–1212.

Schiele F, Artur Y, Bagrel D, Petitclerc C, and Siest G (1981) Measurement of Plasma Gamma-Glutamyltransferase in Clinical-Chemistry - Kinetic Basis and Standardization Propositions. *Clin Chim Acta* **112**:187–195.

Shah VP, Midha KK, Findlay JW, Hill HM, Hulse JD, McGilveray IJ, McKay G, Miller KJ, Patnaik RN, Powell ML, Tonelli A, Viswanathan CT, and Yacobi A (2000) Bioanalytical method validation--a revisit with a decade of progress. *Pharm Res* **17**:1551–1557.

Shin S, and Fung H-L (2011) Evaluation of an LC–MS/MS assay for 15N-nitrite for cellular studies of l-arginine action. *J Pharm Biomed Anal* **56**:1127–1131.

Tate S, and Meister A (1978) Serine-Borate Complex as a Transition-State Inhibitor of Gamma-Glutamyl Transpeptidase. *Proc Natl Acad Sci U S A* **75**:4806–4809.

Wickham S, West MB, Cook PF, and Hanigan MH (2011) Gamma-glutamyl compounds: Substrate specificity of gamma-glutamyl transpeptidase enzymes. *Anal Biochem* **414**:208–214.

Wu W, Gaucher C, Fries I, Hu X, Maincent P, and Sapin-Minet A (2015) Polymer nanocomposite particles of S-nitrosoglutathione: A suitable formulation for protection and sustained oral delivery. *Int J Pharm* **495**:354–361.

Yu H, Schmitt R, Sapin A, Chailbault P, Leroy P (2018) Comparison between two derivatization methods of nitrite ion labeled with 15N applied to liquid chromatography-tandem mass spectrometry. *Anal Methods* **10**:3830–3836.

3. Supplementary study: Comparison between the two intestinal barrier models, Caco-2 cell monolayer and isolated rat intestine in Ussing chamber

The two intestinal barrier models (Caco-2 cell monolayer and isolated rat intestine in Ussing chamber) appear to give complementary data for RSNOs bioavailability studies. Combining data both from above experimental papers and PhD students in EA 3452 (Schmitt R. and Bonetti J.), a comparison between the two models concerning their validation, RSNOs permeability, and influence of GSNO on integrity of intestinal cells or tissue is presently reported.

For Caco-2 cell monolayer model validation, 50 nmol furosemide or 25 nmol propranolol were deposited in the apical compartment, and after a 1-h incubation, permeated furosemide and propranolol were quantified by LC-FL. For isolated intestine in Ussing chamber, 1000 µM sodium fluorescein or 1000 µM propranolol were deposited in the donor compartment, and after a 2-h incubation, permeated fluorescein and propranolol were quantified by FL and LC-FL, respectively. Related P_{app} values were calculated (Peng *et al.* 2014). Parameters of all related instruments, detailed information about measuring intestinal markers and P_{app} values are available in the article (Bonetti *et al.* 2018).

The procedure of RSNOs permeability studies is already described for Caco-2 cell monolayer model (experimental paper submitted to *Rapid Communications in Mass Spectrometry* in Chapter 1) (Bonetti *et al.* 2018), and for rat isolated intestinal model (experimental paper submitted to *Rapid Communications in Mass Spectrometry* in Chapter 1).

The influence of GSNO on the intestinal integrity was checked by measuring transepithelial electrical resistance (TEER) and calculating permeability values of related marker (sodium fluorescein) after GSNO treatment. As a matter of fact, Caco-2 cell monolayer model can be used for more than 4 h, but isolated rat intestine in Ussing chamber should not be used after 2 h due to a loss of tissue viability (TEER less than 30 Ω.cm²; work has been done by PhD students in EA 3452: Schmitt R. and Ming H.). Thus, the intestinal cells were firstly incubated with GSNO for 4 h, then cultured with sodium fluorescein for another 2 h; isolated rat intestine was incubated with GSNO and sodium fluorescein at the same time for 2 h.

Resulting data are shown in Table 1. The standard TEER values as a criterion to define integrity for both models are quite different (500 Ω.cm² for intestinal cells, while

30 Ω.cm² for intestine). Caco-2 cell monolayer model has been well validated by both a high permeable molecule, *i.e.* propranolol, and a low permeable molecule, *i.e.* furosemide. The permeated propranolol concentration is not detectable in the *ex vivo* model using isolated rat intestine in Ussing chamber (LOQ = 0.5 µM). Perhaps, it is trapped in intestine. In addition, sodium fluorescein belongs to high permeability class (P_{app} = (17.27 ± 1.33) x 10^{-6} $cm.s^{-1}$) in the isolated rat intestine model. As a result, permeability values of RSNOs obtanined in both models are consistent.

After GSNO incubation, the TEER values for both models were still above the critical levels, which proved that GSNO showed no influence on the integrity of intestinal cells and tissue. This fact has also been confirmed by permeability of sodium fluorescein (less than 20 % of initial amount). Noteworthy, a much smaller amount of sodium fluorescein was used in the cell model, compared to the intestinal tissue (2.5 vs 25,000 nmol).

Table 1. Permeability of intestinal markers and *S*-nitrosothiols (RSNOs) in intestinal barrier models (GSNO: *S*-nitrosoglutathione; NACNO: *S*-nitroso-N-acetyl-cysteine; SNAP: *S*-nitroso-*N*-acetyl-penicillamine; TEER: Transepithelial electrical resistance; P_{app}: Apparent permeability coefficient)

	Samples	Caco-2 cell monolayer model			Rat isolated intestinal model in Ussing chamber		
		Initial concentration (μM)	Incubation time (h)	P_{app} (10^{-6} cm.s^{-1})	Initial concentration (μM)	Incubation time (h)	P_{app} (10^{-6} cm.s^{-1})
Model control	Sodium fluorescein	-	-	-	1000	2	17.2 ± 1.3
	Furosemide	100	1	0.08 – 0.11	-	-	-
	Propranolol	50	1	3.3 – 41.9	1000	2	*
	TEER (Ω.cm²)	730 ± 53			≥ 30		
RSNOs permeability study	GSNO	100	4	2.6 ± 0.3	100	2	-
	GS^{15}NO	10 -100	1	2.3 ± 0.5	100	2	7.1 ± 0.6
	NACNO	100	4	5.0 ± 0.7	-	-	-
	SNAP	100	4	3.3 ± 0.5	-	-	-

*: under limit of quantification

In conclusion, RSNOs permeability, related transportation mechanism (passive) and preferred absorption site in GIT (jejunum) were studied in an intestinal cell (Caco-2) monolayer model. Meanwhile, GSNO degradation and absorption in intestine, and potential roles of intestinal denitrosationg enzymes (GGT and PDI), thiols and Me^{n+} were explored using isolated rat intestine. All these work give the consistent conclusion that GSNO permeability belongs to medium class according to FDA rules. In addition, GGT activity and PDI identification in rat intestine were measured and performed. Apart from GGT, thiols in intestine also contributed to GSNO degradation, but Me^{n+} showed no significant influence. Less than 1 % GSNO was absorbed and permeated in intestine after a 2-h incubation. Further work focused on protecting GSNO from degradation and improving its absorption after oral administration is of great importance.

General conclusions and perspectives

As mentioned in the general introduction part, the analytical methodologies commonly used in the EA 3452 Cithefor are based on conventional spectroscopic techniques described in the literature. However, their LOQ (defined as the lowest concentration of calibration curve with acceptable RSD, less than 15 %) range between 1 and 0.1 µM; it is is not sufficient for bioavailability study of RSNOs after oral administration. Moreover, in an *in vivo* PK study, it is necessary to distinguish between the different sources of NO: endogenous production, diet and medicine. ^{15}N labeling is a powerful tracer methodology for a better understanding of nitrogen cycle process and metabolism of nitrogen oxides. Using MS to analyze ^{15}N labeled NO species can selectively monitor NO species released from GS^{15}NO, and differentiate them from other sources (endogenous synthesis and diet).

Performances of bioanalytical methods for GS^{15}NO/^{15}N-nitrite ion measurement based on DAN assay is summarized in Table 1. Compositions of PBS, HBSS and Krebs solution are available in the protocol entitled *“Measurement of nitrite, nitrate ions and S-nitrosothiols using the 2,3-diaminonaphthalene assay by spectrofluorometry”*.

Table 1. Summary of bioanalytical method performances for *S*-nitrosoglutathione ($GS^{15}NO$)/^{15}N-nitrite ion measurement based on 2,3-diaminonaphthalene (DAN) derivatization (compositions of PBS/HBSS/Krebs solution are available in appendices)

		Spectrofluorometry	**LC-FL**	**LC-MS/MS**
Media		PBS, HBSS, Krebs solution		
Linearity range (nM)		100-2000		5-200
Limit of quantification (nM) Based on S/B		100		5
Throughput		*ca.* 3 min for 96 samples	15 min per sample	20 min per sample
Storage		r.t. for 2 days	- 80 °C for 3 months (Freezing/defreezing for two times)	
Application to Caco-2 cell monolayer	Initial $GS^{15}NO$ deposit amounts (nmol)	≥ 50	≥ 50	≥ 5 (5 - 50)
	Incubation time (h)	1/4/24	1/4/24	≥ 1
	Quantification spots	Apical and basolateral compartments	Apical and basolateral compartments	Apical and basolateral compartments
Application to isolated intestine in Ussing chamber	Initial $GS^{15}NO$ deposit range (nmol)	> 250	> *ca.* 125	> *ca.* 50
	Incubation time (h)	2	2	2
	Quantification spots	Donor and acceptor compartments	Donor compartment and intestine*	Donor and acceptor compartments

*: to measure *S*-nitrosothiols (RSNOs) and NO_2^- in intestine, see protocol entitled *"Measurement of S-nitrosothiols in the rat intestine with the 2,3-diaminonaphthalene assay by LC coupled with fluorescence detection"*.

The bioanalytical work using ^{15}N labeling and LC-ESI-ITMS/MS is the preamble of future assays of NO species metabolized from labeled $GS^{15}NO$ or other NO donors in the cells or tissues. The transposition of our approach to other biological matrices

(plasma, tissues, organs like aorta) using sample preparation protocols already described (Shin and Fung 2011)(Damacena-Angelis *et al.* 2016) constitutes a natural extension of the fields of application. Noteworwhy, sample pretreatment is a critical point. Consequently, SBC, NEM and EDTA are usually added to stabilize GSNO (Tsikas *et al.* 2017), and acetonitrile (Damacena-Angelis *et al.* 2016)(Wang *et al.* 2018) or solid phase extraction (Chao *et al.* 2016) is performed to purify analytes. In addition, our work has opened the perspective of more fundamental works such as the study of the reactivity of the ion $[NAT+H]^+$ in HCD tandem mass spectrometry in presence of acetonitrile and the mechanism of formation of the fragment ion m/z 156. In the future, Griess assay under HCD mode is promising to be tested to find out the most sensitive novel transition with low interference due to ^{13}C (*e.g.* less than 20 %).

Recently, a paper has described an automated online solid-phase derivatization for quantification of low-molecular-mass RSNOs by LC-MS (Wang *et al.* 2018). Noteworthy, labeling RSNOs by both ^{15}N and ^{13}C contributes to PK studies of both nitroso group carriers and NO species released from RSNOs. A recent review has explained that RSNOs such as SNACET has unique pharmacological profiles for oral use as NO, H_2S and GSH suppliers (Tsikas *et al.* 2018). Compared to nitrite ions, the permeation of the RSNOs species will improve the interest for RSNOs oral administration to provide NO supplementation. In addition, RSNOs have also shown other therapeutic effects, such as anti-cancer (Foster, Hess and Stamler 2009) and anti-inflammatory (Khan *et al.* 2005). For these reasons, exploring NO donors with higher lipophilicity such as *S*-nitrosoglutathione monoethyl ester (Konorev *et al.* 1996) or formulations (Wu *et al.* 2016) to increase RSNOs permeability is in need. In summary, it is vital and eventful to evaluate RSNOs bioavailability more deeply, and the developed and validated analytical method using ^{15}N labeling and LC-ESI-ITMS/MS in a more complex matrix (such as plasma) should be performed to conduct further PK study.

References

Aerssens E, Tiedje J, Averill B. Isotope Labeling Studies on the Mechanism of N-N Bond Formation in Denitrification. *J Biol Chem* 1986;**261**:9652–56.

Akyuez M, Ata S. Determination of low level nitrite and nitrate in biological, food and environmental samples by gas chromatography-mass spectrometry and liquid chromatography with fluorescence detection. *Talanta* 2009;**79**:900–4.

Alberts B, Johnson A, Lewis J, Raff M, Roberts K, Walter P. Carrier Proteins and Active Membrane Transport. *Book of Molecular Biology of the Cell, 4th edition* 2002.

Alqahtani S, Mohamed LA, Kaddoumi A. Experimental models for predicting drug absorption and metabolism. *Expert Opin Drug Metab Toxicol* 2013;**9**:1241–54.

Al-Sa'doni HH, Khan IY, Poston L, Fisher I, Ferro A. A novel family of S-nitrosothiols: chemical synthesis and biological actions. *Nitric Oxide-Biol Chem* 2000;**4**:550–60.

Amidon G, Lennernas H, Shah V, Crison JR. A Theoretical Basis for a Biopharmaceutic Drug Classification - the Correlation of in-Vitro Drug Product Dissolution and in-Vivo Bioavailability. *Pharm Res* 1995;**12**:413–20.

Andresen LC, Michelsen A, Jonasson S, Beier C, Ambus P. Glycine uptake in heath plants and soil microbes responds to elevated temperature, CO_2 and drought. *Acta Oecologica-Int J Ecol* 2009;**35**:786–96.

Andrew PJ, Mayer B. Enzymatic function of nitric oxide synthases. *Cardiovasc Res* 1999;**43**:521–31.

Artursson P. Cell-Cultures as Models for Drug Absorption Across the Intestinal-Mucosa. *Crit Rev Ther Drug Carrier Syst* 1991;**8**:305–30.

Atuma C, Strugala V, Allen A, Holm L. The adherent gastrointestinal mucus gel layer: thickness and physical state in vivo. *Am J Physiol-Gastrointest Liver Physiol* 2001;**280**:G922–9.

Axton ER, Hardardt EA, Stevens JF. Stable isotope-assisted LC–MS/MS monitoring of glyceryl trinitrate bioactivation in a cell culture model of nitrate tolerance. *J Chromatogr B* 2016;**1019**:156–63.

Badhan R, Penny J, Galetin A, Houston JB. Methodology for Development of a Physiological Model Incorporating CYP3A and P-Glycoprotein for the Prediction of Intestinal Drug Absorption. *J Pharm Sci* 2009;**98**:2180–97.

Bai J, Gao H, Xiao R, Wang J, Huang C. A Review of Soil Nitrogen Mineralization as Affected by Water and Salt in Coastal Wetlands: Issues and Methods. *Clean-Soil Air Water* 2012;**40**:1099–105.

Barraclough D. The Use of Mean Pool Abundances to Interpret N-15 Tracer Experiments.1. Theory. *Plant Soil* 1991;**131**:89–96.

Beckman JS, Koppenol WH. Nitric oxide, superoxide, and peroxynitrite: The good, the bad, and the ugly. *Am J Physiol-Cell Physiol* 1996;**271**:C1424–37.

Belcastro E. Thesis manuscript: Inflammation et stress oxydant dans l'athérosclérose: rôle dans les réponses vasculaires des S-nitrosothiols. *Université de Lorraine* 2016

Belcastro E, Wu W, Fries-Raeth I, Corti A, Pompella A, Leroy P, Lartaud I, Caucher C. Oxidative stress enhances and modulates protein S-nitrosation in smooth muscle cells exposed to S-nitrosoglutathione. *Nitric Oxide-Biol Chem* 2017;**69**:10–21.

Benjamin N, Odriscoll F, Dougall H, Duncan C, Smith L, Golden M, Mckenzie H. Stomach NO Synthesis. *Nature* 1994;**368**:502–502.

Bilat PA, Roger E, Faure S, Lagarce F. Models for drug absorbtion from the small intestine: where are we and where are we going? *Drug Discov Today* 2017;**22**:761–75.

Boger RH, Tsikas D, Bode-Boger SM, Phivthong-ngam L, Schwedhelm E, Frolich JC. Hypercholesterolemia impairs basal nitric oxide synthase turnover rate: a study investigating the conversion of L-[guanidino-15N(2)]-arginine to N-15-labeled nitrate by gas chromatography-mass spectrometry. *Nitric Oxide-Biol Chem* 2004;**11**:1–8.

Bojazi MS, Meyer B. Explosive nucleosynthesis of N 15 in a massive-star model. *Phys. Rev. C* 2014;**89**.

Bonetti J, Zhou Y, Parent M, Clarot I, Yu H, Fries-Raeth I, Leroy P, Lartaud I, Gaucher C. Intestinal absorption of S -nitrosothiols: permeability and transport mechanisms. *Biochem Pharmacol* 2018.;**155**:21-31.

Bordeleau G, Savard MM, Martel R, Smirnoff A, Ampleman G, Thiboutot S. Stable Isotopes of Nitrate Reflect Natural Attenuation of Propellant Residues on Military Training Ranges. *Environ Sci Technol* 2013;**47**:8265–72.

Bouressam ML, Meyer B, Boudier A, Clarot I, Leroy P, Genoni A, Ruiz-Lopez M, Giummelly P, Liminana P, Salgues V, Kouach M, Perrin-Sarrado C, Lartaud I, Dupuis F. In vivo and in silico evaluation of a new nitric oxide donor, S,S ’-dinitrosobucillamine. *Nitric Oxide-Biol Chem* 2017;**71**:32–43.

Bramanti E, Angeli V, Mester Z, Pompella A, Paolicchi A, D'Ulivo A. Determination of S-nitrosoglutathione in plasma: Comparison of two methods. *Talanta* 2010;**81**:1295–9.

Bramanti E, Angeli V, Paolicchi A, Pompella A. The determination of S-nitrosothiols in biological samples-Procedures, problems and precautions. *Life Sci* 2011;**88**:126–9.

Braughler J, Mittal C, Murad F. Effects of Thiols, Sugars, and Proteins on Nitric-Oxide Activation of Guanylate-Cyclase. *J Biol Chem* 1979;**254**:2450–4.

Broniowska KA, Diers AR, Hogg N. S-Nitrosoglutathione. *Biochim Biophys Acta* 2013;**1830**:3173–81.

Bryan NS, Fernandez BO, Bauer SM, Bauer SM, Gauria-Saura MF, Milsom AB, Rassaf T, Maloney RE, Bharti A, Rorriguez J, Feelisch M. Nitrite is a signaling molecule and regulator of gene expression in mammalian tissues. *Nat Chem Biol* 2005;**1**:290–7.

Bryan NS, Grisham MB. Methods to detect nitric oxide and its metabolites in biological samples. *Free Radic Biol Med* 2007;**43**:645–57.

Bryan NS, Rassaf T, Maloney RE, Rodriguez CM, Saijo F, Rodriguez JR, Feelisch M. Cellular targets and mechanisms of nitros(yl)ation: An insight into their nature and kinetics in vivo. *Proc Natl Acad Sci U S A* 2004;**101**:4308–13.

Burnette W. Western Blotting - Electrophoretic Transfer of Proteins from Sodium Dodecyl Sulfate-Polyacrylamide Gels to Unmodified Nitrocellulose and Radiographic Detection with Antibody and Radioiodinated Protein-A. *Anal Biochem* 1981;**112**(2):195–203.

Campanella B, Onor M, Pagliano E. Rapid determination of nitrate in vegetables by gas chromatography mass spectrometry. *Anal Chim Acta* 2017;**980**:33–40.

Carpenter AW, Schoenfisch MH. Nitric oxide release: Part II. Therapeutic applications. *Chem Soc Rev* 2012;**41**:3742–52.

Carter BZ, Wiseman AL, Orkiszewski R, Ballard KD, Ou CN, Lieberman MW. Metabolism of leukotriene C-4 in gamma-glutamyl transpeptidase-deficient mice. *J Biol Chem* 1997;**272**:12305–10.

Chan OH, Stewart BH. Physicochemical and drug-delivery considerations for oral drug bioavailability. *Drug Discov Today* 1996;**1**:461–73.

Chao MR, Shih YM, Hsu YW, Liu HH, Chang YJ, Lin BH, Hu CW. Urinary nitrite/nitrate ratio measured by isotope-dilution LC–MS/MS as a tool to screen for urinary tract infections. *Free Radic Biol Med* 2016;**93**:77–83.

Chen D, Chalk P. External-Source Contamination During Extraction Distillation in Isotope-Ratio Analysis of Soil Inorganic Nitrogen. *Anal Chim Acta* 1991;**245**:49–55.

Chobanyan K, Thum T, Suchy MT, Zhu B, Mitschke A, Gutzki FM, Beckmann B, Stichtenoth D, Tsikas D. GC-MS assay for hepatic DDAH activity in diabetic and non-diabetic rats by measuring dimethylamine (DMA) formed from asymmetric dimethylarginine (ADMA): Evaluation of the importance of S-nitrosothiols as inhibitors of DDAH activity in vitro and in vivo in humans. *J Chromatogr B* 2007;**858**:32–41.

Cooke JP, Dzau VJ. Nitric oxide synthase: Role in the genesis of vascular disease. *Annu Rev Med* 1997;**48**:489–509.

Csont T, Ferdinandy P. Cardioprotective effects of glyceryl trinitrate: beyond vascular nitrate tolerance. *Pharmacol Ther* 2005;**105**:57–68.

Curbo S, Gaudin R, Carlsten M, Malmberg KJ, Troye-Blomberg M, Ahlborg N, Karlsson A, Johansson M, Lundberg M. Regulation of interleukin-4 signaling by extracellular reduction of intramolecular disulfides. *Biochem Biophys Res Commun* 2009;**390**:1272–77.

Dahboul F, Leroy P, Gate KM, Boudier A, Gaucher C, Liminana P, Lartaud I, Pompella A, Perrin-Sarrado G. Endothelial *γ*-Glutamyltransferase Contributes to the Vasorelaxant Effect of *S*-Nitrosoglutathione in Rat Aorta. *Plos One* 2012;**7**:e43190.

Dahboul F, Perrin-Sarrado C, Boudier A, Lartaud I, Schneider R, Leroy P. S,S′-dinitrosobucillamine, a new nitric oxide donor, induces a better vasorelaxation than other S-nitrosothiols. *Eur J Pharmacol* 2014;**730**:171–9.

Damacena-Angelis C, Oliveira-Paula GH, Pinheiro LC, Crevelin EJ, Portella RL, Moraes LAB, Tanus-Santos JE. Nitrate decreases xanthine oxidoreductase-mediated nitrite reductase activity and attenuates vascular and blood pressure responses to nitrite. *Redox Biol* 2017;**12**:291–9.

Duan H, Ye L, Erler D, Ni BJ, Yuan Z. Quantifying nitrous oxide production pathways in wastewater treatment systems using isotope technology - A critical review. *Water Res* 2017;**122**:96–113.

Emsley J. Chemistry of the Elements, 1st Edition - Greenwood,NN, Earnshaw, A. *New Sci* 1984;**103**:41–2.

Emsley J. Enriching the Earth: Fritz Haber, Carl Bosch, and the transformation of world food. *Nature* 2001;**410**:633–4.

Fallingborg J, Christensen L, Ingemannielsen M, Jacobsen B, Abildgaard K, Rasmussen H. Ph-Profile and Regional Transit Times of the Normal Gut Measured by a Radiotelemetry Device. *Aliment Pharmacol Ther* 1989;**3**:605–13.

Ferreira JCB, Mochly-Rosen D. Nitroglycerin Use in Myocardial Infarction Patients - Risks and Benefits. *Circ J* 2012;**76**:15–21.

Fetih G, Habib F, Katsumi H, Okada N, Fujita T, Attia M, Yamamoto A. Excellent absorption enhancing characteristics of NO donors for improving the intestinal absorption of poorly absorbable compound compared with conventional absorption enhancers. *Drug Metab Pharmacokinet* 2006;**21**:222–9.

Foster MW, Hess DT, Stamler JS. Protein S-nitrosylation in health and disease: a current perspective. *Trends Mol Med* 2009;**15**:391–404.

Fu XM, Wang P, Zhu BT. Characterization of the Estradiol-Binding Site Structure of Human Protein Disulfide Isomerase (PDI). *Plos One* 2011;**6**:e27185.

Galaon T, Udrescu S, Sora I, David V, Medvedovici A. High-throughput liquid-chromatography method with fluorescence detection for reciprocal determination of furosemide or norfloxacin in human plasma. *Biomed Chromatogr* 2007;**21**:40–7.

Gaucher C, Boudier A, Dahboul F, Parent M, Leroy P. S-nitrosation/Denitrosation in Cardiovascular Pathologies: Facts and Concepts for the Rational Design of S-nitrosothiols. *Curr Pharm Des* 2013;**19**:458–72.

Gill SS, Hasanuzzaman M, Nahar, Macovei A, Tuteja N. Importance of nitric oxide in cadmium stress tolerance in crop plants. *Plant Physiol Biochem* 2013;**63**:254–61.

Giustarini D, Milzani A, Dalle-Donne I, Rossi R. Detection of S-nitrosothiols in biological fluids: a comparison among the most widely applied methodologies. *J Chromatogr B* 2007;**851**:124–39.

Glantzounis GK, Rocks SA, Sheth H, Knight I, Salacinski HJ, Davidson BR, Winyard PG, Selfalian AM. Formation and role of plasma S-nitrosothiols in liver ischemia-reperfusion injury. *Free Radic Biol Med* 2007;**42**:882–92.

Gonçalves JE, Ballerini-Fernandes M, Chiann C, Gai MN, De-Souza J, Storpirtis S. Effect of pH, mucin and bovine serum on rifampicin permeability through Caco-2 cells. *Biopharm Drug Dispos* 2012;**33**:316–23.

Hanff E, Boehmer A, Jordan J, Tsikas D. Stable-isotope dilution LC-MS/MS measurement of nitrite in human plasma after its conversion to S-nitrosoglutathione. *J Chromatogr B* 2014;**970**:44–52.

Hanff E, Eisenga MF, Beckmann B, Bakker SJL., Tsikas D. Simultaneous pentafluorobenzyl derivatization and GC-ECNICI-MS measurement of nitrite and malondialdehyde in human urine: Close positive correlation between these disparate oxidative stress biomarkers. *J Chromatogr B* 2017a;**1043**:167–75.

Hanff E, Luetzow M, Kayacelebi AA, Finkel A, Maassen M, Yancheva GR, Haqhikia A, Bavendiek U, Buck A, Lucke T, Maassen N, Tsikas D. Simultaneous GC-ECNICI-MS measurement of nitrite, nitrate and creatinine in human urine and plasma in clinical settings. *J Chromatogr B* 2017b;**1047**:207–14.

Hanigan MH, Frierson HF. Immunohistochemical detection of gamma-glutamyl transpeptidase in normal human tissue. *J Histochem Cytochem* 1996;**44**:1101–8.

He HB, Li XB, Zhang W, Zhang XD. Differentiating the dynamics of native and newly immobilized amino sugars in soil frequently amended with inorganic nitrogen and glucose. *Eur J Soil Sci* 2010;**62**(1):144–151.

Hekimi S, Lapointe J, Wen Y. Taking a “good” look at free radicals in the aging process. *Trends Cell Biol* 2011;**21**:569–76.

Helmke SM, Duncan MW. Measurement of the NO metabolites, nitrite and nitrate, in human biological fluids by GC-MS. *J Chromatogr B* 2007;**851**:83–92.

Hogg N, Singh RJ, Konorev E, Joseph J, Kalyanaraman B. S-Nitrosoglutathione as a substrate for gamma-glutamyl transpeptidase. *Biochem J* 1997;**323 (Pt 2)**:477–81.

Horyn O, Luhovyy B, Lazarow A, Daikhin Y, Nissim I, Yudkoff M, Nissim I. Biosynthesis of agmatine in isolated mitochondria and perfused rat liver: studies with 15N-labelled arginine. *Biochem J* 2005;**388**:419–25.

Ignarro L, Lippton H, Edwards J, Baricos W, Hyman A, Kadowitz P, Gruetter C. Mechanism of Vascular Smooth-Muscle Relaxation by Organic Nitrates, Nitrites, Nitroprusside and Nitric-Oxide - Evidence for the Involvement. *J Pharmacol Exp Ther* 1981;**218**:739–49.

Ismail A, d’Orlye F, Griveau S, Fracassi-da-Silva JA, Bedioui F, & Varenne A. Capillary electrophoresis with mass spectrometric detection for separation of S-nitrosoglutathione and its decomposition products: a deeper insight into the decomposition pathways. *Anal Bioanal Chem* 2015;**407**:6221–6.

Janzen H, Gilbertson C. Exchange of N-15 Among Plants in Controlled Environment Studies. *Can J Soil Sci* 1994;**74**(1):109–110.

Jernigan H. Metabolism of N-15-Labeled Amino-Acids in Rat Lens. *Exp Eye Res* 1983;**37**:77–84.

Jobgen WS, Jobgen SC, Li H, Meininger CJ, Wu G. Analysis of nitrite and nitrate in biological samples using high-performance liquid chromatography. *J Chromatogr B* 2007;**851**:71–82.

Jones DP. Redox potential of GSH/GSSG couple: Assay and biological significance. *Methods Enzymol* 2002;**348**:93–112.

Kabuto H, Yamamoto M, Yokoi I, Ogawa N. The source of nitrate and nitrite contamination that interferes with their accurate estimation in blood. *Clin Chim Acta* 1997;**266**:199–200.

Kararli T. Comparison of the Gastrointestinal Anatomy, Physiology, and Biochemistry. *Biopharm Drug Dispos* 1995;**16**:351–80.

Keefer LK, Flippen-Anderson JL, George C, Shanklin AP, Dunams TA, Christodoulou D, Saavedra JE, Sagan ES, Bohle DS. Chemistry of the diazeniumdiolates - 1. Structural and spectral characteristics of the [N(O)NO](-) functional group. *Nitric Oxide-Biol Chem* 2001;**5**:377–94.

Kerns EH, Di L, Petusky S, Farris M, Ley R, Jupp P. Combined application of parallel artificial membrane permeability assay and Caco-2 permeability assays in drug discovery. *J Pharm Sci* 2004;**93**:1440–53.

Khan M, Dhammu TS, Baarine M, Kim J, Paintlia MK., Singh I, Singh AK. GSNO promotes functional recovery in experimental TBI by stabilizing HIF-1α. *Behav Brain Res* 2018;**340**:63–70.

Khan M, Dhammu TS, Matsuda F, Singh AK., Singh I. Blocking a vicious cycle nNOS/peroxynitrite/AMPK by S-nitrosoglutathione: implication for stroke therapy. *BMC Neurosci* 2015;**16**:42.

Khan M, Jatana M, Elango C, Paintlia AS, Singh AK, Singh I. Cerebrovascular protection by various nitric oxide donors in rats after experimental stroke. *Nitric Oxide-Biol Chem* 2006;**15**:114–24.

Khan M, Sakakima H, Dhammu TS, Shunmugavel A., Im YB, Gilg AG, Singh AK, Singh I. S-Nitrosoglutathione reduces oxidative injury and promotes mechanisms of neurorepair following traumatic brain injury in rats. *J Neuroinflammation* 2011;**8**:78.

Khan M, Sekhon B, Giri S, Jatana M, Gilg AG, Ayasolla K, Elango C, Singh AK, Singh I. S-Nitrosoglutathione reduces inflammation and protects brain against focal cerebral ischemia in a rat model of experimental stroke. *J Cereb Blood Flow Metab* 2005;**25**:177–92.

Kim HK, Hong JH, Park MS, Kang JS, Lee MH. Determination of propranolol concentration in small volume of rat plasma by LC with fluorometric detection. *Biomed Chromatogr* 2001;**15**:539–45.

Kluge I, Gutteck-Amsler U, Zollinger M, Do KQ. *S*-Nitrosoglutathione in Rat Cerebellum: Identification and Quantification by Liquid Chromatography-Mass Spectrometry. *J Neurochem* 1997;**69**:2599–607.

Konorev EA, Joseph J, Tarpey MM, Kalyanaraman B. The mechanism of cardioprotection by S-nitrosoglutathione monoethyl ester in rat isolated heart during cardioplegic ischaemic arrest. *Br J Pharmacol* 1996;**119**(3):511–518.

Krieger MH, Santos KFR, Shishido SM, Wanschel AC, Estrela HF, Santos L, De-Oliveira MG, Franchini KG, Spadari-Bratfisch RC, Laurindo FR. Antiatherogenic effects of S-nitroso-N-acetylcysteine in hypercholesterolemic LDL receptor knockout mice. *Nitric Oxide-Biol Chem* 2006;**14**:12–20.

Kuzyakov Y, Xu X. Competition between roots and microorganisms for nitrogen: mechanisms and ecological relevance. *New Phytol* 2013;**198**:656–69.

Lash LH, Qian W, Putt DA, Jacobs K, Elfarra AA, Krause RJ, Parker JC. Glutathione conjugation of trichloroethylene in rats and mice: Sex-, species-, and tissue-dependent differences. *Drug Metab Dispos*, 1998;**26**(1):12–19.

Le Ferrec E, Chesne C, Artusson P, Brayden D, Fabre G, Gires P, Guillou F, Rousset M, Rubas W, Scarino ML. In vitro models of the intestinal barrier. The report and recommendations of ECVAM Workshop 46. European Centre for the Validation of Alternative methods. *Altern Lab Anim* 2001;**29**:649–68.

Lehmann J. Nitric oxide donors - current trends in therapeutic applications. *Expert Opin Ther Pat* 2000;**10**:559–74.

Levine AB, Punihaole D, Levine TB. Characterization of the Role of Nitric Oxide and Its Clinical Applications. *Cardiology* 2012;**122**:55–68.

Lewicki K, Marchand S, Matoub L, Lulek J, Coulon J, Leroy P. Development of a fluorescence-based microtiter plate method for the measurement of glutathione in yeast. *Talanta* 2006;**70**:876–82.

Li H, Meininger CJ, Wu G. Rapid determination of nitrite by reversed-phase high-performance liquid chromatography with fluorescence detection. *J Chromatogr B* 2000;**746**:199–207.

Littschwager J, Lauerer M, Blagodatskaya E, Kuzyakov Y. Nitrogen uptake and utilisation as a competition factor between invasive Duchesnea indica and native Fragaria vesca. *Plant Soil* 2010;**331**:105–14.

Li Y, Whitaker JS, McCarty CL. Reversed-phase liquid chromatography/electrospray ionization/mass spectrometry with isotope dilution for the analysis of nitrate and nitrite in water. *J Chromatogr A* 2011;**1218**:476–83.

Loo B, Labugger R, Skepper JN, Bachschmid M, Kilo J, Powell JM, Palacios-Callender M, Erusalimsky JD, Quaschning T, Malinski T, Gyqi D, Ullrich V, Luscher TF. Enhanced Peroxynitrite Formation Is Associated with Vascular Aging. *J Exp Med* 2000;**192**:1731–44.

Lundberg JO, Weitzberg E, Gladwin MT. The nitrate-nitrite-nitric oxide pathway in physiology and therapeutics. *Nat Rev Drug Discov* 2008;**7**:156–67.

Lundstrom J, Holmgren A. Protein Disulfide-Isomerase Is a Substrate for Thioredoxin Reductase and Has Thioredoxin-Like Activity. *J Biol Chem* 1990;**265**:9114–20.

Luo M, Boudier A, Pallotta A, Maincent P, Vincourt JB, Leroy P. Albumin as a carrier for NO delivery: preparation, physicochemical characterization, and interaction with gold nanoparticles. *Drug Dev Ind Pharm* 2016;**42**:1928–37.

Maattanen P, Gehring K, Bergeron JJM, Thomas DY. Protein quality control in the ER: The recognition of misfolded proteins. *Semin Cell Dev Biol* 2010;**21**:500–11.

MacArthur PH, Shiva S, Gladwin MT. Measurement of circulating nitrite and S-nitrosothiols by reductive chemiluminescence. *J Chromatogr B* 2007;**851**:93–105.

Mahmood T, Yang P-C. Western blot: technique, theory, and trouble shooting. *North Am J Med Sci* 2012;**4**:429–34.

Maron BA, Tang S-S, Loscalzo J. S-nitrosothiols and the S-nitrosoproteome of the cardiovascular system. *Antioxid Redox Signal* 2013;**18**:270–87.

Marzinzig M, Nussler AK, Stadler J, Marzinzig E, Barthlen W, Nussler NC, Beger HG, Morris SM, Brückner UB. Improved Methods to Measure End Products of Nitric Oxide in Biological Fluids: Nitrite, Nitrate, and S-Nitrosothiols. *Nitric Oxide-Biol Chem* 1997;**1**:177–89.

McAlister GC, Phanstiel DH, Brumbaugh J, Westphall MS, Coon JJ. Higher-energy Collision-activated Dissociation Without a Dedicated Collision Cell. *Mol Cell Proteomics* 2011;**10**:1-6.

Minamiyama Y, Takemura S, Inoue M. Effect of thiol status on nitric oxide metabolism in the circulation. *Arch Biochem Biophys* 1997;**341**:186–92.

Ming H. Thesis manuscript: Développement de formulations polymériques de *S*-nitrosoglutathion comme traitement *per* os pour prévenir les maladies inflammatoires chroniques de l'intestin. *Université de Lorraine* 2017.

Mitri E, Barbieri L, Vaccari L, Luchinat E. 15 N isotopic labelling for in-cell protein studies by NMR spectroscopy and single-cell IR synchrotron radiation FTIR microscopy: a correlative study. *Analyst* 2018;**143**:1171–81.

Mocellin S, Bronte V, Nitti D. Nitric oxide, a double edged sword in cancer biology: Searching for therapeutic opportunities. *Med Res Rev* 2007;**27**:317–52.

Moncada S, Higgs A. The L-Arginine-Nitric Oxide Pathway. *N Engl J Med* 1993;**329**:2002–12.

Moncada S, Palmer RM, Higgs EA. Nitric oxide: physiology, pathophysiology, and pharmacology. *Pharmacol Rev* 1991;**43**:109–42.

Montano SJ, Lu J, Gustafsson TN, Holmgren A. Activity assays of mammalian thioredoxin and thioredoxin reductase: Fluorescent disulfide substrates, mechanisms, and use with tissue samples. *Anal Biochem* 2014;**449**:139–46.

Mukai Y, Hara H, Taniguchi H. Fluorometric Determinations of Nitrite and Amyl Nitrite with 2,3-Diaminonaphthalene. *Bunseki Kagaku* 1991;**40**:105–7.

Mulholland PJ, Tank JL, Sanzone DM, Wollheim WM, Peterson BJ, Webster JR, Meyer JL. Nitrogen cycling in a forest stream determined by a N-15 tracer addition. *Ecol Monogr* 2000;**70**:471–93.

Münzel T, Steven S, Daiber A. Organic nitrates: Update on mechanisms underlying vasodilation, tolerance and endothelial dysfunction. *Vascul Pharmacol* 2014;**63**:105–13.

Neirinckx E, Vervaet C, Michiels J, De-Smet S, Van-den-Broeck W, Remon JP, De-Backer P, Croubels S. Feasibility of the Ussing chamber technique for the determination of in vitro jejunal permeability of passively absorbed compounds in different animal species. *J Vet Pharmacol Ther* 2011;**34**:290–7.

Numata N, Takahashi K, Mizuno N, Utoguchi N, Watanabe Y, Matsumoto M, Mayumi T. Improvement of intestinal absorption of macromolecules by nitric oxide donor. *J Pharm Sci* 2000;**89**:1296–304.

Ohkouchi N, Chikaraishi Y, Close HG, Fry B, Larsen T, Madigan DJ, Mc-Carthy MD, Mc-Mahon KW, Nagata T, Naito YI, Ogawa NO, Popp BN, Steffan S, Takano Y,

Tayasu I, Wyatt ASJ, Tamaguchi YT, Yokoyama Y. Advances in the application of amino acid nitrogen isotopic analysis in ecological and biogeochemical studies. *Org Geochem* 2017;**113**:150–74.

Okada K, Zhu B-T. S-nitrosylation of the IGF-1 receptor disrupts the cell proliferative action of IGF-1. *Biochem Biophys Res Commun* 2017;**491**:870–5.

Orlowski M, Meister A. Gamma-Glutamyl-Rho-Nitroanilide - a New Convenient Substrate for Determination and Study of L- and D-Gamma-Glutamyltranspeptidase Activities. *Biochim Biophys Acta* 1963;**73**:679 – &.

Pagliano E, Meija J, Sturgeon RE, Mester Z, D'Ulivo A. Negative Chemical Ionization GC/MS Determination of Nitrite and Nitrate in Seawater Using Exact Matching Double Spike Isotope Dilution and Derivatization with Triethyloxonium Tetrafluoroborate. *Anal Chem* 2012;**84**:2592–6.

Parent M, Boudier A, Dupuis F, Nouvel C, Sapin A, Lartaud I, Six JL, Leroy P, Maincent, P Are in situ formulations the keys for the therapeutic future of S-nitrosothiols? *Eur J Pharm Biopharm* 2013a;**85**:640–9.

Parent M, Boudier A, Perrin J, Vigneron C, Maincent P, Violle N, Bisson JF, Lartaud I, Dupuis F. In Situ Microparticles Loaded with S-Nitrosoglutathione Protect from Stroke. *Plos One* 2015;**10**:e0144659.

Parent M, Dahboul F, Schneider R, Clarot I, Maincent P, Leroy P, Boudier A. A Complete Physicochemical Identity Card of S-nitrosoglutathione. *Curr Pharm Anal* 2013b;**9**:31–42.

Parodi O, De Maria R, Roubina E. Redox state, oxidative stress and endothelial dysfunction in heart failure: the puzzle of nitrate-thiol interaction. *J Cardiovasc Med* 2007;**8**:765–74.

Peng Y, Yadava P, Heikkinen AT, Parrott N, Railkar A. Applications of a 7-day Caco-2 cell model in drug discovery and development. *Eur J Pharm Sci* 2014;**56**:120–30.

Pinheiro LC, Amaral JH, Ferreira GC, Portella R L, Ceron CS, Montenegro MF, Toledo-Jr JC, Tanus-Santos JE. Gastric S-nitrosothiol formation drives the antihypertensive effects of oral sodium nitrite and nitrate in a rat model of renovascular hypertension. *Free Radic Biol Med* 2015;**87**:252–62.

Planche T, Macallan DC, Sobande T, Borrmann S, Kun JFJ, Krishna S, Kremsner PG. Nitric oxide generation in children with malaria and the NOS2G-954C promoter polymorphism. *Am J Physiol-Regul Integr Comp Physiol* 2010;**299**:R1248–53.

Pompella A, Emdin M, Passino C, Paolicchi A. The significance of serum gamma-glutamyltransferase in cardiovascular diseases. *Clin Chem Lab Med* 2004;**42**:1085–91.

Prescott LF, Illingworth RN, Critchley JA, Stewart MJ, Adam RD, Proudfoot AT. Intravenous N-acetylcystine: the treatment of choice for paracetamol poisoning. *Br Med J* 1979;**2**:1097–100.

Raturi A, Mutus B. Characterization of redox state and reductase activity of protein disulfide isomerase under different redox environments using a sensitive fluorescent assay. *Free Radic Biol Med* 2007;**43**:62–70.

Rekhi GS, Jambhekar SS, Souney PF, Williams DA. A fluorimetric liquid chromatographic method for the determination of propranolol in human serum plasma. *J Pharm Biomed Anal* 1995;**13**:1499–505.

Richardson G, Benjamin N. Potential therapeutic uses for S-nitrosothiols. *Clin Sci* 2002;**102**:99–105.

Ryu JM, Chung SJ, Lee MH, Kim CK, Shim CK. Increased bioavailability of propranolol in rats by retaining thermally gelling liquid suppositories in the rectum. *J Controlled Release* 1999;**59**:163–72.

Salzman AL, Menconi MJ, Unno N, Ezzell RM, Casey DM, Gonzalez PK, Fink MP. Nitric oxide dilates tight junctions and depletes ATP in cultured Caco-2BBe intestinal epithelial monolayers. *Am J Physiol* 1995;**268**:G361–73.

Saville B. A scheme for the colorimetric determination of microgram amounts of thiols. *Analyst* 1958;**83**:670–2.

Sawicki E, Stanley TW, Pfaff J, D'Amico A. Comparison of fifty-two spectrophotometric methods for the determination of nitrite. *Talanta* 1963;**10**(6):641–655.

Schafer FQ, Buettner GR. Redox environment of the cell as viewed through the redox state of the glutathione disulfide/glutathione couple. *Free Radic Biol Med* 2001;**30**:1191–212.

Schaus R. Griess Nitrite Test in Diagnosis of Urinary Infection. *J Am Med Assoc* 1956;**161**:528–9.

Schiele F, Artur Y, Bagrel D, Petitclerc C, Siest G. Measurement of Plasma Gamma-Glutamyltransferase in Clinical-Chemistry - Kinetic Basis and Standardization Propositions. *Clin Chim Acta* 1981;**112**:187–95.

Schmidt TC, Zwank L, Elsner M, Berg M, Meckenstock RU, Haderlein SB. Compound-specific stable isotope analysis of organic contaminants in natural environments: a critical review of the state of the art, prospects, and future challenges. *Anal Bioanal Chem* 2004;**378**:283–300.

Schreiber F, Stief P, Kuypers MMM, De-Beer D. Nitric oxide turnover in permeable river sediment. *Limnol Oceanogr* 2014;**59**:1310–20.

Sebilo M, Mayer B, Nicolardot B, Pinay G, Mariotti A. Long-term fate of nitrate fertilizer in agricultural soils. *Proc Natl Acad Sci U S A* 2013;**110**:18185–9.

Shah SU, Martinho N, Socha M, Reis CP, Gibaud S. Synthesis and characterization of *S*-nitrosoglutathione-oligosaccharide-chitosan as a nitric oxide donor. *Expert Opin Drug Del* 2015;**12**:1209–23.

Shah SU, Socha M, Fries I, Gibaud S. Synthesis of S-nitrosoglutathione-alginate for prolonged delivery of nitric oxide in intestines. *Drug Deliv* 2016;**23**:2927–35.

Shah VP, Midha KK, Findlay JW, Hill HM, Hulse JD, McGilveray IJ, Mckay G, Miller KG, Patnaik RN, Powell ML, Tonelli A, Viswanathan CT, Yacobi A. Bioanalytical method validation--a revisit with a decade of progress. *Pharm Res* 2000;**17**(12):1551–57.

Sherer EC, Verras A, Madeira M, Hagmann WK, Sheridan RP, Roberts D, Bleasby K, Cornell WD. QSAR Prediction of Passive Permeability in the LLC-PK1 Cell Line: Trends in Molecular Properties and Cross-Prediction of Caco-2 Permeabilities. *Mol Inform* 2012;**31**:231–45.

Shin S, Fung HL. Evaluation of an LC–MS/MS assay for 15N-nitrite for cellular studies of l-arginine action. *J Pharm Biomed Anal* 2011;**56**:1127–31.

Sigman DM, Altabet MA, Michener R, McCorkle DC, Fry B, Holmes RM. Natural abundance-level measurement of the nitrogen isotopic composition of oceanic nitrate: an adaptation of the ammonia diffusion method. *Mar Chem* 1997;**57**(3-4):227–42.

Sigman DM, Casciotti KL, Andreani M, Barford C, Galanter M, Bohlke JK. A bacterial method for the nitrogen isotopic analysis of nitrate in seawater and freshwater. *Anal Chem* 2001;**73**(17):4145–53.

Smith BC, Marletta MA. Mechanisms of S-nitrosothiol formation and selectivity in nitric oxide signaling. *Curr Opin Chem Biol* 2012;**16**:498–506.

Srinivasan B, Kolli AR, Esch MB, Abaci HE, Shuler ML, Hickman JJ. TEER measurement techniques for in vitro barrier model systems. *J Lab Autom* 2015;**20**:107–26.

Stange CF, Spott O, Apelt B, Russow RWB. Automated and rapid online determination of 15N abundance and concentration of ammonium, nitrite, or nitrate in aqueous samples by the SPINMAS technique. *Isotopes Environ Health Stud* 2007;**43**(3):227–36.

Stomberski CT, Hess DT, Stamler JS. Protein S-Nitrosylation: Determinants of Specificity and Enzymatic Regulation of S-Nitrosothiol-Based Signaling. *Antioxid Redox Signal* 2018.

Swartz ME. UPLC (TM): An introduction and review. *J Liq Chromatogr Relat Technol* 2005;**28**(7-8):1253–63.

Tang Y, Jiang H, Bryan NS. Nitrite and nitrate: cardiovascular risk-benefit and metabolic effect. *Curr Opin Lipidol* 2011;**22**:11–5.

Tate S, Meister A. Serine-Borate Complex as a Transition-State Inhibitor of Gamma-Glutamyl Transpeptidase. *Proc Natl Acad Sci U S A* 1978;**75**:4806–9.

Teixeira P, Napoleão P, Saldanha C. S-nitrosoglutathione efflux in the erythrocyte. *Clin Hemorheol Microcirc* 2015;**60**:397–404.

Toledo JC, Augusto O. Connecting the Chemical and Biological Properties of Nitric Oxide. *Chem Res Toxicol* 2012;**25**:975–89.

Toyoda S, Yoshida N, Koba K. Isotopocule analysis of biologically produced nitrous oxide in various environments. *Mass Spectrom Rev* 2017;**36**:135–60.

Tsikas D. Methods of quantitative analysis of the nitric oxide metabolites nitrite and nitrate in human biological fluids. *Free Radic Res* 2005;**39**:797–815.

Tsikas D. GC-MS and LC methods for peroxynitrite (ONOO- and (ONOO-)-N-15) analysis: a study on stability, decomposition to nitrite and nitrate, laboratory synthesis, and formation of peroxynitrite from S-nitrosoglutathione (GSNO) and KO2. *Analyst* 2011;**136**:979–87.

Tsikas D. Pentafluorobenzyl bromide—A versatile derivatization agent in chromatography and mass spectrometry: I. Analysis of inorganic anions and organophosphates. *J Chromatogr B* 2017;**1043**:187–201.

Tsikas D, Boehmer A, Mitschke A. Gas Chromatography-Mass Spectrometry Analysis of Nitrite in Biological Fluids without Derivatization. *Anal Chem* 2010;**82**:5384–90.

Tsikas D, Boger R, Bodeboger S, Gutzki F, Frolich J. Quantification of Nitrite and Nitrate in Human Urine and Plasma as Pentafluorobenzyl Derivatives by Gas-Chromatography Mass-Spectrometry Using Their N-15-Labeled Analogs. *J Chromatogr B* 1994;**661**:185–91.

Tsikas D, Dehnert S, Urban K, Surdacki A, Meyer HH. GC–MS analysis of S-nitrosothiols after conversion to S-nitroso-N-acetyl cysteine ethyl ester and in-injector nitrosation of ethyl acetate. *J Chromatogr B* 2009;**877**:3442–55.

Tsikas D, Duncan MW. Mass Spectrometry and 3-Nitrotyrosine: Strategies, Controversies, and Our Current Perspective. *Mass Spectrom Rev* 2014;**33**:237–76.

Tsikas D, Gutzki FM, Rossa S, Bauer H, Neumann C, Dockendorff K, Sandmann J, Frölich JC. Measurement of Nitrite and Nitrate in Biological Fluids by Gas Chromatography–Mass Spectrometry and by the Griess Assay: Problems with the Griess Assay—Solutions by Gas Chromatography–Mass Spectrometry. *Anal Biochem* 1997;**244**:208–20.

Tsikas D, Raida M, Sandmann J, Rossa S, Forssmann WG, Frölich JC. Electrospray ionization mass spectrometry of low-molecular-mass S-nitroso compounds and their thiols. *J Chromatogr B* 2000a;**742**:99–108.

Tsikas D, Rossa S, Stichtenoth DO, Raida M, Gutzki FM, Frölich JC. Is S-Nitroso-N-acetyl-l-cysteine a Circulating or an Excretory Metabolite of Nitric Oxide (NO) in Man? Assessment by Gas Chromatography–Mass Spectrometry. *Biochem Biophys Res Commun* 1996;**220**:939–44.

Tsikas D, Sandmann J, Frolich JC. Measurement of S-nitrosoalbumin by gas chromatography - mass spectrometry III. Quantitative determination in human plasma after specific conversion of the S-nitroso group to nitrite by cysteine and Cu2+ via intermediate formation of S-nitrosocysteine and nitric oxide. *J Chromatogr B* 2002;**772**:335–46.

Tsikas D, Sandmann J, Gutzki FM, Stichtenoth DO, Frölich JC. Measurement of S-nitrosoalbumin by gas chromatography–mass spectrometry: II. Quantitative determination of S-nitrosoalbumin in human plasma using S-[15N]nitrosoalbumin as internal standard. *J Chromatogr B* 1999a;**726**:13–24.

Tsikas D, Sandmann J, Rossa S, Gutzki FM, Frölich JC. Gas Chromatographic–Mass Spectrometric Detection of S-Nitroso-cysteine and S-Nitroso-glutathione. *Anal Biochem* 1999b;**272**:117–22.

Tsikas D, Sandmann J, Rossa S, Gutzki FM, Frolich JC. Measurement of S-nitrosoalbumin by gas chromatography mass spectrometry - I. Preparation, purification, isolation, characterization and metabolism of S-[N-15]nitrosoalbumin in human blood in vitro. *J Chromatogr B* 1999c;**726**:1–12.

Tsikas D, Sandmann J, Savva A, Luessen P, Boger RH, Gutzki FM, Mayer B, Frolich JC. Assessment of nitric oxide synthase activity in vitro and in vivo by gas chromatography-mass spectrometry. *J Chromatogr B* 2000b;**742**:143–53.

Tsikas D, Schmidt M, Böhmer A, Zoerner AA, Gutzki FM, Jordan J. UPLC–MS/MS measurement of S-nitrosoglutathione (GSNO) in human plasma solves the S-nitrosothiol concentration enigma. *J Chromatogr B* 2013;**927**:147–57.

Tsikas D, Schmidt M, Hanff E, Boehmer A. GC-ECNICI-MS analysis of S-nitrosothiols and nitroprusside after treatment with aqueous sulphide (S2-) and derivatization with pentafluorobenzyl bromide: Evidence of S-transnitrosylation and formation of nitrite and nitrate. *J Chromatogr B* 2017a;**1043**:209–18.

Tsikas D, Schwedhelm KS, Surdacki A, Giustarini D, Rossi R, Kukoc-Modun L, Kedia G, Uckert S. S-Nitroso-N-acetyl-L-cysteine ethyl ester (SNACET) and N-acetyl-L-cysteine ethyl ester (NACET)-Cysteine-based drug candidates with unique pharmacological profiles for oral use as NO, H2S and GSH suppliers and as antioxidants: Results and overview. *J Pharm Anal* 2018;**8**:1–9.

Tsuchiya K, Takiguchi Y, Okamoto M, Izawa Y, Kanematsu Y, Yoshizumi M, Tamaki, T. Malfunction of vascular control in lifestyle-related diseases: Formation of systemic hemoglobin-nitric oxide complex (HbNO) from dietary nitrite. *J Pharmacol Sci* 2004;**96**:395–400.

Vallance P, Leone A, Calver A, Collier J, Moncada S. Accumulation of an Endogenous Inhibitor of Nitric-Oxide Synthesis in Chronic-Renal-Failure. *Lancet* 1992;**339**:572–5.

Walters C, Gillatt P, Palmer R, Smith P. A Rapid Method for the Determination of Nitrate and Nitrite by Chemiluminescence. *Food Addit Contam* 1987;**4**:133–40.

Wang A, Zhu W, Gundersen P, Phillips OL, Chen D, Fang Y. Fates of atmospheric deposited nitrogen in an Asian tropical primary forest. *Forest Ecol Manag* 2018;**411**:213–22.

Wang C, Cassens R, Hoekstra W. Fate of Ingested 15n-Labeled Nitrate and Nitrite in the Rat. *J Food Sci* 1981;**46**:745–8.

Wang X, Garcia CT, Gong G, Wishnok JS, Tannenbaum SR. Automated Online Solid-Phase Derivatization for Sensitive Quantification of Endogenous S-Nitrosoglutathione and Rapid Capture of Other Low-Molecular-Mass S-Nitrosothiols. *Anal Chem* 2018;**90**:1967–75.

Wang Y, Cao J, Wang X, Zeng S. Stereoselective transport and uptake of propranolol across human intestinal Caco-2 cell monolayers. *Chirality* 2010;**22**:361–8.

Warnecke A, Luessen P, Sandmann J, Ikic M, Rossa S, Gutzki FM, Stichtenoth DO, Tsikas D. Application of a stable-isotope dilution technique to study the pharmacokinetics of human N-15-labelled S-nitrosoalbumin in the rat: Possible mechanistic and biological implications. *J Chromatogr B* 2009;**877**:1375–87.

Wickham S, West MB, Cook PF, Hanigan MH. Gamma-glutamyl compounds: Substrate specificity of gamma-glutamyl transpeptidase enzymes. *Anal Biochem* 2011;**414**:208–14.

Wu A, Duan T, Tang D, Zeng Z, Zhu J, Wang R, He B, Cheng H, Feng L, Zhu Q. Review the Application of Chromatography in the Analysis of Nitric Oxide-derived Nitrite and Nitrate Ions in Biological Fluids. *Curr Anal Chem* 2014;**10**:609–21.

Wutzke KD. Development and application of N-15-tracer substances for measuring the whole-body protein turnover rates in the human, especially in neonates: a review. *Isotopes Environ Health Stud* 2012;**48**:239–58.

Wu W. Thesis manuscript: Développement de nanoparticules composites polymériques de *S*-nitrosoglutathion dédiées au traitement oral des maladies cardiovasculaires. *Université de Lorraine* 2017.

Wu W, Gaucher C, Diab R, Fries, I., Xiao YL, Hu XM, Maincent P, Sapin-Minet A. Time lasting S-nitrosoglutathione polymeric nanoparticles delay cellular protein S-nitrosation. *Eur J Pharm Biopharm* 2015a;**89**:1–8.

Wu W, Gaucher C, Fries I, Hu X, Maincent P, Sapin-Minet A. Polymer nanocomposite particles of S-nitrosoglutathione: A suitable formulation for protection and sustained oral delivery. *Int J Pharm* 2015b;**495**:354–61.

Wu W, Perrin-Sarrado C, Ming H, Lartaud I, Maincent P, Hu XM, Sapin-Minet A, Gaucher C. Polymer nanocomposites enhance S-nitrosoglutathione intestinal absorption and promote the formation of releasable nitric oxide stores in rat aorta. *Nanomedicine-Nanotechnol Biol Med* 2016;**12**:1795–803.

Xu DZ, Lu Q, Deitch EA. Nitric oxide directly impairs intestinal barrier function. *Shock* 2002;**17**:139–45.

Yamamoto A, Tatsumi H, Maruyama M, Uchiyama T, Okada N, Fujita T. Modulation of Intestinal Permeability by Nitric Oxide Donors: Implications in Intestinal Delivery of Poorly Absorbable Drugs. *J Pharmacol Exp Ther* 2001;**296**:84–90.

Yamashita S, Furubayashi T, Kataoka M, Sakane T, Sezaki H, Tokuda H. Optimized conditions for prediction of intestinal drug permeability using Caco-2 cells. *Eur J Pharm Sci* 2000;**10**:195–204.

Yang X, Bondonno CP, Indrawan A, Hodgson JM, Croft KD. An improved mass spectrometry-based measurement of NO metabolites in biological fluids. *Free Radic Biol Med* 2013;**56**:1–8.

Yu H, Schmitt R, Sapin A, Chailbault P, Leroy P. Comparison between two derivatization methods of nitrite ion labeled with ^{15}N applied to liquid chromatography-tandem mass spectrometry. *Anal Method* 2018;**10**(31): 3830–36.

Zhu C, Jiang L, Chen TM, Hwang KK. A comparative study of artificial membrane permeability assay for high throughput profiling of drug absorption potential. *Eur J Med Chem* 2002;**37**:399–407.

Appendices

List of protocols

Measurement of nitrite, nitrate ions and *S*-nitrosothiols using the 2,3-diaminonaphthalene assay by spectrofluorometry

1. Principle

The 2,3-diaminonaphthalene (DAN) assay relies upon the reaction between the non-fluorescent reagent DAN and nitrite ion in acidic medium to yield 2,3-naphthotriazole (NAT) adduct, which exhibits in alkaline medium fluorescence at 415 nm after excitation at 375 nm. For *S*-nitrosothiols (RSNOs), mercuric ions are used to cleave the S-NO bond, therefore allowing them to be measured with the DAN assay. Nitrate ions are reduced to nitrite ions by an enzymatic reaction, next they are measured by DAN assay.

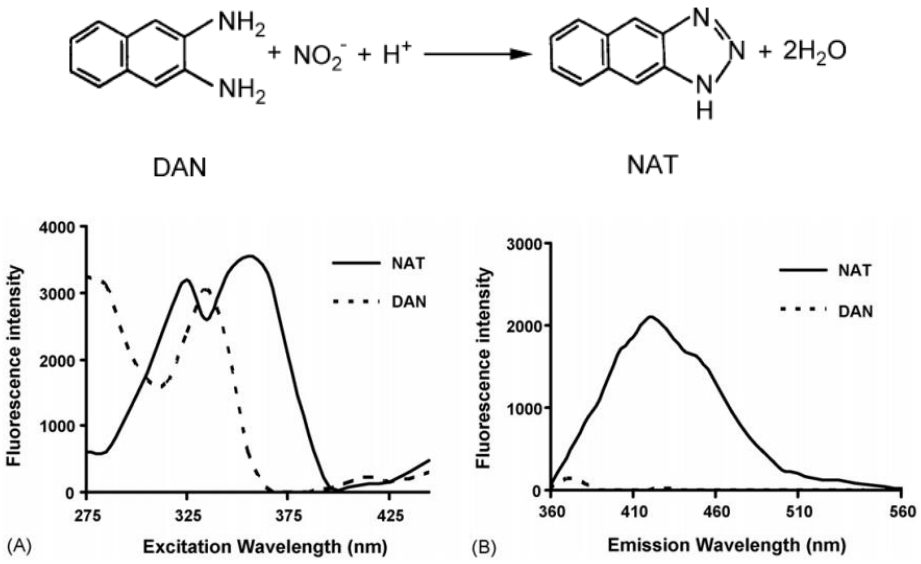

Figure 1. Reaction between nitrite ion and 2,3-diaminonaphthalene (DAN) producing 2,3-naphthotriazole (NAT) and corresponding fluorescence spectra at an excitation wavelength of 375 nm (panel-A) and at an emission wavelength of 415 nm (panel-B) (Jobgen *et al.* 2007).

Reference:

Jobgen WS, Jobgen SC, Li H *et al.* Analysis of nitrite and nitrate in biological samples using high-performance liquid chromatography. *J Chromatogr B* 2007;**851**:71–82.

2. Reagents

All solutions are prepared with fresh cold ultrapure water (> 18.2 MΩ.cm) and

stored at 4°C in the dark for maximum one month unless otherwise specified.

2.1. Physiological media

Conservation time: one week at 4°C after preparation.

Phosphate Buffer Saline (PBS) solution: weigh 8.00 g NaCl, 0.20 g KCl, 2.32 g $Na_2HPO_4 \cdot 12\ H_2O$, 0.20 g KH_2PO_4. Dissolve in 1.0 L of ultrapure water; adjust pH to 7.4 (by using a pH meter) with 10 M NaOH solution**.**

Krebs solution: weigh 6.90 g NaCl, 0.35 g KCl, 1.80 g glucose, 0.16 g KH_2PO_4, 2.02 g $NaHCO_3$, 0.14 g $MgSO_4$, 0.35 g $CaCl_2 \cdot 2\ H_2O$. Dissolve in 1.0 L of ultrapure water, adjust pH to 7.4 (by using a pH meter) with 1.0 M HCl.

Hank's Balanced Salt Solution (HBSS): use commercial HBSS (ref Gibco: 14185-045) made of 8.0 g/L NaCl, 0.4 g/L KCl, 1.0 g/L glucose, 60.0 mg/L KH_2PO_4, 47.5 mg/L Na_2HPO_4, 140.0 mg/L $CaCl_2$, 98.0 mg/L $MgSO_4$ final pH 7.4

2.2. 0.6 M HCl

Transfer 300 mL of 1 M HCl (Mw = 36.46 $g.mol^{-1}$; commercial solution) in a 500 mL volumetric flask and adjust the volume with ultrapure water.

2.3. 0.316 mM DAN

Weigh 5 mg of DAN (Mw = 158 $g.mol^{-1}$; ref Sigma D-2757) in a 100 mL volumetric flask, dissolve and adjust the volume with 0.6 M HCl. Store at 4°C protected from light for 1 month.

2.4. 0.105 mM DAN

Dilute 3-fold of 0.316 mM DAN solution with 0.6 M HCl (500 µL of 0.316 mM DAN + 1000 µL of 0.6 M HCl). Prepare daily.

2.5. 3.17 mM $HgCl_2$

Weigh 86.0 mg of $HgCl_2$ (Mw = 271.5 $g.mol^{-1}$; ref VWR 25384) in a 100 mL volumetric flask, dissolve and adjust the volume with 0.6 M HCl. Store at 4°C protected from light for 1 month.

2.6. 0.105 mM DAN with 1.05 mM $HgCl_2$

Mix 1 volume of 0.316 mM DAN solution, 1 volume of 3.17 mM mercuric chloride solution and 1 volume of 0.6 M HCl. Prepare daily.

2.7. 2.1 M NaOH

Dilute 6-fold 50% NaOH solution with ultrapure water by mixing 5 mL of 50% NaOH solution (Mw = 40 $g.mol^{-1}$; ref Fluka 72064) and 25 mL ultrapure water.

2.8. 10^{-2} M sodium nitrite

Weigh 34.5 mg of sodium nitrite ($NaNO_2$) (Mw = 69 $g.mol^{-1}$; ref Merck 6549) in a 50 mL volumetric flask, dissolve and adjust the volume with PBS. Mix the solution gently for one time. Prepare daily.

2.9. 10^{-2} M sodium nitrate

Weigh 42.5 mg of sodium nitrate ($NaNO_3$) (Mw = 85 $g.mol^{-1}$; ref Sigma S8170) in a 50 mL volumetric flask, dissolve and adjust the volume with PBS. Prepare daily.

2.10. *S*-nitrosoglutathione (GSNO)

Solutions are prepared, titrated and stored according to protocol entitled *"Batch synthesis of S-nitrosoglutathione"*.

2.11. Nitrate/Nitrite fluorometric assay kit

Assay buffer (Item N0. 780022): Transfer the content of the Assay Buffer vial (from the Nitrate/Nitrite fluorometric assay kit Cayman ref. 780051) to a 100 mL volumetric flask, rinse the vial three times with 1 mL of ultrapure water and fill up to 100 mL with ultrapure water. Store at 4 °C for no more than 2 months.

Nitrate Reductase (Item N0. 780010): Reconstitute the content of the vial (from the kit) with 1.2 mL Assay Buffer. Keep on ice during use. Divide into 70 µL aliquots and store at -20 °C for no more than 2 months. Freezing and thawing should be only operated once.

Enzyme Cofactors (Item N0. 780012): Reconstitute the contents of the vial (from the kit) with 1.2 mL Assay Buffer. Keep on ice during use. Divide into 70 µL aliquots and store at -20 °C for no more than 2 months. Freezing and thawing should be only operated once.

2.12. Lysis buffer

Transfer 2 g Triton X-100 (ref Sigma 9002-93-1) in a 500 mL volumetric flask and adjust the volume with 0.1 M HCl.

3. Methods

3.1. Calibration curves for NO_2^- and RSNOs determination

$NaNO_2$/GSNO daughter solution n°1 (10^{-4} M): transfer 100 µL of 10^{-2} M $NaNO_2$/GSNO solution in a 10 mL volumetric flask, adjust the volume with PBS. Mix gently for one time.

$NaNO_2$/GSNO daughter solution n° 2 (2.10^{-6} M): transfer 500 µL of the $NaNO_2$/GSNO daughter solution n°1 in a 25 mL volumetric flask, adjust the volume with sample buffer. Mix gently for one time.

Dilutions for the calibration curve are prepared in 1.5 mL Eppendorf tubes (mix gently each tube for one time), as follows:

Tube n°	1	2	3	4	5	6	7
$NaNO_2$/GSNO daughter solution n°2 (2.10^{-6} M) (µL)	0	50	125	375	500	750	1000
Physiological medium (µL)	1000	950	875	625	500	250	0
$[NO_2^-]$/[RSNO] (µM)	-	0.10	0.25	0.75	1.00	1.50	2.00

100 µL of each standard (concentration range: 0.1 – 2 µM) or sample (in triplicate) is transferred into a black 96-well microplate, and 20 µL of 0.105 mM DAN solution is added. The mixture is shaken for 1 min at 500 rpm at 20-25 °C (Heidolph, VIBRAMAX 110, Schwabach, Germany) before incubation at 37 °C (incubator) in the dark for 10 min. Next, 20 µL of 2.1 M NaOH is added. The mixture is shaken for 5 min at 500 rpm at 20-25 °C, followed by analysis with a spectrofluorimeter (FP-8300iRM, JASCO, Tokyo, Japan) coupled with FMP micro-well plate reader.

For RSNOs or (RSNOs + NO_2^-) measurement, DAN reagent has to be replaced by DAN-$HgCl_2$ reagent.

3.2. Calibration curve for NO_3^- determination

$NaNO_3$ daughter solution n°1 ($2.5.10^{-5}$ M): transfer 50 µL of 10^{-2} M $NaNO_3$ solution in a 20 mL volumetric flask. Adjust the volume with the corresponding physiological medium.

Dilutions for the calibration curve are prepared in Eppendorf tubes, as follows:

Tube n°	1	2	3	4	5	6	7
$NaNO_3$ daughter solution n°1 ($2.5.10^{-5}$ M) (µL)	0	30	60	125	250	500	1000
Physiological medium (µL)	1000	970	940	875	750	500	0
$[NO_3^-]$ (10^{-6} M)	-	0.75	1.50	3.13	6.25	12.50	25.00

According to the kit protocol: 20 µL of each standard (concentration range: 0.75 – 25 µM), or sample (in triplicate) is transferred into a black 96-well microplate, 60 µL of assay buffer and 10 µL enzyme cofactor mixture together with 10 µL nitrate reductase mixture are added. The mixture is shaken for 1 min at 500 rpm (Heidolph, VIBRAMAX 110, Schwabach, Germany) and incubated for 60 min at 20-25 °C in the dark. Next, 10 µL of kit DAN reagent (Item N0. 780070) is added, and the mixture is shaken for 1 min at 500 rpm at 20-25 °C before incubation at 37 °C (incubator) in the dark for 10 min. Finally, 20 µL of 2.8 M kit NaOH solution (Item N0. 780068) is added, followed by shaking for 5 min at 500 rpm and analysis with the spectrofluorimeter coupled with FMP micro-well plate reader.

Fluorescence intensity is measured within 10 min.

3.3. Operating conditions for direct spectrofluorometric reader

FP-8300iRM spectrofluorimeter (JASCO, Tokyo, Japan) parameters are fixed as follows:

- Excitation bandwidth: 5 nm
- Emission bandwidth: 5 nm
- Response time: 0.5 s
- Sensitivity: high
- Excitation wavelength: 375 nm
- Emission wavelength: 415 nm

3.4. Calculations

- Nitrite concentration in samples is calculated with nitrite standard curve equation.
- (RSNOs + nitrite) concentration is calculated with RSNOs standard curve equation.
- (Nitrate + nitrite) concentration is calculated with nitrate standard curve equation.
- RSNOs concentration is calculated by subtracting nitrite concentration to (RSNOs + nitrite) concentration.
- Nitrate concentration is calculated by subtracting nitrite concentration to (nitrate + nitrite) concentration.

Typical calibration curves obtained in a validation process are indicated in Table 1.

Table 1. Resulting calibration curves obtained in the different media without subtracting the blank signal ($r^2 \geq 0.99$, $n \geq 3$)

Medium	Fluorescence intensity (AU) of key points (Mean ± SD)		Equation of calibration curve (Mean ± SD)
	Nitrite	GSNO	
	Blank: 433 ± 69	Blank: 378 ± 53	Nitrite: (1810 ± 138)x + 465 ± 73
PBS	0.1 µM: 635 ± 55	0.1 µM: 632 ± 89	Nitrate: -
	2 µM: 4083 ± 209	2 µM: 3591 ± 163	GSNO: (1549 ± 156)x + 498 ± 173
	Blank: 495 ± 76	Blank: 533 ± 18	Nitrite: (1846 ± 143)x + 585 ± 88
Krebs	0.1 µM: 797 ± 52	0.1 µM: 603 ± 126	Nitrate: -
	2 µM: 4373 ± 307	2 µM: 4677 ± 300	GSNO: (2262 ± 34)x – 204 ± 83
	Blank: 468 ± 66	Blank: 380 ± 24	Nitrite: (1527 ± 96)x + 435 ± 89
HBSS	0.1 µM: 572 ± 67	0.1 µM: 592 ± 83	Nitrate: (264 ± 22)x + 1719 ± 116
	2 µM: 3518 ± 230	2 µM: 3436 ± 253	GSNO: (1451 ± 236)x + 399 ± 98
	Blank: 364 ± 46	Blank: 368 ± 41	Nitrite: (891± 55)x + 510 ± 87
Lysis buffer	0.25 µM: 668 ± 99	0.25 µM: 581 ± 40	Nitrate: -
	2 µM :2279 ± 103	2 µM: 1954 ± 96	GSNO: (787 ± 49)x + 337 ± 58

Nitrate in HBSS: blank, 1652 ± 188; 0.75 µM, 1825 ± 152; 25 µM, 8322 ± 512

Measurement of nitrite, nitrate ions and *S*-nitrosothiols using the 2,3-diaminonaphthalene assay by LC coupled with tandem mass spectrometry

1. Principle

The 2,3-diaminonaphthalene (DAN) assay relies upon the reaction between DAN and nitrite ion in acidic medium to yield 2,3-naphthotriazole (NAT) adduct. For *S*-nitrosothiols (RSNOs), mercuric ions are used to cleave the S-NO bond, therefore allowing them to be measured with the DAN assay. Nitrate ions are reduced to nitrite ions by an enzymatic reaction, next they are measured by DAN assay.

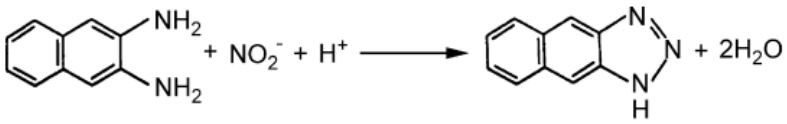

DAN NAT

Figure 1. Reaction between nitrite ion and 2,3-diaminonaphthalene (DAN) producing 2,3-naphthotriazole (NAT).

The resulting NAT adduct is measured by a reversed phase LC method coupled with tandem mass spectrometry to differentiate the NAT adducts labeled either with ^{14}N or ^{15}N, as already reported in Table 1.

Table 1. Literature overview for 2,3-naphthotriazole adduct analysis resulting from derivatization of ^{15}N labeled NO species with 2,3-diaminonaphthalene by using RPLC-MS/MS

Analytes	Columns	Mobile phase components and elution mode	Ion source and mass analyzer (fragmentation modes and transitions)	IS	LOD or LOQ (nM)	Additional informations	Reference
NO_2^- and NO_3^-	C18, 5 µm, 33×2.1 mm	Mixture of methanol (from 49 % to 75 %) and ammonium acetate buffer	ESI; triple quadrupole (CID; m/z: 170 → 115)	$^{15}NO_2^-$	LOQ = 8 / 75 (NO_2^- / NO_3^-, S/N = 10)	2.2 % interference between unlabeled and labeled adducts due to isotopes	(Chao *et al.* 2016)
$^{15}NO_2^-$ and $^{15}NO_3^-$	C18, 5 µm, 150×2.1 mm	Mixture of methanol (from 5 % to 95 %) and ammonium carbonate buffer	ESI; hybrid of triple quadrupole and linear ion trap (CID; m/z: 171 → 115)	No	LLOQ = 1 ($^{15}NO_2^-$ and $^{15}NO_3^-$, S/B = 5)	No interferences between isotopes	(Axton *et al.* 2016)
$^{15}NO_2^-$	C18, 5 µm, 50×2 mm	Mixture of acetonitrile (from 5 % to 95 %) and formic acid	ESI; triple quadrupole (CID; m/z: 171 → 115)	1H-naphth[2,3-d]imidazole	LLOQ = 40 (NO_2^-, S/B = 5) LLOQ = 4 ($^{15}NO_2^-$, S/B = 5)	-	(Shin and Fung 2011)
$^{15}NO_2^-$, $^{15}NO_3^-$ and $RS^{15}NOs$	C18, 3 µm, 150 × 2.1 mm	Mixture of acetonitrile (from 40 % to 80 %) and ammonium acetate buffer	ESI; ion trap (HCD; m/z: 171 → 156)	2-naphthylamine	LOQ = 5 ($^{15}NO_2^-$ and $RS^{15}NOs$, S/B = 4) LOQ = 250 ($^{15}NO_3^-$, S/B = 4)	2 % interference due to isotope ^{13}C	-

$^{15}NO_2^-$: ^{15}N labeled nitrite ion; $^{15}NO_3^-$: ^{15}N labeled nitrate ion; $RS^{15}NOs$: ^{15}N labeled *S*-nitrosothiols; ESI: electrospray ionization; CID: collision induced dissociation; HCD: high collision induced dissociation; IS: internal standard; LOQ: limit of quantification; LLOQ: lower limit of quantification; S/N: signal-over-noise ratio; S/B: signal over blank response ratio; RPLC: reverse phase liquid chromatography.

References:

Chao MR, Shih YM, Hsu YW *et al.* Urinary nitrite/nitrate ratio measured by isotope-dilution LC–MS/MS as a tool to screen for urinary tract infections. *Free Radic Biol Med* 2016;**93**:77–83.

Axton ER, Hardardt EA, Stevens JF. Stable isotope-assisted LC–MS/MS monitoring of glyceryl trinitrate bioactivation in a cell culture model of nitrate tolerance. *J Chromatogr B* 2016;**1019**:156–63.

Shin S, Fung HL. Evaluation of an LC–MS/MS assay for 15N-nitrite for cellular studies of l-arginine action. *J Pharm Biomed Anal* 2011;**56**:1127–31.

2. Reagents

All solutions are prepared with fresh cold ultrapure water (> 18.2 MΩ.cm) and stored at 4°C in the dark for maximum one month unless otherwise specified.

2.1. Physiological media

Conservation time: one week at 4°C after preparation.

Phosphate Buffer Saline (PBS) solution: weigh 8.00 g NaCl, 0.20 g KCl, 2.32 g $Na_2HPO_4 \cdot 12\ H_2O$, 0.20 g KH_2PO_4. Dissolve in 1.0 L of ultrapure water; adjust pH to 7.4 (by using a pH meter) with 10 M NaOH solution**.** Sterilize and aliquot in 35 mL fractions.

Hank's Balanced Salt Solution (HBSS): use commercial HBSS (ref Gibco: 14185-045) made of 8.0 g/L NaCl, 0.4 g/L KCl, 1.0 g/L glucose, 60.0 mg/L KH_2PO_4, 47.5 mg/L Na_2HPO_4, 140.0 mg/L $CaCl_2$, 98.0 mg/L $MgSO_4$ final pH 7.4

2.2. 0.6 M HCl

Transfer 300 mL of 1 M HCl (Mw = 36.46 $g.mol^{-1}$; commercial solution) in a 500 mL volumetric flask and adjust the volume with ultrapure water. Aliquot in 2 mL fractions.

2.3. 0.316 mM DAN

Weigh 5 mg of DAN (Mw = 158 $g.mol^{-1}$; ref Sigma D-2757) in a 100 mL volumetric flask, dissolve and adjust the volume with 0.6 M HCl. Store at 4°C protected from light for 1 month. Aliquot in 1 mL fractions.

2.4. 0.105 mM DAN

Dilute 3-fold of 0.316 mM DAN solution with 0.6 M HCl (500 µL of 0.316 mM DAN + 1000 µL of 0.6 M HCl). Prepare daily.

2.5. 3.17 mM $HgCl_2$

Weigh 86.0 mg of $HgCl_2$ (Mw = 271.5 $g.mol^{-1}$; ref VWR 25384) in a 100 mL volumetric flask, dissolve and adjust the volume with 0.6 M HCl. Store at 4°C protected from light for 1 month. Aliquot in 1 mL fractions.

2.6. 0.105 mM DAN with 1.05 mM $HgCl_2$

Mix 1 volume of 0.316 mM DAN solution, 1 volume of 3.17 mM mercuric chloride solution and 1 volume of 0.6 M HCl. Prepare daily.

2.7. 10^{-4} M NaOH

Transfer 1 mL of 1.0 M NaOH titrated solution (commercial solution; ref Sigma S2770) in a 100 mL volumetric flask, and adjust the volume with ultrapure water to obtain 10^{-2} M NaOH solution. Dilute 100-fold of NaOH solution in ultrapure water by transferring 1 mL of 10^{-2} M NaOH in a 100 mL volumetric flask and adjust the volume with ultrapure water.

2.8. 10^{-2} M sodium nitrite

Weigh 35.0 mg of sodium nitrite ($Na^{15}NO_2$) (Mw = 70 $g.mol^{-1}$; ref Cambridge Isotope Laboratories 68378-96-1, purity: 98 %) in a 50 mL volumetric flask, dissolve and adjust the volume with PBS. Mix the solution gently for one time. Prepare daily.

2.9. 10^{-2} M sodium nitrate

Weigh 43 mg of sodium nitrate ($Na^{15}NO_3$) (Mw = 86 $g.mol^{-1}$; ref Sigma 364606, purity: 98 %) in a 50 mL volumetric flask, dissolve and adjust the volume with PBS.

Prepare daily.

2.10. S-nitrosoglutathione ($GS^{15}NO$)

Solutions are prepared, titrated and stored according to protocol entitled *"Batch synthesis of S-nitrosoglutathione"*, except that $Na^{15}NO_2$ instead of $Na^{14}NO_2$ is used.

2.11. Nitrate/Nitrite fluorometric assay kit

Assay buffer (Item N0. 780022): Transfer the content of the Assay Buffer vial (from the Nitrate/Nitrite fluorometric assay kit Cayman ref. 780051) to a 100 mL volumetric flask, rinse the vial three times with 1 mL of ultrapure water and fill up to 100 mL with ultrapure water. Store at 4 °C for no more than 2 months.

Nitrate Reductase (Item N0. 780010): Reconstitute the content of the vial (from the kit) with 1.2 mL Assay Buffer. Keep on ice during use. Divide into 70 µL aliquots and store at -20 °C for no more than 2 months. Freezing and thawing should be only operated once.

Enzyme Cofactors (Item N0. 780012): Reconstitute the contents of the vial (from the kit) with 1.2 mL Assay Buffer. Keep on ice during use. Divide into 70 µL aliquots and store at -20 °C for no more than 2 months. Freezing and thawing should be only operated once.

2.12. 10^{-2} M CH_3COOH

Dilute 0.285 mL of glacial acetic acid solution (volumetric mass = 1.05 g/mL; Mw = 60.05 $g.mol^{-1}$) with 500 mL with ultrapure water, and filter with 0.45-µm HV membrane (Durapore®).

2.13. Rinsing mobile phase

Mix 500 mL acetonitrile and 500 mL of ultrapure water, filter with 0.45-µm HV membrane (Durapore®).

2.14. 0.02 mM 2-naphthylamine (internal standard, IS)

Weigh 7 mg of 2-naphthylamine (Mw = 143 $g.mol^{-1}$, ref Sigma 91598) in a 10 mL volumetric flask, dissolve and adjust the volume with rinsing mobile phase to

obtain 5 mM 2-naphthylamine solution. Dilute 250-fold 2-naphthylamine solution by transferring 0.04 mL of 5 mM 2-naphthylamine solution in a 10 mL volumetric flask and adjust the volume with rinsing mobile phase. Prepare daily.

2.15. 1.24 mM pure NAT

Weigh 21 mg NAT (Mw = 169.2 $g.mol^{-1}$; ref Chemodex 269-12-5; purity: 98.2 %) in a 100 mL volumetric flask, dissolve in 10 mL of methanol, and adjust the volume with 0.1 M HCl solution. Divide into aliquots of 2 mL and store at -80°C for 1 year.

3. Methods

3.1. Calibration curve for pure NAT determination

The pure NAT daughter solution (2.10^{-6} M): defreeze 1.24 mM NAT solution, sonicate for 1 min, transfer 2 mL to a 200 mL volumetric flask, add 2.96 mL of CH_3CN-H_2O (25/75, V/V), and adjust the volume with ultrapure water to obtain 0.012 mM NAT. Next, transfer 1.65 mL of 0.012 mM NAT to a 10 mL volumetric flask and adjust the volume with ultrapure water.

The dilutions for the calibration curve are prepared in 1.5 mL Eppendorf tubes, as follows:

Tube n°	1	2	3	4	5
Pure NAT daughter solution (2.10^{-6} M) [µL]	50	500 µL of n° 1	200 µL of n° 2	500 µL of n° 3	500 µL of n° 4
Ultrapure water [µL]	950	500	800	500	500
[NAT] (nM)	100	50	10	5	2.5

3.2. Calibration curves and quality controls for $^{15}NO_2^-$ and RS^{15}NO determination

$Na^{15}NO_2$/GS^{15}NO daughter solution n°1 (10^{-4} M): transfer 100 µL of 10^{-2} M $Na^{15}NO_2$/GS^{15}NO solution in a 10 mL volumetric flask, adjust the volume with PBS. Mix gently for one time.

$Na^{15}NO_2$/GS^{15}NO daughter solution n° 2 (2.10^{-6} M): transfer 500 µL of the $Na^{15}NO_2$/GS^{15}NO daughter solution n°1 in a 25 mL volumetric flask, adjust the volume

with sample buffer. Mix gently for one time.

200 nM $Na^{15}NO_2$/$GS^{15}NO$ is prepared by mixing 0.1 mL of 2.10^{-6} M $Na^{15}NO_2$/$GS^{15}NO$ and 0.9 mL of HBSS.

100 nM $Na^{15}NO_2$/$GS^{15}NO$ is prepared by mixing 0.6 mL of 200 nM $Na^{15}NO_2$/$GS^{15}NO$ and 0.6 mL of HBSS.

Lower $Na^{15}NO_2$/$GS^{15}NO$ concentrations are prepared as follows:

Tube n°	1	2	3	4	5	6
$Na^{15}NO_2$/$GS^{15}NO$ solution (100 nM) (µL)	0	50	100	200	500	320
HBSS (µL)	1000	950	900	800	500	0
$[^{15}NO_2^-]$/$[GS^{15}NO]$ (nM)	-	5	10	20	50	100

180 nM $Na^{15}NO_2$/$GS^{15}NO$ as the quality control is prepared by mixing 0.9 mL of 200 nM $Na^{15}NO_2$/$GS^{15}NO$ and 0.1 mL of HBSS.

50 nM $Na^{15}NO_2$/$GS^{15}NO$ as the quality control is prepared by mixing 0.5 mL of 100 nM $Na^{15}NO_2$/$GS^{15}NO$ and 0.5 mL of HBSS.

15 nM $Na^{15}NO_2$/$GS^{15}NO$ as the quality control is prepared by mixing 0.15 mL of 100 nM $Na^{15}NO_2$/$GS^{15}NO$ and 0.85 mL of HBSS.

300 µL of each standard (concentration range: 5 – 200 nM), quality controls, or sample are transferred into a 1.5-mL Eppendorf tube, and 60 µL of 0.105 mM DAN solution are added. The mixture is shaken for 0.1 min by vortex at 20-25 °C before incubation at 37 °C in the dark for 10 min. Next, 36 µL of 1 M and 4 µL of 10^{-4} M NaOH are added. The mixture is shaken for 0.1 min by vortex at 20-25 °C, followed by freezing at -80 °C. 10 µL of 0.02 mM IS are added before analysis with LC-MS/MS.

For $RS^{15}NO$ or ($RS^{15}NO$ + $^{15}NO_2^-$) measurement, DAN reagent has to be replaced by DAN-$HgCl_2$ reagent.

3.3. Calibration curve for $^{15}NO_3^-$ determination

$Na^{15}NO_3$ daughter solution n°1 (10^{-4} M): transfer 100 µL of 10^{-2} M $Na^{15}NO_3$ solution in a 10 mL volumetric flask. Adjust the volume with PBS.

5000 nM $Na^{15}NO_3$ is prepared by transferring 0.5 mL of 10^{-4} M $Na^{15}NO_3$ in a 10 mL volumetric flask. Adjust the volume with HBSS;

2500 nM $Na^{15}NO_3$ is prepared by mixing 0.6 mL of 5000 nM $Na^{15}NO_3$ and 0.6 mL of HBSS.

Lower $Na^{15}NO_3$ concentrations are prepared as follows:

Tube n°	1	2	3	4	5
$Na^{15}NO_3$ solution (2500 nM) (µL)	0	100	200	500	400
HBSS (µL)	1000	900	800	500	0
$[^{15}NO_3^-]$ (nM)	-	250	500	1250	2500

4000 nM $Na^{15}NO_3$ as the quality control is prepared by mixing 0.8 mL of 5000 nM $Na^{15}NO_3$ and 0.2 mL of HBSS.

2500 nM $Na^{15}NO_3$ as the quality control is prepared by mixing 0.5 mL of 5000 nM $Na^{15}NO_3$ and 0.5 mL of HBSS.

300 nM $Na^{15}NO_3$ as the quality control is prepared by mixing 0.6 mL of 500 nM $Na^{15}NO_3$ and 0.4 mL of HBSS.

According to the kit protocol: 40 µL of each standard (concentration range: 250 – 5000 nM), quality controls, or sample are transferred into a 1.5-mL Eppendorf tube, 120 µL of assay buffer and 20 µL enzyme cofactor mixture together with 20 µL nitrate reductase mixture are added. The mixture is shaken for 0.1 min by vortex and incubated for 60 min at 20-25 °C in the dark. Next, 40 µL of 0.105 mM DAN solution is added. The mixture is shaken for 0.1 min by vortex at 20-25 °C before incubation at 37 °C in the dark for 10 min. Then, 24 µL of 1 M and 3 µL of 10^{-4} M NaOH are added. The mixture is shaken for 0.1 min by vortex at 20-25 °C, followed by freezing at -80 °C.

7 µL of 0.02 mM IS are added before analysis with LC-MS/MS.

3.4. Operating conditions for LC-MS/MS

All reversed phase columns used for the present method have to exhibit a number of theoretical plates per meter equal to at least 15,000 for the anthracene peak.

The operating conditions for LC (DIONEX, Ultimate 3000) are as follows:

- Column: Acclaim 120 C18 3 µm, 2.1 X 150 mm (Thermo Scientific).
- Gradient mobile phase: start at 40% B for 10 min (equilibrating the column) + 2 min; change linearly to 80% B over 3.5 min; hold at 80% B for 2.5 min (mobile phase A: 10^{-2} M acetic acid; mobile phase B: CH_3CN)
- Flow rate: 0.2 $mL.min^{-1}$; column temperature: 25 °C; resulting back pressure: 105 bars for 40% B, 65 bars for 80 % B.
- Loop size: 20 µL
- Software: Chromeleon (running time: 7 min; peak range: 5.3 min – 5.5 min)
- Rinsing conditions: use CH_3CN-H_2O (50/50, V/V) at a flow rate of 0.2 $mL.min^{-1}$ and at 25 °C for 10 min.

The operating conditions for MS/MS (LTQ Velos Pro, Thermo Fisher Scientific, San José, CA, USA) are as follows:

- Ion source: ESI (source voltage: 5.00 kV; source current: 3.5 µA; source temperature: 280 °C; sheath / aux / sweep gas (N_2) flow rate: 10.00 / 5.00 / 0.05 arb; capillary temperature: 250 °C）
- Analyzer: dual-pressure linear ion trap (monitor transition: m/z 171 → 156 for ^{15}N-NAT, m/z 170 →156 for ^{14}N-NAT)
- Software: Thermo Tune Plus, (MRM; Act type: HCD; collision energy: 50 %; Act Q: 0.25; Act time: 10 ms)
- A valve between LC and MS is used to throw sample for the first 3 min into waste and transfer sample for the next 4.5 min into detector.

3.5. Calculations

- Nitrite concentration is calculated with nitrite standard calibration curve equation.
- (RSNOs + nitrite) concentration is calculated with RSNOs standard calibration curve equation.
- (Nitrate + nitrite) concentration is calculated with nitrate standard calibration curve equation.
- RSNOs concentration is calculated by subtracting nitrite concentration to (RSNOs + nitrite) concentration.
- Nitrate concentration is calculated by subtracting nitrite concentration to (nitrate + nitrite) concentration.

The signal value obtained in the blank is subtracted to all signal values obtained for standards.

Typical validation data are shown in Table 2. They are checked daily by comparing with quality control.

Table 2. Inter-day and intra-day variability of quality control samples for ^{15}N-nitrite *S*-nitrosoglutathione (GS^{15}NO) and ^{15}N-nitrate analysis with IS. Accuracy was determined as the deviation (%) of calculated concentrations from the nominal concentrations. Precision was determined as the relative standard deviation (RSD) of the 6 measurements.

NO species	Concentration (nM)	Intra-day		Inter-day	
		Accuracy (%)	Precision (%)	Accuracy (%)	Precision (%)
^{15}N-nitrite	15	105.2 ± 6.4	6.1	104.7 ± 7.0	6.7
	50	99.0 ± 6.8	6.9	94.7 ± 2.8	3.0
	180	98.6 ± 5.3	5.4	102.7 ± 7.3	7.1
GS^{15}NO	15	98.1 ± 13.1	13.4	93.3 ± 11.8	12.6
	50	99.1 ± 10.9	11.0	96.0 ± 7.4	7.7
	180	100.0 ± 12.7	12.7	101.5 ± 11.4	11.3
^{15}N-nitrate	300	105.2 ± 6.4	6.1	104.7 ± 7.0	6.8
	2500	99.0 ± 6.8	6.9	94.7 ± 2.8	8.7
	4000	98.6 ± 5.3	5.4	102.7 ± 7.3	8.1

Measurement of *S*-nitrosothiols in the rat intestine with the 2,3-diaminonaphthalene assay by LC coupled with fluorescence detection

1. Principle

The present analytical method is aimed at being applied to experiments on rat intestine isolated. *S*-nitrosothiols (RSNOs) were measured by the 2,3-diaminonaphthalene/mercuric ions (DAN/Hg^{2+}) assay; the derivatization step was directly operated on smashed tissue as previously described (Shin and Fung 2011)(Damacena-Angelis *et al.* 2016), and resulting naphthotriazole (NAT) adduct extracted with acetonitrile was analyzed by reversed phase LC coupled with spectrofluorimetric detection (LC/FL). The method should be further applied to other tissues and organs by using LC coupled with tandem mass spectrometry (LC-MS/MS) after GSNO labeling with ^{15}N.

References:

Shin S, Fung HL. Evaluation of an LC–MS/MS assay for 15N-nitrite for cellular studies of l-arginine action. *J Pharm Biomed Anal* 2011;**56**:1127–31.

Damacena-Angelis C, Oliveira-Paula GH, Pinheiro LC *et al.* Nitrate decreases xanthine oxidoreductase-mediated nitrite reductase activity and attenuates vascular and blood pressure responses to nitrite. *Redox Biol* 2017;**12**:291–9.

2. Reagents

All solutions are prepared with fresh cold ultrapure water (> 18.2 MΩ.cm) and stored at 4°C in the dark for maximum one month unless otherwise specified.

2.1. Physiological media

Conservation time: one week at 4°C after preparation.

Phosphate Buffer Saline (PBS) solution: weigh 8.00 g NaCl, 0.20 g KCl, 2.32 g $Na_2HPO_4 \cdot 12\ H_2O$, 0.20 g KH_2PO_4. Dissolve in 1.0 L of ultrapure water; adjust pH to 7.4 (by using a pH meter) with 10 M NaOH solution**.**

0.1 M Tris buffer (pH = 7.4): weigh 1.576 g of Trizma-HCl (Mw = 158 $g.mol^{-1}$, ref Sigma T040) and dissolve in 100 mL of ultrapure water; adjust the pH to 7.40 ± 0.05 with 10 M NaOH solution.

2.2. 0.6 M HCl

Transfer 300 mL of 1 M HCl (Mw = 36.46 $g.mol^{-1}$; Commercial solution) in a 500 mL volumetric flask and complete with ultrapure water.

2.3. 0.316 mM DAN

Weigh 5 mg of DAN (Mw = 158 $g.mol^{-1}$; ref Sigma D-2757) in a 100 mL volumetric flask, dissolve and adjust the volume with 0.6 M HCl. Store at 4°C protected from light for 1 month.

2.4. 0.105 mM DAN

Dilute 3-fold of 0.316 mM DAN solution with 0.6 M HCl (500 µL of 0.316 mM DAN + 1000 µL of 0.6 M HCl). Prepare daily.

2.5. 3.17 mM $HgCl_2$

Weigh 86.0 mg of $HgCl_2$ (Mw = 271.5 $g.mol^{-1}$; ref VWR 25384) in a 100 mL volumetric flask, dissolve and adjust the volume with 0.6 M HCl. Store at 4°C protected from light for 1 month.

2.6. 0.105 mM DAN with 1.05 mM $HgCl_2$

Mix 1 volume of 0.316 mM DAN solution, 1 volume of 3.17 mM mercuric chloride solution and 1 volume of 0.6 M HCl. Prepare daily.

2.7. 10 M NaOH

Weigh 10 g of NaOH (Mw = 40 $g.mol^{-1}$, ref Prolabo- 28252.293) and dissolve in 25 mL of ultrapure water, use ice to cool the mixture.

2.8. 10^{-2} M sodium nitrite

Weigh 34.5 mg of sodium nitrite ($NaNO_2$) (Mw = 69 $g.mol^{-1}$; ref Merck 6549) in a 50 mL volumetric flask, dissolve and adjust the volume with PBS. Mix the solution gently for one time. Prepare daily.

2.9. *S*-nitrosoglutathione (GSNO)

Solutions are prepared, titrated and stored according to protocol entitled *"Batch synthesis of S-nitrosoglutathione"*.

2.10. 1.24 mM pure NAT

Weigh 21 mg NAT (Mw = 169.2 $g.mol^{-1}$; ref Chemodex 269-12-5; purity: 98.2 %) in a 100 mL volumetric flask, dissolve in 10 mL of methanol and adjust the volume with 0.1 M HCl. Divide into aliquots of 2 mL and store at -80°C for 1 year.

2.11. Mobile phase $CH_3CN–CH_3COONH_4$ (10^{-2} M, pH = 7.2) (28/72, V/V)

Dilute 0.57 mL of glacial acetic acid solution (volumetric mass = 1.05 g/mL; Mw = 60.05 $g.mol^{-1}$; ref Sigma 64-19-7) with 1 L of ultrapure water, and adjust the pH to 7.2 with 10 times diluted ammonia solution (ca. 25% NH_3; volumetric mass = 0.91 g/mL; Mw = 17.03 $g.mol^{-1}$; ref Sigma 1336-21-6); mix 280 mL acetonitrile and 720 mL ammonium acetate solution and filter with 0.45-µm HV membrane (Durapore®).

3. Methods

3.1. Calibration curves for NO_2^- and GSNO determination

50 µM $NaNO_2$ or GSNO solutions are prepared by transferring 50 µL of 10^{-2} M $NaNO_2$ or GSNO in a 10 mL volumetric flask. Adjust the volume with Tris buffer. Further dilutions for the calibration curve are prepared in 1.5 mL Eppendorf tubes (mix gently each tube for one time), as follows:

Tube n°	1	2	3	4	5	6
$NaNO_2$/GSNO solution (50 µM) (µL)	0	125	250	500	750	1000
Tris buffer (µL)	1000	875	750	500	250	0
$[NO_2^-]$/[GSNO] (µM)	-	6.25	12.5	25	37.5	50

Remove Wistar rat intestine (length: around 2 cm, weight: 100 ± 5 mg) after sacrifice (anesthetized with sodium pentobarbitone (60 $mg.kg^{-1}$, intraperitoneal

injection, Sanofi Santé Nutrition Animale, Libourne, France); administrated with heparin (1000 IU.kg^{-1} heparin Choay, penis vein and sacrificed by exsanguination)). Rinse quickly with 1 mL cold PBS for 2 times, use tissue paper to dry the intestine each time; freeze the rat intestine with liquid N_2. Smash the intestine in liquid N_2 with a pestle in a mortar, weigh 20 ± 2 mg intestine powder in a 2-mL Eppendorf tube. Spike the powder with 20 µL of $NaNO_2$ or GSNO standard solutions. Add 600 µL DAN or DAN/Hg^{2+} in 0.6 M HCl, followed by vortex for 30 s. Incubate the mixture in the dark in an incubator (37 °C, Jouan IG150) for 10 min under rotation (80 rpm, MX-RD-E Classic Rotator, Labtech, Cernusco, Italy), add 40 µL of 10 M NaOH, mix by vortex for 10 s, add 600 µL acetonitrile, mix by vortex for 30 s, and centrifuge at 18,000 x *g* for 15 min at 4 °C (VWR Hitachi, CT15RE); collect the supernatant and store at 4 °C for a maximum period of 24 h before measurement by LC-FL.

3.2. Quantification of RSNOs after incubation of isolated rat intestine with GSNO

Rinse the isolated rat intestine (100 ± 5 mg) quickly with 1 mL of cold PBS for 2 times, use tissue paper to dry the intestine each time; incubate intestine with 5 mL of 100 µM GSNO in a 15-mL tube at 37°C for 60 min under rotation (35 rpm, CAT Roller RM5-40, Dordrecht, Netherlands), rinse intestine quickly with 5 mL of cold PBS for 3 times. Then freeze intestine and quantify NaNO2/RSNOs as described above.

For RSNOs or (RSNOs + nitrite) measurement, DAN reagent has to be replaced by DAN-$HgCl_2$ reagent.

3.3. Operating conditions for LC-FL

All reversed phase columns used for the present method have to exhibit a number of theoretical plates per meter equal to at least 15,000 for the anthracene peak.

The operating conditions are as follows:

- Column: ZORBAX SB-Aq C18 4.6 X 150 mm, 3.5 µm (Agilent) + precolumn (NUCLEODUR® EC4/3 C-18 Htec, 5 µm)
- Mobile phase: CH_3CN–CH_3COONH_4 (10^{-2} M, pH = 7.2) (28:72, V/V)
- Flow rate: 0.8 $mL.min^{-1}$; column temperature: 40°C; resulting back pressure: 95-105 bars.
- Auto-sampler with cooling device set at 4 °C (loop size: 20 µL)
- Spectrofluorometric detection: λ_{exc} = 375 nm and λ_{em} = 415 nm; sensitivity: low (RF-10A XL, Shimadzu, Kyoto, Japan) + software: LC Solution, (running time: 15 min; peak range: 9 – 11 min)
- Rinsing conditions: use CH_3CN-H_2O (50:50, V/V) at a flow rate of 0.8 $mL.min^{-1}$ and at 40 °C for 10 min.

3.4. Calculations

- Nitrite concentration is calculated with nitrite standard calibration curve equation.
- (RSNOs + nitrite) concentration is calculated with RSNOs standard curve equation.
- RSNOs concentration is calculated by subtracting nitrite concentration to (RSNOs + nitrite) concentration.

Retention times of the DAN excess and NAT adduct are within 8 and 10 min, respectively. Typical chromatograms are shown in Figure 1.

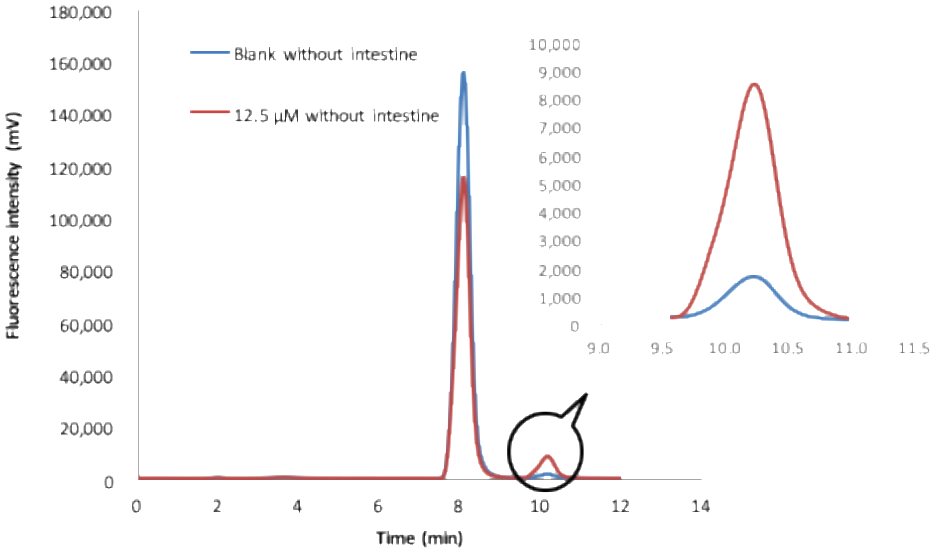

(A)

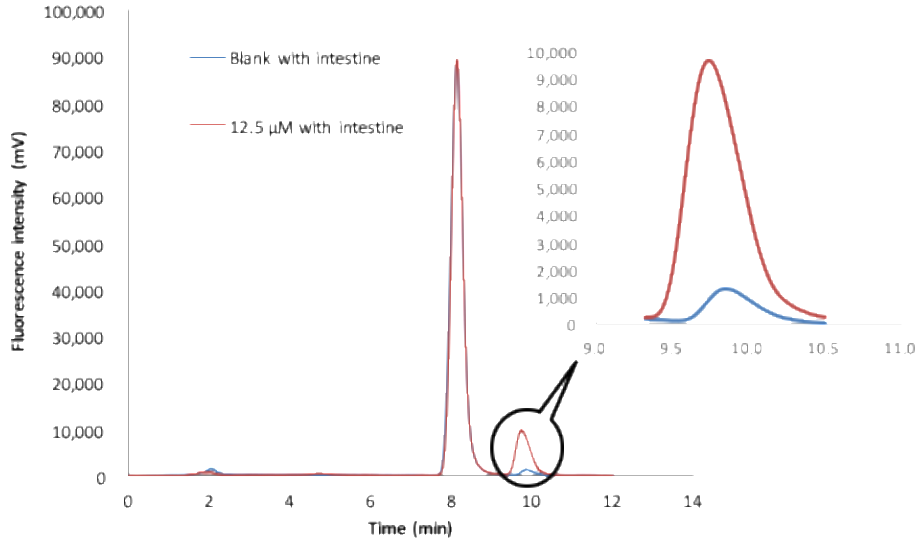

(B)

Figure 1. Chromatograms of NAT resulting from derivatization of 12.5 µM GSNO in the (A) absence and (B) presence of rat intestine by LC-spectrofluorimetry at λ_{exc} = 375 nm and λ_{em} = 415 nm.

Typical validation data are shown in Table 1.

Table 1. Validation data for GSNO quantification in the rat intestine

NO species	Linearity (6.25 – 50 µM, n ≥ 3) Slope (a) ; intercept (b) ; determination coefficient (r^2)	Concentration (µM)	Accuracy (%)	Precision (%) (n ≥ 3) Intra-day	Inter-day
GSNO	a : 15308 ± 1160 b : -51365 ± 56834 r^2 : 0.996 ± 0.005	6.25	113.3	0.7	10.2
		12.5	97.0	8.2	11.9
		25	98.6	6.4	5.7
		37.5	104.0	4.6	4.3
		50	100.3	4.5	5.6
Nitrite	a : 16572 ± 218 b : -40458 ± 29394 r^2 : 0.995 ± 0.005	6.25	99.9	2.9	11.3
		12.5	100.2	0.4	2.0
		25	112.9	3.8	7.9
		37.5	101.8	2.1	7.9
		50	98.4	6.5	4.7

A 50 µM pure NAT solution has been used to check extraction efficiency of the protocol described above, the recovery is 88 % according to peak area ratio of pure NAT with and without intestine (n = 1).

Recoveries when compared to GSNO standard solutions derivatized in the absence of intestine (injected concentration range: 6.25-50 µM): *ca.* 85%

Intestinal permeability studies of *S*-nitrosothiols using a Caco-2 cell monolayer model

1. Principle

The Caco-2 cell line is a continuous cell of heterogeneous human epithelial colorectal adenocarcinoma. Although derived from a colon (large intestine) carcinoma, when cultured under specific conditions, the cells become differentiated and polarized so that their properties (phenotype, morphology and functions) are similar to those of the enterocytes lining the small intestine. When cultured on a cell culture insert filter (*e.g.* Transwell®; Figure 1), the cells differentiate to form a polarized epithelial cell monolayer that provides a physical and biochemical barrier to the passage of ions and small molecules. The Caco-2 monolayer is widely used in the pharmaceutical industry as an *in vitro* model to predict the absorption of orally administered drugs (Wu *et al.* 2016) (Bilat *et al.* 2017).

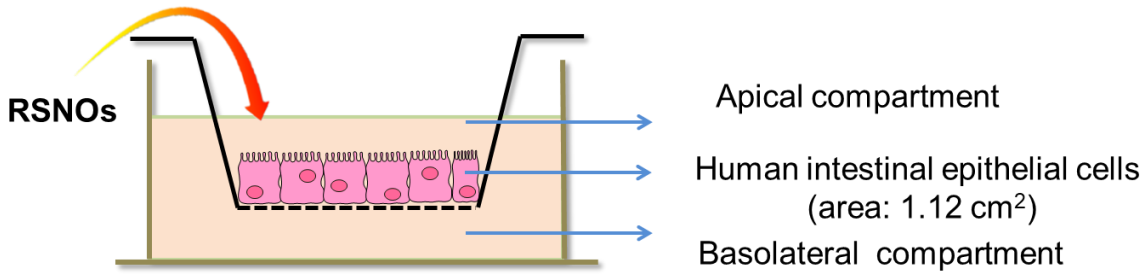

Figure 1. Representation of Caco-2 cells in a Transwell® plate and its application for permeability evaluation of *S*-nitrosothiols (RSNOs).

References:

Wu W, Perrin-Sarrado C, Ming H *et al.* Polymer nanocomposites enhance S-nitrosoglutathione intestinal absorption and promote the formation of releasable nitric oxide stores in rat aorta. *Nanomedicine-Nanotechnol Biol Med* 2016;**12**:1795–803.

Bilat PA, Roger E, Faure S *et al.* Models for drug absorbtion from the small intestine: where are we and where are we going? *Drug Discov Today* 2017;**22**:761–75.

2. Reagents

All solutions are prepared with fresh cold ultrapure water (> 18.2 MΩ.cm) and stored at 4°C in the dark for maximum one month unless otherwise specified.

2.1. Physiological medium

Conservation time: one week at 4°C after preparation.

Hank's Balanced Salt Solution (HBSS): use commercial HBSS (ref Gibco: 14065-056) made of 8.0 g/L NaCl, 0.4 g/L KCl, 1.0 g/L glucose, 60.0 mg/L KH_2PO_4, 47.5 mg/L Na_2HPO_4, 140.0 mg/L $CaCl_2$, 98.0 mg/L $MgSO_4$ final pH 7.4

Hank's Balanced Salt Solution (HBSS) without Ca^{2+}/Mg^{2+}: use commercial HBSS (ref Gibco: 14185-045) made of 8.0 g/L NaCl, 0.4 g/L KCl, 1.0 g/L glucose, 60.0 mg/L KH_2PO_4, 47.5 mg/L Na_2HPO_4, final pH 7.4

2.2. 5 µM sodium fluorescein

Weigh 18.8 mg of sodium fluorescein (Mw = 376 $g.mol^{-1}$; ref Sigma F-1628) and dissolve with 1 mL ultrapure water to obtain 50 mM sodium fluorescein. Next, dilute 100-fold to obtain 500 µM (10 µL of 50 mM sodium fluorescein + 990 µL of HBSS). Finally, dilute 100-fold to obtain 5 µM (100 µL of 500 µM sodium fluorescein + 9900 µL of HBSS).

3. Methods

3.1. Preparation of cells

Seed Caco-2 cells (ATCC number: HTB-37) on the insert (pore diameter: 0.4 µm) of a 12-well transwell plate (Transwell®, Corning, USA) at a density of 2.10^5 cells/mL and 0.5 mL/well in the apical compartment. Fill the basolateral compartment with 1.5 mL of cell culture medium (Eagle's Minimum Essential Medium (EMEM) supplemented with 10 % (v/v) fetal bovine serum, 1 % (v/v) of a mixture of 10,000 U of Penicillin and 10 $mg.mL^{-1}$ streptomycin and 1 % (v/v) of a 100 mM sodium pyruvate solution, 1 % (v/v) of non-essential amino acids). Cells are cultivated at 37 °C under O_2-CO_2 (95:5, V/V) mixture supplying in a humidified incubator. Change medium every two days in the first week, then change medium every day to inhibit the

differentiation of Caco-2 cells into polarized ones till the 15th day. Control the monolayer confluency by transepithelial electrical resistance (TEER) measurement with a Millicell®-Electrical Resistance system (Millipore, USA) (on the 15th day, a TEER value ≥ 500 Ω.cm^2 indicates a confluent monolayer). Usually, the differentiation phase is achieved after 14-18 days of incubation, when TEER values reach 730 ± 53 Ω.cm².

3.2. Validation of the model using reference molecules

Furosemide and propranolol are fluorescent molecules. Furosemide is known as a low permeability molecule through intestinal epithelium layer and propranolol as a high permeability one. LC coupled with spectrofluorimetric detection is used to quantify these molecules. See protocol entitled *"dosage du furosémide et du propranolol par CLHP à polarité de phases inversée couplée à une détection spectrofluorimétrique "* (In lab EA 3452).

	Apparent permeability coefficient (P_{app}) (10^{-6} cm.s^{-1})
Furosemide	0.08 – 0.11
Propranolol	3.30 – 41.90

3.3. Treatment of cells

Replace the culture medium in basolateral compartment with 1.5 mL of HBSS, and the one in apical compartment with 0.5 mL of HBSS. Then incubate at 37 °C for 15 to 20 min on an orbital shaker at 500 rpm, followed by TEER measurement.

Next, replace the HBSS in basolateral compartment with 1.5 mL of fresh one and the solution in apical compartment with 0.5 mL of RSNOs solution prepared in HBSS (*e.g.* 50 µM) or HBSS or HBSS without Ca^{2+}/Mg^{2+} (tight junctions opening, as a positive control of barrier integrity). Incubate cells at 37 °C for 1 or 4 h on a orbital shaker at 500 rpm, before harvesting the full volume of HBSS in both compartments.

Finally, rinse the cells by the addition of 0.5 mL of fresh HBSS in apical compartment and 1.5 mL of fresh one in basolateral compartment, followed by TEER measurement and sodium fluorescein (5 μM) permeability assessment to evaluate monolayer integrity. Briefly, replace the medium in basolateral compartment with 1.5 mL of HBSS and the one in apical compartment with 0.5 mL of sodium fluorescein or HBSS or HBSS without Ca^{2+}/Mg^{2+} after TEER measurement; incubate at 37 °C for 2 h, measure the fluorescence intensity of both compartments at λ_{exc} = 460 nm, λ_{em} = 515 nm (Fluorimetric Detector, Biotek) (a permeability value of sodium fluorescein ≤ 20 % indicates a confluent monolayer (Wu et al. 2016), calculated according to a calibration curve with stadards of 0.05, 0.0625, 0.125, 0.25, 0.5, 5 μM).

3.4. Quantification of nitrite, nitrate ions and RSNOs in both compartments

See protocol entitled *"Measurement of nitrite, nitrate ions and S-nitrosothiols using the 2,3-diaminonaphthalene assay by spectrofluorometry"* and *"Measurement of nitrite, nitrate ions and S-nitrosothiols using the 2,3-diaminonaphthalene assay by LC coupled with tandem mass spectrometry"*.

3.5. Calculations

Calculate the cumulative amounts of RSNOs permeated through the Caco-2 monolayer by the concentrations measured in the basolateral compartment. Calculate the P_{app} values using the following equation:

$$P_{app} = \frac{dQ}{dt} \times \frac{1}{A \times C_0}$$

dQ/dt (mol·s^{-1}) refers to the quantity of permeated NO related species (dQ) in the basolateral compartment at the time of quantification (dt), A refers to membrane diffusion area (1.12 cm^2), and C_0 refers to the initial concentration of RSNOs in the apical compartment (from 10^{-5} to 10^{-4} M).

Permeability studies of *S*-nitrosothiols in isolated rat intestine using Ussing chamber

1. Principle

The Ussing chamber was invented by the Danish zoologist and physiologist Hans Henriksen Ussing in 1946. The basic design of a classical Ussing chamber is illustrated in Figure 1. The membrane (cells, tissues or synthetic one) is situated vertically in the middle of the model, and separates it into two compartments (equal volume): a donor compartment (also referred to the apical, mucosal or luminal-side membrane) and an acceptor compartment (also referred to the basolateral, serosal, nutrient, or blood-side membrane). The Ussing chamber is an apparatus for measuring the transport of ions, nutrients or drugs across various epithelial cells, tissues or synthetic membrane. Thus, it is useful to explore drug absorption process and barrier functions of living tissues. It is widely used in the pharmaceutical industry as an *ex vivo* model to predict the absorption of orally administered drugs (Bilat *et al.* 2017)(Neirinckx *et al.* 2011). We presently use it for studying the permeability of *S*-nitrosothiols (RSNOs) by quantifying RSNOs and their metabolites (nitrite and nitrate ions).

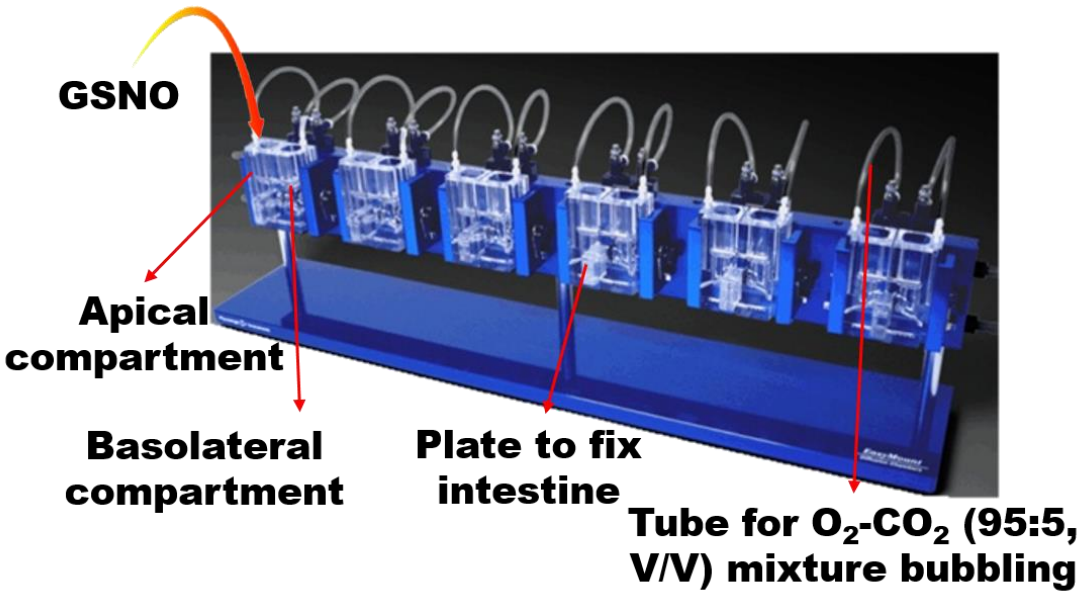

Figure 1. Scheme of 6 Ussing chambers for studying drug permeability, *e.g.* *S*-nitrosothiols (RSNOs)

References:

Bilat PA, Roger E, Faure S *et al.* Models for drug absorbtion from the small intestine: where are we and where are we going? *Drug Discov Today* 2017;**22**:761–75.

Neirinckx E, Vervaet C, Michiels J *et al.* Feasibility of the Ussing chamber technique for the determination of in vitro jejunal permeability of passively absorbed compounds in different animal species. *J Vet Pharmacol Ther* 2011;**34**:290–7.

2. Reagents

All solutions are prepared with fresh cold ultrapure water (> 18.2 MΩ.cm) and stored at 4°C in the dark for maximum one month unless otherwise specified.

2.1. Physiological medium

Conservation time: to prepare daily.

Krebs solution: weigh 6.90 g NaCl, 0.35 g KCl, 1.80 g glucose, 0.16 g KH_2PO_4, 2.02 g $NaHCO_3$, 0.14 g $MgSO_4$, 0.35 g $CaCl_2 \cdot 2\ H_2O$. Dissolve in 1.0 L of ultrapure water. Equilibrate at 37 ^oC in a water bath for 30 min with an O_2/CO_2 (95 %/5 %) mixture bubbling before to adjust pH to 7.4 (by using a pH meter) with 1.0 M HCl. Solution should be kept at 37°C during the experiment, with continuous bubbling.

3. Methods

3.1. Preparation of rat intestine

Set the Ussing chamber at 37 ^oC with an O_2-CO_2 (95:5, V/V) mixture bubbling. Harvest Wistar rat intestine (ileum) after sacrifice (anesthetized with sodium pentobarbitone (60 $mg.kg^{-1}$, intraperitoneal injection, Sanofi Santé Nutrition Animale, Libourne, France)). Remove the fat tissue along the mesenteric attachment and open the intestine longitudinally. Rinse segments from the distal portion of the ileum with pre-heated Krebs solution. Mount the intestine (length: around 2 cm, weight: around 100 mg) as a flat sheet on pins of the tissue holding device, followed by fitting the device to the Ussing chamber (EM-CSYS-6, Physiologic Instruments Inc., CA, USA) with the help of screws. Add 2.5 mL of Krebs solution in both donor and acceptor compartments and equilibrate for 10 min. Measure the transepithelial electrical

resistance (TEER) value with electrodes (Electrode kit for Ussing chamber, WPI). Discard tissue samples that have a TEER value less than 30 Ω.cm^2 directly after having placed the intestine.

Replace the Krebs solution in acceptor compartment with 2.5 mL of fresh one and the solution in donor compartment with 2.5 mL of RSNOs solution (*e.g.* 100 µM) or Krebs solution. Next, incubate intestine at 37 °C with bubbling for maximum 2 h, harvest 0.25 mL of the medium from acceptor compartment at regular time intervals and replace it with pre-heated buffer. Measure also TEER values at these same times.

3.2. Quantification of nitrite, nitrate ions and RSNOs in both compartments

See protocol entitled *"Measurement of nitrite, nitrate ions and S-nitrosothiols using the 2,3-diaminonaphthalene assay by spectrofluorometry"* and *"Measurement of nitrite, nitrate ions and S-nitrosothiols using the 2,3-diaminonaphthalene assay by LC coupled with tandem mass spectrometry"*.

3.3. Quantification of nitrite ion and RSNOs in the rat intestine

See protocol entitled *"Measurement of S-nitrosothiols in the rat intestine with the 2,3-diaminonaphthalene assay by LC coupled with fluorescence detection"*.

3.4. Quantification of proteins in the rat intestine

Quantify intestinal proteins with BCA assay, see procedure 3.2 from protocol entitled *"Western blot for protein disulfide isomerase identification in tissues"*.

3.5. Calculations

Calculate the cumulative amounts of RSNOs permeated through the intestine by the concentrations measured in the acceptor compartment. Calculate the apparent permeability coefficient (P_{app}) values using the following equation:

$$P_{app} = \frac{dQ}{dt} \times \frac{1}{A \times C_0}$$

dQ/dt (mol·s^{-1}) refers to the quantity of permeated NO related species (dQ) in the acceptor compartment at the time of quantification (dt), A refers to membrane diffusion

area (0.25 cm^2), and C_0 refers to the initial concentration of RSNOs in the donor compartment.

Measurement of *γ*-glutamyltransferase activity by spectrophotocolorimetry

1. Principle

γ-Glutamyltransferase (GGT, EC 2.3.2.2) is a membrane-bound protein that catalyzes the transfer of γ-glutamyl moieties to acceptor molecules such as amino acids or peptides. As GGT can catalyze the transfer of a *γ*-glutamyl group from the colorless substrate of L-γ-glutamyl-3-carboxy-4-nitroanilide, to the acceptor of glycylglycine with production of the colored product of 3-carboxy-4-nitroanilide, the enzyme activity is related to the absorbance measured at 405 nm, with molar absorbance (ε) equal to 9,500 $L.mol^{-1}.cm^{-1}$ (Schiele *et al.* 1981). The reaction is shown below:

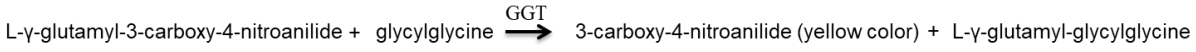

Reference:

Schiele F, Artur Y, Bagrel D, Petitclerc C, Siest G. Measurement of Plasma Gamma-Glutamyltransferase in Clinical-Chemistry - Kinetic Basis and Standardization Propositions. *Clin Chim Acta* 1981;**112**:187–95.

2. Reagents

All solutions are prepared with fresh cold ultrapure water (> 18.2 MΩ.cm) and stored at 4°C in the dark for maximum one month unless otherwise specified.

2.1. Physiological media

Conservation time: one week at 4°C after preparation.

0.1 M Tris buffer (pH = 7.4): weigh 1.576 g of Trizma-HCl (Mw = 158 $g.mol^{-1}$, ref Sigma T040), dissolve with 100 mL of ultrapure water; and adjust the pH to 7.40 ± 0.05 with 10 M NaOH solution.

0.1 M Phosphate buffer (pH = 7.4): Weigh 1.36 g of KH_2PO_4 (Mw = 136.09 $g.mol^{-1}$, ref Merck 646A148973) and 0.074 g of $EDTANa_2{\cdot}2H_2O$ (Mw = 372.24 $g.mol^{-1}$), dissolve with 100 mL of ultrapure water, and adjust the pH to 7.40 ± 0.05 with 10 M NaOH.

2.2. Substrate solution

Weigh 6.6 mg of L-γ-glutamyl-3-carboxy-4-nitroanilide (Mw = 328.3 $g.mol^{-1}$, ref Sigma AC98), 40.6 mg of $MgCl_2 \cdot 6H_2O$ (Mw = 203.31 $g.mol^{-1}$, ref Sigma M9272) and 52.8 mg of glycylglycine (Mw = 132.1 $g.mol^{-1}$, ref Sigma G1002), dissolve with 20 mL of Tris buffer. Protect solution from light. The same solution is prepared without adding the substrate for the blank.

2.3. *γ*-glutamyltransferase (GGT)

Weigh 1 mg of GGT (26 UI*/mL, bovine kidney, EC 2.3.2.2, ref G8040), dissolve with 1 mL of phosphate buffer, divide the solution in aliquots of 100 µL (1.1 UI/mL) and store them at -20°C for maximum five months (determine the GGT concentration by the BCA Protein Assay kit (Pierce™ BCA Protein Assay Kit, ref Thermo Fisher 23225)).

2.5. 100 mM Serine-borate complex (SBC)

Weigh 0.503 g of sodium borate (Mw = 201.372 $g.mol^{-1}$, ref Sigma S4500) and 0.2665 g of serine (Mw = 105.09, ref Sigma G100), dissolve with 25 mL of Tris buffer, adjust the pH to 7.40 ± 0.05 with 10 M NaOH.

2.6. Solution with substrate and enzyme inhibitor

Prepare 20 mM SBC by mixing 5 mL of 100 mM SBC and 20 mL of 100 mM Tris buffer. Weigh and dissolve 6.6 mg of L-γ-glutamyl-3-carboxy-4-nitroanilide (Mw = 328.3 $g.mol^{-1}$, ref Sigma AC98) with 20 mL of 20 mM SBC solution. Protect solution from light. Prepare daily.

3. Methods

3.1. Measurement of purified GGT activity

Equilibrate the temperature of the incubator at 37°C, transfer 5 mL of solution with substrate to a 1.5-mL Eppendorf tube, and incubate at 37°C in the dark for 5 min. Next, dilute GGT (1.1 UI/mL) 1:10 in Tris buffer, and add 25 µL of GGT diluted solution to the EP tube above. The blank with substrate is prepared in the same way but without adding GGT. Read absorbance at 405 nm at different time shown in Table 1.

Table 1. Measurement of purified GGT activity at different times (n = 3)

Incubation time (min)	0	10	20	30
Group 1 (blank)	Substrate without GGT			
Group 2	Substrate with GGT			

3.2. Measurement of GGT activity in rat intestine

Remove Wistar rat intestine (length around 2 cm, weight around 100 mg) after sacrifice (anesthetized with sodium pentobarbitone (60 $mg.kg^{-1}$, intraperitoneal injection, Sanofi Santé Nutrition Animale, Libourne, France); administrated with heparin (1000 $IU.kg^{-1}$ heparin Choay, penis vein and sacrificed by exsanguination)). Rinse quickly with 1 mL cold PBS for 2 times, use tissue paper to dry the intestine each time. Next, place the intestine tissue in a 5-mL tube and add 5 mL of solution with/without substrate in the dark. The blank with substrate is prepared in the same manner but without intestine. Incubate all the tubes in the dark at 37°C for 10/20/30 min, transfer 1 mL of the solution at different time shown in the above table to Eppendorf tube, centrifuge at 14,000 rpm for 30 s, collect the supernatant to the plastic cuvette, and read absorbance at 405 nm shown in Table 2.

Table 2. Measurement of intestine GGT activity at different time intervals

Incubation time (min)	0	10	20	30
Group 1 (blank)	Substrate without intestine			
Group 2	Substrate with intestine			
Group 3	Without substrate but with intestine			

For manipulations with SBC (GGT inhibitor): the procedure is the same, except solution with substrate is replaced with solution with substrate and enzyme inhibitor.

3.3. Calculation

Calculate the concentration of produced 3-carboxy-4-nitroanilide by using the Beer-Lambert law ($A = \varepsilon \times l \times c$, ε = 9,500 $L.mol^{-1}.cm^{-1}$). Take into consideration of the optical length (l = 1 cm in plastic cuvette and 0.15 cm on microplate) and the possible dilution factor. Next, define the enzymatic activity = Amonut of 3-carboxy-4-nitroanilide/incubation time ($nmol.min^{-1}$).

Specific enzyme activity ($nmol.min^{-1}.mg^{-1}$ of proteins) is calculated by dividing enzyme activity by the quantity of proteins (proteins are measured by the BCA Protein Assay kit).

- Specific purified GGT activity: 3200 $nmol.min^{-1}.mg^{-1}$ of proteins
- Specific rat intestine GGT activity: 6.83 $nmol.min^{-1}.mg^{-1}$ of proteins

Western blot for protein disulfide isomerase identification in tissues

1. Principle

Protein disulfide isomerase (PDI) is an enzyme located in the endoplasmic reticulum or on the plasmic membrane surface of eukaryotes, catalyzing the formation and breakage of disulfide bonds between cysteine residues within proteins during their folding. Its denitrosating action has been identified in isolated aorta (Dahboul *et al.* 2014).

PDI is presently extracted from the rat intestine, separated on a denaturing gel under electric field and identified using specific anti-bodies (Mahmood and Yang 2012).

Reference

Dahboul F, Perrin-Sarrado C, Boudier A *et al.* S,S′-dinitrosobucillamine, a new nitric oxide donor, induces a better vasorelaxation than other S-nitrosothiols. *Eur J Pharmacol* 2014;**730**:171–9.

2. Reagents

All solutions are prepared with fresh cold ultrapure water (> 18.2 MΩ.cm) and stored at 4°C in the dark for maximum one month unless otherwise specified.

2.1. Physiological medium

Conservation time: one week at 4°C after preparation.

0.1 M Phosphate buffer (pH = 7.4): weigh 1.36 g of KH_2PO_4 (Mw = 136.09 $g.mol^{-1}$, ref Merck 646A148973) and 0.074 g of $EDTANa_2 \cdot 2H_2O$ (Mw = 372.24 $g.mol^{-1}$), dissolve with 100 mL of ultrapure water, and adjust the pH to 7.40 ± 0.05 with 10 M NaOH.

2.2. 1.5 M Tris buffer (pH = 8.9)

Weigh 2.364 g of Trizma-HCl (Mw = 158 $g.mol^{-1}$, ref Sigma T040), dissolve with 10 mL of ultrapure water; and adjust the pH to 8.90 ± 0.05 with 10 M NaOH solution.

2.3. 0.5 M Tris buffer (pH = 6.8)

Dilute 3-fold 1.5 M Tris buffer with ultrapure water (3 mL of 1.5 M Tris buffer + 6 mL of ultrapure water); and adjust the pH to 6.80 ± 0.05.

2.4. Laemmli Lysis-buffer

Use commercial Laemmli Lysis-buffer (ref Sigma 38733) made of 0.004 % bromophenol blue, 400 mM dithiothreitol glycerol (DTT), 20 % glycerol, 4 % SDS, and 0.125 M TRIS.

2.5. Lysis buffer

Dissolve 1 Medium Complete Mini (Roche) tablet in 7.8 mL of ultrapure water, add reagents as indicated in the following table and vortex for 0.5 min. Store at 4 °C for maximum 2 weeks.

Lysis buffer	Volume (final volume = 10 mL)	Final concentration
Tris-HCl (0.5 M, pH = 6.8)	1 mL	0.050 M
NaCl (1.5 M)	1 mL	0.15 M
Sodium dodecyl sulfate (SDS, 10 %)	0.1 mL	0.1 % (w/v)
Pure Triton X-100	0.1 mL	1 % (v/v)

2.6. 9.34 μM protein disulfide isomerase (PDI) solution

Weigh 1 mg of PDI purified from bovine liver (Mw = 107 kDa, EC 5.3.4.1, ref Sigma P3818), dissolve in 1 mL of phosphate buffer, divide the solution in aliquots of 40 µL and store them at -20°C.

2.7. Bicinchoninic acid (BCA) solution (working reagent, from the BCA Protein Assay kit (Pierce™ BCA Protein Assay Kit, ref Thermo Fisher 23225))

Mix 49 units of reagent A (sodium carbonate, sodium hydrogenocarbonate, bicinchoninic acid and sodium tartrate in 0.1 M NaOH) with 1 unit of reagent B (copper sulfate 4 % (w / v)).

2.8. Buffers for migration, transfer and labeling:

Prepare as indicated in the following table. Store at 4 °C for 1 month.

	Electrophoresis buffer	Transfer buffer	Tris-buffered saline - Tween 20 (TBST) buffer	Blocking buffer (TBST-milk 5 %)
Trizma base (ref Sigma T6066)	3 g	3.03 g	2.42 g	-
Glycine (ref Sigma G8898)	14.4 g	14.4 g	-	-
SDS	1 g	-	-	-
NaCl	-	-	8 g	-
Ultrapure water	1000 mL	800 mL	1000 mL	-
Methanol (ref Carlo Erba V5A473035B)	-	200 mL (add daily)	-	-
Tween 20 (ref Sigma P1379)	-	-	1 mL (add daily)	-
TBST buffer	-	-	-	20 mL
Milk powder	-	-	-	1 g
pH	8.3	8.3	7.6	-

2.9. Stripping buffer

Prepare as indicated in the following table. Store at 4 °C for 1 month.

	Volume / weight	Final concentration
Tris-HCl (0.5 M, pH=6,8)	12.5 mL	62.5 mM (pH=6.7)
SDS	2 g	2 % (w/v)
β-Mercaptoethanol (Sigma M6250)	0.141 mL	0.14 % (v/v)
Ultrapure water	67.4 mL	

2.10. Denaturing polyacrylamide gels

Polyacrylamide separation gel: prepare as indicated in the following table (10 %, followed by using 1 mL of propanol to smooth the gel and use ultrapure water to eliminate propanol). Store at 4 °C for 1 month.

	Volume (final volume = 10 mL)	Final concentration
Acrylamide (40 %, ref CSACR01)	3.3 mL	13.2 % (w/v)
Ultrapure water	4 mL	
SDS (10 %)	0.1 mL	0.1 % (w/v)
Tris-HCl (1.5 M, pH = 8,9)	2.5 mL	375 mM
Ammonium persulfate (APS, 10 %, ref Sigma A3678)	0.05 mL (initiate polymerization)	0.05 % (w/v)
N,*N*,*N*′,*N*′-Tetramethylethylenediamine (TEMED, ref Sigma T9281)	0.005 mL	0.05 (v/v)

Polyacrylamide concentration gel (4 %): prepare as indicated in the following table. Store at 4 °C for 1 month.

	Volume (final volume = 5 mL)	Final concentration
Acrylamide (40 %)	0.67 mL	5.4 % (w/v)
Ultrapure water	3 mL	
SDS (10 %)	0.050 mL	0.1 % (w/v)
Tris-HCl (500 mM, pH = 6,8)	1.25 mL	125 mM
APS (10 %)	0.025 mL (initiate polymerization)	0.05 % (w/v)
TEMED	0.005 mL	0.1 % (v/v)

3. Methods

3.1. Treatment of rat intestine

Remove Wistar rat intestine (ileum) (length: around 2 cm, weight: around 100 mg) after sacrifice (anesthetized with sodium pentobarbitone (60 $mg.kg^{-1}$, intraperitoneal injection, Sanofi Santé Nutrition Animale, Libourne, France); administrated with heparin (1000 $IU.kg^{-1}$ heparin Choay, penis vein and sacrificed by exsanguination)). Rinse quickly with 1 mL cold PBS for 2 times, use tissue paper to dry the intestine each time; freeze the rat intestine with liquid N_2. Smash the intestine in liquid N_2 with a pestle in a mortar, transfer the intestine powder to a 5-mL tube (ca. 100 mg). Add lysis buffer (1 mL of lysis buffer per 40 mg tissue powder) in each tube. Vortex for 10 s and incubate the tubes for 10 min on ice in the dark. Vortex the tubes for 10 s, divide samples into 1.5-mL Eppendorf tubes, then centrifuge at 18,000 $\times$ *g* for 15 min at 4 °C, and transfer the supernatant to a 15-mL tube. Precipitate proteins with pure acetone (1 mL supernatant + 3.3 mL acetone), and store the mixture for 1 h at -20 °C. Centrifuge at 3,000 $\times$ *g* for 10 min at 4 °C, and resuspend the pellet in 200 µL of lysis buffer before storing the tissue lysate at -80 ° C.

3.2. Quantification of proteins in the rat intestine

The suspension prepared in 3.1 is stored at -20 °C, before quantification by the BCA Protein Assay kit. Briefly, transfer 25 µL of sample or a standard solution of Bovine Serum Albumin (BSA) (from 25 to 1000 µg/mL) to a transparent 96-well microplate, add 200 µL of working reagent, incubate the mixture at 37 °C for 30 min. Finally, read the absorbance at 570 nm in a microplate reader (BioTek EL 800).

3.3. Electrophoresis of intestinal proteins

Dilute proteins to 0.8 µg/µL in lysis buffer and further dilute to 0.4 µg/µL with Laemmli Lysis-buffer (33 µL Laemmli Lysis-buffer + 33 µL of 0.8 µg/µL proteins solution); next heat the mixture at 95 °C with heating plate for 10 min to denature proteins.

Deposit molecular weight markers (PM marker, Biorad 161-0375), PDI diluted in lysis buffer (molecular weight of monomer around 55 kDa, ≤1µg, positive control)

and proteins samples (rat intestine homogenate) (8 µL marker and 50 µL samples) on the gel in the following order (from left to right); put the gel in the tank with the electrophoresis buffer, perform migration with following conditions:

- 25 min at 50 V
- 90 min to 150 V
- 20 min to 180 V

3.4. Transfer of intestinal proteins to nitrocellulose membrane

Activate the nitrocellulose membrane in methanol for 1 min, and in transfer buffer for 5 min.

The proteins after migration, are subjected to an electro-transfer on nitrocellulose membrane (Whatman Protran) in Transfer buffer (pH = 8.3) for 1 h at constant voltage of 100 V.

After the transfer, wash the membrane in 20 mL of TBST for 5 min and blocking the membrane in blocking buffer (20 mL, TBST-milk 5 %) for 2 h at r.t. or overnight at 4 ° C.

3.5. Labeling of intestinal proteins

Dilute the primary antibody (anti-PDI, Santa cruz Biotechnology) for 1000-fold in the TBST-Milk 5 % buffer (final volume = 20 mL) and use it to cover the membrane. Incubate for 30 min at r.t. with gentle stirring (Heidolph Polymax 1040 stirrer, Schwabach, Germany). Wash the membrane in TBST for 4 times (5 min for each wash) (Do not load the antibodies of Anti-PDI and the anti-Actin at the same time):

Sample type	Rat intestine
Dilution of anti-PDI	1/1000[e]
Dilution of anti-Actin	1/7500[e]
Exposure time for anti-PDI	30 s
Exposure time for anti-Actin	30 s

Dilute the secondary antibody (Goat anti-Rabbit HRP, Santa Cruz Biotechnology) for 5000-fold in the TBST-Milk 5 % buffer (final volume = 20 mL), and use it to cover the membrane. Incubate for 60 min at r.t. with gentle stirring (Heidolph Polymax 1040

stirrer, Schwabach, Germany). Wash the membrane in TBST for 4 times (5 min for each wash).

3.6. Analysis of intestinal proteins

Enhanced chemiluminescence (ECL) revelation: Tap the membrane on filter paper and place it in a crystallizer. Mix 1 mL of solution 1 and 1 mL of ECL solution 2 (BIO-RAD, Clarity Western ECL Substrate, Ref: 170-5061) (use 2 different tips and don't mix these two solutions in the original vials). Use this mixture to cover the membrane completely and avoid bubbles. Incubate for 5 min in dark and take out the membrane with a forceps and drain it, next, wrap the membrane with cellophane (attention to bubbles). Place the membrane in the revelation cassette: fix the cellophane in the cassette with scotch (wearing gloves).

Development: Take out the film, cut it to the proper size and cut off the top right corner; place the film on the diaphragm (align the film in the upper left corner); Expose (30 s for anti-Actin, 30 s for anti-PDI); Remove the film in a dry flash. Develop the film for 30 s and fix for 1.5 min. Rinse the film in ultrapure water and dry it. Place the film on the membrane again in the cassette: mark molecular weights according to the marker and note the contours of the membrane on the film. Rinse the membrane in TBST for 5 min under rotation, and store the membrane wrapped with cellophane at 4 ° C. The whole procedure is in dark.

Stripping: Rinse the membrane in TBST for 2 h at r.t. under rotation, incubate for 30 min at 50 °C in stripping buffer; rinse the membrane in TBST for 5 min under rotation for 4 times, block the membrane again and label anti-actin as procedure 3.5.; analyze proteins as procedure 3.6..

A representative result is shown in Figure 1.

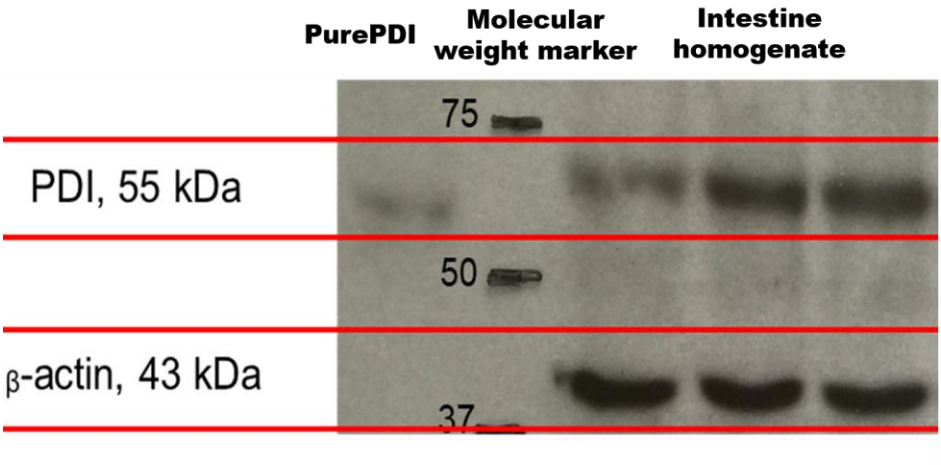

Figure 1. Western blot analysis of PDI (55 kDa) in isolated rat intestine homogenate with different concentrations, and β-actin was used as a reference protein (43 kDa).

Purification of azo adduct and 2,3-naphthotriazole adduct by LC coupled with UV/Vis detection

1. Principle

The Griess method is based on diazotation between nitrite ion (NO_2^-) and sulfanilamide. The resulting diazonium salt is then coupled to *N*-(1-naphthyl)ethylenediamine (NED), forming an azo adduct which strongly absorbs at λ_{max} = 540 nm (Figure 1).

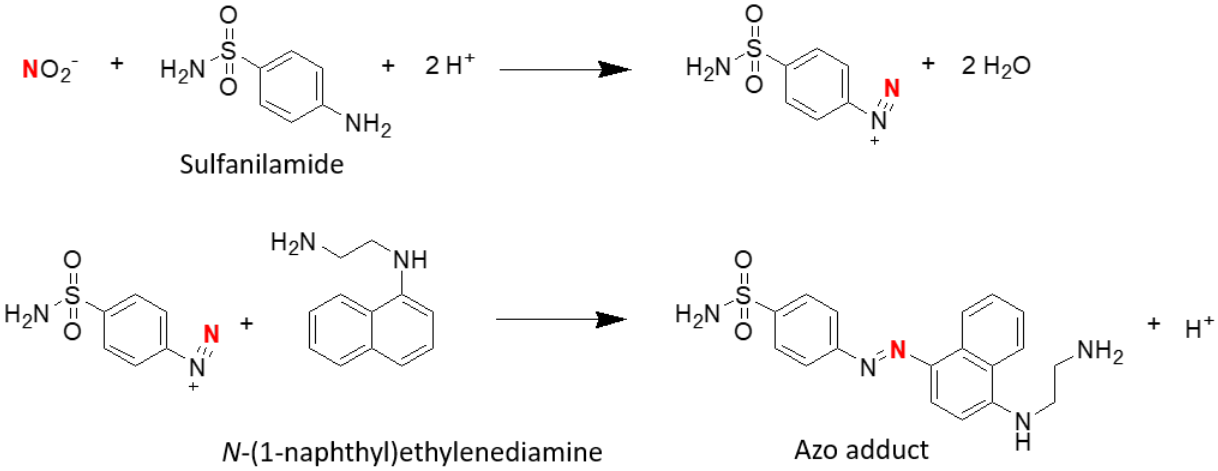

Figure 1. Scheme of the Griess reaction.

Principle of 2,3-diaminonaphthalene (DAN) assay is shown in protocol entitled *"Measurement of nitrite, nitrate ions and S-nitrosothiols using the 2,3-diaminonaphthalene assay by spectrofluorometry"*.

Stable nitrogen isotope (^{15}N) labeled azo adduct and 2,3-naphthotriazole (NAT) adduct are not available in the market. When ^{15}N labeled nitrite ion reacts with Griess or DAN reagents, ^{15}N labeled azo adduct or NAT adduct is produced. High performance liquid chromatography (LC) is used to separate produced adducts from excess of derivatization reagents, Next, purified adducts are collected for further research, such as optimizing method sensitivity using mass spectrometry.

Reference:

Marzinzig M, Nussler AK, Stadler J *et al.* Improved Methods to Measure End Products of Nitric Oxide in Biological Fluids: Nitrite, Nitrate, andS-Nitrosothiols. *Nitric Oxide-Biol Chem* 1997;**1**:177–89.

2. Reagents

All solutions are prepared with fresh cold ultrapure water (> 18.2 MΩ.cm) and stored at 4°C in the dark for maximum one month unless otherwise specified.

2.1. 10^{-2} M sodium nitrite

Weigh 35.0 mg of sodium nitrite ($Na^{15}NO_2$) (Mw = 70 $g.mol^{-1}$; ref Cambridge Isotope Laboratories 68378-96-1, purity: 98 %) in a 50 mL volumetric flask, dissolve and adjust the volume with ultrapure water. Mix the solution gently for one time. Prepare daily.

2.2. 1.75 M acetate buffer pH 2.5

Mix 50 mL of glacial acetic acid solution (Mw = 60.05 $g.mol^{-1}$) with 400 mL of ultrapure water, adjust the pH to 2.50 ± 0.05 with 12 M NaOH (Mw = 40.0 $g.mol^{-1}$), and fill up to 500 mL with ultrapure water.

2.3. Sulfanilamide (Griess reagent)

Weigh and transfer 0.6 g of sulfanilamide (Mw = 172.2 $g.mol^{-1}$) in a 100-mL volumetric flask, dissolve in 40 mL of 1 M HCl (Mw = 36.46 $g.mol^{-1}$) and adjust the volume with ultrapure water.

2.4. *N*-1-(naphthyl)ethylenediamine dihydrochloride (NED)

Weigh and transfer 0.45 g of NED (Mw = 259.2 $g.mol^{-1}$) in a 100-mL volumetric flask, add 30 mL of 1 M HCl, and adjust the volume with ultrapure water.

2.5. 1.24 mM pure NAT

Weigh 21 mg NAT (Mw = 169.2 $g.mol^{-1}$; ref Chemodex 269-12-5; purity: 98.2 %) in a 100 mL volumetric flask, dissolve and adjust the volume with 0.1 M HCl solution containing 10 % methanol. Divide into aliquots of 2 mL and store at -80°C for 1 year.

2.6. 0.6 M HCl

Transfer 300 mL of 1.0 M HCl (commercial solution; Mw = 36.46 $g.mol^{-1}$) in a 500.0 mL volumetric flask and complete with ultrapure water.

2.7. 3.16 mM DAN

Weigh 5 mg of DAN (Mw = 158 $g.mol^{-1}$; ref Sigma D-2757) in a 10 mL volumetric flask, dissolve and adjust the volumewith 0.6 M HCl.

2.8. 1.2 M NaOH

Dilute NaOH solution with ultrapure water by mixing 0.12 mL of 10 M NaOH solution and 0.88 mL ultrapure water.

2.9. Mobile phase CH_3CN-H_2O (25/75, V/V) + 0.1 % trifluoroacetic acid (TFA)

Mix 250 mL acetonitrile and 750 mL ultrapure water and 1 mL TFA, filter with 0.45-µm HV membrane (Durapore®).

2.10. Mobile phase CH_3CN–CH_3COONH_4 (10^{-2} M, pH = 7.2) (28/72, V/V)

Dilute 0.57 mL of acetic acid (volumetric mass = 1.05 g/mL; Mw = 60.05 $g.mol^{-1}$; ref Sigma 64-19-7) with 1 L of ultrapure water, and adjust the pH to 7.2 with 10 times diluted ammonia solution (ca. 25% NH_3; volumetric mass = 0.91 g/mL; Mw = 17.03 $g.mol^{-1}$; ref Sigma 1336-21-6); mix 280 mL acetonitrile and 720 mL ammonium acetate solution and filter with 0.45-µm HV membrane (Durapore®).

3. Methods

3.1. Operating conditions for collecting purified azo adduct

100 µL of 10^{-2} M $NaNO_2$ solution is transferred to a 1.5 mL Eppendorf tube, 900 µL of acetic acid and 200 µL of sulfanilamide are added. The mixture is vortexed for 5 s and kept at 20-25 °C for 3 min in dark. Next, 50 µL of NED is added. The mixture is vortexed again for 5 s and kept at 20-25 °C for 5 min in dark, before injecting into the LC-UV/Vis system and the appropriate volume (around 0.5 mL) of mobile phase fraction containing azo adduct is collected. The resulting solution is stable at 4 °C for a maximum period of 24 h and -80 °C for a maximum period of one month.

The operating conditions are as follows:

- Injector with loop size: 100 µL
- Column: CC 250/4.6 NUCLEOSIL 100-5 C18 AB (Macherey Nagel, Germany) + precolumn (LiChrospher ® 100 RP-18 (5 µm) 4 x 4 mm)
- Mobile phase: $CH_3CN–H_2O$ (25/75, V/V) + 0.1 % trifluoroacetic acid (TFA)
- Flow rate: 1.2 $mL.min^{-1}$; column temperature: 40 °C; resulting back pressure: 135-137 bars
- Spectrophotometric detection: fixed wavelength at 220 nm (UV/VIS-155, GILSON, Middleton, USA) + software: Azur®, Datalys (running time: 20 min; peak range: 10.5 – 12.5 min)
- Rinsing conditions: use CH_3CN-H_2O (50/50, V/V) at a flow rate of 0.8 $mL.min^{-1}$ and at 40°C for 10 min.

Retention time of the azo adduct is within 12 min. Typical chromatograms are shown in Figure 2.

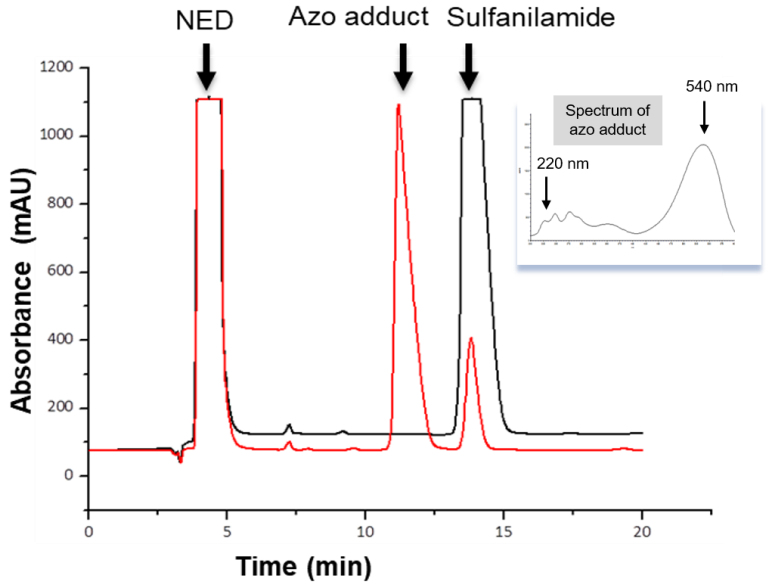

Figure 2. Chromatograms corresponding to azo adduct resulting from derivatization of 10^{-2} M NO_2^- in red or blank (ultrapure water) in black by LC-UV/Vis at λ = 220 nm.

3.2. Operating conditions for collecting purified NAT

300 µL of 5 mM $NaNO_2$ solution (obtained by mixing 500 µL of the 10^{-2} M $NaNO_2$ and 500 µL of ultrapure water) is transferred to a 1.5-mL Eppendorf tube, and

600 µL of 3.16 mM DAN is added (excess: 26.4 %, pH = 0.4). The mixture is vortexed for 5 s and incubated in an oven at 37°C for 10 min and in dark. Next, 310 µL of 1.2 M NaOH are added. The mixture is stored at -80°C (for maximum 3 months) before injecting into the LC-UV/Vis system and the appropriate volume (around 0.5 mL) of mobile phase fraction containing NAT is collected. The operating conditions are as follows:

- Injector with loop size: 100 µL
- Column: CC 250/4.6 NUCLEOSIL 100-5 C18 AB (Macherey Nagel, Germany) + precolumn (LiChrospher ® 100 RP-18 (5 µm) 4 x 4 mm)
- Mobile phase: CH_3CN–CH_3COONH_4 (10^{-2} M, pH = 7.2) (28/72, V/V)
- Flow rate: 0.8 mL.min^{-1}; column temperature: 40°C; resulting back pressure: 100 bars.
- Spectrophotometric detection: fixed wavelength at 330 nm (UV/VIS-155, GILSON, Middleton,USA) + software: Azur®, Datalys (running time: 15 min; peak range: 11 – 13 min)
- Rinsing conditions: use CH_3CN-H_2O (50/50, V/V) at a flow rate of 0.8 mL.min^{-1} and at 40 °C for 10 min.

Retention time of the NAT adduct is within 12 min. Typical chromatograms are shown in Figure 3.

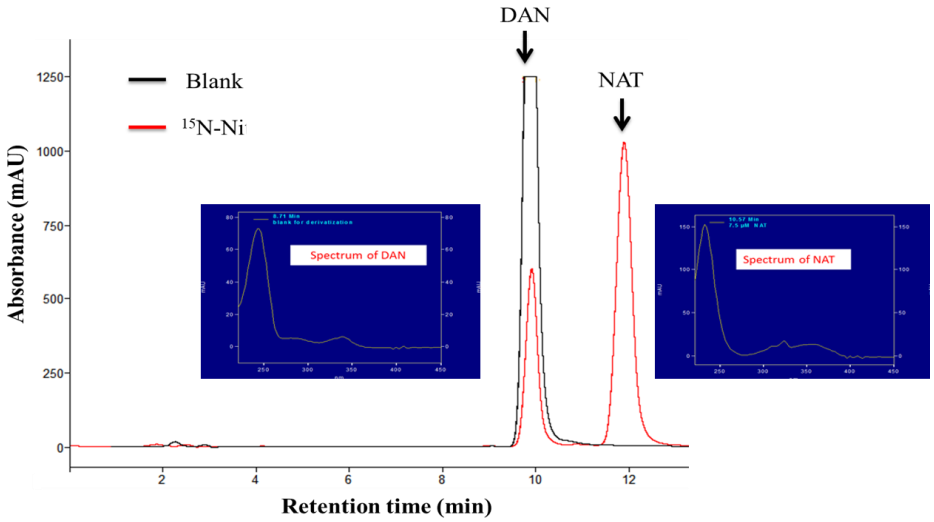

Figure 3. Chromatograms corresponding to NAT adduct resulting from derivatization of 5 mM NO_2^- in red or blank (ultrapure water) in black by LC-UV/Vis at λ = 330 nm.

3.3. Quantification of purified azo adduct by spectrophotometry

The purified azo adduct is 20-fold diluted with ultrapure water (50 µL sample in 1-mL ultrapure water), followed by spectrophotometry (UV-1800, Shimadzu, Lognes, France) at wavelength of 540 nm. Nitrite concentration is calculated by the Beer-Lambert law ($A = \varepsilon \times l \times c$, $\varepsilon = 37700 \pm 5000\ M^{-1}.cm^{-1}$).

3.4. Operating conditions for purified NAT quantification

Purified NAT is diluted for 50-fold in mobile phase, 2 µM nitrite (1.5 µM NAT) in ultrapure water and blank (ultrapure water) is derivatized as standards:

300 µL of each $NaNO_2$ solution are transferred to a 1.5-mL Eppendorf tube and 60 µL of 0.105 mM DAN solution are added. Next, the mixture is vortexed for 5 s, and then incubated in an oven at 37°C for 10 min and in dark. Next, 40 µL of 1 M NaOH are added. The mixture is cooled and stored at 4°C before injecting into the LC-FL.

The operating conditions for LC are the same as above, except for the following conditions:

- Injector with loop size: 20 µL
- Column: ZORBAX SB-Aq C18 4.6 X 150 mm, 3.5 µm (Agilent) or the one used for NAT collection + precolumn (NUCLEODUR® EC4/3 C-18 HTec, 5 µm)
- Spectrofluorometric detection: λ_{exc} = 375 nm and λ_{em} = 415 nm; sensitivity: low (RF-551, Shimadzu, Kyoto, Japan) + software: Azur® (running time: 12 min; peak range: 8 min - 10 min).

Etude de la biodisponibilité orale du *S*-nitrosoglutathion au moyen de modèles de la barrière intestinale par chromatographie en phase liquide couplée à la spectrométrie de masse après marquage par l'isotope 15 de l'azote

Résumé : Le développement de nouveaux donneurs d'oxyde nitrique (NO) dans le traitement chronique des maladies cardiovasculaires nécessite l'étude de leur biodisponibilité après administration par voie orale. Les *S*-nitrosothiols (RSNOs) apparaissent d'intéressants candidats médicaments pour ce faire, et l'étude de leur perméabilité intestinale est une première étape indispensable. Il est nécessaire de disposer d'une méthodologie analytique suffisamment sensible et sélective, en particulier permettant de différencier entre la production endogène de NO, l'apport alimentaire en ions nitrites et nitrate et le médicament lui-même. Nos travaux de thèse ont consisté à utiliser le *S*-nitrosoglutathion (GSNO) comme modèle après son marquage par l'isotope stable 15 de l'azote (^{15}N). La dérivation du ^{15}NO libéré par deux méthodes conventionnelles (méthode de Griess conduisant à la formation d'un adduit azoïque ; réaction avec le 2,3-diaminonaphtalène (DAN) formant l'adduit 2,3-naphtotriazole (NAT)) et l'étude de la fragmentation en spectrométrie de masse tandem (MS/MS) des deux adduits correspondants ont mené à sélectionner la dérivation par le DAN comme étant la plus sensible. Une transition originale résultant de la fragmentation du NAT en mode *Higher-energy Collisional Dissociation* (HCD) au lieu du mode conventionnel *Collisionally Induced Dissociation* (CID) a été mise en évidence ; elle permet d'atteindre une limite de quantification de 5 nM (soit 20 fois plus basse que celle offerte par la fluorescence). La méthode LC-MS/MS a été validée et appliquée à l'étude de la perméabilité intestinale du GS^{15}NO par deux modèles : l'un *in vitro* (monocouche de cellules épithéliales type Caco-2), l'autre *ex vivo* (intestin de rat isolé (iléum) dans une chambre de Ussing). Les valeurs de perméabilité apparente calculées à partir des concentrations des métabolites du GS^{15}NO (ions nitrites, nitrates et RSNOs) le classent comme un médicament de perméabilité intermédiaire. En outre, des études sur les mécanismes de dénitrosation du GSNO ont été menées sur intestin isolé, démontrant en particulier le rôle d'enzymes telles que la γ-glutamyltransférase et la protein disulfide isomerase.

Mots clés : donneurs de NO; *S*-nitrosothiols; azote 15; dérivation; chromatographie en phase liquide; spectrométrie de masse tandem.

Oral bioavailability studies of *S*-nitrosoglutathione using intestinal barrier models by liquid chromatography coupled with mass spectrometry after labeling with the nitrogen isotope 15

Abstract: The development of innovative nitric oxide (NO) donors for the chronic treatment of cardiovascular diseases implies their bioavailability studies after oral administration. *S*-nitrosothiols (RSNOs) look interesting drug candidates for this purpose and evaluating their intestinal permeability appears the first step to be realized. Thus, an analytical method offering high sensitivity is needed; moreover this method should be selective by differentiating between the endogenous production of NO, the intake of nitrite and nitrate ions *via* the diet, and the drug itself. Our work consisted in using *S*-nitrosoglutathione (GSNO) labeled with the stable nitrogen isotope 15 (^{15}N) as a model. Released ^{15}NO species were derivatized by two conventional methods: Griess method leading to the formation of an azo adduct; reaction with 2,3-diaminonaphthalene (DAN) producing 2,3-naphtotriazole (NAT); fragmentation studies of the two adducts by tandem mass spectrometry (MS/MS) allow the selection of DAN method because it provides the highest sensitivity. An original transition resulting from the NAT fragmentation in *Higher-energy Collisional Dissociation* (HCD) mode instead of the conventional *Collisionally Induced Dissociation* (CID) mode was pointed out and permitted to reach a limit of quantification of 5 nM (20 fold less than when using fluorescence). The LC-MS/MS method was validated and applied to the GS^{15}NO intestinal permeability studies with two models: *in vitro* (a monolayer of Caco-2 epithelial cells), and *ex vivo* (isolated intestine of rat (ileum) in an Ussing chamber). The apparent permeability values calculated with concentrations of GS^{15}NO metabolites (nitrite, nitrate ions and RSNOs) classify it as a middle permeable drug. Studies on GSNO denitrosating processes using isolated rat intestine demonstrate that the enzymes *γ*-glutamyltransferase and protein disulfide isomerase play a pivotal role.

Keywords: NO donors; *S*-nitrosothiols; nitrogen 15; derivatization; liquid chromatography; tandem mass spectrometry.